The aerodynamics of long lorry platoon in a tunnel

By

Xiaotian Zhang

A thesis submitted to
the University of Birmingham
for the degree of
DOCTOR OF PHILOSOPHY

School of Civil Engineering
University of Birmingham
April 2022

ABSTRACT

In recent years, the concept of vehicle platooning has gained widespread attention for its highly efficient road usage and lower fuel consumption. However, the aerodynamics of vehicle platoons travelling in a tunnel are not well understood, even though more and more road tunnels have been built to alleviate the traffic congestion problem. This research aims to improve our understanding of the aerodynamic phenomena associated with a long vehicle platoon running through a tunnel. The effect of the tunnel existence, blockage ratio, symmetry of the traffic lane and the inter-vehicle spacing on the aerodynamics performance of the long platoon will be investigated. To achieve this goal, both model-scale experiments and numerical simulations (IDDES) were conducted, and the results are compared to a similar study conducted in the open air.

The slipstream velocity and pressure, the lorry surface pressure, as well as the drag coefficient, were investigated systematically. The results show greater pressure variations when the platoon is running through the tunnel than in open air. The piston effect in the tunnel leads to a lower approaching velocity and a weaker flow separation compared to the case in the open air. All vehicles, in both the tunnel and the open air, experience a drag reduction due to platooning. Interestingly, the drag reduction in the tunnel is 20% greater than that in the open air, implying a greater potential in fuel saving.

When the blockage ratio decreases, the piston effect becomes less effective, making the flow field and the variation drag reduction ratio approach the pattern observed in the

open air. Unlike a single lorry, increasing the blockage ratio does not lead to an increase of the drag of every lorry in the platoon. In a small tunnel, the some intermediate lorries have smaller drag coefficients, while others have larger drag coefficients compared to the lorries in large tunnels. Therefore, the overall drag coefficients of the platoons are not affected by the blockage ratio, except for the platoon with $0.1L$ spacing. It is further found that the travelling on the asymmetrical traffic lane may results in some asymmetry of the flow field, but has little influence on the drag and side forces experienced by the lorries.

In the open air, the drag coefficients of all lorries are monotonically decreasing with the spacing due to the stronger shielding effect. When the spacing reduces to $0.25L$, the intermediate lorries have larger drag coefficients than the same lorries in the platoon with larger spacings due to the change of the wake structure and the confinement of tunnel walls. Therefore, the overall drag reduction ratio does not monotonically increase with the decreasing spacing. The inter-vehicle spacing control strategy should be reconsidered when a long platoon travelling from the open air into a road tunnel.

ACKNOWLEDGMENTS

Without the help and encouragement of others, this work would not be possible.

First of all, I would like to convey my particular thanks to my supervisor, Dr. Hassan Hemida and Dr Shi-Di Huang, for their patient guidance and inspiration during the process of this work. Their expertise in this topic, availability for discussions and meetings and their provision of constructive feedback, were essential to the success of the research.

I would also like to acknowledge the support of my second supervisor, Dr. David Soper and Dr Bruño Fraga for their useful feedback and suggestions. I would like to convey my heartfelt appreciation to Dr Francis Robertson and Dr Mingzhe He of the University of Birmingham for their cooperation with the TRAIN rig experiments.

I would like to thank a number of people who reviewed my research and acknowledged its importance. The internal examiner Professor Chris J. Baker and external examiner Dr Dominic Flynn gave me useful advice for the thesis. The anonymous reviewers of the published journal articles, who gave insightful remarks, also made a significant contribution to the quality of this thesis.

I am thankful to present and past colleagues in the department of civil engineering in UOB and department of mechanics and aerospace engineering in SUSTech for together creating such an pleasant working environment. All the discussions over lunch, joint trips to conferences, presentations, research discussions, group meeting and so on, have made my stay at the departments quite memorable. In particular I would like to thank Mr Yi Wang and Mr Peijiang Qin

Family encouragement has been critical during this period, both for the completion of this thesis and the journey preceding it. I am eternally thankful to them for their tireless efforts and never-ending patience.

This work was supported by an EPSRC funded project entitled 'The aerodynamics of close running ground vehicles - EP/ N004213/1' and the Department of Science and Technology of Guang-dong Province (Grant No. 2019B21203001). The author also would like to thank the computational support from BlueBEAR at the University of Birmingham and the Center for Computational Science and Engineering at Southern University of Science and Technology.

Contents

List of Figures

List of Tables

Nomenclature

$\triangle P_N$	Nominal differential pressure
$\delta \triangle P$	Accuracy of static velocity
$\delta\rho$	Accuracy of the air density
δu	Accuracy of longitudinal velocity
δu_{res}	Accuracy of horizontal velocity
δv	Accuracy of lateral velocity
δV_{plat}	Accuracy of experimental platoon speed
δV_{lorry}	Accuracy of platoon speed of each run
Δ	Filter width
δ_{ij}	Kronecker delta
Δ_{max}	Grid spacing
ℓ_m	Mixing length
ℓ_S	Smagorinsky length sacle
ϵ	Dissipation rate
η	Kolmogorov length scale
$\hat{U}$	Filtered velocity
κ	Von Karman constant
μ	Dynamics viscosity
ν	Kinematic viscosity
ν_r	Residual eddy viscosity
ν_t	Eddy viscosity
Ω	Vorticity tensor
ω	Specific rate of dissipation
$\overline{C_{P_k}}$	Mean surface pressure coefficient of Tap k
$\overline{u_i' u_j'}$	Reynold stress tensor
Φ	Relative humidity
ρ	Air density
σ_{C_ξ}	Standard deviation of general non-dimensional coefficient
τ	Normalised time/Time scale
τ_{ij}^r	Residual stresses
τ_{ij}	Viscous stresses
Vol_{RT}	Time average value
Re	Reynolds number
$\widehat{\mathcal{S}}$	Filtered rate of strain
b_k	General measured quantity coefficient
c	General signal
C_1, C_2, C_3	Cubic calibration coefficients
$C_\omega, C_{dt1}, C_{dt2}, C_l, C_t$	Constants for IDDES
C_ξ	General non-dimensional coef-

	ficient
C_p	Pressure coefficient
C_S	Smagorinsky coefficient
C_{des}	Constant in DES model
C_{d1}, C_{d2}	Constant
d_ω	distance to the nearest wall
E_{BIAS}	General bias uncertainty
E_{BIAS}	General total uncertainty
E_{RND}	General random uncertainty
$E_{ACC,k}$	Calibration error
F_1, F_2	Blending function
f_e	Elevating function
f_{samp}	Sampling frequency
F_{DDES}	Blending function of DDES
h_{max}	Maximum edge length of the cell
k	Kinetic energy
L, W, H	Length, width and height of the model-sacle lorry
L_t	Turbulent length scale
N_{samp}	Sample number
P	Pressure
p_0	Ambient reference pressure
P_{atm}	Atmospheric pressure
R	Gas constant
T	Measured temperature
t_{samp}	Re-sampled time
U, V, W	Dimensionless speed of longitudinal, lateral and vertical-component
u, v, w	Air velocity of longitudinal, lateral and vertical component
u'	Filter-out velocity
$u'(x,t)$	Fluctuating component of velocity
$U_(x,t)$	Mean component of velocity
u_i	Velicity component
U_{res}	Dimensionless speed of overall horizontal velocity
v	Velocity scale
V_{plat}	Experimental speed of the platoon
V_{nom}	Nominal speed of the platoon
y^+	Dimensionless wall distance
Y_k	Dissipation term of turbulent kinetic energy

Chapter One

Introduction

1.1 Outline of studies

The thesis reports an investigation into the aerodynamics of a long lorry platoon travelling trough a partially-enclosed road tunnel. Two method are used: physical experiments using a moving model-scale and computational simulation based on the sliding mesh technique. The simulations were validated by comparing the experiments and numerical result of one case. Then the effect of the tunnel existence, tunnel size, symmetry of traffic lane and the inter-vehicle spacing are investigated numerically. The slipstream velocity and pressure, the lorry surface pressure, as well as the drag coefficient, were investigated systematically and compared with the results obtained in the open air. The results of this study have been published in two journal:

- X.-T. Zhang, F. H. Robertson, D. Soper, H. Hemida and S.-D. Huang, 2021. Investigation of the aerodynamic phenomena associated with a long lorry platoon running through a tunnel. Journal of Wind Engineering and Industrial Aerodynamics. DOI: 10.1016/j.jweia.2020.104514
- X.-T. Zhang, D. Soper, B. Fraga, H. Hemida and S.-D. Huang, 2022. Numerical investigation of the aerodynamics of lorry platooning travelling through road tunnels. Journal of Wind Engineering and Industrial Aerodynamics (Under-review).

and present at:

- The 15th International conference on Wind Engineering, Beijing (China), 1-6 September 2019.

This Ph.D programme is a joint programme by University of Birmingham (UoB) and Southern University of Science and Technology (SUSTech). The author spent the first 15 month conducting the experimental work at UoB in the UK and then the remaining period conducting the simulation work at SUSTech in China.

1.2 Research Background

Road traffic has been continuously increasing over the years. The road transport in Europe increased by 27.2% from 2000 to 2018. Trucks carry 73.1% of all freight transported over land in the European Union (Commission, Mobility, and Transport 2020) and 73.1%. The expansion of vehicles is detrimental to society and the environment. It increases fuel consumption, air pollution, traffic congestion, and accident rates. To deal with the growing traffic demand and the consequent environmental problem due to increasing pollutant emissions, the concept of platooning has long been proposed as a potential solution (Shladover et al. 1991). Platooning, or vehicle convoys, refers to the case where several vehicles form a road-train, with relatively small gaps between vehicles that are maintained autonomously. Thanks to the recent fast development of autonomous road vehicles, the platooning strategy has once again become an important topic in both academic and industrial fields (Robbert Janssen 2015).

With the advancement of digital technologies in vehicle industry, the notion of vehicle-to-vehicle (V2V) communication can be used to enhance the operation of Heavy-Duty Vehicles (HDVs). Platooning is one of the possible uses of this technology. A set of onboard sensors monitors the truck's environment, while communication modules communicate vehicle information to the convoy's other trucks. An autopilot can handle braking, acceleration, and even steering based on these data. Due to the V2V communications convey command

signals such as joining and braking, the autopilot may react swiftly to the other truck's actions. The benefits of platooning can be summarised as Robbert Janssen (2015):

- **Fuel Consumption** Close running arrangement of the vehicles provides aerodynamic benefits. Reduced aerodynamic drag benefits all vehicles in a platoon, resulting in decreased fuel consumption.
- **Safety** V2V connections will enable trailing vehicles to automatically slow down in response to the slowing of the leading vehicle. The risk of a head-to-tail collision is reduced when the response time is shorter.
- **Traffic Flow** The distance of road occupation to deliver a given number of cargo can be minimised with the help of close following strategy of the vehicles. The traffic congestion due to the fluctuating following distances will be largely alleviated with the rapid response time.
- **Driver Occupation** Fully automated driving control systems can allow drivers to take a break from the wheel or undertake other administrative tasks.

The potential in fuel-saving been identified by wind tunnel experiments (Le Good et al. 2018; McAuliffe and Ahmadi-Baloutaki 2018; Salari and Ortega 2018; Tsuei and Savaş 2001; Zabat et al. 1995) and fuel consumption track tests (Hong et al. 1998; Browand, Mcarthur, and Radovich 2004; Lammert et al. 2014; Humphreys and Bevly 2016; Bergenhem et al. 2010; Davila, Aramburu, and Freixas 2013; Browand, Mcarthur, and Radovich 2004). These studies illustrated that the drag reduction mainly results from the changes in the frontal and rear surface pressures of the vehicles. Briefly, the trailing vehicles are shielded from the high-speed air, therefore the drag force on the frontal surface is reduced. In addition, thanks to the trailing vehicles, the leading vehicle also enjoys an increased pressure in its rear region, resulting in less pressure differential between its frontal and rear surfaces.

To achieve greater fuel saving, researchers have also explored the optimal inter-vehicle spacing (Davila, Aramburu, and Freixas 2013; Robertson et al. 2019; Tsuei and Savaş 2001; Schito and Braghin 2012). The SARTRE (Safe Road Trains for the Environment) project, which aimed to develop a system that allows platoons to travel on public highways, showed

that higher drag reduction and fuel saving could be achieved with smaller inter-vehicle spacing. (Schito and Braghin 2012) found that a 6-vehicle platoon with smaller inter-vehicle spacing has smaller drag coefficient, and this finding is valid for a variety of vehicle geometries. In a recent experimental study of an 8-lorry platoon, Robertson et al. (2019) also reported that the drag decreases as the inter-vehicle spacing decreases from $1.5L$ to $0.5L$, where L is the vehicle length. They demonstrated that the shielding effect is more effective at smaller inter-vehicle spacing by reducing the frontal pressure. However, some other studies showed that platooning does not necessarily lead to a drag reduction for certain inter-vehicle spacings (Browand, Mcarthur, and Radovich 2004; Ebrahim and Dominy 2020; Le Good et al. 2018; Mirzaei and Krajnović 2016; Watkins and Vino 2008; Zabat, Frascaroli, and Browand 1994; Pagliarella, Watkins, and Tempia 2007). A so-called "drag penalty" phenomenon for a two-vehicle platoon with small inter-vehicle spacing (Pagliarella, Watkins, and Tempia 2007). The drag properties associated with vehicles in platooning depend on the geometry of the vehicle and the platoon configuration (Le Good et al. 2018). Therefore, more detailed studies are required to understand the effects of the inter-vehicle spacing for different types of vehicle platoon.

Meanwhile, more road tunnels has been built in recent years to improve the urban traffic conditions (Chung and Chung 2007). When vehicles travel in a road tunnel, the tunnel's wall will not only restrict the airflow motion, but will also modify the flow dynamics around the vehicles. One of the most important effects is the 'piston effect'. Specifically, in contrast to the case of vehicles travelling in the open space, where the air displaced by the vehicles can freely move away to most directions, the airflow around vehicles in a tunnel is largely forced to flow parallelly to the vehicles' movement direction. As a result, a high-pressure region is formed in the front of the vehicle and a low-pressure region behind it, where the wake structures act as an air-sucker. These changes in the flow field lead to significant variations in the aerodynamic forces. Therefore, investigating the aerodynamics of vehicles travelling through road tunnels is critical for optimising the platooning strategy. In the road tunnel, the blockage ratio of the tunnel has a significant effect on the drag coefficient (Lee, Park, and Kim 2018), it is worthy to check whether the above finding is valid in a large tunnel. In addition, as the majority of road tunnels have multiple traffic lanes, the effect of the traffic lane (i.e., the laterally unsymmetrical flow field) is also of interest.

1.3 Proposed scope and aims

This work aims to investigate the aerodynamic phenomena associated with a long vehicle platoon running through a road tunnel in order to provide information for the future platooning formation that will achieve greater fuel savings. To achieve this goal, both model-scale experiments and numerical simulations were conducted. Several key variables in platooned conveyed will be exploiting:

- Compare the aerodynamics behaviors of a long platoon travelling through a road tunnel and the open air:

  Conduct and validate numerical simulations of a $1.5L$ spaced platoon in a road tunnel in order to determine the confinement effect of the tunnel walls on the aerodynamics characteristics of the platoon. The slipstreams properties, surface pressure variation and the drag reduction will be compared in the tunnel and in the open air.

- The effects of blockage ratio of the tunnel and the symmetry of traffic lane;

  Analyse the numerical simulations of a $1.5L$ spaced platoon in tunnels with different blockage ratio and different traffic lane in order to determine their effect on the slipstream, drag and side force of the platoon.

- The effects of inter-vehicle spacing on platoon aerodynamic performance in a road tunnel.

  Analyse the numerical simulations of different spaced platoon in road tunnels to determine the best inter-vehicle spacing of the platoon under different running conditions.

1.4 Structure of thesis

This study will be confined to the investigation of slipstream, surface pressure, aerodynamic forces and flow structures that arise from the flow interactions of the platoon and the tunnel walls. The model-scale experiments were performed with novel moving models at the University of Birmingham TRansient Aerodynamic INvestigation (TRAIN) rig facility. The

slipstream properties and vehicle surface pressure were measured to provide a benchmark for validating the Computational Fluid Dynamics (CFD) results. For the numerical simulation, a sophisticated Detached Eddy Simulation (DES) method (Gritskevich et al. 2012) was utilised to obtain high-quality information of the unsteady flow. These results enable us for the first time to have a full understanding of the aerodynamic behaviour of a long platoon travelling through a tunnel. A platoon travelling in the open air and a platoon running through a road tunnel will be compared first in terms of aerodynamic performance. The influence of the tunnel's blockage ratio and the position of the traffic lanes as two factors affecting aerodynamics will then be explored. While this is going on, the most crucial factor in platooning - the spacing between vehicles - will be investigated in each of the scenarios.

The rest of this thesis is organised as follows. In Chapter 2, the relevant literature concerning vehicle platoon in the open air and in the road tunnel is discussed and the related research methodology including experiment and numerical simulation. The TRAIN rig facility, experiment setup and the preliminary data processing are described in Chapter 3. The numerical simulation setup, which includes the introduction of the Improved Delayed Detached Eddy Simulation (IDDES), the mesh generation, the calculation setting, and the validation of the numerical results, will be discussed in Chapter 4. The results analysis is from Chapter 5 to Chapter 8. In Chapter 5, the aerodynamics performance of a single vehicle in four different cases will be explored as a baseline to better understand the aerodynamics of the platoon in general. In Chapter 6, the effect of the tunnel will be thoroughly discussed. Four characteristics, including slipstream properties, flow structures, surface pressure, and drag coefficients, will be analysed and compared between an open air environment and a road tunnel environment. In Chapter 7, the effect of the blockage ratio of the road tunnel and the traffic lane position on the aerodynamic performance (including the slipstream properties, flow structure, drag and side force coefficients) of the platoon will be analysed. In Chapter 8, the effect of inter-vehicle spacing on the platoon in each of the four scenarios will be thoroughly addressed. The flow field, flow structure, surface pressure and aerodynamics forces will be discussed. The main findings of this work will be summarized in Chapter 9 along with several difficulties that need to be addressed in future research on vehicle platooning in a road tunnel.

Chapter Two

Literature review

2.1 Projects of platooning

Due to the promising future of the platoon, several programs have studied various aspects of vehicle platooning during the last few decades. These programs developed platooning characteristics, platoon objects, and platoon actions in accordance with their own concepts. The following part summarizes these platooning projects, together with their associated platooning attributes, operations, and project objectives.

- **PATH** - A truck platooning project based in the United States, sought to increase road capacity, safety, and fuel consumption through platooning. The platooning vehicles in this project are entirely automated in terms of lateral and longitudinal control. The platoon properties included the vehicles number in the platoon, platoon length, inter-vehicle spacing, platooning vehicle types, vehicle acceleration or deceleration, and highway driving speed (Carbaugh, Godbole, and Sengupta 1998; Rajamani et al. 2000; Michael et al. 1998). This project evaluated operations such as *lane keeping*, *changing*, *join*, and *split*.

- **SARTRE** - A European platooning project Safe Road Trains for the Environment (SARTRE), aimed at the energy saving, congestion control, enhancement of the safety, and the driver convenience and comfort. SARTRE allowed for vehicle type diversity

and attempted to achieve platooning without requiring any changes to the road infrastructure. The platooning vehicles in this project are also automated in terms of lateral and longitudinal control. Different platoon operations, such as *creating platoon*, *adding platoon*,*maintaining platoon*, *leaving platoon*, and *dismissing platoon*, are specified as platoon case studies (Bergenhem et al. 2010; Robinson, Chan, and Coelingh 2010).

- **SCANIA** - Two platooning project launched by the Swedish truck maker SCANIA: Distributed Control of a Heavy-Duty Vehicle Platoon, and iQFleet (Bergenhem et al. 2012) with the primary objective of fuel-saving. In contrast to other projects, the controlling mechanism is dispersed, which means that each vehicle is responsible for self-control according to data from on-board sensor system (e.g., cameras, radar) and signal exchanged via V2V communication. iQFleet focused on the platoon control with respect to road topology and infrastructure.

- **Other** - The Japanese platooning project Energy Intelligent Transport Systems (ITS) also aimed at energy saving and driver support (Tsugawa, Kato, and Aoki 2011). CHAUFFEUR, a European platooning project, analysed potential failure situations and the coupling protocol (Fritz et al. 2004). KONVOI, a German platooning initiative, intended to enhance traffic flow and also analysed fuel savings associated with inter-platoon gaps (Wille, Röwenstrunk, and Debus. 2008).

Meanwhile, more road tunnels has been built in recent years to improve the urban traffic conditions (Chung and Chung 2007). When vehicles travel in a road tunnel, the tunnel's wall will not only restrict the airflow motion, but will also modify the flow dynamics around the vehicles. One of the most important effects is the 'piston effect'. Specifically, in contrast to the case of vehicles travelling in the open space, where the air displaced by the vehicles can freely move away to most directions, the airflow around vehicles in a tunnel is largely forced to flow parallelly to the vehicles' movement direction. As a result, a high-pressure region is formed in the front of the vehicle and a low-pressure region behind it, where the wake structures act as an air-sucker. These changes in the flow field lead to significant variations in the aerodynamic forces. Therefore, investigating the aerodynamics of vehicles travelling through road tunnels is critical for optimising the platooning strategy.

2.2 Aerodynamics of vehicle platoon in open air

A literature review related to the vehicle platoon in open air will be discussed in this section. First, an overview of the single vehicle will be presented, followed by an explanation of the platoon concept in general. The literature on ground vehicle platoon will be presented in detail in relation to several key platoon aspects, including inter-vehicle spacing, drag penalty, vehicle numbers, and others. Finally, the research on the aerodynamic characteristics of freight trains which are analogous to vehicle platoon, will be presented.

2.2.1 Heavy single vehicle

The transportation of goods is essential to the economy, and the number of goods transported is closely linked to economic growth (*ITF Transport Outlook* 2019). Over the past few decades, road freight transport has become the dominant mode of surface freight transportation. In China, compared to other types of transportation, such as inland waterways or rail, lorries account for around half of all surface freight. The Heavy-Goods Vehicles (HGVs) are capable of reaching practically any location where goods need be moved to or from. Due to the aerodynamic inefficiency of the majority of heavy goods vehicles, a large quantity of fuel is spent to help address the aerodynamic drag imposing on the high-speed vehicles. At 100 kilometres per hour on the highway, aerodynamic drag accounts for approximately 62% of the energy necessary to drive a typical heavy lorry (McCallen et al. 1999). In long-haul journeys, buses and HGVs face an aerodynamic drag of up to 65 percent (Altaf, Omar, and Asrar 2014). The aerodynamic drag of a 36-ton freight vehicle travelling at 105 km/h contributes roughly 21% of the energy loss (Bradley et al. 2000). A 40% reduction in drag force on a large truck might save US$ $10,000$ in fuel consumption per year, according to Hsu and Davis (2010). Bradley et al. (2000) also predicted that 20% reduction in drag force on a large truck may result in a 4% reduction in fuel consumption when operating at high speeds.

The airflow around a vehicle can be characterized by temporal and spatial variations in velocities and pressures. The flow structure of various vehicles has been widely researched, both theoretically and experimentally, using simplified models and actual vehicles. The

Ahmed body, conceived and utilized by Ahmed, Ramm, and Faltin (1984b), is amongst the most extensively used simplified vehicle models to study the ground vehicles' aerodynamics and flow structures. The flow structure is basically constituted of a recirculating vortex on the slant surface and a wake zone behind the vertical base. Additionally, a pair of counter rotating vortices originated from the slant face's side edge. However, the data acquired of the Ahmed body could not be used to represent the general flow structure of the lorry since most lorries have square-back instead of the fast-back designs. For square-back vehicles, the General Motor (GM) model was a popular choice for a simplified model, which the location of flow separation is anchored at the rear edge. Due to the flow separation, massive recirculating vortices forms downstream of the vehicle body. Additionally, downstream of the base of this model, two counter-rotating, spanwise vortices are generated. The existence of these vortices considerably decreases the base pressure and thus increasing the drag (Altaf, Omar, and Asrar 2014; Patel et al. 2019). However, the GM model still unable to study the flow features of tractor-trailers or articulated lorries. To explore the flow characteristics of articulated lorries, the Ground Transport System (GTS) (Roy, Payne, and McWherter-Payne 2006) and the Generic Conventional Model (GCM) (Hyams et al. 2011) were proposed and employed. The GTS model is based on the CAB-OVER-ENGINE (COE) configuration of articulated lorries that are popular throughout Europe. While in the United States and Australia, the GCM model exemplifies the standard tractor-trailer arrangement.

Understanding the aerodynamics of lorry is critical not only because it is highly related to pollutant emission and fuel consumption, but also because wind-related accidents can lead to the death or destruction of people and property. Studies based on the GCM and GTS models showed that there are several principal origins of drag: the stagnation region in the front, underbody flow region, the wake and the gap region. Figure 2.1 depicts the primary drag domains of a tractor-trailer lorry are the tractor frontal face, tractor-trailer gap, wheels and undercarriage, and the wake Drollinger (1987).

Indeed, significant drag reductions have been realized during the last few decades. Improved add-on devices and front-end shape design, especially the frontal shape, greatly reduced the drag of the lorry (Burton et al. 2013; Leuschen and Cooper 2006). Mariotti and Buresti (2013) demonstrated that lowering separation and optimizing aerodynamic contact between the cabin and trailer resulted in significant drag reduction. Landman et al. (2009)

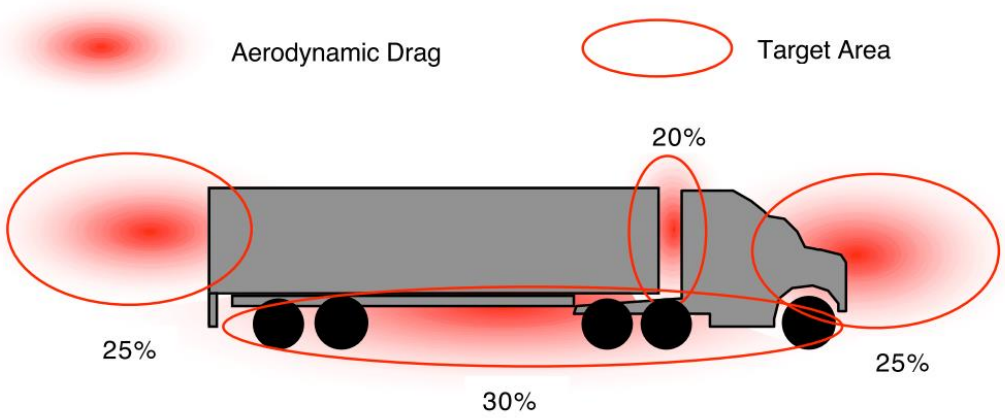

Figure 2.1: The distribution of the aerodynamic drag on a tractor-trailer truck (Drollinger 1987).

discovered that side skirts and wheel coverings on the back of the vehicle were effective at reducing stagnation and preserving attached flow on underbody. Many other studies have shown that aerodynamic drag can also be reduced with the add-on devices like boat-tails, side-extenders, and side skirts (Burton et al. 2013; Cooper 2012; Leuschen and Cooper 2006).

The most often used technique for investigating the aerodynamics of a single vehicle are full-scale measurements and scale-down experiments in wind tunnel (Coleman and Baker 1990, 1994; Baker 1991a, 1991b; Quinn et al. 2007; Cheli et al. 2011; Patel et al. 2019; Cheli et al. 2006). Cheli et al. (2011), Cheli et al. (2006), and Quinn et al. (2007) focused on the aerodynamic moments and forces while Patel et al. (2019) concentrated on the flow structures around this lorry. Typically, wind-induced instability is a challenge for a high-sided vehicle. Cheli et al. (2006) studied this lorry model in a wind tunnel and combined the experimental and numerical method for determining the wind loading in real wind conditions. At the same time, Quinn et al. (2007) performed the full scale experiments using this lorry. The rolling moments and the pressure were monitored in several places on the lorry container box.

Understanding the aerodynamics of a single lorry is essential for determining the advantages of the platoon formation. Although a great deal of prior research has examined various aspects of the heavy single vehicle, it is still necessary to investigate the single lorry

used under related conditions in the present work to determine the advantage of platooning.

2.2.2 General platoon concepts

The earliest investigation of bluff body dates back to early twentieth-century research on the struts and wires of biplane wings. Pannell, E. A. Griffiths, and Coales. (1915) studied circular cylinders along the stream, referred to as 'tandem', and reported the overall drag of a pair of cylinders in tandem was smaller than twice that of a single one. In case of two bodies placed one behind another, the drag of the second one is usually smaller than in free flow, because of reduced dynamic pressure within the wake of the first body. This phenomena is termed as "shielding effect". Biermann, D. and Herrnstein, William H. (1933) investigated the effect of separating spacing on drag values of a pair of cylinders in tandem. The critical separation distance was $3 - 3.5$ diameter length at which the measured drag becomes discontinuous. This discontinuity is caused by a change in flow field occurring between three to four diameters separation, according to the further visualisation study (Ishigai et al. 1972). Under this separation range, the flow separates off the leading cylinder re-attaches to the downstream one, while beyond 3.5-diameters length, a secondary stagnation point generates on the trailing body. As a result, both the leading and trailing bodies experience an increase in drag, which is confirmed by later study by using surface pressure measurements (Zdravkovich and Pridden 1977).

Researchers attempted to characterize the flow structures and evaluate the drag using basic geometries, such as cylindrical tubes (Ljungkrona and Sundén 1993), thin circular disk (Morel and Bohil 1980), a rectangular plate placed behind an oval plate (Bull et al. 1996) and a flat disc followed by a cylinder (Koenig and Roshko 1985). They found that the optimal spacing for the maximum drag reduction allowed for developing a stable quasi-steady vortex in the gap region and the separated shear layers from the leading body to re-attach onto the downstream body. However, it should be noticed that no ground plane induced asymmetric flow was presented.

The investigation of related phenomena on automobile began in motor-sports - "slip-streaming" - with an original research by Romberg, Chianese, and Lajoie (1971). Vehicles

were controlled by an automated highway system in order to minimize the amount of space between them, allowing for an increase in traffic capacity on current main roadways. The findings of contemporaneous studies have brought a renewed focus in tandem vehicle configurations. Most of related studies focus primarily on force measurements instead of the underlying flow phenomena. In general, significant reductions in overall platoon drag are achieved when the spacing is smaller than the length of a vehicle (Browand, Mcarthur, and Radovich 2004; Tsuei and Savaş 2001; Zabat, Frascaroli, and Browand 1994; Zabat et al. 1995; Abdel Azim and Abdel Gawad 2000). Ioannou (2013) even recommends grouping cars with the same destination into platoons to maximize stability. These studies confirmed that the distance between the lead and trailing bodies has a significant impact on drag.

2.2.3 Ground vehicle platoons

2.2.3.1 The effect of the inter-vehicle spacing

Inter-vehicle spacing is one of the most significant factors affecting the benefit of ground vehicle platoons. Extensive studies looked into the effect of the inter-vehicle spacing on the aerodynamic force of the platoon. A wide range of geometries have been explored in these works, from heavy truck and simplified vehicle model to replicas in great detail. Furthermore, the fact that these results varied for different vehicle models suggests that the vehicle's geometry produce a significant impact on the drag of platoon (Ioannou 2013; Hammache, Michaelian, and Browand 2002; Watkins and Vino 2008; Ebrahim and Dominy 2020). Ahmed body is an important example of a simplified vehicle. This model can replicates the main wake structures of vehicle (Ahmed, Ramm, and Faltin 1984a). Watkins and Vino (2008) observed that as the spacing between two Ahmed bodies rose, a stronger downwash flow was generated as streamlines from the leading vehicle failed to reattach on the trailing one. For the tandem Ahmed bodies, Rajamani (2006) and Pagliarella (2009) found that the axial C-pillar vortices would impinge on the frontal face of the downstream vehicle with very short inter-vehicle spacing. The stagnation point of the downstream body is close to the outer and top edges of the frontal, which is considerably higher than single model. Furthermore, the existence of the trailing body generates an increase in pressure upstream, which in turn

induces a rise in base pressure of the lead model. Because the total drag of bluff body, such as an Ahmed body or a lorry, is mostly contributed by the rear surface pressure, lowering this component has a considerable effect on the drag reduction. This explains why the leading vehicle had a lower drag than the trailing one with small spacing (Watkins and Vino 2008).

However, this behaviour is not universal in other vehicle platoon studies. Hammache, Michaelian, and Browand (2002) observed that the drag values of smooth and idealised vehicles, which removes the characteristic features and wheels, was significantly different from that of more realistic vehicles (those keeps more structural details). It was also discovered that the leading body of a smooth idealised truck had lower drag than the trailing truck, whereas the contrary was discovered for a "dirty" truck model. Romberg, Chianese, and Lajoie (1971) found that for a "dirty" model, the following vehicle exhibited 37% drag reduction at more than one vehicle length downstream but only a moderately higher reduction at narrower spacings. There were no discontinuities or inflections in the drag with varying spacing, as in the case of simple smooth geometry bodies. Ebrahim and Dominy (2020) characterised the changes associated with the pressure field and flow structures of a Nissan passenger three-vehicle platoon. Their findings revealed that some design features optimized for a single vehicle could negatively impact platoon performance. These results indicated that the separation from the lead model and subsequent re-attachment to the trailing model might be possible only for simple shape model. Models with varied drag results showed that the drag of three-dimensional bluff body is highly sensitive to the geometry.

Figure 2.2 depicts the potential performance of platoons (Zabat, Frascaroli, and Browand 1994; Zabat et al. 1995) including previous results from Romberg, Chianese, and Lajoie (1971). Generally, the aerodynamic advantages of platooning comprised of square-back van were best realised where the platoon length was maximized and the inter-vehicle spacing was minimised. Zabat et al. (1995) then investigated drag force at close ranges (half a vehicle length and lower), as shown in Figure 2.3. The drag was not linearly proportional to the vehicle spacing at smaller spacing. The drag reduction were dependent on the vehicle position and platoon size. The trailing vehicle experienced the most considerable drag reduction before the phenomena reverse as the spacing decreasing below 0.5L. They also found that the middle vehicle in a 3-vehicle platoon experienced the most considerable drag reduction at spacing less than 0.5L. The complex formation of the platoon at close spacings

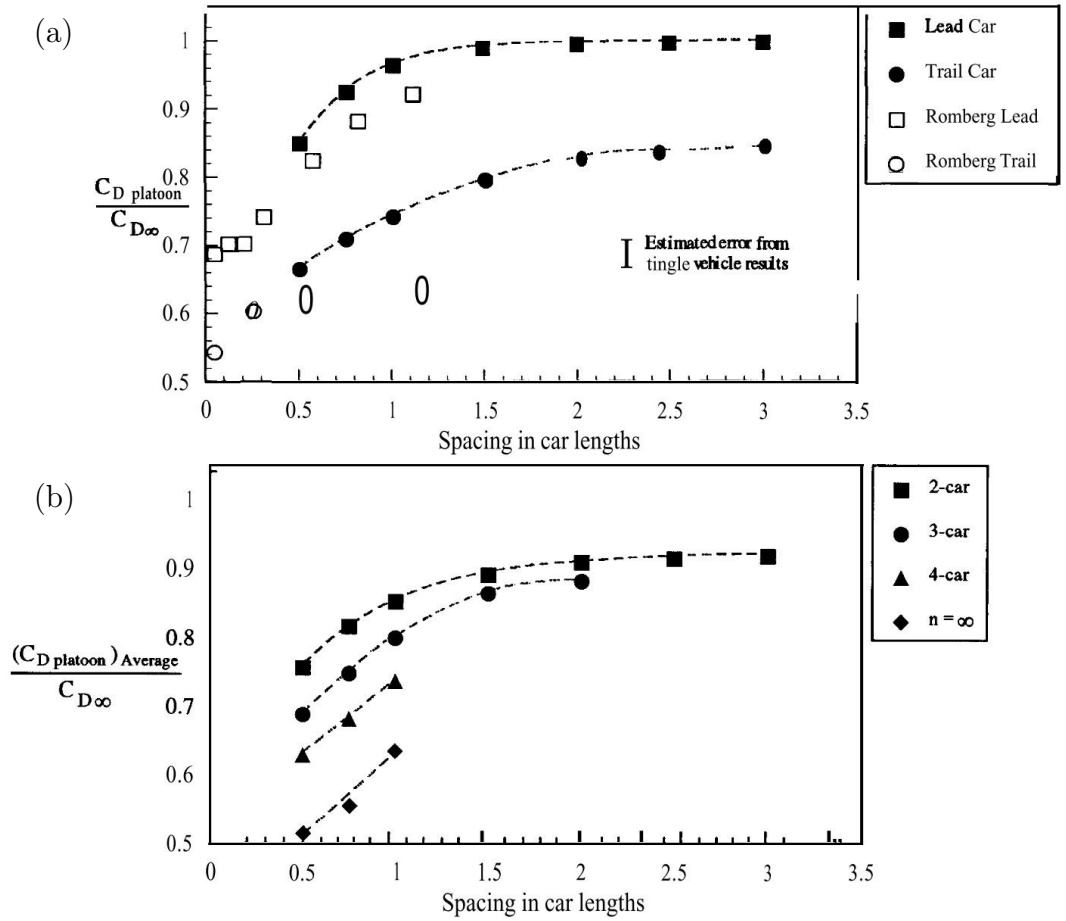

Figure 2.2: (a) Comparison of minivan model drag fraction (versus drag of isolated car) in two-vehicle platoon with stock car. (b) Overall drag reduction (versus drag of isolated car) for platoons of 2-4 and extrapolated infinite number of minivans (Romberg, Chianese, and Lajoie 1971).

altered the flow field, which lead to a more complicated drag behaviour. This behaviour is referred to as the “strong interaction regime”. These findings were also verified through later on-road measurements by Hong et al. (1998) and Browand, Mcarthur, and Radovich (2004). Mirzaei and Krajnović (2016) investigated the drag penalty phenomenon reported in Pagliarella, Watkins, and Tempia (2007) and Watkins and Vino (2008) on a two-vehicle platoon with different spacings (0.3, 0.5, and 1.0 vehicle length) using Large Eddy Simulation (LES) simulations. Their findings indicated a drag penalty for the two shorter spacings, which is consistent with the experimental results.

In automobile forms, the existence of a ground plane and blunt base geometries leads to a low static pressure above the base and a high static pressure beneath. As the result of the up-wash from the under-body, the flow separates at the intersection of the base, bottom and centreline. A square-back after-body allows the dominance of such a feature in the near wake. For a two-bus platoon, this vortex might be formed in a steady way in the gap region, allowing lead model after-body pressures to be raised, hence lowering drag. The increased gap enabled the vortex to grow and oscillate at even greater distances (Fletcher and Stewart 1986). Increased impingement on the frontal of downstream vehicle resulted in an increase in the trailing vehicle’s drag exceeding the isolation values, as shown in Figure 2.4 (visualised along the centreline). The penalty influence of the vortex’s impingement was partly alleviated by physically separating the downstream model fore-body from the vortex.

When it comes to the notch-back and fast-back automobile, the transferability of the above argument is complicated by differences. A delta-wing-like axial vortex pair is formed by the C-pillars of and results in distinctive behaviors for these two automobile. Abdel Azim and Abdel Gawad (2000) investigated two notch-back vehicle platoon at ultra close spacing and observed the flow field. They found that significantly decreased flow within the gap region would obtain a lowest overall drag. A slightly greater spacing allowed for the formation of dominant vortices from the C-pillars, which impinged on the trailing model’s fore-body. The fast-back vehicles are the most extreme case of "C-pillar" vortex generation. Wolf-Heinrich (1997) verified that in two-vehicle platoon, higher base pressure in the leading model would increased trailing model fore-body pressure for high, medium and low-drag configured fast-back models. The net effect was a reduction in net platoon drag, for each configuration studied, the trailing model drag force was increased at tight spacing. Similar

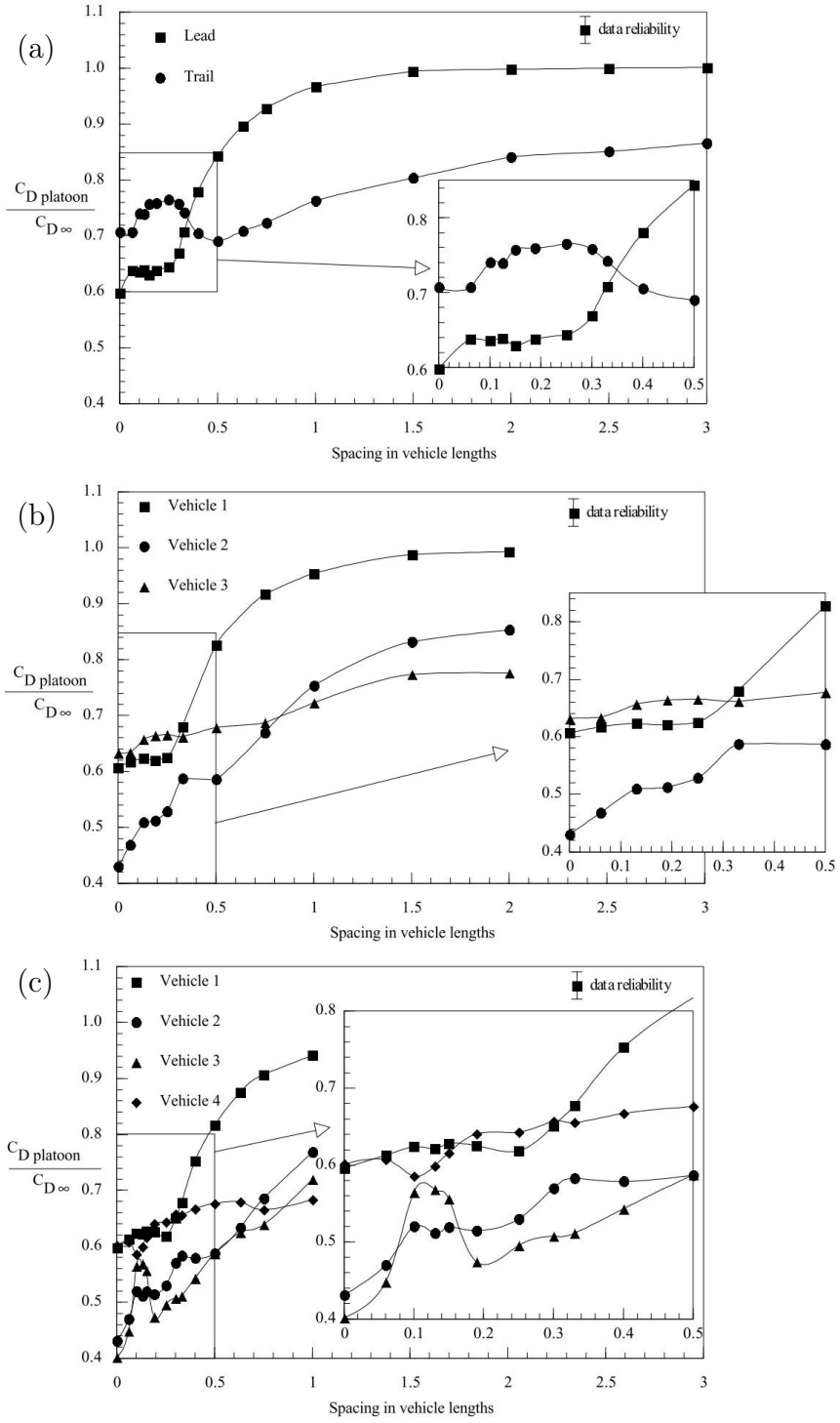

Figure 2.3: The measured drag for multi-vehicle platoon (Zabat et al. 1995).

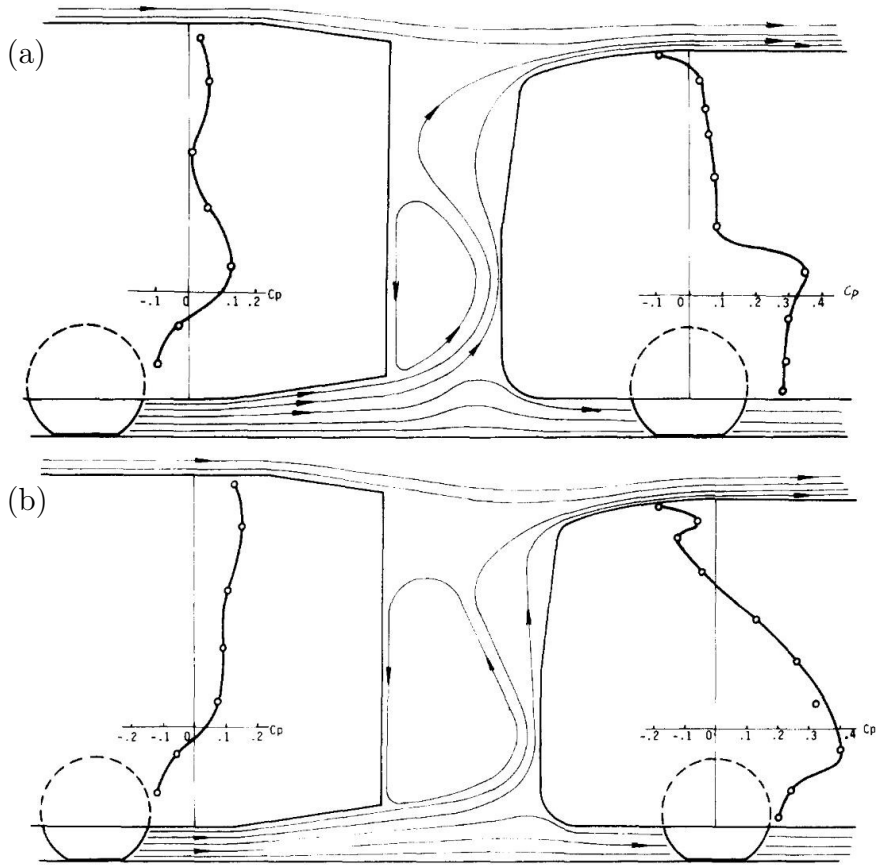

Figure 2.4: Centreline flow structure of the gap region in a two-vehicle platoon formation. The left one is the tail of the leading bus and the right one is the fore-body of the trailing bus. (a) Gap=0.314D, (b) Gap=0.472D (Fletcher and Stewart 1986).

phenomena was observed in Zabat et al. (1995) when the vehicles were placed in reverse orientation. Additionally, Carlino, Cardano, and Cogotti (2007) and Carlino and Cogotti (2006) noticed that when a range of practical vehicles were put in a typical downwash wake, the drag force increased. Watkins and Vino (2008) and Pagliarella (2009) also noted a drag penalty for the square back trailing vehicle in a platoon of two vehicle at small spacing. The leading one achieved the largest reduction of drag, while the vehicle in the downstream yielded penalty drag (larger than isolated vehicle).

Pagliarella (2009) later discussed platoon forces using surface pressure, wake structures and force measurements. The results revealed that the rear pressure of the leading model rose because of the suppression of the roll-up bottom vortices and C-pillar vortices. The drag of the trailing model increased primarily because of the increasing frontal pressure due to the impingement of the flow. The sensitivity of fore-body geometry of basic lorry on drag with modifications on small edge was reported by Gheyssens and Van Raemdonck (2016) . Le Good et al. (2018) and Le Good et al. (2021) also mentioned an combined drag penalty for three to five vehicles platoons at one fourth length spacing, with a simplified shape of different back slant angles. The optimum drag reduction combination for a three-vehicle platoon was 0°, 25° and 25° combinations.

Despite the fact that, in general, the shorter the inter-vehicle spacing, the greater the drag reduction of the platoon, the relationship is still highly sensitive to geometry of the vehicle (e.g. the front and back face, vehicle type). Therefore, the effect of inter-vehicle spacing should be thoroughly examined, particularly for spacings shorter than half the length of the vehicle.

2.2.3.2 The effect of vehicle number

With the development of the digital technique, the platooning technology will eventually allow platoon beyond two or three vehicles (Janssen et al. 2015). Current studies mostly concentrated on relatively short platoons. Extensively studies are focused on the two-vehicle platoon (Hammache, Michaelian, and Browand 2002; Browand, Mcarthur, and Radovich 2004; Abdel Azim and Abdel Gawad 2000; McAuliffe and Ahmadi-Baloutaki 2018; Lammert

et al. 2014; Altinisik, Yemenici, and Umur 2015; Vegendla et al. 2015; Watkins and Vino 2008; Humphreys and Bevly 2016; Mirzaei and Krajnović 2016; Pagliarella, Watkins, and Tempia 2007). The three-vehicle platoon, consisting of a lead, a trail, and one interior vehicle, is the shortest platoon to contain all the essential platoon elements. It was pointed out by Ebrahim and Dominy (2020) that the flow interaction stayed basically identical to a two-vehicle platoon when the number of vehicles is increased from 2 to 3. Bruneau, Khadra, and Mortazavi (2017) studied three-vehicle platoon based on a square back simplified vehicle and found that more drag reduction was achieved when the vehicle number increased from two to three. Gheyssens and Van Raemdonck (2016) investigated the influence of the front edge and of a truck model and inter-vehicle spacing on the aerodynamic behaviour of a three-vehicle platoon. As the increasing of spacing, the drag of the upstream vehicle asymptotically increased to the magnitude of a single vehicle, while downstream vehicle's drag decreases compared to the value of isolated vehicle. The middle vehicle's drag was affected by the lead and the last vehicles combined. Salari and Ortega (2018) found that increasing the platoon member from 2 to 3 would increase the overall drag benefit. They also found that the third vehicle would not alter the benefit of the leading one except at the smallest spacing.

Other researchers extend the platoon to four to six vehicles (Tsuei and Savaş 2001; Le Good et al. 2018; Le Good et al. 2021; Schito and Braghin 2012). Tsuei and Savaş (2001) investigated up to four-box platoons. Their findings indicated that the more platoon members, the greater the average drag reduction. Le Good et al. (2018) and Le Good et al. (2021) analyzed platoons include up to five vehicles and discovered that the vehicles sheltered in the center of the platoon benefited the most. Both the leading and last cars seemed to be unaffected to the car number. When the number of cars increased from three to four to five, the center car gained the highest drag reduction. Schito and Braghin (2012) investigated the 6-vehicle platoon based on the different type of vehicles. After the fourth vehicle, the drag coefficient of the second-to-last vehicle remained relatively constant. The entire drag of the platoon consist of square-back van decreased until reaching a number of 6 vehicle.

Robertson et al. (2019), Robertson, Soper, and Baker (2021), and He et al. (2019) investigated the eight lorries platoon according to the consideration of the understanding of the boundary layer formation of container freight trains (Soper, Baker, and Sterling 2014).

Robertson et al. (2019) found that the overall drag reduction for eight-lorry platoon could estimated by extrapolating method suggested by Zabat et al. (1995). Zabat et al. (1995) studied the effect of the vehicle number of a platoon by considering 2, 3, 4-vehicle platoon. They mentioned that the flow field details showed consistent trend when the vehicle number increased. The interior vehicle has the lowest drag, however due to flow-induced resonance, there were some unusual small plateau regions around 0.1 to 0.2 vehicle length. According to their results, a linear relationship existed between the reciprocal of the number of vehicle and the drag reduction ratio. The relationship could be used to predict the overall drag of any number vehicle platoon by extrapolating the existing data.

By increasing the number of vehicles in the platoon, a greater reduction in drag can be achieved. The chosen number of vehicles must take into account the platoon's essential elements as well as the experimental and numerical resources required.

2.2.3.3 Other factors

Other studies considered a more realistic scenario, namely that longitudinal stability which is difficult to maintain when travelling. Tsuei and Savaş (2001) investigated the "in-line oscillations" of a 4-vehicle platoon and analysed the transient and steady force on each vehicle. Marcu and Browand (1999) considered the crosswind at 10° yaw on individual of a 3-vehicle platoon. According to the side force measured with the $1/8th$ scale models, the leading model showed almost no increase beyond model in isolation values, while the side force of the following models decreased exponentially with increasing spacing, possibly because the progressive realignment of the flow in the direction of the platoon. Misalignment is another frequently observed phenomenon that occurs when cars leave or join the platoon. Marcu (1998) discovered that the center vehicle's drag and side forces were the most affected by misalignment. When the middle vehicle was placed nearer to the leading one, it reduced drag throughout a wide range of misalignments, and vice versa when it was placed closer to the following vehicle. Although it is difficult to draw convincing conclusions, the altered wake shape results in greater drag and side force due to flow asymmetry and pressure decrease at the base. Chan (2012), Davila and Nombela (2012), and Davila, Aramburu, and Freixas (2013) outlined the three year SARTRE project funded by the European Commission. This

project considered a variety of vehicle types inside platoons, including passenger vehicles and commercial vehicles, to determine the feasibility of integrating control systems into traditional vehicle designs and application scenario, such as platooning. In addition, the overtaking and passing platoon formation scenario was also studied (Gilliéron and Noger 2004).

Another issue that is less well understood is the unsteady forces generated by running vehicles in close formation. Frequency analysis of base pressure measurements or wake velocity is frequently applied to analyze coherent structures and oscillating forces generating from a single vehicle (Grandemange, Gohlke, and Cadot 2013; Lahaye, Leroy, and Kourta 2014; Volpe, Devinant, and Kourta 2015; McArthur et al. 2018). In a stock car race, when one car drives in the wake of the front car, it has a significant impact on vehicle handling (Katz 2006). The trail vehicle in a two-vehicle platoon is discovered to be suffered from buffeting, which may have been caused by the vortices shed by the leading one (Humphreys and Bevly 2016). He et al. (2019) applied numerical simulation on the eight-lorry platoon and noticed that the trailing lorries suffered from considerable oscillating lateral forces that increased in intensity along the platoon. Robertson, Soper, and Baker (2021) used Fourier spectrum analysis and wavelet analysis to analyze the experimental results for an eight-vehicle platoon. Two types of unsteady flow were identified: the low frequency mode affected the whole platoon, while the high frequency only affected certain vehicles. However, the Delayed Detached Eddy Simulation (DDES) simulation from He et al. (2019) can only capture the low frequency mode because the high frequency mode requires much smaller time step. It is necessary to conduct a more in-depth spectral analysis of the platoon in the future.

2.2.4 Freight train

Visually, a platoon of lorries is comparable to a container freight train; both consist of a series of cuboids moving in a straight line in a uniform formation. However, it is somewhat ironic that road vehicles have diverted freight traffic away from the railways. The shape difference between a single vehicle and a single container has little effect on qualitative trends in side velocity and pressure, indicating that a great deal can be learned about the aerodynamics of platoons by analysing the aerodynamics of freight trains (Robertson et al. 2019). The

loading efficiency or inter-wagon spacing of a freight train is comparable to the inter-vehicle spacing of a vehicle platoon.

Soper, Baker, and Sterling (2014) characterised the flow around the freight train as a continually growing boundary layer punctuated with a series of velocity peaks relating to the front edge of each individual container where a large flow separation occurs. It was discovered that boundary layer velocities increased as container loading efficiencies decreased (Soper 2016) or inter-wagon spacing increased (Flynn et al. 2014). Golovanevskiy, Chmovzh, and Girka (2012) noted that for a purpose of investigating the aerodynamic phenomena of the inter-carriage inside a long freight train, eight railcars were sufficient and optimal in length. The drag coefficient of all containers except the 3 first and 3 last cars were almost the same. (Robertson et al. 2019; He et al. 2019) found that the patterns of the slipstream development of a long platoon showed great similarity to those of a freight train with 50% and 33% loading efficiencies, especially the latter consist in Soper, Baker, and Sterling (2014). Robertson et al. (2019) also mentioned that the airflows around freight train and vehicle platoon could raise concern of instabilities on other road users.

2.3 Aerodynamics of vehicle platoon in road tunnel

The number of road tunnels has increased dramatically to improve urban traffic conditions (Chung and Chung 2007; Dong et al. 2017). When vehicles travel in a tunnel, tunnel walls restrict the airflow motions and additional aerodynamic forces act on these vehicles. The tunnel walls can modify the flow field, including the separation of flow, wake structure as well as vortex shedding. The interaction between the tunnel walls and bluff vehicles also leads to considerable variations of the flow field, drag and lateral force. Therefore, investigating the aerodynamic phenomena associated with vehicles travelling in tunnels is essential for automatic control platoons.

2.3.1 Single Vehicle

To better comprehend the aerodynamic performance of a platoon, the flow information of a single vehicle travelling in a tunnel is crucial. Studies related to a single travelling inside a tunnel is relatively rare. Because the tunnel space is relatively sealed, a vehicle entering a tunnel will experience strong air flow and significant pressure variations (Ogawa and Fujii 1997; Khayrullina et al. 2015, 2015). Liu et al. (2017) studied pressure variations resulted from a single high velocity vehicle travelling through a tunnel. The relative movement between the vehicle and the tunnel led to a large increase in pressure inside the tunnel compared to the case in open air. Liu et al. (2018) developed an two-dimensional method to predict the piston effect induced by a single cube passing though a tunnel. The rising drag compared to the vehicle travelling in open air are also observed. Meng, Zhou, and Wang (2019) performed a moving model investigation on the slipstream and pressure field of a metro train travelling inside the road tunnel. Increased vehicle speed increased transient pressure and slipstream velocity, but had little influence on the slipstream's spatial distribution. Research into the flow structural differences between a single vehicle in the tunnel and the free air is lacking.

2.3.2 Ground vehicle platoon

2.3.2.1 The mean flow information in the tunnel

Early studies focused on how time-averaged flow quantities, such as the mean drag coefficient, vary with the vehicles' size, speed, and number (Chen, Lee, and Hsu 1998; Chen, Chung, and Wang 2002; Jang and Chen 2000, 2002; Sambolek 2004; Katolický and Jícha 2005; Barmpas, Ossanlis, and Moussiopoulos 2011; Wang et al. 2014; Wang et al. 2011; Tong et al. 2016; Lee, Park, and Kim 2018). Chen, Lee, and Hsu (1998) experimentally studied the effects of jet fans and moving vehicles on ventilation in a rotating-belt scale-down tunnel. They mentioned that piston effect was not confined to the nearby of the vehicles since the air velocity in the top area of the tunnel was about 40% of that near the vehicle. The traffic generated mostly axial flow within the tunnel. Chen, Chung, and Wang (2002) experimentally and numerically

studied the pollutant dispersion and airflow in a cross harbor tunnel. The pollutants were carried downstream by the traffic wind, resulting in an increase in pollutants concentrations with distance. The concentrations were found to be almost vertically stratified at the cross-sectional plane. Jang and Chen (2002, 2000) developed a one-dimensional model to predict wind speed and pressure field in a tunnel and compared it with their field measurements. The wind speed increased as the number of vehicles grew, but it was not linearly proportional. The one-dimensional theoretical model predicted the wind-induced air velocity, but it largely depends on the properness of the aerodynamic coefficients of their model. One of the crucial coefficients, the drag coefficient, was measured for an individual vehicle under uniform flow, while in real situations, the vehicle might move in the shedding vortices generated by the preceding vehicle. Jang and Chen (2002) later applied optimization method to improve their approach to predict the drag coefficients of vehicles in transient condition. The averaged drag coefficients decreased from around 0.35 to 0.22 when the traffic volume increased from below eight to 8-to-23 vehicles per lane per kilometre. Sambolek (2004) studied the parameters affecting the design of the ventilation system using a 1/25 scale tunnel and discovered that the air resistance coefficient was highly dependent on the Reynolds number. Katolický and Jícha (2005) reported that the airflow rate was strongly influenced by the vehicle velocity, tunnel length and traffic volume. However, at a certain high traffic rate, the airflow rate generated by the growing traffic volume finally approached the limit. With the increase of the length of tunnel, the traffic flow arrived a maximum value that results from the balance between drag and inertial forces.

Above all, these research focused on the averaged aerodynamics behaviour of the traffic instead of the moving vehicles itself. The vehicles were simulated as "still " objects with momentum sources (Tong et al. 2016; Yang et al. 2000) or Turbulent Kinetic Energy (TKE) source (Brohus, Balling, and Jeppesen 2006). Lee, Park, and Kim (2018) used a factorial design method to study the influence of inter-vehicle spacing, Blockage Ratio (BR) (ratio of the vehicle frontal area to cross sectional area of the tunnel) and Reynold number on the drag of platoons in a two-deck road tunnel. The blockage ratio was shown to be the most important factor, while the Reynolds number was the least important factor. The Reynolds number and inter-vehicle spacing showed a negative correlation, indicating high traffic case with fast travelling vehicle can reduce the overall mean drag. These indirect method are computationally faster. However, the reliability of the CFD modelling techniques

in predicting flow in enclosed environments is still inconclusive. Unless validated by high-quality experimental data, the reliability of the approximations made in the CFD models would remain questionable.

2.3.2.2 The moving vehicle simulation

With the development of experimental technology and computational power, more research started to focus on the transient aerodynamic flow generated by moving vehicles in the tunnel (Barmpas, Ossanlis, and Moussiopoulos 2011; Wang et al. 2014; Wang et al. 2011; Dong et al. 2017; Bhautmage and Gokhale 2016; Song and Zhao 2019; Zhao et al. 2020; Sike, Yanfeng, and Guangli 2015). Barmpas, Ossanlis, and Moussiopoulos (2011) investigated the aerodynamic effects of the flow around moving vehicles on the dispersion in the wake area behind the cars. The average pollutant concentration for two moving vehicles was higher by approximately 17% than one moving vehicles. They also mentioned that the flow separation at the wall of the vehicles and the resulting aerodynamic forcing can lead to a increase in pollutant concentrations due to the formation of intense entrapment phenomena. Ashrafi et al. (2012) treated the travelling cars as porous jump sliding wall and obtained the distribution of TKE in a road tunnel, which achieved good consistency between modelling and measurement data. Wang et al. (2014) combined the one dimensional model and CFD to analyse the aerodynamics of two-vehicle travelling inside a curved tunnel. For a moving isolated vehicle in a curved tunnel, the drag increased as the radius of curvature decreased, while the drag coefficient of a two-car platoon were lower than the drag coefficients of a single vehicle (Wang et al. 2011). The effective drag coefficients was shown to grow greatly the inter-vehicle spacing and marginally increased as travelling speed goes down. Dong et al. (2017) applied dynamic mesh method to analyse the effect of the platoon velocity on carbon dioxide concentration. The vehicle platoon with running through the tunnel once were treated as a baseline cycle. The result of flow domain were interpolated as the initial condition for next run to achieve continuous running. The piston effect could discharge pollutants adequately at 40 km/h, but at 10 km/h, substantial CO_2 concentrations were observed at the tunnel downstream and exit portal.

Bhautmage and Gokhale (2016) investigated the effect of shape of vehicle on the

pollutant dispersion in a high way tunnel with moving traffic. In the wake area, the TKE for SUVs decreased more rapidly than for buses. The SUV generated a larger near wake, while the bus generated a larger far wake. Compared to single-vehicle traffic, mixed traffic generated a higher near-wake. Sike, Yanfeng, and Guangli (2015) analysed the effect of traffic conditions on the flow field in a 1/10 scale tunnel. The air velocity distribution was influenced more by vehicle speed than by inter-vehicle distance. A linear rise in air velocity was seen as vehicle speed increased in the tunnel. The air velocity near the vehicles was more than 40% of the vehicle speed. In the stable phase, the air velocity in the tunnel had a logarithmic relationship with its heights. Song and Zhao (2019) investigated the effect induced by vehicle platoons travelling through road tunnel on the dispersion of pollutant. Although the spacing was quite large (10 time vehicle length), the drag coefficients were decreased with the increase of the platoon speed. However, their simulations were merely validated by comparing the experimental and numerical results of one vehicle passing across the tunnel. Zhao et al. (2020) analysed the unsteady turbulence, dispersion characteristics and deposition of ultra-fine particles in the process of a four-vehicle platoon passing through a road tunnel. The piston effect-induced wind speed was not stable in the tunnel and insensitive to the platoon speed. The particle concentration reached its maximum when the vehicles arrived the middle of tunnel.

2.3.2.3 The effect of the traffic lane

The platoon's side force in the tunnel is currently unexplored. Miau and Liu (1990) found that axisymmetric bluff bodies could be used to create unsteady flow near the wall. Miau and Hsu (1992) further explored various circular disks in a confined channel within the range of limiting blockage ratio of 35.4%. The vortex shedding frequency increased with the increase blockage ratio. However, beyond the limiting blockage ratio the vortex shedding phenomenon was completely suppressed. Yu et al. (2011) studied 2D flow past a rectangular bluff body and also reported that the Strouhal number St increased with smaller gap, mainly due to the enhanced vortex shedding from the bluff body by the interaction with the boundary layers on the sidewall. The side force of multi-body inside a tunnel is unclear.

In this work, the side force induced by the unsymmetrical flow field is mainly con-

cerned. In reality, more tunnels are multi-lane, with vehicles travelling in a single lane, naturally creating an asymmetric flow field. The side force in this scenario will be studied. Chen, Lee, and Hsu (1998) found that the moving vehicle on either lane in the tunnel produced similar velocity distributions of the air. Similar investigations were carried out in the street canyon (a less confined space than a road tunnel). In the wind tunnel experiment reported by Kastner-Klein, Fedorovich, and Rotach (2001), the vehicle induced wind velocity and turbulence fluctuation would be closer to the corner, as traffic lanes were close to the buildings. The concentration distribution throughout the canyon has exhibited significant lateral skewness as a result of the organised motion caused by one-way traffic moving in one direction.

2.3.2.4 Blockage ratio

Apart from the inter-vehicle spacing, the blockage ratio of the tunnel is another critical factor that affect the aerodynamics of a platoon travelling through a road tunnel. The blockage ratio of road tunnel depends upon the number of traffic lanes. Therefore, the effect of the blockage ratio will be investigated in the work. However, there is a scarcity of relevant research, with most studies focusing on blockage correction in a wind tunnel. In the wind tunnel, the restriction of the flow around the bluff body, along with the flow's interaction with the tunnel wall, alters the flow field. Therefore, wall interference corrections (blockage corrections) need to be applied to the experimental results. However, from a physical phenomenal point of view, wall interference in a wind tunnel differs from blockage ratio in a tunnel with a moving vehicle. The blockage correction method in wind tunnel experiments can not be applied in current work.

2.3.3 Train in confined space

Since the slipstream development of a long platoon resembles that of a freight train with different loading configurations, a great deal can also been learn about the aerodynamics by studying the aerodynamics of trains in tunnel, particularly freight trains. When a train enters a tunnel, additional drag components are present due to the formation of a repeated

pattern of reflective pressure waves (Novak 2006). The drag in the tunnel is composed of skin friction and pressure drag. Skin friction drag increases with increasing blockage ratio (Vardy 1996). (Iliadis et al. 2019; Iliadis et al. 2020) investigated the effect of loading efficiency of a freight train passing through a road tunnel. They found that the 33% loaded train showed a second pressure peak at the tunnel wall before the arrival of the nose to the monitor point, which is different from the fully loaded case. They suggested that the analytical models for fully loaded train were not valid for partially loaded trains. However, the detailed analysis of the flow structure in the gap region between containers and the drag of each container were missed.

The majority of tunnel studies involving trains are fully enclosed. In real world, the flow of the train can be constraints by by various structures (e.g. hoardings, station walls, partially-enclosed tunnels). The road vehicle tunnels are closer to partially-enclosed tunnels, which is of greater concern to the present study. A positive pressure peak followed by a negative one was identified for slipstream measurements in all kinds of 'flow constraints' cases (Baker 2014). Gilbert, Baker, and Quinn (2013b) and Gilbert, Baker, and Quinn (2013a) studied the aerodynamics transition from open air to double vertical wall, partially enclosed spaces and fully sealed tunnels based on a single train. It was discovered that the side wall and tunnels increase the peak pressure magnitudes relative to the open air. All the confined cases, gusts occur over a longer duration than in the open air. In addition, they mentioned that the gaps in the un-sealed tunnel may cause the pressure waves to dissipate quickly.

2.4 Research method for platoon

2.4.1 Experimental method

The experimental methodology related to vehicle platoon can roughly categorised to three type: full-scale on-track experiment (Hong et al. 1998; Browand, Mcarthur, and Radovich 2004; Lammert et al. 2014; Tsugawa, Kato, and Aoki 2011; Humphreys and Bevly 2016; Roberts, Mihelic, and Roeth 2016; McAuliffe and Ahmadi-Baloutaki 2018; Robinson, Chan,

and Coelingh 2010; Bergenhem et al. 2010; Davila, Aramburu, and Freixas 2013; Browand, Mcarthur, and Radovich 2004; Alam, Gattami, and Johansson 2010; McAuliffe and Chuang 2016), wind tunnel experiment (Hammache, Michaelian, and Browand 2002; Watkins and Vino 2008; Rajamani 2006; Pagliarella 2009; Watkins and Vino 2008; Hammache, Michaelian, and Browand 2002; Le Good et al. 2018; Pagliarella, Watkins, and Tempia 2007; Altinisik, Yemenici, and Umur 2015; Salari and Ortega 2018; Törnell, Sebben, and Elofsson 2021), moving model-scale experiment (Robertson et al. 2019; Zhang et al. 2021).

The full scale on-track experiments can possess the complexity of the real vehicles operating on a roadway at much higher Reynolds numbers. The track tests can also evaluate the real fuel consumption and pollutant emission in real world and under what conditions platoon will perform best. (Hong et al. 1998) reported that full-scale track tests predicted 10 percent lower drag coefficients for two-vehicle platoons at nearly all spacings. (Roberts, Mihelic, and Roeth 2016) summarizes the platoon on-track experiments. A 7.0% fuel efficiency improvement can be achieved on average between the two trucks versus a truck operating in isolation. However, due to the stringent testing conditions required, it would have been impossible to conduct any track testing with a platoon of five vehicles (Davila, Aramburu, and Freixas 2013). The uncontrollable variations in environment conditions would compromise the accuracy of the measurements. In addition The cost to conduct on track test is also significantly higher than wind tunnel experiments and CFD simulations (McAuliffe and Ahmadi-Baloutaki 2018).

Wind tunnel experiments are commonly used for evaluating the aerodynamics performance for vehicle platoons (McAuliffe and Ahmadi-Baloutaki 2018). It is a reliable fine-tuning design tool of experimental aerodynamics, with the experimental error usually kept below 5% (Golovanevskiy, Chmovzh, and Girka 2012). However, the wind tunnel experiment is not a direct representation of the real world, The disparities between model- and full-scale include: the model's absence of underbody and trim detail, the absence of rolling wheels, and the presence of an undesirable wind tunnel ground plane boundary layer. A turbulent boundary layer would be generated when the air streaming above the ground plane. Correctly simulating the relative motion between the ground and vehicles was frequently highlighted as a tough job (Zabat et al. 1995; Tsuei and Savaş 2001; Wolf-Heinrich 1997). The suction slot (Chen, Savas, and Hedrick 1997) and porous ground plane (Zabat et al. 1995) both failed

to show a substantial difference in results before and after their methods were applied. Furthermore, the relative motion between the tunnel wall and vehicle platoon in present work cannot be modelled by wind tunnel experiments. Another drawback for applying wind tunnel method to vehicle platoon is the ability to install two or more vehicle model in the wind tunnel at the desired separation distances due to the length of the test section (McAuliffe and Chuang 2016). The wind tunnel experiments in previous research are usually carried out at Reynolds numbers around one order of magnitude smaller than those in real-world conditions.

The majority of wind tunnel tests were conducted with relatively small platoons, and the tests employed static models in the wind tunnel with unrealistic ground simulations. Robertson et al. (2019) first conducted moving model experiments with a eight-lorry platoon on a moving model rig, with a correct ground simulation. They observed that the maximum velocities occurred at low altitudes due to the confinement the ground plane. The experiments were conducted at the University of Birmingham TRAIN rig facility, which is ideal for examining the transient aerodynamics of moving vehicles as it correctly models the relative movement between vehicles and ground/tunnel (Gilbert, Baker, and Quinn 2013a; Gilbert, Baker, and Quinn 2013b; Iliadis et al. 2019; Soper et al. 2017; Soper, Baker, and Sterling 2014). This moving model rigs originally developed specially to address the advent of high-speed railway.They are primarily used to investigate the environmental effect of slipstreams and wakes of high-speed trains on people (e.g. track-side workers and passengers on platforms etc.) and infrastructure (e.g. tunnels, train stations and road signs) (Baker 2001; Sterling et al. 2008). Gilbert, Baker, and Quinn (2013a) and Gilbert, Baker, and Quinn (2013b) investigated the aerodynamics transition of a train from open air to confined spacing (double vertical walls, partially-enclosed tunnel and fully-enclosed tunnel). The partially-loaded freight train (resembling the vehicle platoon) passing through a road tunnel was investigated by Iliadis et al. (2019). This facility has been used and performs well in for numerous aerodynamic tests including tunnel flows. slipstream flow development, crosswind effect and platooning vehicles (Iliadis 2019).

2.4.2 Simulation method

With the rapidly growing ability of computational methods to reliably and affordably simulate complex flows, CFD has become a powerful tool to reveal detailed flow dynamics around moving vehicles. Of the many different simulation approaches available, the Reynolds-Averaged Navier-Stokes (RANS) equations with the $k - \epsilon$ model is the most widely used in the academic literature, considering the computational cost, robustness and reliability (Munoz-Paniagua, García, and Lehugeur 2017). Li et al. (2009) used dynamic mesh techniques to numerically simulate the aerodynamics of one van running into a tunnel. They found that the drag coefficient increased sharply near the tunnel entrance, about 13% more than that in the open air. They later adopted the renormalisation group method (Yakhot and Orszag 1986) to study the process of two vans running in a tunnel (Li et al. 2010b). It was found that the aerodynamic characteristics around the first van were similar to that of a single van, and the aerodynamic forces on the downstream van did not have an obvious change. By performing a numerical study combining a one-dimensional mathematical model and a RANS simulation, Wang et al. (2014) performed RANS simulation of a two-vehicle platoon moving in a curved tunnel. Song and Zhao (2019) also conducted RANS simulations to investigate the flow patterns induced by a fleet of vehicles inside a road tunnel. Their results showed that the drag coefficient fluctuated dramatically during the vehicle passing period, which could be attributed to the unstable traffic wind during the transient movement process.

However, many authors reported that while the predicted drag coefficients in vehicle aerodynamics were acceptable, the pressure distributions were often inaccurate. For example, Humphreys and Bevly (2016) pointed out that RANS modelling was only valid in predicting drag reduction for short platoons (with less than four vehicles), and its description of the flow field was far from satisfactory and sometimes non-physical. In addition, the one-dimensional model could result in either underestimating or overestimating the drag forces, depending on the traffic conditions, e.g., the speed and number of the vehicles (Eftekharian, Abouali, and Ahmadi 2015). In this context, DES is a more suitable numerical approach (Spalart et al. 1997). Indeed, some researchers have used DES to study platoon aerodynamics and obtained good agreement with experiments at a low computational cost compared to Large Eddy Simulation (LES) (He et al. 2019; Humphreys and Bevly 2016). Nevertheless, previous

simulation works pertaining to the phenomena of vehicle platoons in a tunnel have mostly been based on RANS in the academic literature, despite its deficiencies. In this study, the aerodynamic performance of the long platoon in various cases were investigated by IDDES based on Shear Stress Transport (SST) $k-\omega$ turbulence model. Meng, Zhou, and Wang (2019) and Meng et al. (2021) investigated the slipstreams induced by train passing through a tunnel using IDDES. The results of the simulation were in excellent accordance with those of the experiments and the pressure amplitude difference was within 5%. The IDDES model outperforms DES and DDES when simulates mixed flow with both separated and attached flow (Gritskevich et al. 2012).

2.5 Conclusions for literature review

Previous work about the platoon in the open air are extensively studied. From a two-vehicle platoon to an eight-vehicle platoon, from an Ahmed body to a track-trailer lorry, the platoon's benefits have been widely recognized. The influence of inter-vehicle spacing on the aerodynamics of various geometry configurations is complex, particularly at close separation. Within a specific range of inter-vehicle spacing, certain types of vehicles were identified to have a drag penalty, whilst other vehicles exhibited a different trends. Following a thorough investigation of the flow structure, it was discovered that the up-wash vortex formed by the leading vehicle increased impingement on the trailing vehicle's front face, which had a negative influence on the trailing vehicle's aerodynamic drag. Some design features optimized for a single vehicles can negatively impact platoon performance. Furthermore, these studies were mostly limited to relatively short platoons. Few studies touch the long platoon cases. By studying the longer platoon (eight-vehicle platoon) than considered previously, it is possible to determine if the potential benefits of the drag reduction will extend to the end of the platoon of a length suitable for the realistic freight transport.

Moreover, the traffic wind induced by vehicle platoons running in the tunnel has been rarely studied. The effect of the inter-vehicle on the aerodynamic performance of the platoon inside the tunnel is barely investigated. The previous studies of platoon travelling in a road tunnel focused on turbulence induced by moving vehicles under the stable or quasi-static

assumptions. The real flow structure are, however, quite different from the assumptions. Previous studies are more focused on the traffic speed and traffic volume instead of focusing on the inter-vehicle spacing, which lacks detailed research. Other significant factors in the tunnel cases, such as the blockage ratio and traffic lane position is barely mentioned.

Chapter Three

Experimental methodology

3.1 Apparatus

3.1.1 TRAIN rig introduction

The TRansient Aerodynamic INvestigation (TRAIN) rig facility is a purpose-built facility in Derby to examine transient aerodynamics of vehicles (Baker 2001). The reduced-scale vehicle models can be propelled along a series of 150 m long tracks at speeds up to 75 m/s. They are fired by pre-tensioned elastic bungee ropes without additional propulsion and then run at a relatively constant specified speed within a 50m firing section before decelerating by a friction device. Compared with a typical wind tunnel, the advantage of the moving model rig is that it can properly simulate the relative movement between the ground/structure and the vehicle. More detail about the rig facility firing system can be found in Soper (2016).

The method performs well when simulating a train consisting of multiple jointed carriages or a single vehicle. To generate a platoon effect by firing multiple models in rapid succession, this research adopted a new method to install a group of model vehicles in a row configuration on a long spine system. Therefore, they can run as a single unit at the same speed and at a fixed inter-lorry spacing (Robertson et al. 2019).

3.1.2 Vehicle model

The vehicle model was a 1/20th scale commercial box-type lorry (see Figure 3.1), with the length(L), width(W) and height(H) being 0.395 m, 0.125 m and 0.175 m, respectively. This lorry model was simplified from a typical commercial vehicle Leyland DAF 45-130, which has been extensively investigated either as a single-vehicle (Quinn et al. 2007; Cheli et al. 2011; Patel et al. 2019) or in a platoon formation (He et al. 2019; Robertson et al. 2019). Therefore, there are abundant results to offer useful references and necessary validations of the present experiments and numerical simulations. Furthermore, by using the same vehicle shape as in previous studies by the same research group (He et al. 2019; Robertson et al. 2019), direct comparisons of the results obtained in the tunnel and in the open air can be shown, which is the focus of the present study. Note that some detailed features of the original lorry, such as side mirrors and windshield overhangs, were removed or simplified in the present lorry model. This simplification is related to the simulation efforts, as including these features has a negligible effect on the aerodynamic performance, but it would require intensive meshing design and result in an exponential growth in the number of mesh cells.

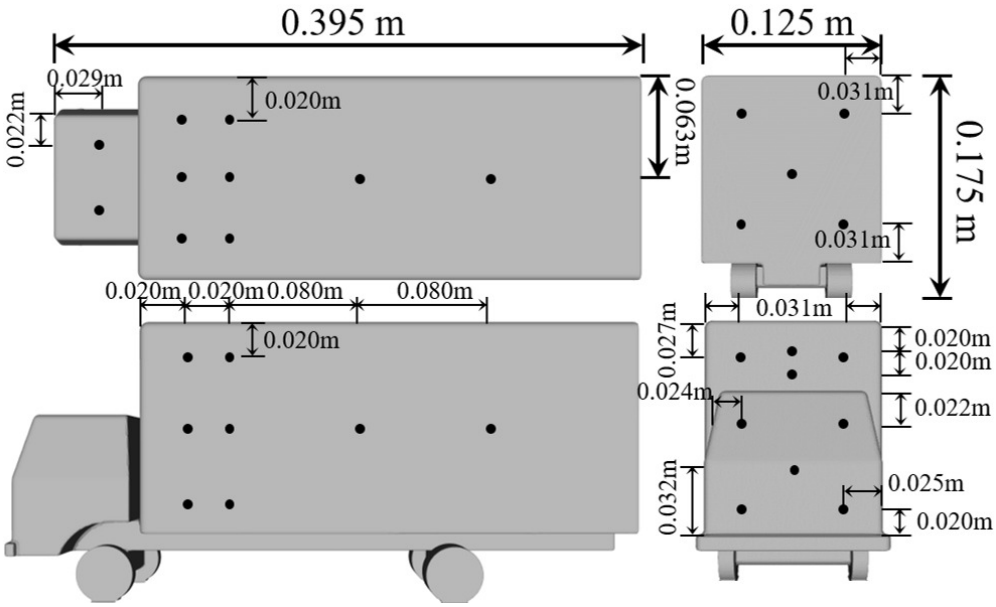

Figure 3.1: The shape and dimensions of the reduced-scale lorry model.

3.1.3 Tunnel model

The scaled tunnel with a rectangular cross-section in shape was built on the plane, with the length, width and height being 10 m, 0.26 m and 0.215 m, respectively (see Figure 3.2). Figure 3.2 shows the photographs of the platform and the lorry platoon on the rig. Note that in Figure 3.2, the roof of the tunnel was temporally removed to show the lorries and cobra probes inside. The cross-section of the scaled tunnel is $0.0559m^2$, leading to the blockage ratio (proportion of the frontal area of the vehicle to the cross-sectional area of the tunnel) to reach around 35.8%. The blockage ratio is larger than the real situation, which is from 10% to 15%. However, owing to the limited amount of room available in the rig, the tunnel has reached its maximum width. The impact of the blockage ratio will be explored in the simulation, with the experimental findings serving as a benchmark to verify the simulation.

Figure 3.2: Photographs of the platform and the lorry platoon on the train rig.

The ground plane was composed of two suspended plane halves with a minimised gap of 10 mm in width. The slot gap around the vehicle mounting posts was kept as small as possible, at 5mm on each side, to minimize any influence on the flow around the lorries caused by the supporting system. With this gap, the tunnel appears more like a partially enclosed space than a traditional tunnel. No doubt, there is a vast difference in aerodynamic

phenomena if the gap on the ground is absent. There is no 'gap' on the ground in the actual situation. The effect of is leakage of the tunnel is analysed and discussed in Appendix A. Above all, the gap on the ground was an acceptable setting given the limitations of the experiment setting. The gap will also be modeled in simulations.

3.2 Instrumentation

3.2.1 Cobra Probe

The slipstream velocities and pressures were measured by multi-hole probes (Turbulent Flow Instrumentation (TFI) Series 100 Cobra probes). This kind of probe (see Figure 3.3 (a)) can measure three velocity components of the airflow and also the static pressure, with the accuracies being $0.3m/s$ and ± 5 Pa for velocity and pressure measurements, respectively. The maximum frequency response of this probe is 2000 Hz, enabling it particularly well suited for the experiments of high turbulent flow. TFI Device Control software converts voltage data from the Cobra Probe into three components of velocity data based on a predetermined calibration. The software also "zeroed" the Cobra probe before the platoon was fired for each measurement. This guaranteed that measurements were taken in the context of a static air environment.

A disadvantage of the Cobra probe is that the cone-of-acceptance is only 45 degree, which restricts the flow detecting scope. Data produced when flow beyond this range is set to zero. While previous studies (Soper et al. 2018; Robertson et al. 2019) have shown that most of the slipstream flow are within ± 20 flow angles. Indeed, based on the data collected in this research, average flow angles suggest a comparable range of values. The probe is configured in such a way that the central measuring hole is positioned at the desired measurement position on the tunnel's side wall. Figure 3.3 (b) shows a set of specially constructed probe holders or clamp stands are used to support the Cobra probes.

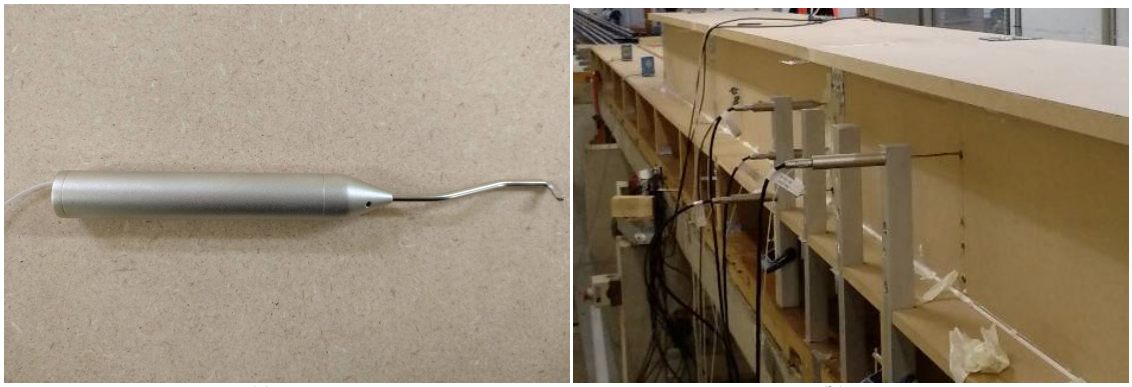

(a) (b)

Figure 3.3: (a) Series 100 Cobra probe. (b) The probe holders.

3.2.2 Position finder

The speed of the model was measured using five photoelectric position finders and reflectors in opposition that were installed on the ground plane. The monitored velocity was estimated to an accuracy of 0.1 m/s using the time required for the vehicle to break both beams. Separately, two pairs of finders were set at 0.5 m and 1.5 m away from the inlet and outlet of the tunnel (see Figure 3.4 (a)). In order to assist in data alignment, another couple of position finders was installed on the roadside in accordance with the measuring head of Cobra probe. Each position finder pairs calculated and output the speed on the interface unit screen before inputting it in Excel. The data from the position finders was saved and then used to align the data.

3.2.3 Monitors of the environment condition

The environment conditions were measured with an BAR208HGA advanced weather station of Oregon Scientific, which measured relative humidity Φ and temperature T with a precision of 1% and 1 centigrade, and an accuracy of 10% and 2 centigrade, respectively. The atmospheric pressure P_{atm} was measured using a GBP3300 Digital Barometer with a resolution of $\pm$1mb/100Pa and a 200Pa accuracy. Sensors were positioned on a supporting pillar in the rig adjacent to the setup of the experiment to record the ambient conditions (see Figure 3.4 (b)). The estimated air density was derived from the measured T, Φ and P_{atm} and the gas

constant $R = 287(J/kg \cdot K)$. Here is the mean standard deviation of the ambient condition: $P_{atm} = 99.63 \pm 1.62$kPa, $T = 16.34 \pm 0.53$°C, $\Phi = 67.67 \pm 1.67$ and $\rho = 1.19 \pm 0.004$kg $\cdot$ m^{-3}.

(a) (b)

Figure 3.4: (a) Position finders were mounted on the ground to measure the speed of the platoon and (b) the ambient condition monitors positioned on the supporting pillar.

3.2.4 On-board pressure monitoring systems

In addition to roadside data, the surface pressure of each lorry were also monitored. All vehicles were equipped with a set of customized on-board pressure monitoring devices with independent data loggers (see Figure 3.5 (a)). The system comprises of a standalone battery-powered data logger, linked to 14 miniature difference pressure transducers from FirstSensor Ltd through a specific circuit board system. The logger with a 16-bit resolution can monitor up to fifteen channels with a largest sampling rate of 3000 Hz. The measurement ports of the pressure transducer were linked through silicon pipe to metal pipe adapters cemented into the wall of the lorry, which served as pressure taps (see Figure 3.5 (b)).

The manifold in each lorry was connected to the reference ports via silicon tubing and then linked to a shared sealed reservoir, which served as a synchronized reference pressure.

To avoid the effect of perturbation in reservoir due to temperature fluctuations, the system was equipped with a vent that was opened after each run. (Dorigatti 2013).

(a) (b)

Figure 3.5: (a) The on-board pressure monitoring systems. (b) The pressure taps on the lorry body.

3.3 Experiment setup

3.3.1 Measuring positions and coordinate system

A coordinate system was defined such that the x-axis was aligned in the direction of platoon motion; the z-axis was in the vertical direction measured from the ground plane; the y-axis was on the horizontal plane and perpendicular to the direction of platoon motion. The original point of x-axis is set at the tunnel's entrance.

Cobra probe measurements were taken using four probes from the lorry side and above the ground plane (see Table 3.1). To monitor the changes of the slipstream in the vertical direction, three probes are used: Probe A, B, and C. These probes are positioned close to the height of the wheel center, height of the lorry center, and $0.14H$ under the roof of the lorry, respectively. Probes A and D are positioned at the same height but at various distances from the lorry body to detect horizontal slipstream changes.

Due to the limited number of pressure transducers on the on-board pressure monitoring systems (as described in in Subsection 3.2.4), only fourteen taps are used to measure the surface pressure of each lorry. As indicated in Figure 3.7, eight of all taps are utilized in

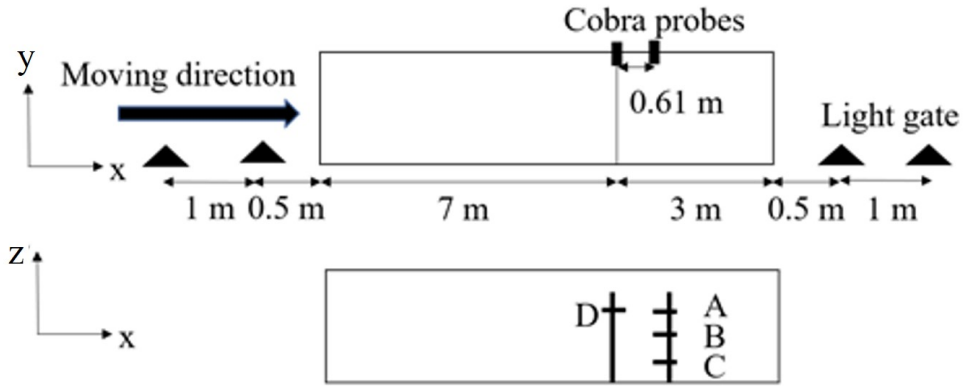

Figure 3.6: Coordinate system and measuring positions of the cobra probes.

Probe number	Height from ground level(z/H)	Distance from lorry body side (y/H)
A	0.86	0.14
B	0.45	0.14
C	0.11	0.14
D	0.86	0.28

Table 3.1: The positions of the multi-hole probes for measuring the slipstream properties. Here, H is the height of the lorry model.

later validation, with their positions marked.

3.3.2 Experiment method

The slipstream experiments on the TRAIN rig model scale included collecting Cobra probe measurements throughout a series of runs for the platoon. Due to the highly temporal variations in velocity and pressure obtained from individual measurement, multiple runs (of the order of 10–20) are required to ensure that the standard deviation of the ensemble average is comparable to the turbulence level (Baker 2001). Therefore, 20 runs of the experiment were conducted in the present study to ensure statistically converged ensemble averages (Robertson et al. 2019; Sterling et al. 2008). The lorry platoon was propelled at a speed of

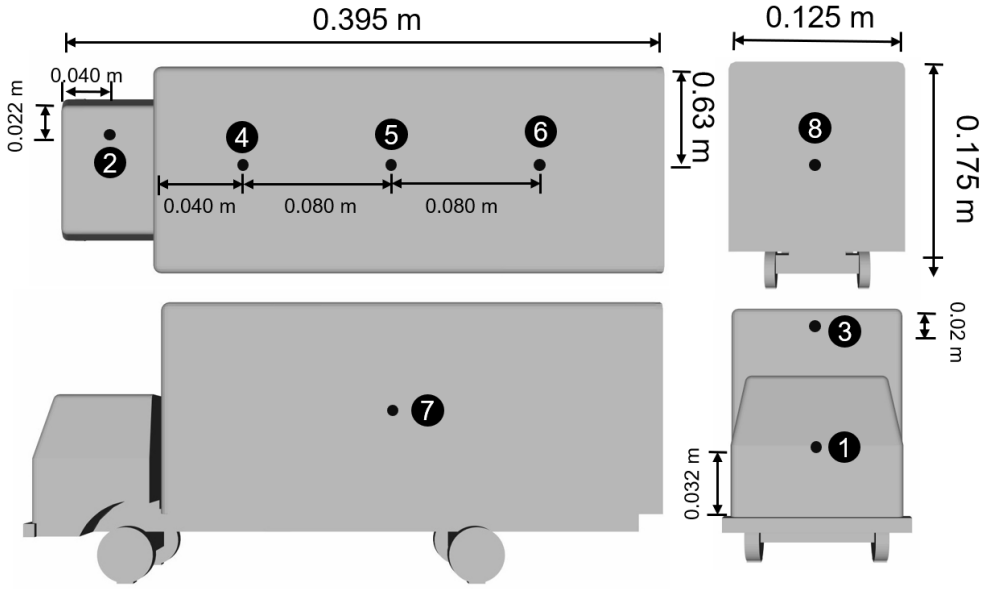

Figure 3.7: The positions of the pressure taps for surface pressure measurements are indicated by the numbers on the lorry.

$V_{\text{plat}} = 25 \pm 1\text{m/s}$ to reflect typical road speeds. To get at this particular platoon velocity, multiple preliminary firings were conducted to determine the tension of the rope. Because of the aerodynamic drag on the lorry models and the friction between the vehicle mounting point and the rig, there is a slight decrease in the speed (1.17 m/s) of the lorry platoon when it left the tunnel. For this 1/20th scale model experiment, based on the platoon speed 25 m/s and the characteristic height of 0.175 m, the Reynolds number is,

$$\text{Re} = \frac{V_{\text{plat}} L_{\text{ref}}}{\nu} = \frac{25 \times 0.175}{0.000015} = 2.92 \times 10^5 \tag{3.1}$$

The comparable Reynolds number of experiment and full scale can be obtained by high wind speed or large models. However, the Reynolds number in current experiments can only reach $Re \sim 3 \times 10^5$ due to the limitations of wind tunnel, which is an order lower than the full scale experiments ($Re \sim 9 \times 10^6$). This discrepancy raises the question of whether turbulent flow will be fully developed around the model in experiments conducted in wind tunnel (Tsuei and Savaş 2001).

According to the British Standards Institution (EN 2013) , in order to guarantee the results are representative of full-scale experiments, scale down slipstream experiments with a

moving vehicle are expected to be carried out at a Reynolds number greater than 2.5×10^5, to guarantee the results are representative of full-scale experiments. Previous studies related to the train passing trough tunnel (Iliadis et al. 2019; Johnson and Dalley 2002; Gilbert, Baker, and Quinn 2013b) conducted in TRAIN rig and the comparison between the pressure inside the tunnel with full scale results showed excellent agreement. As for the ground vehicle (Ahmed), Cooper suggested that for scale down experiment it was important to ensure that the flow over fore-body edges were turbulent (Cooper 1993). The critical Reynolds number as low as 3×10^4 has been tested (Spohn and Gilliéron 2002). (Salari and Ortega 2018) reported that the Reynolds number effects were taken to be negligible above 2×10^5 for a heavy truck. Robertson et al. (2019) compares the averaged surface pressure distribution between a isolated model vehicle and full-scale measurements with a one order higher Reynolds number from Quinn et al. (2007). They discovered that, despite the fact that the model C_p is considerably smaller, the overall patterns in both full-scale and model data were highly consistent. The authors pointed out that there was yet to be enough data to corroborate the Reynolds number effect. Above all, the Reynolds number of this scale down experiments is sufficient to investigate the aerodynamic phenomena of the long lorry platoon.

3.4 Data process methodology

3.4.1 Data conversion

The measured data is collected in its most basic form, consisting of a sequence of voltage signals. These signals could be transferred to useful quantities by using conversion and calibration formulae provided by instrument-maker and the experiments of calibration.

The Cobra probe constantly records data in a digitally sampled analog format at 5000 Hz. The TFI data recorder converts the sampled data from a sequence of voltage signals to useful values. All data were recorded at a sampling frequency of 5 kHz and filtered using a 650 Hz low-pass filter to reflect the maximum frequency response of the probe. More detail information about the data conversion can be found in Soper (2016).

The surface pressure was recorded via the stand-alone monitoring system. All 15 pressure transducers are powered by a 5 Volt supply and have a ground reference provided by the circuit board, which also integrates a 4GB data storage memory card. The connection between the logger and a computer is accomplished via the use of a USB cable, and a special software program has been created to operate the device. This program allows for the configuration, real-time and sampling monitoring, and data downloading of the system (into a .csv file). The raw data is then converted to usable values via Matlab.

3.4.2 Non-dimensionalised variables

The sampled result is expressed using a sample number N_{samp}, and then transferred to sampling time,

$$t_{\text{samp}} = \frac{N_{\text{samp}} - 1}{f_{\text{samp}}} \tag{3.2}$$

where f_{samp} is the sampling frequency and $N_{\text{samp}} = 1, 2, \ldots$ is the sample number. In order to analyse the results in convenience, the data is realigned (in Subsection 3.4.3) with the sample point when the frontal face of the leading lorry passes the tunnel entrance defined as $t = 0$. The time is also realigned to measurement around the frontal face of the leading lorry, rather than measurements from the beginning of the time history during realigning process.

The slipstream velocity, static pressure, and the surface pressure are presented in dimensionless form throughout this study. In accordance with past slipstream investigations

(Robertson et al. 2019), the convention of non-dimensioning data has been used:

$$\begin{aligned} U(\tau) =& \frac{u(\tau)}{V_{plat}} \\ V(\tau) =& \frac{v(\tau)}{V_{plat}} \\ W(\tau) =& \frac{w(\tau)}{V_{plat}} \\ U_{res}(\tau) =& \sqrt{\left(\frac{u(\tau)}{V_{plat}}\right)^2 + \left(\frac{v(\tau)}{V_{plat}}\right)^2} \\ C_P(\tau) =& \frac{p(\tau) - p_0}{\frac{1}{2}\rho V_{plat}^2} \end{aligned} \tag{3.3}$$

Here, $\tau = V_{plat}t/L$ is the normalised time in terms of the platoon speed V_{plat} and the lorry model's length L. Note that τ is taken as zero when the first lorry enters the tunnel for presenting the slipstream properties of the platoon, or when each lorry enters the tunnel for presenting their surface pressures and drag properties. U, V and W represent the normalised velocity for the longitudinal, lateral and vertical components, respectively. U_{res} is the overall normalised horizontal velocity. The pressure coefficient C_p is calculated with respect to an ambient reference pressure p_0 and the air density ρ.

3.4.3 Data aligned

Experimental results for velocity and pressure are aligned with the nose of the leading lorry passing at the tunnel entrance, which is defined as origin. The signal of the light source and detector were recorded to an extra channel in the data logger. In order to align the beam of light with the Cobra probe head's measuring face, the light source was positioned. An event finder for the lorry front is created that records a time series of data along with the Cobra probe, which allows the pressure and velocity measurements to be synchronized with the auxiliary channel measurements. The cobra probes were installed 7 meters from the tunnel entrance. Therefore, the original point is then shifted to the moment when the leading lorry entering the tunnel according to the platoon speed V_{plat} and the sampling frequency.

Because the velocity and pressure are non-dimensionalised in relation to the platoon

speed V_{plat}, the results need to first be resampled to the nominal platoon speed $V_{nom} = 25m/s$. For instance, the platoon is travelling at either end of a $V_{\text{plat}} = 25 \pm 1m/s$ speed window covers a distance of a 10-meters in 0.402s and 0.398s respectively. There is a difference of 20 samples for a sampling frequency of 5000Hz. The raw data is resampled to the nominal platoon speed V_{nom} in order to negate differences in platoon speed. After that, the normalised pressure and velocity are resampled at the initial sampling frequency using a linear interpolation for both on-board pressure monitoring system and cobra probes.

3.4.4 Ensemble averaging

Due to the stochastic nature of the turbulent flow forming around a platoon, such brief time history exhibited a substantial run-to-run fluctuation. Experimental data may include significant test-to-test variations, making it impossible to calculate averages using a conventional methodology. As a result, in order to get reliable estimates of mean aerodynamic coefficients, the computation of their ensemble averages, which was based on a sequence of repeated runs, proved to be very advantageous (Soper et al. 2017). According to previous experimental measurement of slipstream properties, an experiment should be repeated at least 20 times in order to verify the findings and provide ensemble averages (Gil, Baker, and Roberts 2008).

Let us start with a general signal $c(x)$ measured n times with the location of axial coordinates x. The ensemble average $\bar{c}(x)$, variance $var(x)$ and the standard deviation σ can be defined as (Deeg et al. 2008):

$$\bar{c}(x) = \frac{1}{n}\sum_{r=1}^{n} c_r(x), \quad \overline{c^2} = \frac{1}{n}\sum_{r=1}^{n} c_r^2(x), \quad \text{var}(x) = \overline{c^2} - \bar{c}^2 \quad \sigma(x) = \sqrt{\overline{c^2} - \bar{c}^2}, \tag{3.4}$$

where r represents the r^{th} passage of the platoon and n is the ensemble size.

To comprehend the ensemble averaging, Figure 3.8 presents the normalised longitudinal velocity $U(\tau)$ and pressure coefficient C_p, for all 20 runs and the black line indicated the ensemble average time history. The test-to-test variations, particularly in the boundary layer, are clearly evident. The 45 degree cone-of-acceptance of the Cobra probe, which is a limitation of the ensemble averaging approach and the Cobra probe data, causes a series of

zeros in the output time history when it is exceeded. It is clear in the longitudinal velocity in dimensionless time between 18 to 27 in Figure 3.8 (a), the Cobra probes are unable to record a flow reversal that happens when the leading edge of the first lorry passes and the flow separates. To address this issue, the zero data is excluded in the ensemble averaging procedure.

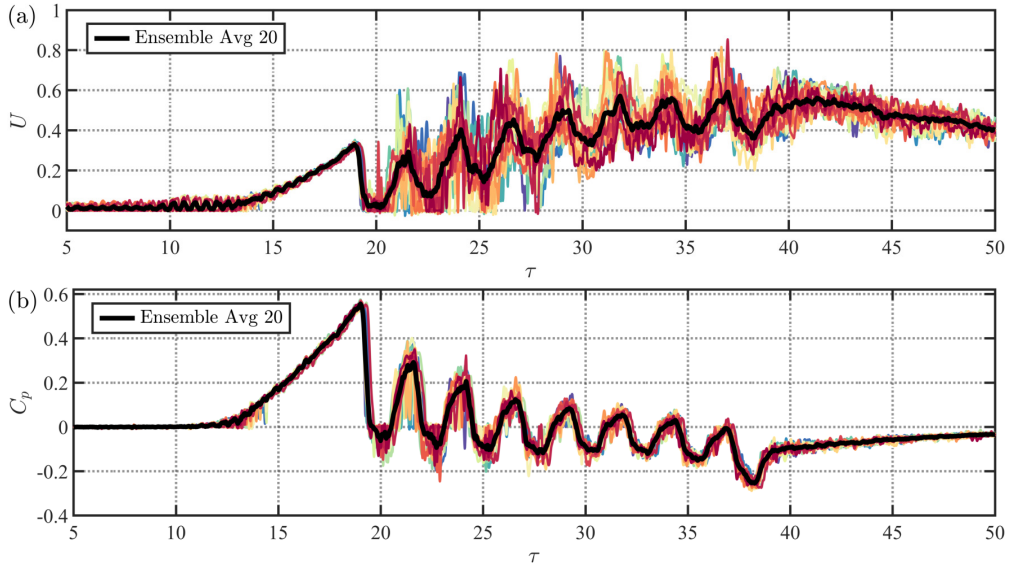

Figure 3.8: Example of the ensemble averaging adopting (a) normalised horizontal velocity U and (b) pressure coefficient C_p from Probe B. The individual result of each run and the ensemble average (black line) are shown together.

Figure 3.9 presents the surface pressure coefficient of the Tap 1, 5, 7 and 8 of Lorry 1 (see Figure 3.7), for all 20 runs and the black line indicates the ensemble average time history. All time series display short time scale oscillations throughout the duration of the data collection, which are not synchronized among different runs. However, there is good agreement between each runs in the short period during the entering and exiting tunnel process as well as the long time-scale variations, both of which are clearly obvious in the time history of ensemble averages.

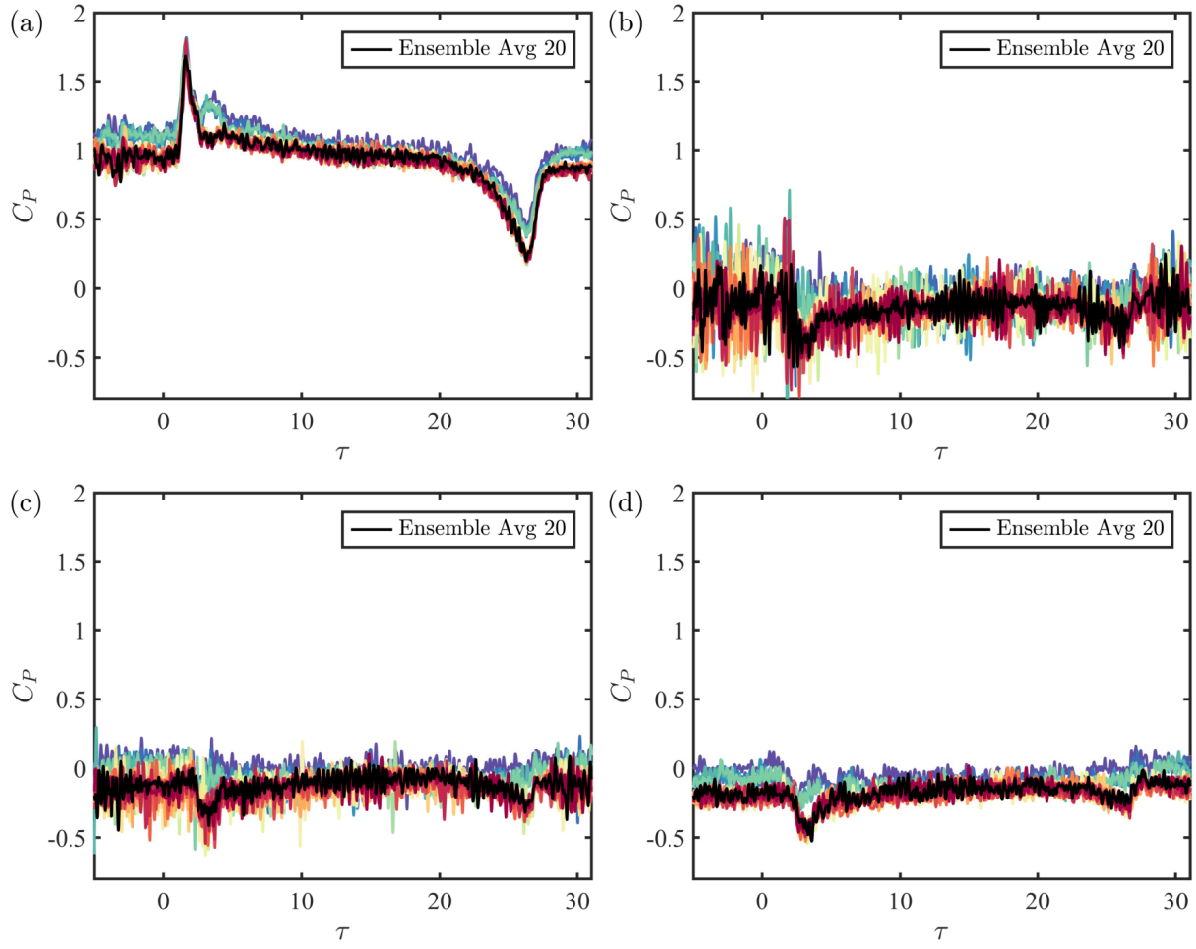

Figure 3.9: Example of the ensemble averaging using surface pressure coefficient from (a) Tap 1, (b) Tap 5, (c) Tap 7 and (d) Tap 8 (see Figure 3.7) of Lorry 1. The individual result of each run and the ensemble average (black line) are shown together.

3.4.5 Uncertainty analysis

For simplicity, the uncertainty analysis for the measured quantities, including the velocity and static pressure of the slipstream and the surface pressure of the lorry, is discussed in detail in Appendix B. The discrepancy between the true and observed values of a certain direct measured or derived quantity is called measurement error (Taylor 1997; Tavoularis 2005). Based on the data reduction methods and experimental techniques, there are two major causes of the uncertainty of experiments: bias limit and random uncertainty.

In accordance with the prior aerodynamics investigations (Gil et al. 2010; Baker et al. 2016), the uncertainties of the slipstream are calculated using maximum values for horizontal velocities and pressure of the slipstream. The mean and maximum uncertainties value for experiments in open air and the tunnel are listed in Table 3.2. The uncertainties for each cobra probes are also calculated in the Appendix B. In comparison to random uncertainties, the values of the bias limit are fairly small. The values for random uncertainty in the open air experiments are relatively larger in comparison to that in the tunnel.

	Slipstream velocities		Static pressure	
	Mean	Maximum	Mean	Maximum
In tunnel	0.047	0.054	0.36	0.38
In open air	0.066	0.070	0.33	0.42

Table 3.2: The total uncertainties for slipstream velocities and static pressure for two series of experiments. The mean and maximum values are presented.

The mean surface pressure uncertainties is calculated for all pressure taps on all lorries in the platoon travelling through the tunnel. The mean surface pressure coefficients in tunnel are calculated for 1 meter length near the cobra probe (7 meters from tunnel inlet to 8 meters from the tunnel inlet), in accordance with the experiments in the open air (Robertson et al. 2019). To obtain the accuracy of the pressure transducers, the actual cubic calibration is undertaken. The error of all other pressure transducers tested have the same magnitudes of the order of $\pm$9Pa. The peak values occurs on Tap 5, where the flow stagnates. The random uncertainties are approximately the same for measurement taps located in other

regions. The total uncertainties of the mean surface pressure coefficients is in the range of $0.02 - 0.08$.

Chapter Four

Numerical simulation setup

This chapter describes simulation methodology for this project. This chapter discuss the general CFD approach and the accuracy associated with it. The IDDES will be thoroughly introduced in this chapter. And then the grid generation techniques, discretisation and numerical schemes will be presented.

4.1 Turbulence Theory

With the rapidly growing ability of computational methods to reliably and affordably simulate complex flows, CFD has become a powerful tool to reveal detailed flow dynamics around moving vehicles. In this section, the theory behind the numerical simulation is briefly stated and explained.

4.1.1 The governing equations

The main mathematical equations in CFD are the continuity equation (mass conservation), momentum equation (Navier-Stokes), and energy equation (energy conservation). The scope of this dissertation does not include any heat transmission, hence it is assumed that the flow is isothermal. Therefore, this study discusses just the continuity and conservation of

momentum equations. The flow is also considered to be incompressible, as the vehicle speed is slower than the sound speed (less than 0.3 mach). The governing equations are displayed below:

$$\begin{gathered} \frac{\partial u_i}{\partial x_i} = 0 \\ \frac{\partial u_i}{\partial t} + u_j \frac{\partial u_i}{\partial x_j} = -\frac{1}{\rho}\frac{\partial p}{\partial x_i} + \frac{\partial \tau_{ij}}{\partial x_j} \\ \tau_{ij} = \nu \left(\frac{\partial u_i}{\partial x_j} + \frac{\partial u_j}{\partial x_i} \right) \end{gathered} \tag{4.1}$$

where u_i denotes a velocity component, ν is the kinematic viscosity and p is the pressure. τ_{ij} represents the viscous stresses (Pope 2000).

4.1.2 Large Eddy Simulation

To solve the Navier Stokes Equations directly without modelling would require the resolution of the smallest length and time scales of turbulence, through the Kolmogorov micro-scales. However, for such a high Reynolds number case, The required computational resources vastly outweigh current capabilities (Pope 2000). For this reason, a Direct Numerical Simulation (DNS) is currently inappropriate for modelling road vehicle aerodynamics. The complexity of the problem must be reduced in order to reduce the computational needs of DNS. LES divides the Navier Stokes Equations into resolved and unresolved components, allowing for coarse grid resolutions overall. This must be done correctly for an accurate simulation, capturing the large anisotropic energy-carrying eddies and leaving only the smallest scales of isotropic turbulence to be modelled (Pope 2000). LES performs a filtering operation to decompose the velocity and pressure into filtered terms and filtered-out (unresolved) terms.

Let us assume that the LES with sufficient near wall resolution is employed for a lorry and 80% of the energy is resolved everywhere. Fröhlich et al. (2005) determined that a filter width 12 times larger than the Kolmogorov length scale was ideal when investigating the LES of separated channel flow. Considering the same Kolmogorov length and time scale. The required length scale increases to 0.165 mm and time scale to 0.154 ms, requiring 3 billion cells to resolve the 50 mm volume near the lorry body. A three orders of magnitude improvement, but still out of reach for even the most powerful High Performance Computing

(HPC) systems available today. Although there are variants of LES with near-wall modelling which could reduce the grid spacing requirements, the number of the cells is still 4 orders of magnitude away from a feasible solution.

4.1.3 RANS models

The least computationally intensive method of simulating turbulent flow in CFD is to apply Reynolds Averaging to the Navier-Stokes equations. In Reynolds average approach, the scale separation relies on the averaging and the whole turbulent energy spectrum is modelled. The variable of instantaneous flow is split into its mean and fluctuating components. For example, the velocity can be expressed as:

$$u(x,t) = \bar{u}(x,t) + u'(x,t) \tag{4.2}$$

The RANS equations can be written as follow,

$$\begin{aligned} \frac{\partial \bar{u}_i}{\partial x_i} &= 0 \\ \frac{\partial \bar{u}_i}{\partial t} + \bar{u}_j \frac{\partial \bar{u}_i}{\partial x_j} &= -\frac{1}{\rho}\frac{\partial \bar{p}}{\partial x_i} + \frac{1}{\rho}\frac{\partial \tau_{ij}}{\partial x_j} - \frac{\partial \overline{u_i' u_j'}}{\partial x_j} \end{aligned} \tag{4.3}$$

The additional component, $\overline{u_i' u_j'}$, is the Reynolds Stress tensor, which presents the influence of the fluctuating turbulence to the mean flow. The Reynolds-stress tensor is a symmetric tensor, it yields six additional unknowns in the time-averaged momentum equations, which means the system is not closed. Therefore, developing the turbulence models to predict the Reynolds stress tensor become a necessity.

One of the most common used turbulence models is the $k-\omega$ model, which is a two-equation model. Two partial differential equations for kinetic energy k and specific rate of dissipation ω along with the RANS equations (Equation 4.3) are computed (Wilcox 1998). The transport equations of k and ω are as follows. The eddy viscosity is calculated from $\mu_t = \rho k/\omega$.

$$\begin{aligned} \frac{\partial \rho k}{\partial t} + \frac{\partial \left(\rho u_j k\right)}{\partial x_j} &= \frac{\partial}{\partial x_j}\left(\left(\mu + \sigma_k \frac{\rho k}{\omega}\right)\frac{\partial k}{\partial x_j}\right) + P - \beta^* \rho \omega k \\ \frac{\partial \rho \omega}{\partial t} + \frac{\partial \left(\rho u_j \omega\right)}{\partial x_j} &= \frac{\partial}{\partial x_j}\left(\left(\mu + \sigma_\omega \frac{\rho k}{\omega}\right)\frac{\partial \omega}{\partial x_j}\right) + \frac{\gamma \omega}{k} P - \beta \rho \omega^2 \end{aligned} \tag{4.4}$$

where,

$$\begin{aligned} P &= \tau_{ij}\frac{\partial u_i}{\partial x_j} \\ \tau_{ij} &= \mu_t\left(2S_{ij} - \frac{2}{3}\frac{\partial u_k}{\partial x_k}\right) - \frac{2}{3}\rho k\delta_{ij} \\ S_{ij} &= \frac{1}{2}\left(\frac{\partial u_i}{\partial x_j} + \frac{\partial u_j}{\partial x_i}\right) \end{aligned} \tag{4.5}$$

The $k-\epsilon$ is another a two-equation model, which is widely used in industrial area (Jones and Launder 1972). The $k-\epsilon$ model uses a turbulent energy dissipation rate ϵ. Each model, however, has disadvantages. The $k-\epsilon$ trends towards higher eddy-viscosity $\nu_t = \epsilon^2/k$ near the wall as k tends towards zero near the wall, which requires additional damping functions. The $k-\omega$ model performs better in the viscous near-wall region. However, a non-zero at inlet boundaries on ω is required to be specified, and the results is sensitive to this value. These shortcomings were addressed by Menter (1994) who combined two models into SST model using $k-\epsilon$ model within the fully developed turbulent region far from the wall and $k-\omega$ model in the sub-layer of the boundary layer. The $k-\omega$ SST Menter model is presented as follow,

$$\begin{aligned} \frac{\partial k}{\partial t} + \frac{\partial u_j k}{\partial x_j} &= P - \beta\omega k + \frac{\partial}{\partial x_j}\left[\left(\mu + \sigma k\mu_t\right)\frac{\partial k}{\partial x_j}\right] \\ \frac{\partial \omega}{\partial t} + \frac{\partial u_j \omega}{\partial x_j} &= \frac{\gamma}{\nu_t}P - \beta\omega^2 + \frac{\partial}{\partial x_j}\left[\left(\mu + \sigma_\omega\mu_t\right)\frac{\partial \omega}{\partial x_j}\right] + 2\left(1-F_1\right)\frac{\sigma_{\omega 2}}{\omega}\frac{\partial k}{\partial x_j}\frac{\partial \omega}{\partial x_j} \end{aligned} \tag{4.6}$$

where the blending function F_1 and F_2 are defined as:

$$\begin{aligned} F_1 &= \tan\left\{\left\{\min\left[\max\left(\frac{\sqrt{k}}{\beta^*\omega d_\omega}, \frac{500v}{d_\omega^2\omega}\right), \frac{4\rho\sigma\omega^2 k}{CD_{k\omega}d_\omega^2}\right]\right\}^4\right\} \\ CD_{K\omega} &= \max\left(2\rho_{\omega 2}\frac{1}{\omega}\frac{\partial k}{\partial x_i}\frac{\partial \omega}{\partial x_i}, 10^{-10}\right) \\ F_2 &= \tanh\left[\left[\max\left(\frac{2\sqrt{k}}{\beta^*\omega d_\omega}, \frac{500v}{d_\omega^2\omega}\right)\right]^2\right] \end{aligned} \tag{4.7}$$

Here d_ω is the distance to the nearest wall. This model's details are beyond the scope of this study, therefore readers are encouraged to visit the National Aeronautics and Space Administration (NASA) turbulence modelling verification website (https://turbmodels.larc.nasa.gov).

The RANS models only require enough resolution to capture velocity gradients and underlying geometry. When wall functions are applied at no-slip wall boundary circumstances, the necessity to capture velocity gradients becomes less stringent, allowing for faster wall normal growth rates of near wall cells. RANS is also widely used to simulate the aerodynamics of vehicles in a tunnel (Li et al. 2009; Wang et al. 2014; Dong et al. 2017). The mesh density requirement of RANS is lower than that for LES. However, the limitations of RANS simulations were pointed out by Humphreys and Bevly (2016), who validated the accuracy of RANS in estimating the overall drag reduction trend when platoon was restricted to 4 vehicle lengths.

4.1.4 Improved Delayed Detached-Eddy simulation

The excessive cost for LES and inaccuracy for RANS in for high Reynolds number flows make hybrid RANS/LES models become attractive for high Reynolds number flows. The most popular methods are DES proposed by Spalart et al. (1997). DES models switch explicitly between RANS and LES models simulations according to the turbulent length scale and local grid spacing (Gritskevich et al. 2012). DES uses LES in separated regions and RANS models in the boundary layer. The LES zone is typically associated with the core turbulent region, which is dominated by large unstable turbulence scales. DES models were specifically developed to address flows with high Reynolds numbers and are a more affordable alternative to LES simulations for wall-bounded turbulent flows, such as the high Reynolds number external flow. The DES model can be based on $k-\epsilon$, standard $k-\omega$, SST $k-\omega$ and so on. Using DES models, the computational costs are smaller than the computational costs of the LES models, but higher than those of the RANS models.

In Equation 4.6, dissipation term of the turbulent kinetic energy, for simplicity, is written in Y_k here.

$$Y_k = \rho\beta^* k\omega \tag{4.8}$$

where f_β and β can be derived from Equation 4.6 and Equation 4.7. In DES, this term is modified as described in Menter, Kuntz, and Langtry (2003) such that,

$$Y_k = \rho\beta^* k\omega F_{DES} \tag{4.9}$$

where F_{DES} is expressed as:

$$F_{DES} = \max\left(\frac{L_t}{C_{des}\Delta_{\max}}, 1\right) \tag{4.10}$$

where c_{des} is a calibration constant with a value of 0.61 in the DES model, and $\Delta_{\max}$ is the grid spacing. L_t is the turbulent length scale that defines in the RANS model: $L_t = \sqrt{k}/\beta^*\omega$. DES model switches from RANS to LES once $L_t > C_{des}\Delta_{\max}$. By relying on wall distance and grid size, the LES zones need not be known a priori.

However, the standard DES model has some drawbacks reported by Menter, Kuntz, and Langtry (2003) and Spalart et al. (2006). Reducing the maximum cell edge length in the wall boundary layer of an airfoil simulation might result in an artificial separation (Spalart et al. 2006). This effect was termed as (GIS) as the separation determined by the mesh size instead of the mechanics of the flow. GIS is clearly the result of a abrupt grid refinement that converts the RANS to LES model without compensating for the decrease of eddy viscosity. Spalart et al. (2006) proposed the term Modeled Stress Depletion (MSD) to describe the influence of decreasing eddy viscosity from RANS to LES with no balance of resolved quantities. GIS is the result of MSD. For wall-bounded flows, it needs many boundary thicknesses to develop sufficient LES content to compensate the reduction of RANS model. Therefore, the MSD is particularly evident in wall-bounded flows. Menter, Kuntz, and Langtry (2003) used the blending function of SST model to shield the RANS model from the DES formula for boundary layers to avoid the GIS. The resulting formula was named as Delayed Detached Eddy Simulation (DDES). The blending function is given by:

$$F_{DDES} = \tanh\left[\left(C_{d1}r_d\right)^{C_{d2}}\right] \tag{4.11}$$

where $C_{d1} = 20$, $C_{d2} = 3$ and

$$r_d = \frac{v_t + v}{\kappa^2 d_w^2 \sqrt{0.5 \cdot (S^2 + \Omega^2)}} \tag{4.12}$$

where S is the strain rate tensor, Ω is the vorticity tensor, d_w is the wall distance, and $\kappa = 0.41$ is the von Karman constant. The DES limiter is deactivated if the function $f_d = 0$.

Another drawback of DES and DDES is Logarithmic Layer Mismatch (LLM). The DES and DDES models use two logarithmic layers: the inner and outer log-layer. The formal layer is built by the the RANS model and the latter is constructed by LES, which

is functioning well when all local grid-sizes are lower than the distance to the wall (Travin et al. 2006; Shur et al. 2008). However, the two log-layers turn out mismatched which underestimates the skin-friction coefficient by 15 to 20%. Travin et al. (2006) proposed Improved DDES (IDDES) by combining the advantages of the wall-modelled LES (WMLES) and DDES. In this combined approach, the empiric function is similar to the function in DDES to provide shielding.

The govern equations of the SST-IDDES model read as:

$$\begin{aligned}
&\frac{\partial \rho k}{\partial t} + \nabla \cdot (\rho \vec{U} k) = \nabla \cdot \left[(\mu + \sigma_k u_t) \nabla k \right] + P_k - \rho \sqrt{k^3} / l_{\mathrm{IDDES}} \\
&\frac{\partial \rho \omega}{\partial t} + \nabla \cdot (\rho \vec{U} \omega) = \nabla \cdot \left[(\mu + \sigma_\omega u_t) \nabla \omega \right] + 2 (1 - F_1) \rho \sigma_{\omega 2} \frac{\nabla k \cdot \nabla \omega}{\omega} \alpha \rho S^2 + \alpha \frac{\rho}{u_t} P_k - \beta \rho \omega^2 \\
&u_t = \rho \frac{\alpha_1 k}{\max (\alpha_1 \omega, S F_2)}
\end{aligned} \tag{4.13}$$

F_1 and F_2 denote the SST blending functions described in Equation 4.7. The production term P_k reads as follows:

$$P_k = \min \left(\mu_t S^2, 10 \cdot C_\mu \rho k \omega \right). \tag{4.14}$$

The IDDES length scale in Equation 4.13 reads as follows:

$$\begin{aligned}
l_{IDDES} &= \tilde{f}_d \cdot (1 + f_e) \cdot l_{RANS} + \left(1 - \tilde{f}_d \right) \cdot l_{LES} \\
l_{LES} &= C_{DES} \Delta \\
l_{RANS} &= \frac{\sqrt{k}}{C_\mu \omega} \\
C_{DES} &= C_{DES1} \cdot F_1 + C_{DES2} \cdot (1 - F_1)
\end{aligned} \tag{4.15}$$

The filter length Δ in LES is:

$$\Delta = \min \left\{ C_w \max \left[d_w, h_{\max} \right], h_{\max} \right\} \tag{4.16}$$

where h_{max} denotes the maximum edge length of the cell. The empiric blending function in

Equation 4.15 is determined based on the following relations:

$$\begin{aligned} \tilde{f}_d &= \max\left\{\left(1-f_{dt}\right), f_b\right\} \\ f_{dt} &= 1-\tanh\left[\left(C_{dt1}\cdot r_{dt}\right)^{C_{dn}}\right] \\ r_{dt} &= \frac{v_t}{\kappa^2 d_w^2\sqrt{0.5\left(S^2+\Omega^2\right)}} \\ f_b &= \min\left\{2\exp\left(-9\alpha^2\right), 1.0\right\} \\ \alpha &= 0.25-d_w/h_{\max} \end{aligned} \tag{4.17}$$

The elevating function f_e in Equation 4.15 reads as follows:

$$\begin{aligned} f_e &= f_{e2}\cdot\max\left(\left(f_{e1}-1.0\right), 0.0\right) \\ f_{e1} &= \begin{cases} 2\cdot\exp\left(-11.09\cdot\alpha^2\right), \alpha\geq 0 \\ 2\cdot\exp\left(-9.0\cdot\alpha^2\right), \alpha<0 \end{cases} \\ f_{e2} &= 1.0-\max\left(f_t, f_l\right) \\ f_t &= \tanh\left(\left(C_t^2\cdot r_{dt}\right)^3\right) \\ f_l &= \tanh\left(\left(C_l^2\cdot r_{dl}\right)^{10}\right) \\ r_{dl} &= \frac{v}{\kappa^2 d_w^2\sqrt{0.5\left(S^2+\Omega^2\right)}} \end{aligned} \tag{4.18}$$

In addition to the model constants in the governing equations Equation 4.13, the constants are introduced in SST-IDDES model:

$$C_w = 0.15, C_{dt1} = 20, C_{dt2} = 3, C_l = 5.0, C_t = 1.87 \tag{4.19}$$

.

The present work adopted IDDES to gain an instantaneous view of the flow field of the platoons with different inter-vehicle spacings travelling through the tunnel. The flow involving recirculation, rotation, separation and boundary layers with adverse pressure gradients could be better simulated (Gritskevich et al. 2012).

4.1.5 Sliding Mesh

To accurately simulate the relative motion between the moving lorry platoon and the road tunnel, two main methods introduced in literature are the sliding meshing method and the

dynamic meshing method. The dynamic mesh approach enables the boundaries of a cell zone to be moved relative to the boundaries of other cell zones, hence adjusting the mesh accordingly. Because nodes in the domain's cells need to be updated as time passes, dynamic mesh solutions are unstable by default. In addition, the performance and computational sources of the dynamic mesh method are unsatisfied, and the mesh distortion is complex and difficult to control due to the mesh reconstruction (Chen et al. 2017).

Sliding mesh is a subset of general dynamic mesh. The whole domain, including the cells and the boundaries, move locksteps in a rigid body movement. Therefore, the cells defined by the grid points do not deform when the whole domain is moving. This technique has been widely used to simulate a vehicle travelling in a tunnel (Chen et al. 2017; Khayrullina et al. 2015; Liu, Hemida, and Liu 2014). The flow field is separated into two computational domains (see Figure 4.1). Moving domain II consists of the space around the lorry body, while stationary domain I encompasses the region far outside the platoon. A grid interface is used to represent the interplay between two different domains. The boundary of the moving domain is basically in the middle if the tunnel wall and lorry body (see Figure 4.1 (b)). To be specific, during the simulation, the moving sub-domain slides relative to stationary sub-domain along the interfaces without mesh generation at every time step, and thus the nodes do not need to be re-aligned at the interfaces.

In each time step, the fluxes across each grid point inside the non-conformal interface zones were computed. The intersection grids (points b to i in Figure 4.2) are determined at every time step to calculate the fluxes. The intersection grids are used to determine fluxes across the grid interface. Between two adjacent domains, physical information can be exchanged.

In order to study the surface pressure variation, a User-Defined Function (UDF) was added to the CFD code to simulate the surface pressures on the moving lorries. The UDF is a function based on C language that can be loaded dynamically into the ANSYS FLUENT to improve its standard features.

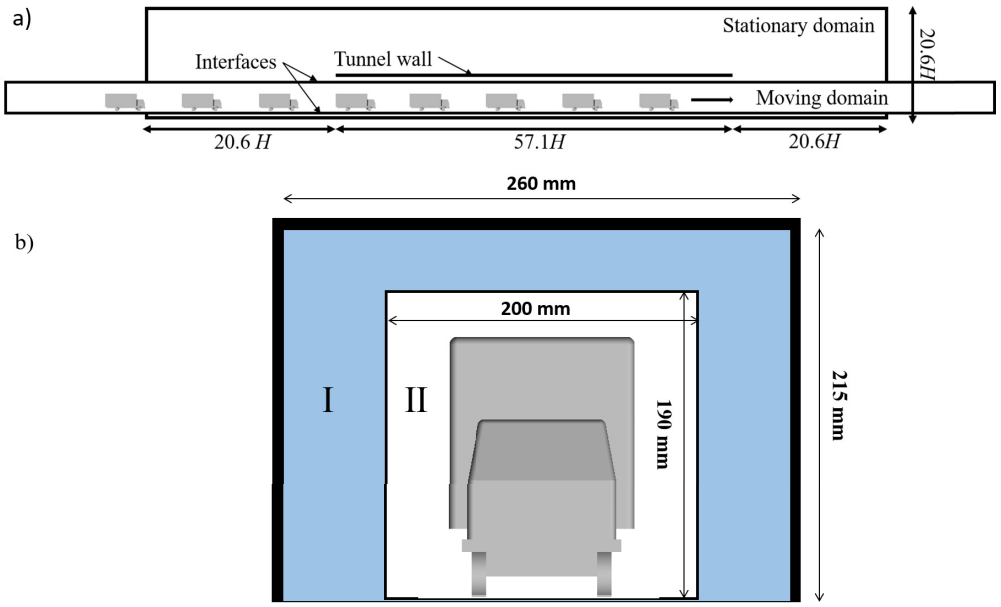

Figure 4.1: Schematic diagram of the stationary and moving domain.

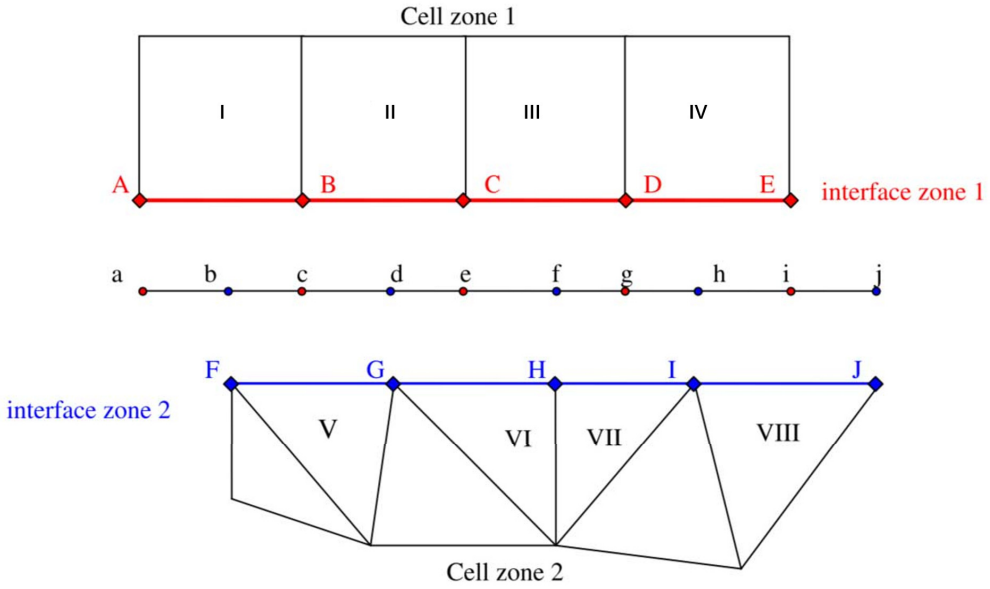

Figure 4.2: Schematic figure of sliding mesh technique for computing the flux across the interface (Chu et al. 2014).

4.2 Computational domain and boundary conditions

The computational domain consists of both stationary and moving sub-domains. The computational domain is illustrated in Figure 4.3. A coordinate system was defined such that the x-axis was aligned in the platoon travelling direction originating from the tunnel portal, the z-axis was in the vertical direction measured from the ground plane, and the y-axis was on the horizontal plane and perpendicular to the platoon travelling. The width and height of the stationary domain are $40.14H$ and $20.6H$, respectively.

Based on the best practice recommendations (Khayrullina et al. 2015; Chu et al. 2014), the numerical simulation of the blockage ratio must be no more than 15%. If the the blockage ratio of tunnel cross-sectional area to the whole computational domain cross-sectional area is between 5% and 15%, and the results must be corrected. In this work, the blockage ratio is 3.3% for large tunnel cases and 2% for small tunnel cases; thus, the calculation results do not need to be amended.

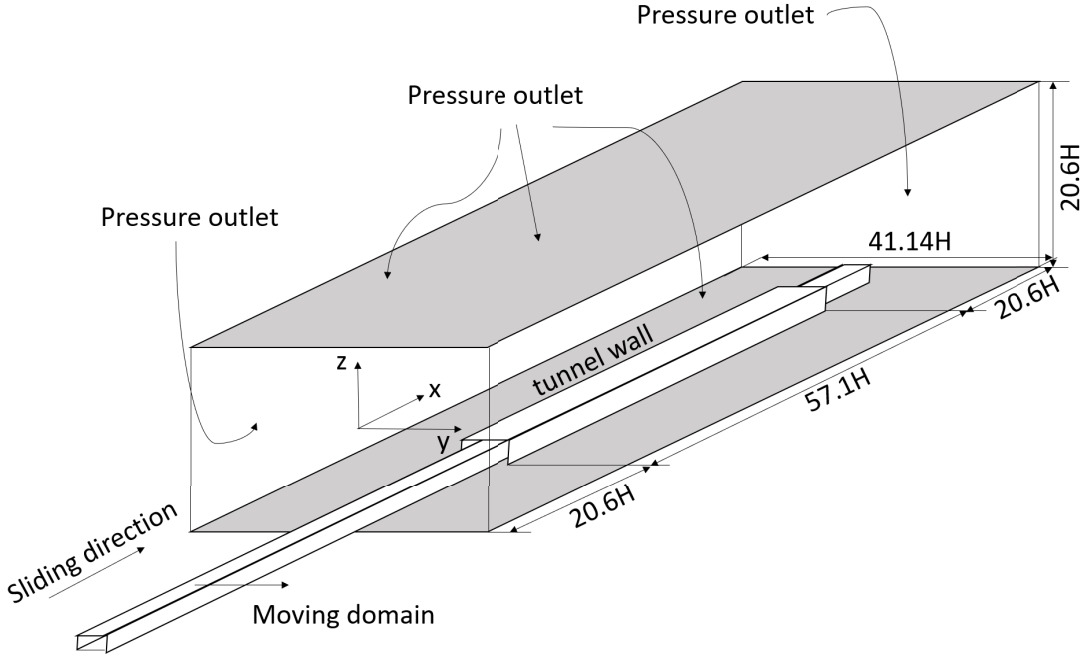

Figure 4.3: Overview of the computational domain for lorries in platoon travelling through a tunnel. The boundary conditions and the dimensions of the domains are also presented.

The boundary condition for the computational domain is also shown in Figure 4.3.

The front, top, back and side faces of the computational domain are defined as the pressure outlet boundaries and the reference pressure is 0 Pa. The no-slip wall boundary conditions were specified for the lorry's surface, ground plane and tunnel wall. To ensure the flow field is fully developed before the platoon enters the tunnel and avoid the influence of boundary conditions on the flow structure around the lorry platoon, the leading lorry in the platoon was initially placed at a distance 20.6H from the tunnel portal and stopped when the last lorry was outside the tunnel at a distance of 20.6H away from the exit. When two interfaces do not overlap, a temporary wall surfaces will be generated by default in ANSYS FLUENT.

4.3 Mesh generation scheme

The IDDES method is highly mesh-dependent because the blending process between the RANS and LES is greatly depended on the grid size. The surface grid of one lorry is shown in Figure 4.4 (a). Figure 4.4 (b) shows a horizontal cross-section of the whole domain meshes. The stationary domain is shown with a red colour. The computational meshes in the current work are structured hexahedral meshes generated by commercial software Ansys ICEM-CFD. Sufficient refinement close to the solid walls was made to resolve the critical flow features. On the lorry body ten prisms layer are added by O-block to solve the near wall gradient. Using the prism layer is crucial since the largest gradients are concentrated near the walls.

Three groups of meshes, coarse, medium, and fine, were adopted to check the independence of the meshes. The details of the meshes around the lorry surface are presented in Table 4.1. The minimum grid size on the tunnel and the lorry surface in the moving direction x was 0.0004 m and 0.009 m, respectively. In the published paper (Zhang et al. 2021), the coarse mesh is used as fine mesh. Although the y^+ value is above 30, which violates the requirement of the SST $k-\omega$ model's condition, the results are in excellent agreement with the experimental measurements. Later work refines the grid and reduces the y^+ value to roughly 1. The Courant-Friedrichs-Lewy (CFL) number (CFL= $V_{plat}\Delta t/\Delta x$, where Δx is the length of cells and Δt is the time step) remains below 1 with a small number of localized exceptions occurring. This minor infringement on the stringent CFL requirement has no significant effect on the simulation (Xia et al. 2017; Wang et al. 2017).

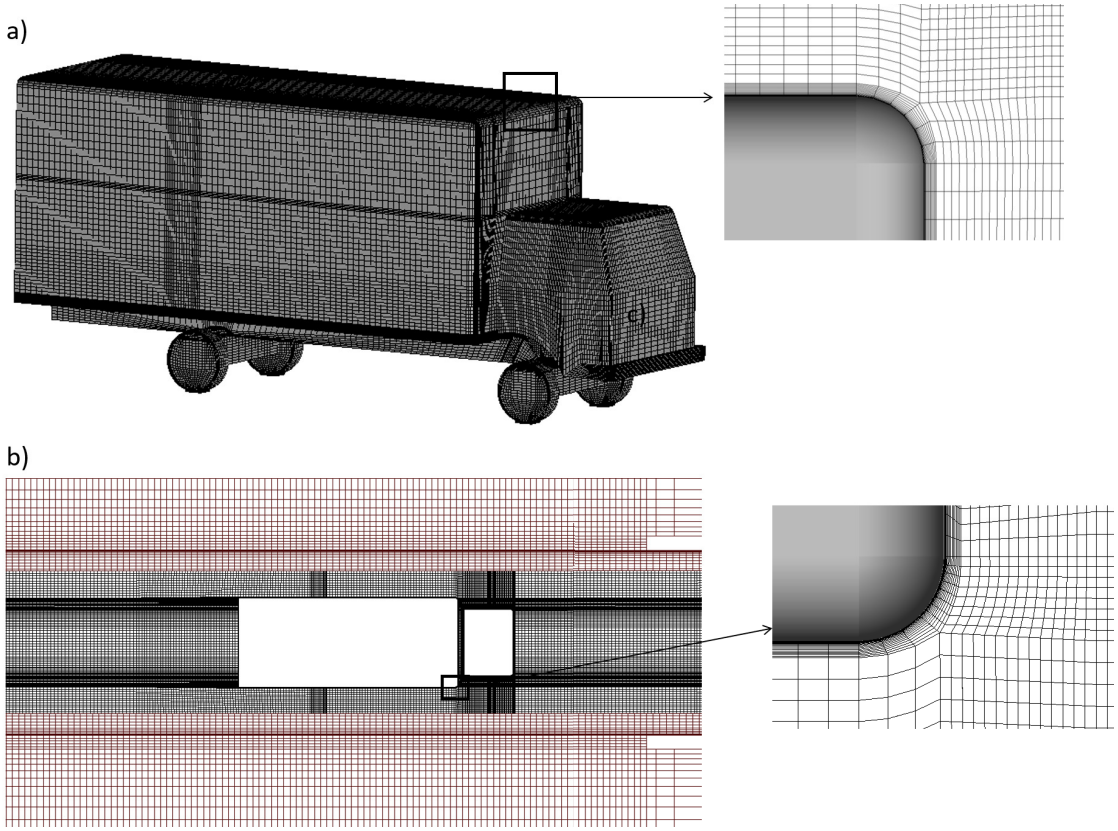

Figure 4.4: Computational grid used in this study: (a) surface mesh around the lorry cab and box; (b) horizontal cross-section of the whole domain at $z/H = 0.57$.

The pressure coefficients C_p of the IDDES simulations based on three different numbers of cells are shown in Figure 4.5. The testing point is located at a position of $0.45H$ above the ground and $0.14H$ away from the lorry body. The differences in the positive pressure peaks between the fine and middle meshes are relatively small. However, the results using coarse mesh have relatively large deviations, especially at $37 < \tau < 38$. The horizontal velocity at the same testing point are also computed in Figure 4.5 (b). Results of the middle and fine grids correspond well to each other. As for the surface pressure variation of the Tap 1 on Lorry 1 (see Figure 4.5 (c)), results of the fine and middle grids show good agreement with each other, however the coarse grid produces slightly different surface pressure before the lorry entering the tunnel and after the lorry leaving the tunnel. Therefore, the fine mesh was used in this study.

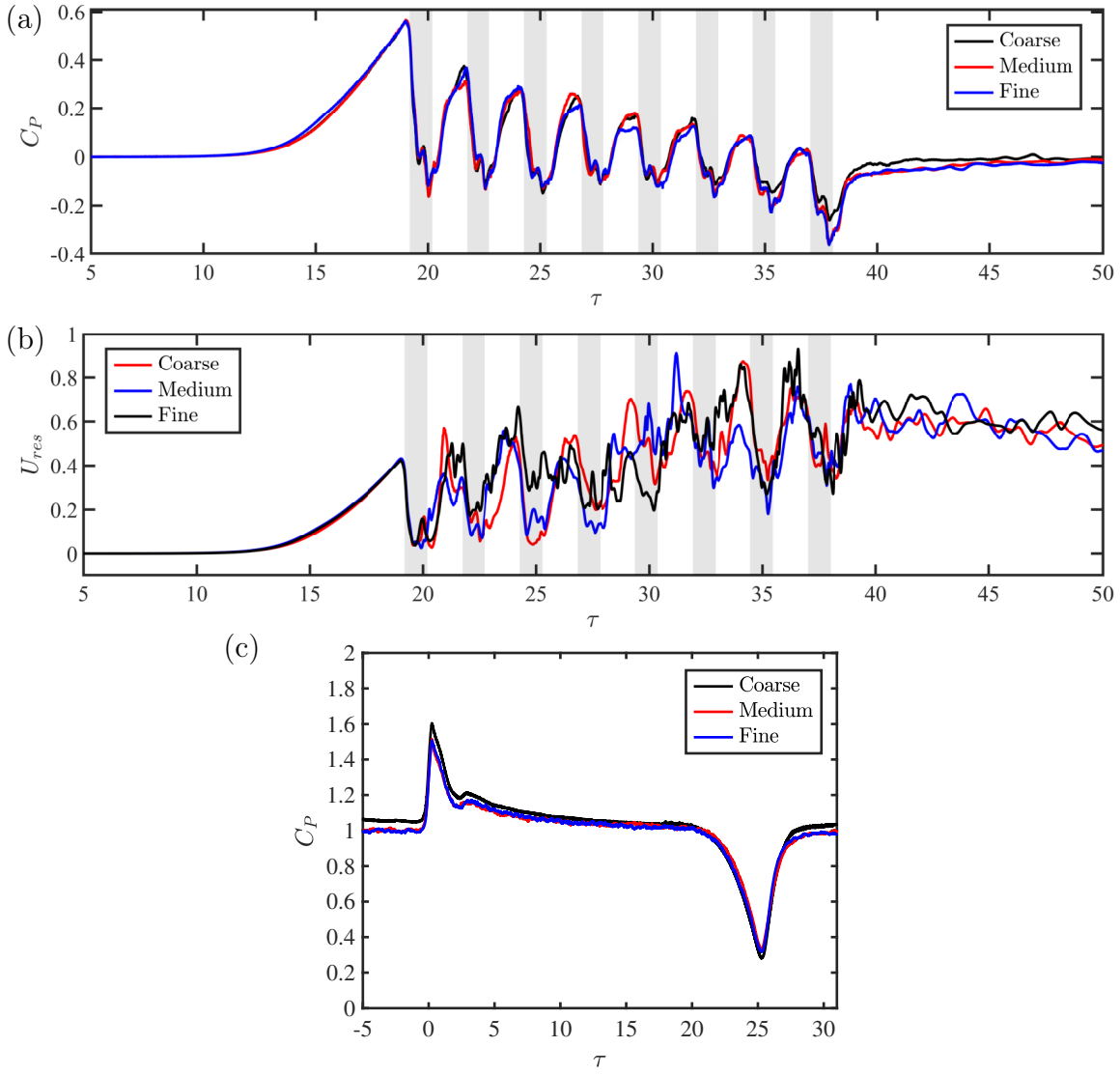

Figure 4.5: (a) Pressure coefficients for different mesh densities. The shaded rectangles indicate the time duration for each lorry to pass the probes; (b) Horizontal velocity for different mesh densities; (c) Surface pressure coefficient of Tap 1 on Lorry 1 for different mesh densities.

	Coarse	Medium	Fine
Averaged y^+	33	2	1
Number of mesh cells in moving domain (million)	20.3	28.2	35.5
Number of mesh cells in stationary domain (million)	14.6	14.6	14.6
Total number of mesh cells (million)	34.9	42.8	50.1

Table 4.1: The parameters for the grid sensitivity testing in the simulations.

4.4 Calculation setting

This program performed the simulations by commercial CFD software ANSYS FLUENT 18.2 based on a pressure solver with the finite volume method. The method is listed in Table 4.2. The Semi-Implicit Method for Pressure-Linked Equations (SIMPLE) algorithm was adopted to solve the velocity and pressure coupling equations.

A bounded central differencing method was adopted to solve the momentum equation. The low numerical diffusion of this scheme makes it an excellent choice for a wide variety of problems. Unfortunately, it often leads to non-physical oscillations in the solution region. The problem is aggravated by the LES region's typically very low turbulent diffusivity on a subgrid scale. The bounded central differencing scheme is developed mostly on the Normalized Variable Diagram (NVD) methodology (Leonard 1991), as well as the convection boundedness requirement. This scheme is a composite NVD scheme composed of a first-order upwind scheme, a blended second-order upwind and central differencing scheme, and original central differencing scheme. Notably, the first-order scheme is only employed when the Convection Boundedness Criterion (CBC) is violated. The second-order upwind scheme was applied to solve the k and ω transport equations. The time-advancement was conducted using a second-order implicit scheme, and the time step was set to $1 \times 10^{-4}s$, in keeping with studies in Hemida and Krajnović (2009) and Niu et al. (2017). For every step of time, the number of iterations was 50. The simulations are preliminary performed by using HPC system BlueBEAR at the University of Birmingham and then finally performed Langchao at Southern University of Science and Technology. The Langchao system runs on Intel Xeon E5-2690v3. In the present study, in general, 6 nodes with a total of 120 cores are

Parameter	Method
Pressure-Velocity Coupling	SIMPLE
Pressure	Second Order
Momentum	Bounded Central Differencing
Turbulent Kinetic Energy	Second Order Upwind
Turbulent Dissipation Rate	Second Order Upwind
Transient formulation	Second Order Implicit

Table 4.2: The simulation solution method.

employed for each case.

4.5 Validation of the numerical simulations

To validate the CFD results, Figure 4.6 shows the simulated normalised velocities and pressure coefficients at the position of multi-hole probe B together with the ensemble-averaged pressure from experiments. The trends of the pressure data obtained from the numerical simulations are consistent with the experimental results. Whilst the velocity data deviate a lot in detail, the numerical data mostly fall within one standard deviation of the experimental values. To understand the discrepancy in velocity data, note that although the gap in the ground plane has been modelled in the simulations, the exact boundary conditions for this region are difficult to define. Another reason could come from the multi-hole probe. The velocity component in the direction of platoon motion is sensitive to the alignment of the probe. The ± 45 degree cone of acceptance of the probe might also restrict the detection of air flow (Soper 2016; Soper et al. 2017).

Figure 4.7 compares the surface pressure coefficients between the simulations and the experiments. Figure 4.7 (a) and (b) represent the data at the cab front and rear points of the leading lorry, respectively. It is seen in Figure 4.7 (a) that the data from the numerical simulations compare well with the experimental results. When the lorry is running inside the tunnel, the simulated frontal surface pressure decreases slower than the experimental cases.

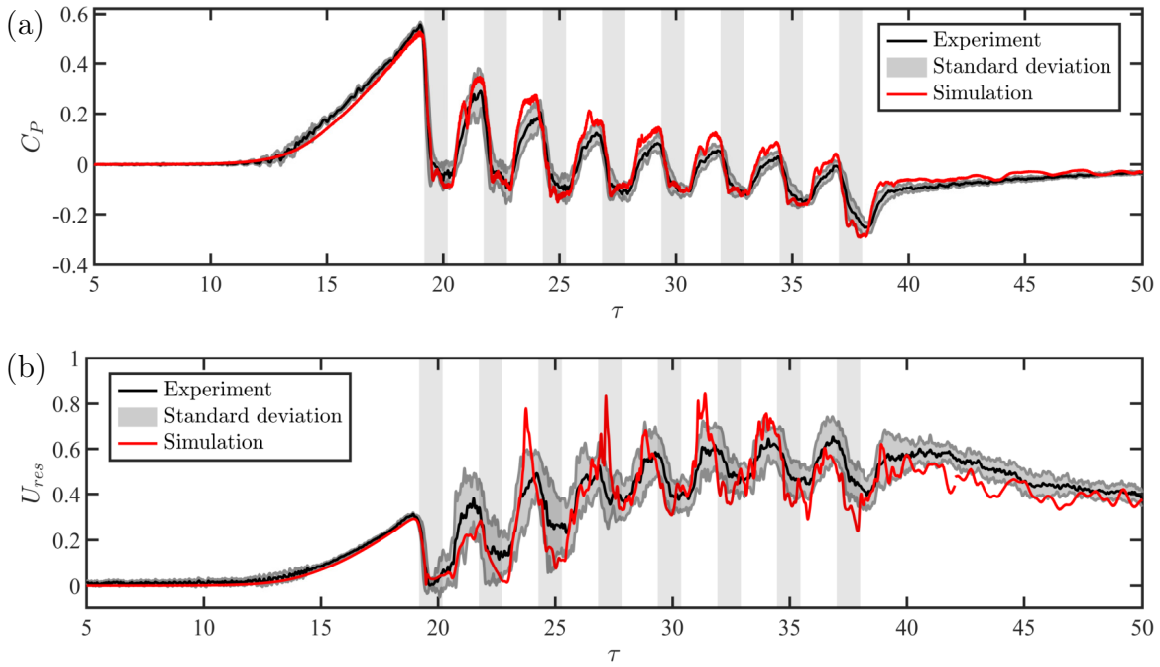

Figure 4.6: Comparison between the ensemble-averaged values from experiments and numerical simulations measured at the position of multi-hole probe B: (a) normalized horizontal velocity; (b) pressure coefficient.

This can be ascribed to a gradual decrease in the speed of the platoon in the experiments (as a result of the rig friction and the aerodynamic drag aforementioned), in contrast to the constant speed used in the simulations. The experimentally measured C_p drops from around 1 prior to the inlet to around 0.9 after leaving the tunnel (beyond entry. Indeed, direct measurement with laser sensors shows that the $\tau = 27$), suggesting that the platoon speed at the exit is 95% of that at the platoon speed reduces by 4.6%, which provides support for the conclusion that the lower C_p of the experiments is due to the slowing down of the lorry model when running through the tunnel. For the rear region of the lorry where separated flow exists (Figure 4.7 (b)), the simulation data are also in good agreement with the experimental values (typically within one standard deviation).

The last important quantity to be validated is the mean drag coefficient as defined below:

$$C_d = \frac{F_x}{\frac{1}{2}\rho V_{\text{plat}}^2 A_f} \tag{4.20}$$

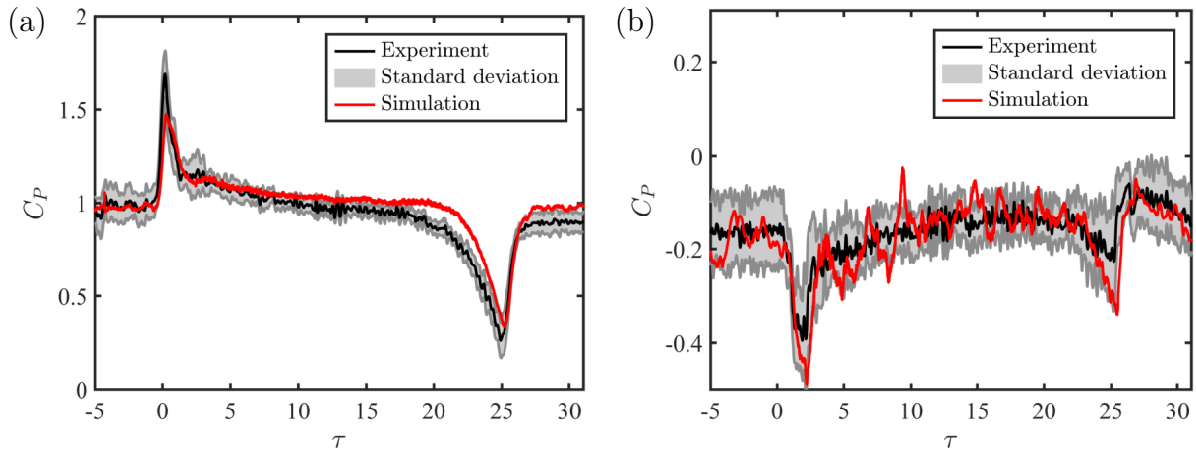

Figure 4.7: The surface pressure coefficients from the experiments and simulations. The monitoring positions are at (a) the central point at front face and (b) central point at rear face.

Here, F_x is the effective drag force, and A_f is the reference area derived from the projected area of the lorry. V_{plat} is the nominal platoon speed aforementioned. Note that the calculation of mean drag coefficient requires integrating pressure over a discrete geometry of the lorry surface and thus sufficient data should be acquired to make the integration (Dorigatti et al. 2015). One of the sources of error in this method is not considering friction. Extending a polygon from each tapping point half-way to the edge of surface generates discretized areas or to the adjacent point. The drag coefficients can be estimated as:

$$C_d = \frac{F_x}{\frac{1}{2}\rho V_{\text{plat}}^2 A_f} = -\frac{\sum_i \left(\overline{C_{P_i}} A_i n_i \times x\right)}{A_{ref}} \tag{4.21}$$

where A_i is the discretised area of pressure tapping i and n_i represents the normal unit vector. The $\overline{C_{P_i}}$ is the ensemble average pressure coefficient. The leftmost negative sign is inserted to ensure that the adopted coordinate system contains positive drag coefficients. The drag was calculated using 12 pressure taps: five on the cab front, five on the rear (see Figure 4.8 (b)), and two on the front of the box-section (see Figure 4.8 (a)).

In this work, the pressures along the lorry surface were experimentally measured at fourteen positions only. This low resolution of pressure data prevents us from obtaining a reliable drag coefficient. Therefore, the numerical model is validated here by comparing the drag coefficient simulated in the open air with the experimental results obtained by Robertson

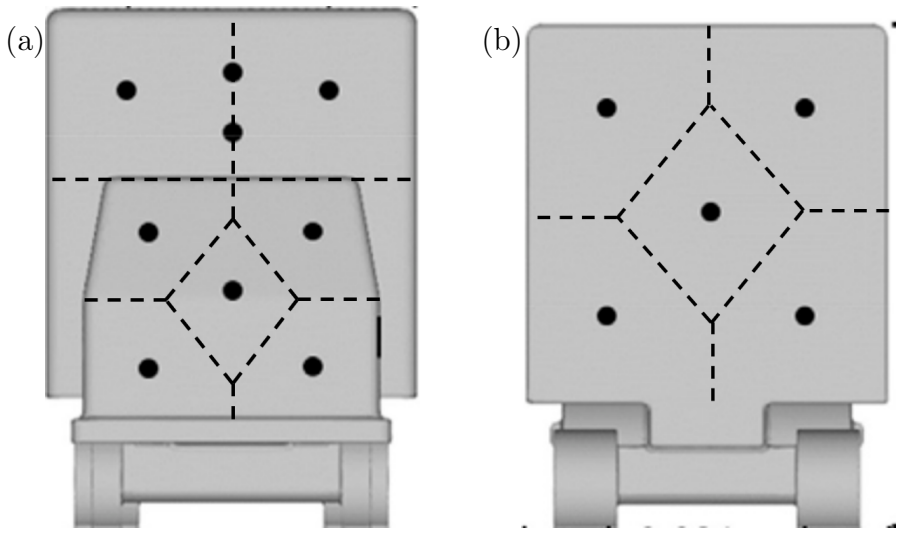

Figure 4.8: The discretized regions used for calculating the drag coefficients.

et al. (2019). The error bars in Figure 4.9 indicate the root-mean-square (rms) magnitudes for the simulations, while for the experiments they are uncertainties calculated by applying the uncertainty transfer formula based on the uncertainties of the pressure coefficients at all the locations. The directly simulated drag values and the integrated value from the simulated surface pressure (indicated by the blue line) are also presented in Figure 4.9.

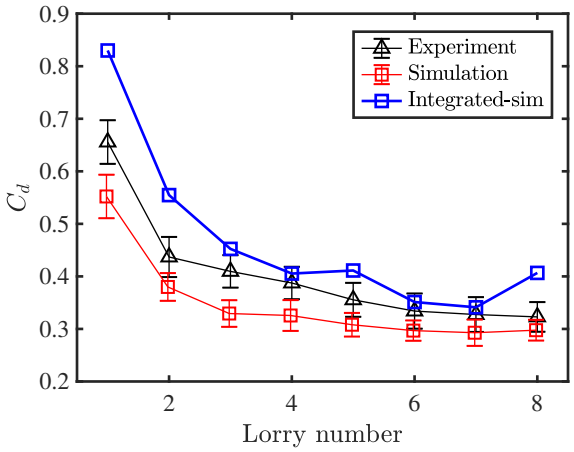

Figure 4.9: Mean drag coefficient in the open air from the experiments and simulations. The experiment results are obtained by Robertson et al. (2019)

It is seen that there is a discrepancy between the experimental and numerical results, which may be due to the relatively low resolution of surface pressure taps in the experiments.

As noted by Robertson et al. (2019), the experimental data only provides an estimated drag coefficient and the uncertainty may be less than the true error, because the assumption of uniform pressure across the discretised area might be inaccurate. In addition, the skin fiction is not considered in his work. Compared with the direct simulation drag coefficient with the integrated value from all surface elements, the integral value of the 12-points simulated surface pressure overestimates the drag coefficient. Therefore, it is logical to assume that experimental drags using the same calculation method will also be overestimated. Nevertheless, it will be shown in conclusion that there is a good agreement between the experimental and IDDES values in the surface pressure coefficients for lorries both inside the tunnel and in the open air. This gives us confidence in the reliability of the present results.

4.6 Simulation cases

To investigate the effect of the inter-vehicle spacing, blockage ratio and the lane location, multiple simulations were conducted. Figure 4.10 shows that six inter-vehicle spacing, as well as the single lorry cases are discussed in this study. Experiments are also conducted to evaluate the simulation methods at the maximum inter-vehicle distance (1.5L). Initially, the plan included experimental studies with 0.5L and 1.0L spacing, but owing to damage to the experimental equipment, the idea was forced to be abandoned. The experiments of 0.5L, 1.0L and 1.5L platoon in open air was conducted by Robertson et al. (2019) and Robertson, Soper, and Baker (2021).

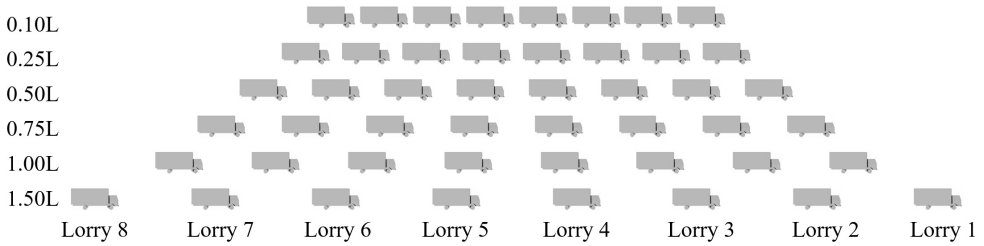

Figure 4.10: Diagram of the different platoons to be simulated.

Four cases are simulated: Open Air (OA), Small Tunnel (ST), Large Tunnel (LT) and Right lane in the Large Tunnel (RLT) (see Figure 4.11). The open air cases have been

widely studied in the literature and are also simulated as reference work. The small tunnel cases are identical to the experiments and are compared to open air cases to investigate the tunnel's effect on aerodynamics of long platoon. The large tunnel cases are designed to investigate the effect of the blockage ratio. The width and height of the tunnel increased from 0.26m and 0.215m of small tunnel to 0.52m and 0.275m to large tunnel, respectively. The blockage ratio is 35.8% for the small tunnel and 15.3% for the large tunnel. Finally, the large tunnel right lane cases is to investigate the effect of multi-lane. The traffic lane of the whole platoon is shifted 0.11m from the middle to the right of the travelling direction. The effect of the inter-vehicle spacing is discussed in each case separately.

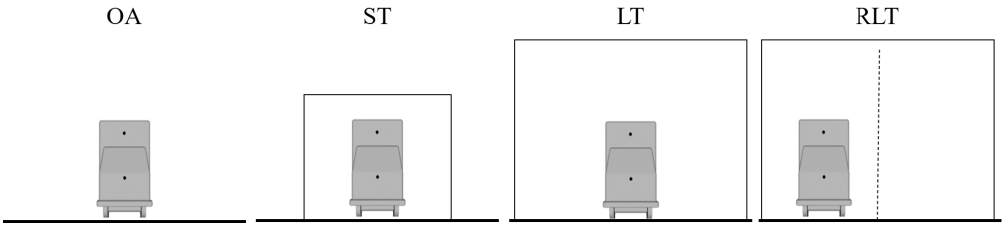

Figure 4.11: The platoon running in (a) open air, (b) small tunnel, (c) large tunnel and (d) right lane in the large tunnel.

Table 4.3 provides a summary of the author's experiments and simulations, as well as the results of related investigations from other researchers. The experiments of platoon with $0.5L, 1.0L$ and $1.5L$ spacing travelling in the open air were conducted by Dr. Francis Robertson (Robertson et al. 2019). The experimental results are used in numerical validation in Section 4.5. The following chapters are mainly based on the simulations.

<table>
<tr><th colspan="2" rowspan="2"></th><th colspan="2">The authur</th><th colspan="2">Other researchers</th></tr>
<tr><th>Experiment</th><th>Simulation</th><th>Experiment</th><th>Simulation</th></tr>
<tr><td colspan="2">Open air</td><td>–</td><td rowspan="4">Single
0.1L 0.25L 0.5L
0.75L 1.0L 1.5L</td><td>single
0.5L 1.0L 1.5L
(Robertson et al. 2019)</td><td>Single
(Patel et al. 2019)
Single 0.5L
(He et al. 2019)</td></tr>
<tr><td rowspan="3">Tunnels</td><td>ST</td><td>1.5L</td><td colspan="2" rowspan="3">–</td></tr>
<tr><td>LT</td><td>–</td></tr>
<tr><td>RLT</td><td>–</td></tr>
</table>

Table 4.3: The experiments and simulations conducted by the author and related research by other scholars.

Chapter Five

Results and Discussion of a single lorry

In this chapter, the aerodynamics of a single lorry is discussed. Inspection of the flow parameters of lorry under isolated conditions provides some information into the behaviors of expected properties within a platoon of varied cases.

A typical commercial vehicle Leyland DAF 45-130 was selected. This type of vehicle has been extensively investigated as a single vehicle (Quinn et al. 2007; Patel et al. 2019). The drag coefficient from the current work of a single lorry in the open air are listed and compared with the previous simulation and experiments (see Table 5.1). The differences of current simulated drag coefficient over wind tunnel result is 6.1%. However, in the wind tunnel, the ground is static, there are no relative movement between ground and lorry. The results show that the moving model simulation shows better agreement with the moving vehicle experiment conducted by Robertson et al. (2019) than with wind tunnel measurement. Browand (2005) states that almost 90% of the aerodynamic drag is generated by the pressure differential from the front to the rear of the vehicle while driving and additional 10% is due to the friction losses in the boundary layer (see Figure 5.1). In comparison, an airfoil is a streamlined body with little drag caused by friction between the airfoil and the surrounding air. The amount of drag from each source is dependent on the designed shape of the lorry.

The airflow induced by vehicles in the tunnel, known as the "piston effect", is driven by the tunnel wall adjacent to the moving vehicle (see Figure 5.2). When a vehicle is travelling in open area, the air pushed by the vehicle can flow in all directions to the sides of

	Drag coefficient	Differences of the drag over wind tunnel result %
Current simulation	0.62	6.1
Experiment (Robertson et al. 2019)	0.63	4.6
DDES (He et al. 2019)	0.67	1.5
LES (Patel et al. 2019)	0.61	7.58
Wind tunnel	0.66	

Table 5.1: Drag coefficient comparisons between current research and previous research.

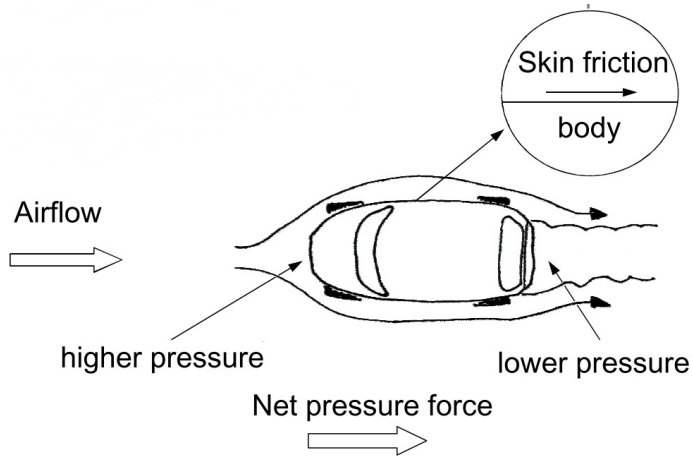

Figure 5.1: Drag component of a single vehicle (Browand 2005).

the vehicle. When the vehicle enters a tunnel, however, the ability of the vehicle to disperse air to the sides diminishes. A significant amount of air will flow in front of the vehicle, as the air unable completely flow to the rear region of the vehicle. This results in the formation of a high-pressure zone in front of the vehicle and a low-pressure zone behind it, as well as the formation of a wake that acts as a sucker for air from behind the vehicle. Considering that the bulk flow generated by the piston effect is moving in the same direction as the vehicle, the approaching velocity may be lower than in the open air, and this may weaken flow separation.

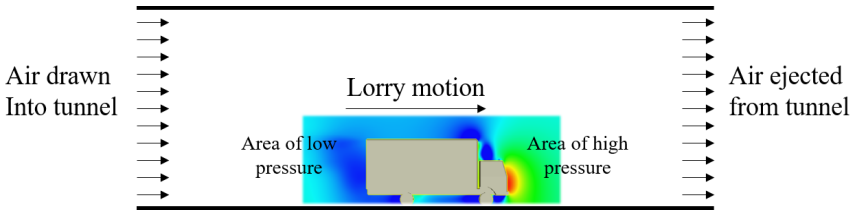

Figure 5.2: Schematic representation of the piston effect of a single lorry in the tunnel.

Figure 5.3 shows the time-averaged horizontal velocity, pressure and y-axis component velocity field of a single lorry on the horizontal plane in open air, large tunnel, right lane of large tunnel and small tunnel. The piston effect is clearly observed in the small tunnel and less so in the large tunnels. In the tunnels, the pressure surrounding the entire lorry box is negative, whereas in the open air, the negative pressure area occurs only at the front edge of the box. As the decrease of the tunnel size, the pressure in the wake and box side region decreases and the horizontal velocities in the side and wake region increases. As for the effect of the traffic lane, the box side region on the near wall side and the cab side region on the opposite side are identified as having higher horizontal velocities. The high pressure zone in front of the vehicle slight deviates from the symmetrical position towards the near wall. The pressure on the near wall size of the lorry is slightly lower than the other size, and the wake pressure distribution deviates slightly from the symmetrical position. The y-axis component velocity field on the right panel also shows that the side wall will restrict the passage of air to the wall near the cab and to the wake zone.

The iso-surfaces of the second invariant of velocity gradient tensor, Q, are utilized to visualize the flow structures around the lorries. Iso-surfaces with a positive Q value indicate regions where the rotation's strength exceeds the strain, implying the presence of vortical

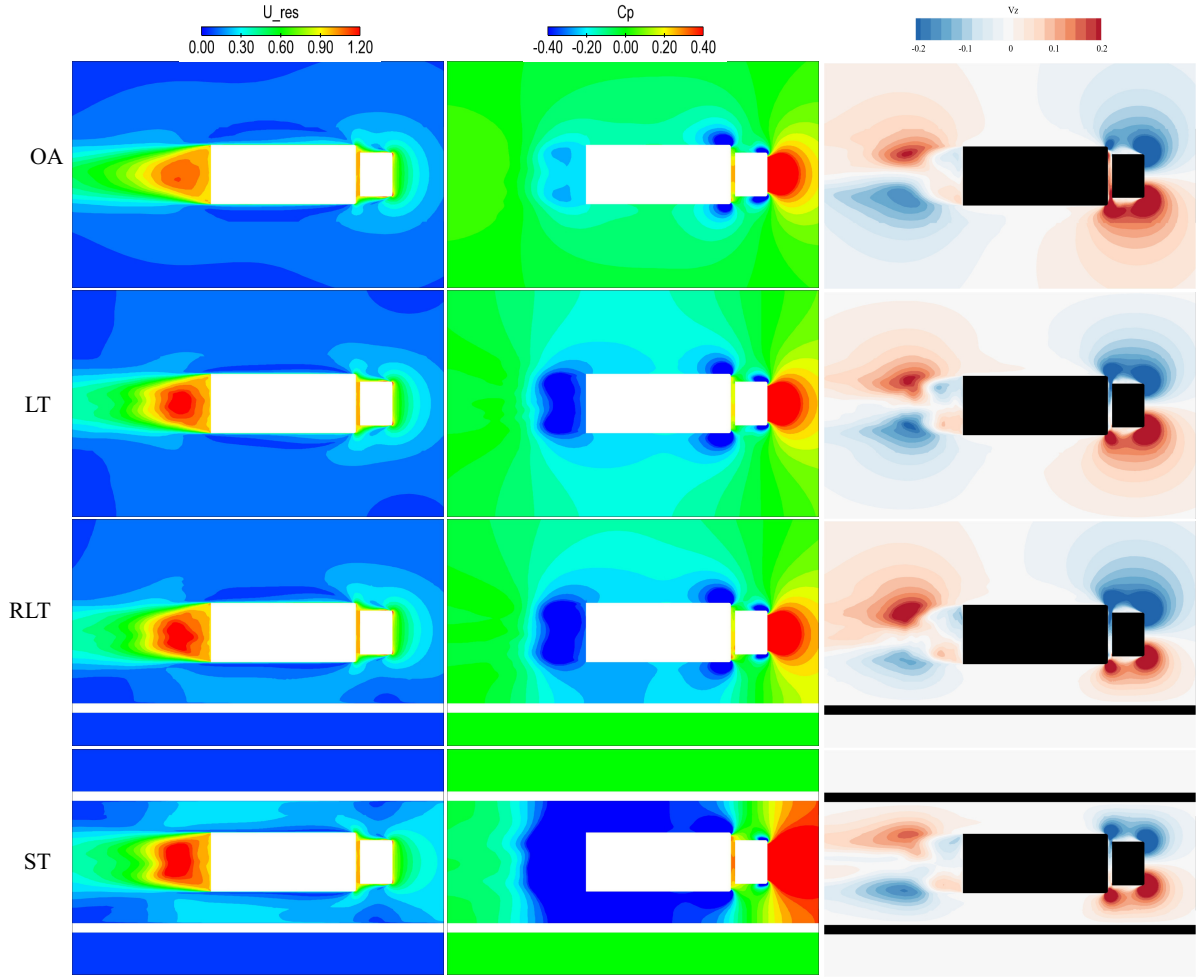

Figure 5.3: Left panel: The horizontal velocity fields of a single lorry for four cases; Middle panel: The horizontal pressure distribution of a single lorry in four cases; Right plane: y-axis component velocity field.

structures (Jeong and Hussain 1995). Q is defined as,

$$Q = -\frac{1}{2}\left(\bar{S}_{ij}\bar{S}_{ij} - \bar{\Omega}_{ij}\bar{\Omega}_{ij}\right), \tag{5.1}$$

where $\bar{S}_{ij}$ and $\bar{\Omega}_{ij}$ are the symmetric and anti-symmetric parts of the velocity gradient tensor. Q represents the local balance between shear strain rate and vorticity magnitude.

Patel et al. (2019) introduced the detailed flow structure of a single vehicle. Figure 5.4 illustrates a schematic figure of the main vortex cores. $Vc1$ formed at the leading edge of the lorry and then re-attached on the top surface. $Vc2$ illustrates the position of vortices shed off from the sides of the lorry. $Vc3$ illustrates a circulation region at the front of the container box induced by a powerful positive pressure. The flow through the wheels of the lorry generates $Vc4$. $Vc5$ is created by the rear edge of the lorry box and represents the original zone of recirculation. The $Vc6$ is created by air sinks from the top, as well as the air from beneath the lorry pushes up because the low pressures behind the vehicle. $Vc7$ is caused by the collection of vortices in the wake of the lorry. The $Vc7$ are known as hairpin vortices.

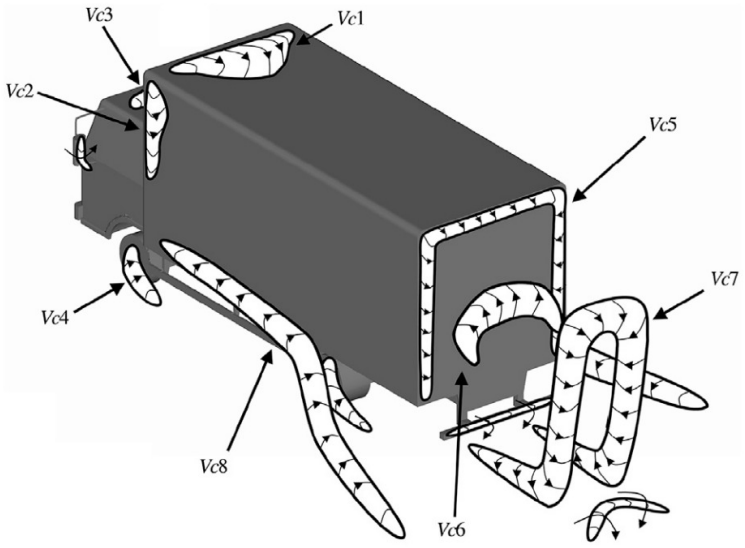

Figure 5.4: Schematic figure of the main time-averaged vortex structures (Patel et al. 2019).

Figure 5.5 shows the streamlines time-averaged flow field behind a single lorry in different cases. The mean flow fields are calculated by averaging the intermediate 4-meters when lorry is travelling inside tunnels and the corresponding section in the open air. It is

depicted how the air flows along the boundary of the lorry box and separates at the sharp corner. The free shear layer is a thin layer that exists between the fast-moving free stream and the stagnant air behind the vehicle box. High Reynolds numbers lead to unstable shear layers that roll up into separate eddies as shown in the side view. Entrainment of the stagnant air by the large eddies reduces the gradient of velocity between the two zones. The mixing layer is the turbulent region between the free-flowing air and the stagnant air. Vortical structures can be seen in the images of unsteady flow from the top perspective. Through the aforementioned entrainment mechanism, the mixing layer decreases the pressure of the near-wake region and, as a result, the rear pressure. Due to the low base pressure, the mixing layer deviates away from the symmetrical position and arrives the stagnation point called the reattachment zone. The mixing layer balances the air evacuated from the dead air with the reflux from the stagnation point. As a result of this motion, the near wake exhibits visible recirculation zones. The ring-type recirculating zones, also named "toroidal", is shown in Figure 5.4. The $Vc6$ and $Vc7$, which is shown in Figure 5.4, can be easily identified in Figure 5.5. The upper vortex $Vc6$ in the side view becomes larger in tunnels than in open air. When examine the effect of traffic lane by comparing the $Vc7$ vortex horizontal view in two large tunnels, the vortex in the far wall side becomes slightly larger than the near-wall side.

As for the aerodynamics forces, the tunnel wall impose constrains flow around the model. The BR is critical in causing the wall interference effect in vehicle. It has a considerable effect on drag coefficient as well. The drag coefficient of a single lorry is 0.96 ± 0.03 in small tunnel (BR=35.8%) and 0.71 ± 0.02 in the large tunnel (BR=15.3%), both of which are higher than the value in the open air (0.62 ± 0.02). The drag coefficients and their root mean square values for a single lorry in different cases are listed in Table 5.2.

When a lorry travels in the middle lane of the tunnel, the side force is expected to be zero. The side force coefficient is defined as follow:

$$C_s = \frac{F_y}{\frac{1}{2}\rho V_{\text{plat}}^2 A_f}, \tag{5.2}$$

where F_y is the effective side force. The side force coefficients C_s of a single lorry travels in different cases are also listed in Table 5.2. Note that the side force coefficient in the tunnel is averaged over the intermediate 4-meters when each lorry is travelling inside the tunnel.

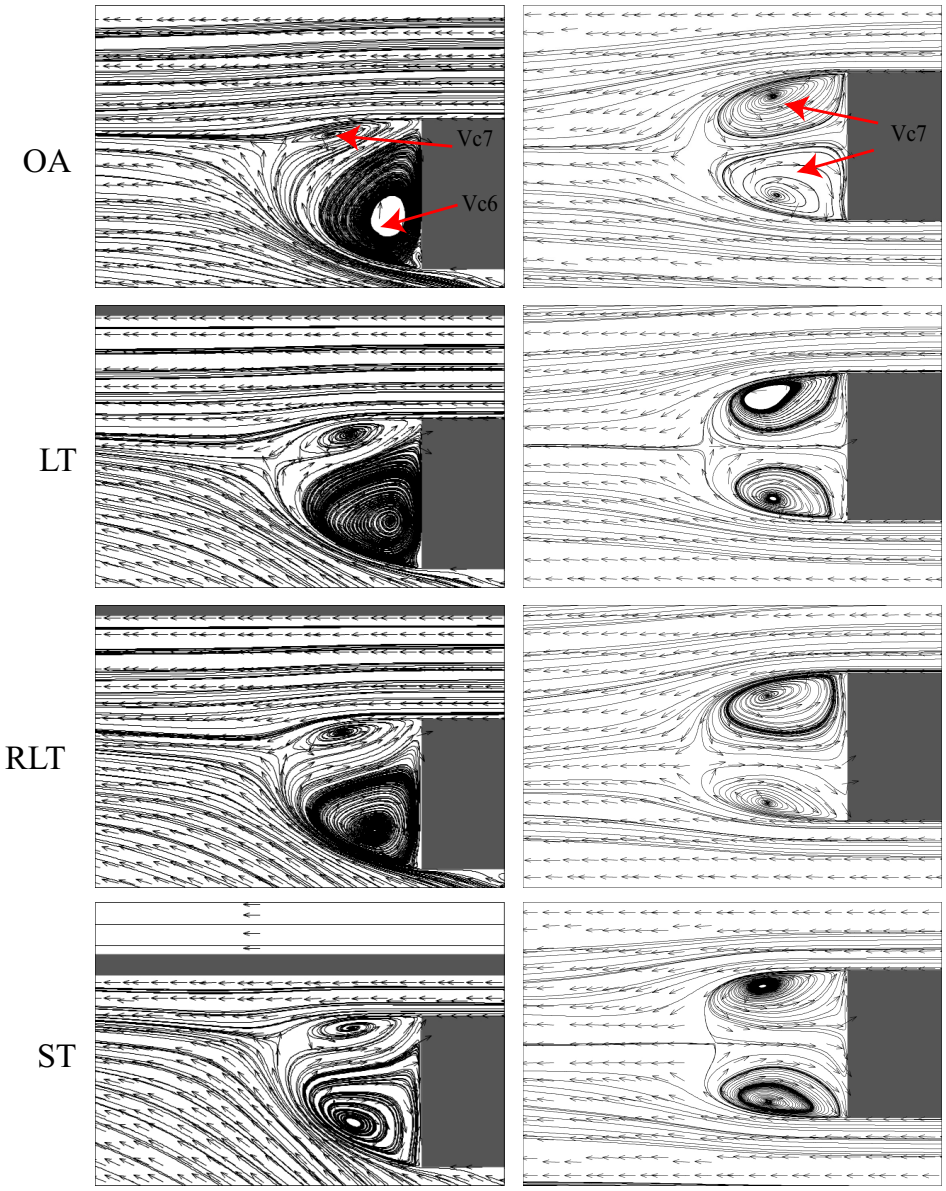

Figure 5.5: Streamlines for time-averaged flow field behind a single lorry in different cases. Left panel illustrates the side view at $y/H = 0$. Right panel shows the top view at $z/H = 0.57$.

This non-zero value is primarily caused by turbulence and an insufficient amount of time for averaging. The side force coefficient Cs in the right lane of the large tunnel is 2.7 times that in ST and LT cases, owing to the asymmetric flow field. However, the r.m.s value is even an order higher than the side force coefficient itself. The side force coefficients of a single lorry in these cases are too small to consider the laterally instability. The conclusion that the asymmetrical traffic lane has any discernible influence on the side force of a single lorry is inconclusive.

	C_d	r.m.s	C_S	r.m.s
Open air	0.62	0.02	0.0035	0.0386
Small tunnel	0.98	0.03	0.0026	0.0461
Large tunnel	0.71	0.02	0.0027	0.0419
Large tunnel right lane	0.71	0.02	0.0072	0.0413

Table 5.2: The coefficients of side force and their rms values for a single lorry travelling in four different scenarios.

Figure 5.6 compares the instantaneous flow structures around the a single lorry running in the middle of the tunnels and in the open air. A large number of vortices are generated around the cab, box side and rear regions, due to the bluff nature of the box lorries. However, some differences in the vortical structures can be found for the single lorry in the tunnel: fewer vortices are appearing at the lorry sides. As mentioned above, the piston effect induced by movement of the vehicle leads to a lower approach velocity, which results in weaker flow separations. While the piston effect weakens in the large tunnels, side vortices appear to increase to the level of those seen in the open air. Traffic lane position has no significant impact on the flow structure.

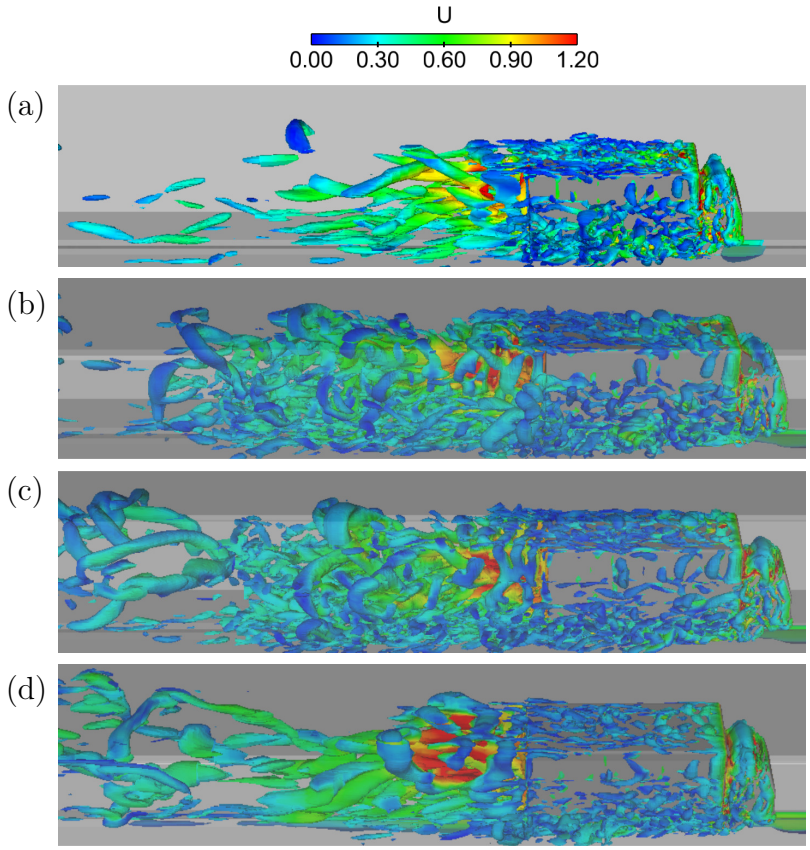

Figure 5.6: The instantaneous iso-surface of Q of a single lorry in each of the following cases: (a) open air, (b) large tunnel, (c) right lane of the large tunnel and (d) small tunnel. Here, Q is set to be $50000s^{-2}$ and coloured by the normalised velocity.

Chapter Six

Results and Discussion of the effect of tunnel [1]

In this chapter, the effect of the tunnel on the aerodynamic performance will be thoroughly investigated. Platoon running in a small tunnel with a $1.5L$ spacing is selected for this purpose. Note that this separation distance can reflect typical road conditions more appropriately. It is not uncommon for lorries to travel at a separation comparable to this distance, while smaller separations could only be achieved through autonomous vehicle technology. It is also worth mentioning that the aerodynamics of platoons in the open air were qualitatively similar for different separation distances from $0.5L$ to $1.5L$ (Robertson et al. 2019). Therefore, the selection of the separation distance was not a major concern in the present chapter. The focus of this chapter is to compare different behaviours of lorry platoons in the tunnel and in the open air.

[1] The results in this Chapter have been published in Journal of Wind Engineering and Aerodynamics (Zhang et al. 2021).

6.1 Slipstream properties

Figure 6.1 shows the aerodynamic flow around the lorry platoon, in terms of the simulated normalised horizontal velocity in the slipstream. The data monitored in the tunnel and in the open air are plotted together for comparison. In the open air, the flow created by the moving platoon is characterised by a continually growing boundary layer punctuated with pulse peaks near the front of each lorry (Robertson et al. 2019). While in the tunnel, the piston effect induced by the movement of the lorry platoon causes the bulk flow through the tunnel. Therefore, the horizontal velocity starts rising long before the arrival of the first lorry. It is also observed in Gilbert, Baker, and Quinn (2013b), where a train passes through two vertical walls and a partially-sealed tunnel, that the velocity begins to increase further upstream of the leading frontal face than in the open air. Due to the pressure-driven piston effect, the velocity in tunnels and partially enclosed tunnels increases between the points where the train's nose enters the tunnel and it passes the sensor. The bulk flow in the tunnel also leads to a smaller approach flow velocity for the platoon. Fluctuations are recorded due to the complex flow patterns. The peaks associated with the lorries are more obvious in the tunnel than in the open air. It is further seen that the horizontal velocity does not approach the maximum value until the sixth lorry passes, suggesting that at least this number of vehicles are needed to study the aerodynamic phenomena of a long platoon in the tunnel.

Figure 6.2 presents the simulated pressure coefficients at different heights from the ground level and at different distances away from the lorry. Also shown in the figure are the simulated data for the same platoon configuration running in the open air. The pressure coefficients for different positions have a similar trend as time evolves. To be specific, the pressure coefficients rise until the first lorry arrives at the positions where the cobra probes were installed. When the first lorry passes by the cobra probes, the slipstream pressures due to the so-created turbulent flow have lower values than the ambient fluid. The pressure coefficients therefore drop drastically after the first lorry leaves the location of the probes. As the platoon moves forward, all the lorries induce similar variations in the local pressure. Thus, there are eight peaks as seen in the figure, corresponding to eight lorries in the platoon. These phenomena are the same in both the tunnel and the open air. The first positive peak

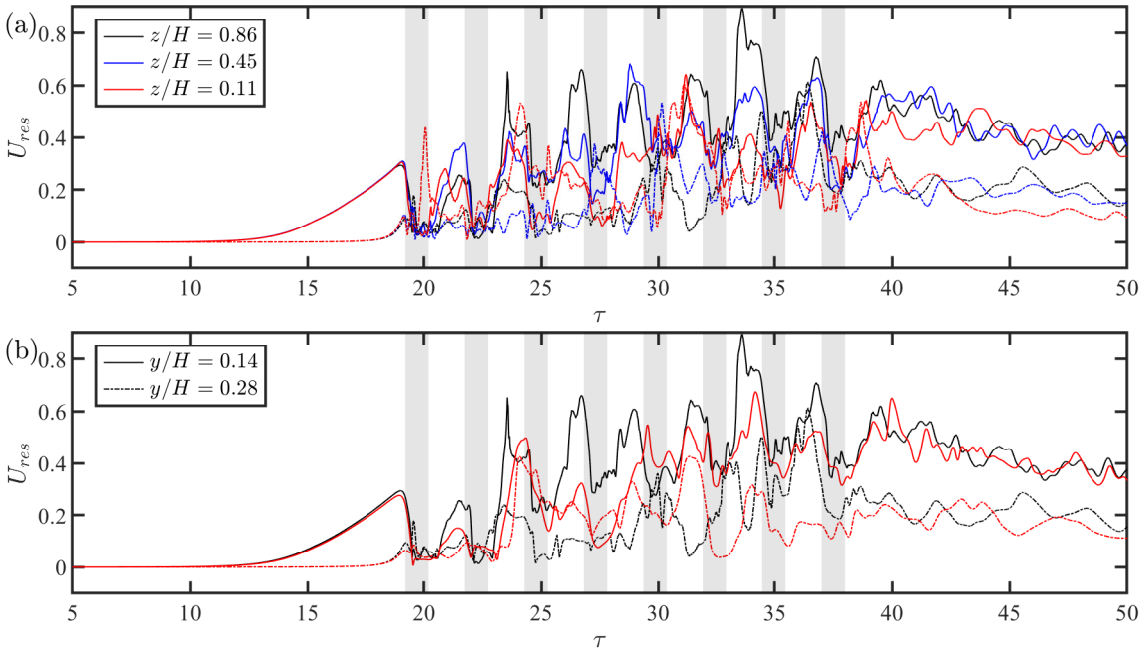

Figure 6.1: The simulated normalised horizontal velocity as a function of the normalised time: (a) at various heights from the ground level with the same location of $y/H = 0.14$ away from the lorry side; (b) at different locations away from the lorry side with the same height of $z/H = 0.86$ from the ground level. The solid lines denote the results obtained in the tunnel and the dotted lines denote the results obtained in the open air. The shaded rectangles indicate the time duration for each lorry to pass the probes.

induced by the leading lorry and the last negative peak induced by the last lorry follow the same pattern as a train passing through a partially-sealed tunnel, as described in Gilbert, Baker, and Quinn (2013b) and Baker (2014). The intermediate pressure fluctuations induced by the leading face of each lorry resembles those of the 33% loaded freight train passing through a tunnel (Iliadis et al. 2019). However, since the tunnel in (Iliadis et al. 2019) was fully sealed, the peak positive pressure caused by the downstream carriage of the train did not exhibit a gradual decline.

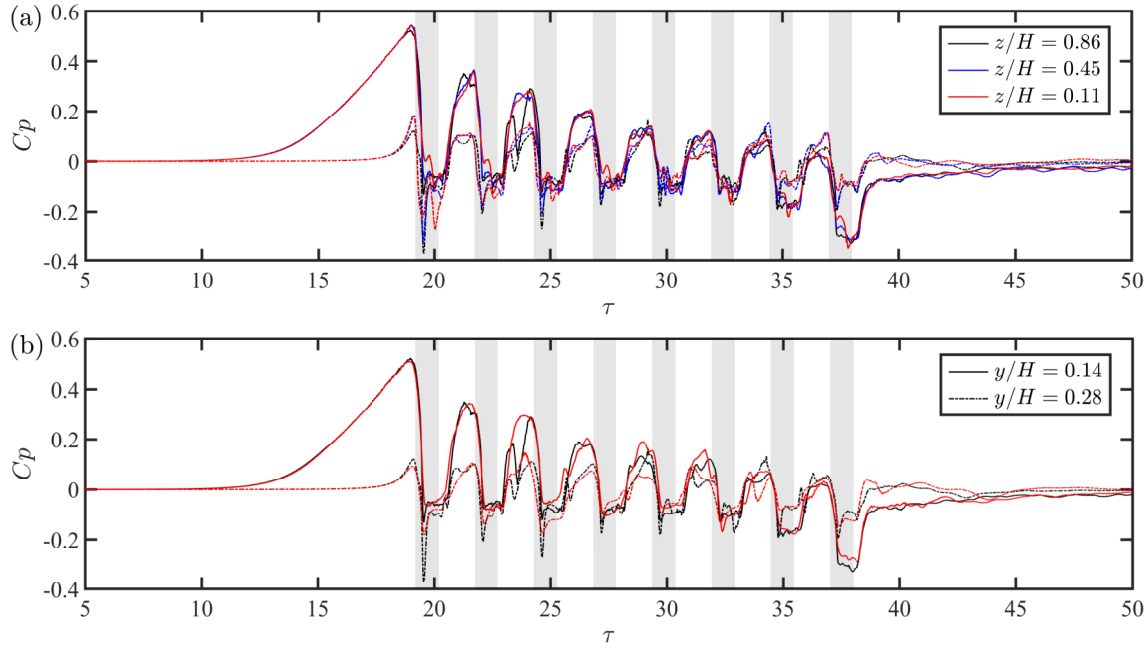

Figure 6.2: The simulated temporal variations of the pressure coefficients: (a) at various heights from the ground level with the same location of $y/H = 0.14$ away from the lorry side; (b) at different locations away from the lorry side with the same height of $z/H = 0.86$ from the ground level. The solid lines denote the results obtained in the tunnel and the dotted lines denote the results obtained in the open air. The shaded rectangles indicate the time duration for each lorry to pass the probes.

However, when considering the magnitude of the pressure coefficient, significant differences are observed between the data in the tunnel and in the open air. When the platoon runs in the tunnel, the air around the lorries is largely forced to flow parallel to the travelling direction of the platoon because of the spatial confinement. This results in a slower

dissipation in the frontal pressure. Therefore, the first peak of pressure coefficient reaches a value as large as 0.55 in the tunnel, while the value in the open air is about 25% of the former. This difference gets progressively smaller for the following lorries and the pressure coefficients for different situations become almost identical for the fifth to seventh lorries in the platoon. On the other hand, as less airflow is able to penetrate into the rear region of the platoon in the tunnel, the low-pressure behind the last lorry is strongly intensified, leading to a great fall in the value of pressure coefficient (as low as -0.25). This is in strong contrast to the almost constant value (around -0.1) of the negative peaks for the platoon in the open air. Note that the above differences in the pressure coefficient are observed for all the positions shown in Figure 6.2. Since frontal and rear pressure difference contributes a large part to the drag of a lorry (another part is skin fiction) (Vardy 1996), these much larger pressure variations in the tunnel indicate the drag coefficients might be different when the platoon passes by compared to the case in the open air.

To have a better understanding of the aerodynamic flow created by the lorry platoon in the tunnel, the numerical results are presented for detail. Figure 6.3 presents the top view of the horizontal velocity at the height $z/H = 0.57$ above the ground. The transient velocity fields at three distinct times during the platoon passing through the tunnel are shown, together with the results in the open air. The highest speed appears in the rear regions and a small frontal region of all the lorries, regardless of in the tunnel or in the open air. However, when the platoon is running inside the tunnel, stronger flows are induced in the frontal and rear regions of the platoon. The velocity in the regions between each lorry is also larger than that in the open air. For the lateral sides of the platoon, the influenced regions expand gradually as the platoon moves forward. While the sides of the first two lorries have a relatively weak airflow, the horizontal velocity around the last four lorries increases to a constant value of 0.6 inside the tunnel. These findings are in good agreement with the experimental results as shown in Figure 6.1.

Figure 6.4 shows the corresponding TKE of the velocity fields in Figure 6.3. It is seen that high turbulent kinetic energy value is observed in the rear regions of all the lorries. This is originated from small-scale turbulent structures due to the large-scale flow separations in these regions. Interestingly, the TKE seems to be weaker for some intermediate lorries in the tunnel than in the open air, suggesting that the transient flow created by these lorries is

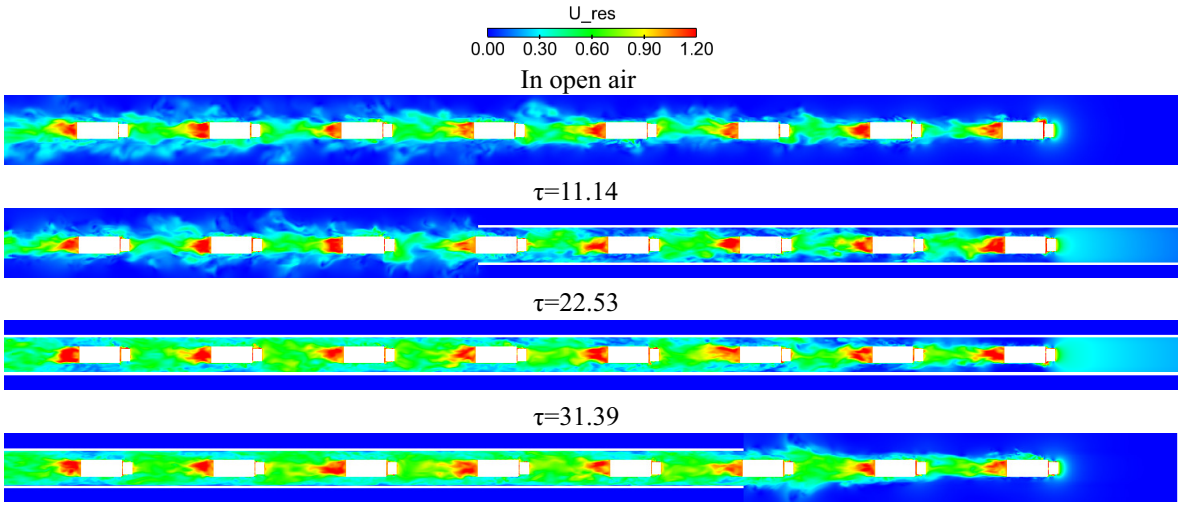

Figure 6.3: The simulated velocity fields during the lorry platoon passing through the small tunnel at three distinct times on the horizontal plane of $z/H = 0.57$. The top panel shows the data in the open air for comparison.

less fluctuating.

Figure 6.5 shows the side view of the pressure distribution at $y/H = 0.076$. The results reveal a significant piston effect induced by the movements of the lorry platoon inside the tunnel. As the platoon enters the tunnel, the pressures at the cab front of the leading lorries increase greatly, especially for the first one. When the whole lorry platoon is inside the tunnel, the frontal positive pressure continuously decreases from the leading lorry to the last one, which is consistent with the experimental results shown in Figure 6.2. Moreover, the experimentally-observed smaller positive pressure at the front region and larger negative pressure at the rear region of the last lorry are more clear here. As the platoon begins to leave the tunnel, the pressures around the lorries reduce again quickly, with the frontal positive pressures of some lorries (e.g., the second and the third ones) even smaller than those in the open air.

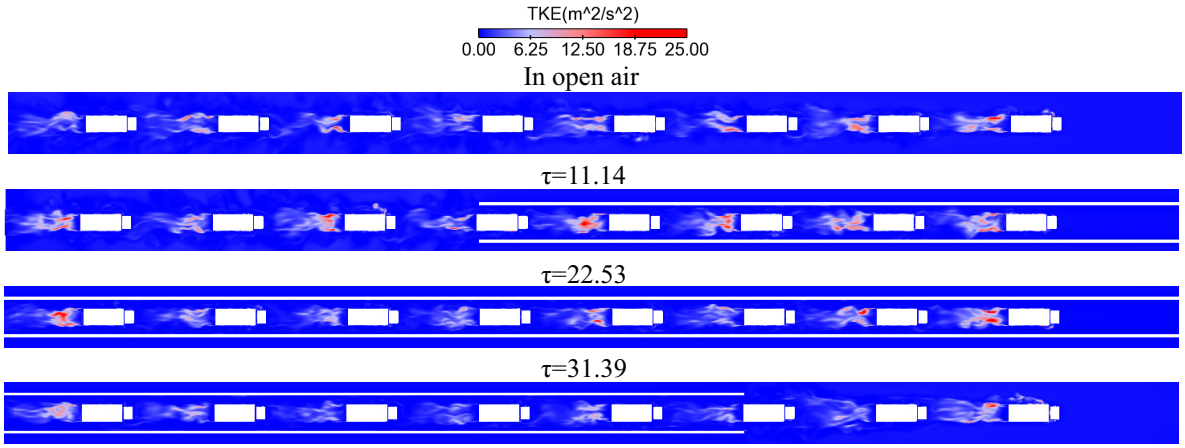

Figure 6.4: The instantaneous turbulent kinetic energy during the lorry platoon passing through the tunnel at three distinct times on the horizontal plane of $z/H = 0.57$. The top panel shows the data in the open air for comparison.

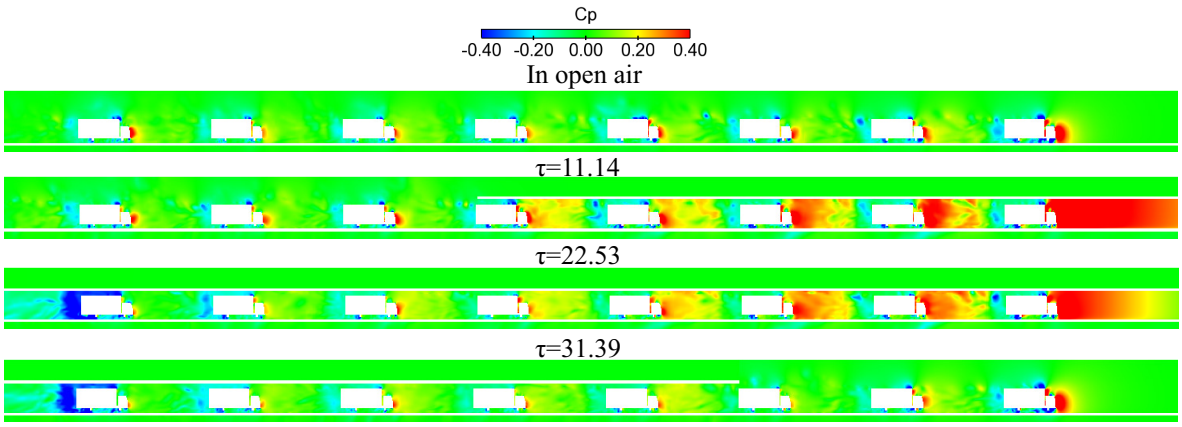

Figure 6.5: The pressure distribution during the lorry platoon passing through the tunnel at three distinct times on the vertical plane of $y/H = 0.076$. The top panel shows the data in the open air for comparison.

6.2 Flow structures

To have a closer look at the aerodynamic flow created by the platoon, the iso-surfaces of the second invariant Q are used to extract the flow structures around the lorries. Figure 6.6 compares the instantaneous flow structures around the first, the fifth and the last lorries running in the middle of the tunnel and in the open air. Based on the analysis of slipstream above, the overall flow field for all the intermediate lorries is similar, especially when compared to the lorries at each end, despite the slight difference caused by the development of the slipstream. Thus, only Lorry 5 is used as a representative of the intermediate lorries. The distributions of the vortices around the leading lorries are similar in these two cases. As shown in Figure 6.6 (a) and (b), a large number of vortices are generated around the cab, box side and rear regions, due to the bluff nature of the box lorries. However, some differences in the vortical structures can be found for the platoon in the tunnel: fewer vortices are appearing at the lorry sides. This difference is also observed but less obvious for the fifth and the last lorries as shown in Figure 6.6 (c) to (f). As mentioned in Section 6.1, the piston effect induced by the movement of the platoon leads to a lower approach velocity, which results in weaker flow separations. Thanks to the shielding effect, there are fewer vortices around the fifth and the last lorries compared to those around the leading lorries in both the tunnel and the open air.

Figure 6.7 compares the streamlines at the centreline plane in the frontal region of three representative lorries in the platoon. As clearly indicated in Figure 6.7 (a) and (d), the recirculation region close to the frontal edge of the lorry box is obviously larger in the open air than in the tunnel for the leading lorry. This phenomenon is also identified in the same region of the fifth lorry (see Figure 6.7 (b) and (e)). When it comes to the last lorry, the separation almost disappears compared to the leading lorries due to the shielding effect in both the tunnel and the open air.

Figure 6.8 compares the corresponding streamlines in the rear region. The figure shows two counter-rotating recirculation vortices in the near wake region. The most noticeable difference in the flow structures between the lorries travelling in the tunnel and in the open air is the size of the bottom vortex and the upper vortex. It is clear that the presence of the tunnel enlarges the upper vortices for all the lorries in the tunnel. As will be shown in

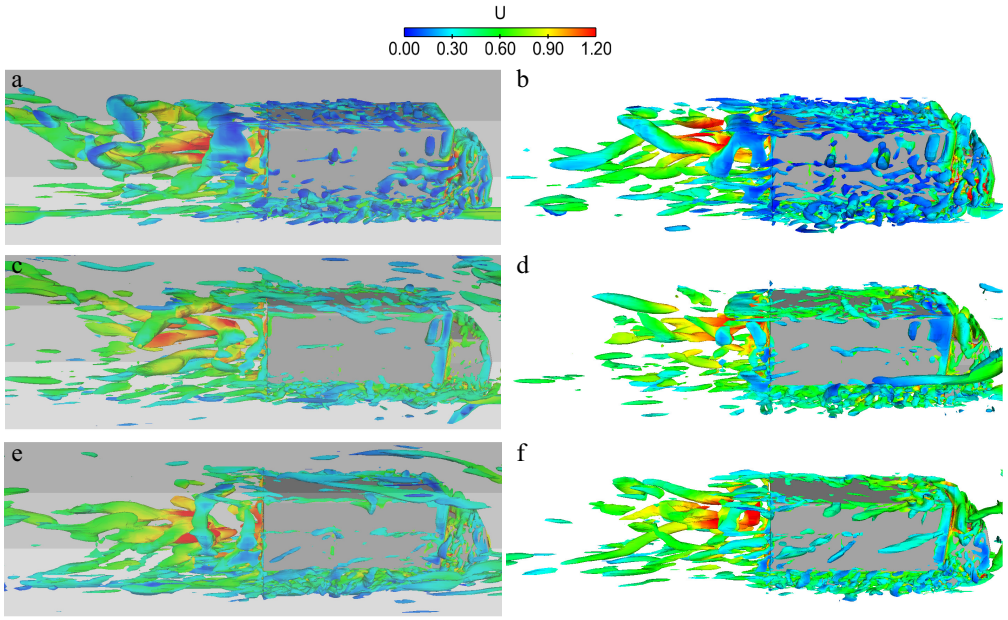

Figure 6.6: The instantaneous iso-surfaces of the second invariant Q. Left panel: (a), (c) and (e) are the lorries 1, 5 and 8 in the tunnel. Right panel: (b), (d) and (f) are the lorries 1, 5 and 8 in the open air. Here, Q is set to be $50000s^{-2}$ and coloured by the normalised velocity.

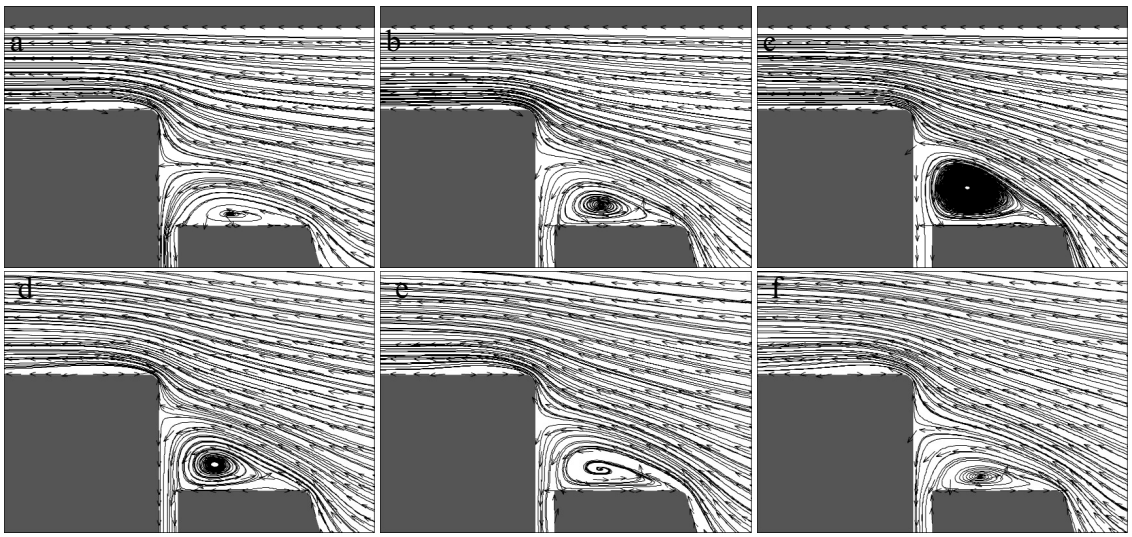

Figure 6.7: Illustrations of the frontal flow structures of three representative lorries in the platoon at $y/H = 0$. Top panel: (a), (b) and (c) are the lorries 1, 5 and 8 in the tunnel. Bottom panel: (d), (e) and (f) are the lorries 1, 5 and 8 in the open air.

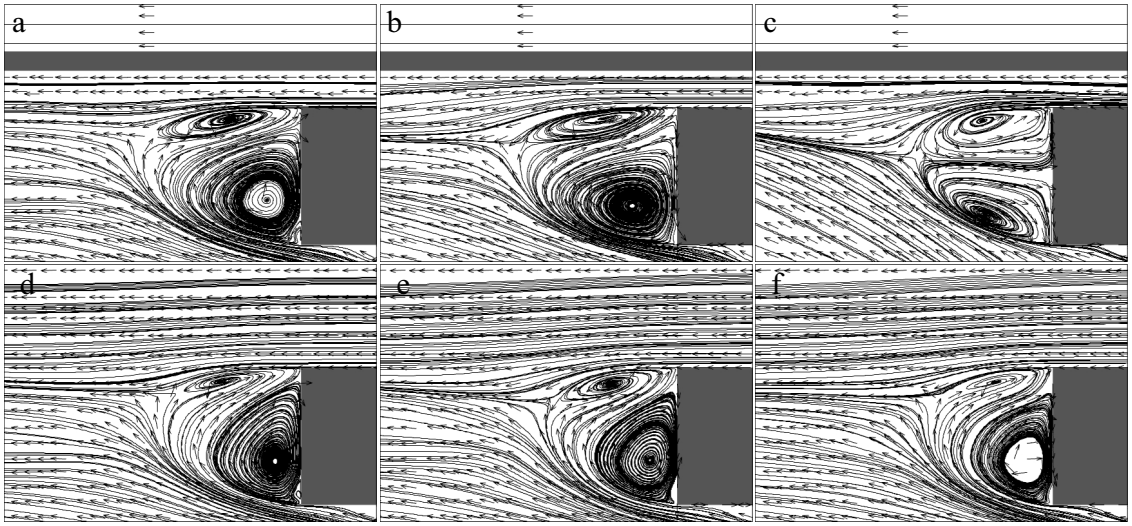

Figure 6.8: Illustrations of the wake flow structures of three representative lorries in the platoon at $y/H = 0$. Top panel: (a), (b) and (c) are the lorries 1, 5 and 8 in the tunnel. Bottom panel: (d), (e) and (f) are the lorries 1, 5 and 8 in the open air.

next section, these differences in flow structures provide direct support for interpreting the surface pressure results.

6.3 Surface pressure analysis

As the aerodynamic flow created by the platoon running in the tunnel is largely different from that in the open air, it is natural to expect that the pressure distributions on the lorries' surfaces are also different. However, in contrast to the case in the open air, the flow field around the platoon is strongly unsteady, and the positions of the lorries relative to the tunnel change with time. In order to study the surface pressure variation, a user-defined function was added to the CFD code to simulate the surface pressures on the moving lorries.

Figure 6.9 presents the time history of the simulated surface pressure coefficient C_P at two typical surface positions of each lorry in the tunnel and in the open air. Note that the data is aligned with respect to the time when each lorry arrives at the entrance of the tunnel. The shielding effect is obvious for the results shown in Figure 6.9 (a) and (b). In

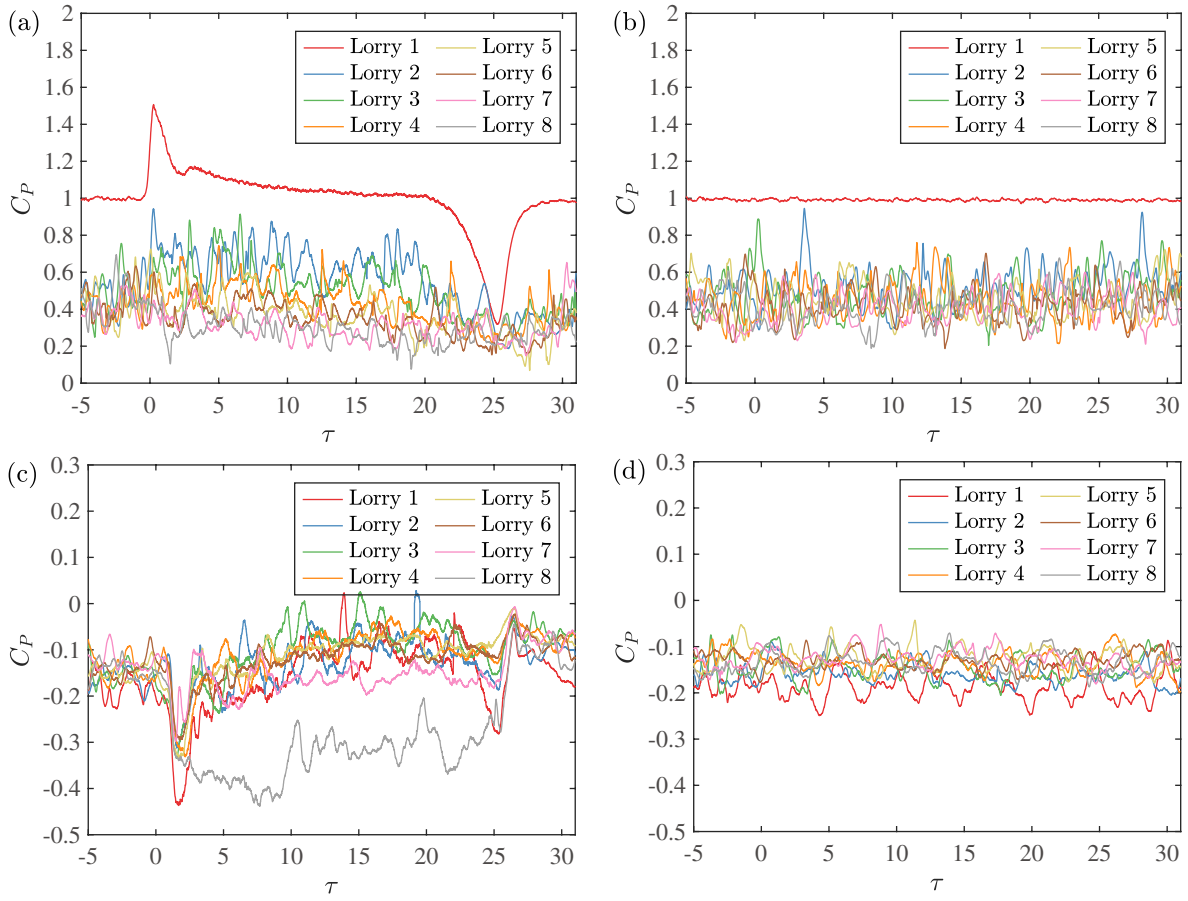

Figure 6.9: The simulated surface pressure coefficients of all the lorries as a function of the normalised time: (a) cab front in the tunnel; (b) cab front in the open air: (c) box rear in the tunnel; (d) box rear in the open air.

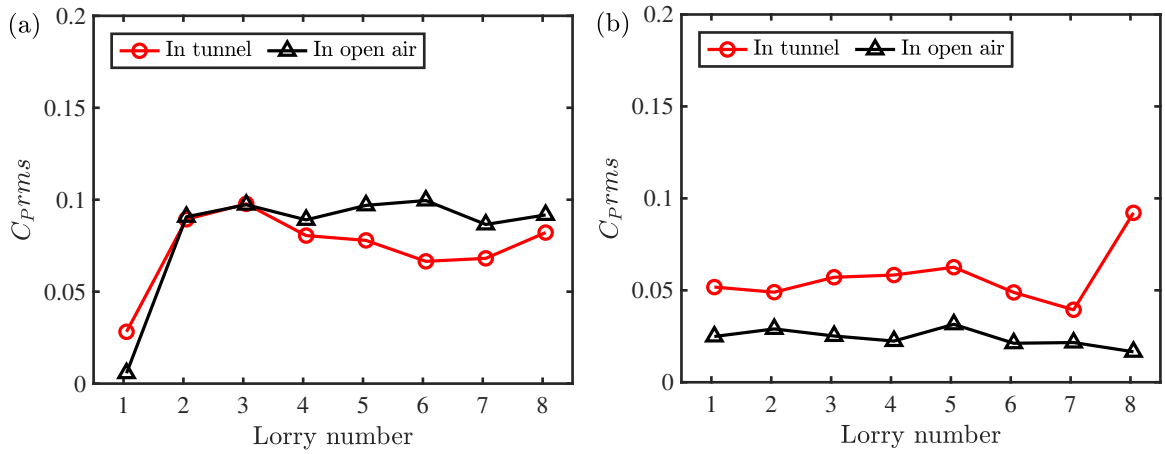

Figure 6.10: A comparison of the r.m.s value of the simulated surface pressure between the lorries in platoon in the tunnel and in the open air: (a) cab front; (b) box rear.

the tunnel, the surface pressure on the cab front decreases for the first four lorries, with the largest drop occurring at the second one, and then keeps relatively constant for the last four lorries. Also thanks to the shielding effect, the pressure variations for the trailing lorries in the tunnel are not as drastic as those for the leading lorries during entering and leaving the tunnel. However, frequent and small fluctuations are observed for the trailing lorries in both the tunnel and the open air, which are induced by the separated flow structures from the upwind stream as shown in Figure 6.6. When it comes to the box rear regions of the lorries in the tunnel (see Figure 6.9 (c)), almost all the lorries experience larger surface pressure fluctuations when entering the tunnel, but only the first and the last lorries have obvious changes in the surface pressure when leaving the tunnel. The last lorry has the lowest rear pressure coefficient in the tunnel, which is consistent with pressure distribution as shown in Figure 6.5. In addition, except for the last lorry, the pressures on the box rear fluctuate at similar levels for the other lorries. Figure 6.10 compared the r.m.s value of the simulated surface pressure of each lorry's cab front and rear box in the tunnel and in the open air. As for the cab front region, the trend along the platoon is roughly the same. The frontal surface pressure fluctuation of all trailing lorries is greater than those of the leading lorries. For the box rear surface pressure (Figure 6.10 (b)), the fluctuation along the platoon in the tunnel is higher than that in the open air. The fluctuation of the last lorry without trailing lorry in the tunnel is significantly higher than the preceding lorries.

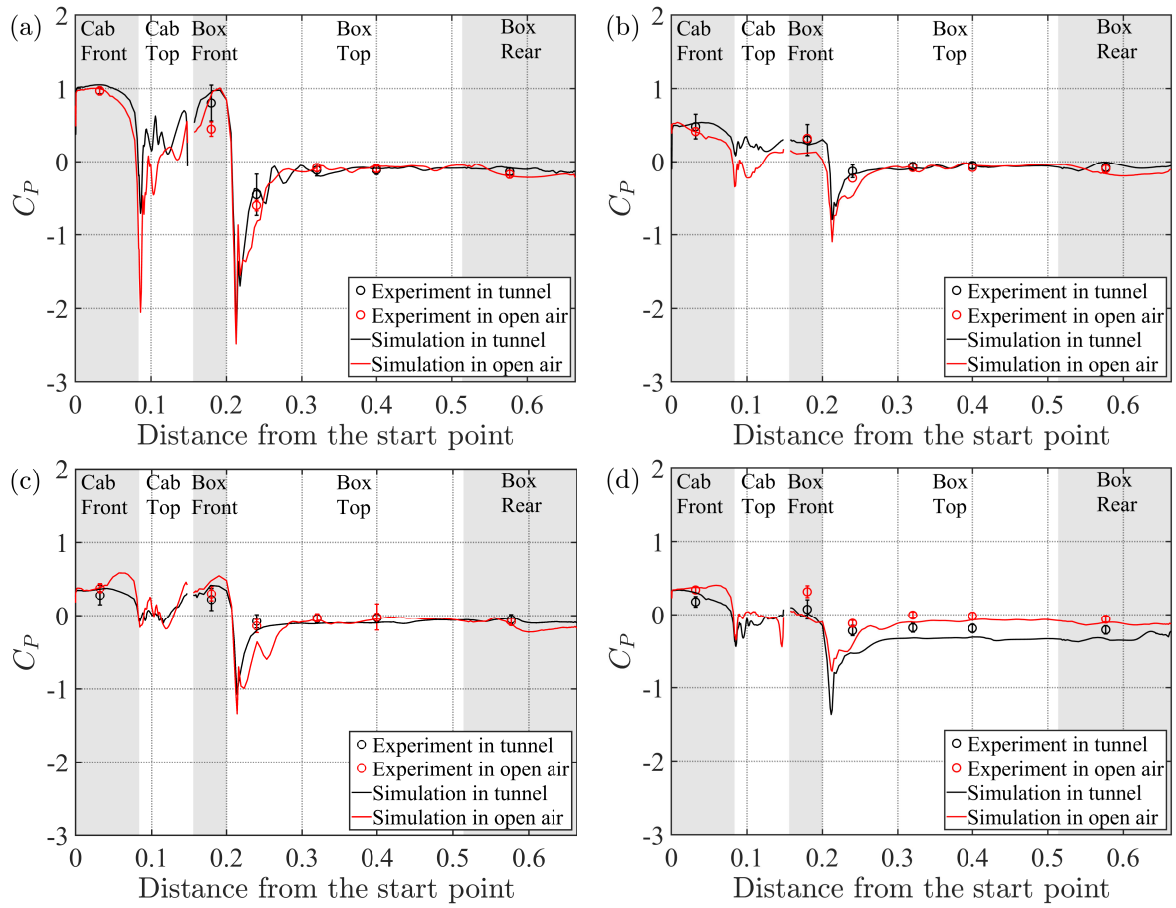

Figure 6.11: The mean surface pressure coefficients of different lorries along the central line of the platoon: (a) Lorry 1; (b) Lorry 3; (c) Lorry 5; (d) Lorry 8. Both experimental and numerical results are shown for the cases in the tunnel and in the open air. The shaded area is used to help to distinguish different regions along the lorry's surface.

Figure 6.11 shows the time-averaged surface pressure coefficients of Lorry 1, Lorry 3, Lorry 5 and Lorry 8 along the central line in the platoon. Both experimental and numerical results are plotted together, and a comparison is made between the data in the tunnel and in the open air (Robertson et al. 2019). Note that the surface pressure coefficient in the tunnel is averaged over the intermediate 4-meters when each lorry is travelling inside the tunnel. In the experimental study presented in Robertson et al. (2019), a short (5 meters) section was averaged and subtracted from the entire time history. Considering the effect of entering and leaving process, a slightly shorter section is used here as an time averages. The shaded

areas are employed to distinguish different regions along the lorry's surface. It is seen that the data predicted by the simulations are generally in good agreement with the experimental data. The mean surface pressure coefficients have a similar trend for different lorries both inside and outside the tunnel. To be specific, the surface pressure along the central line of each lorry drops significantly in the regions where the strongest flow separations occur (see Figure 6.6 to Figure 6.8),and then becomes almost unchanged for the box top and rear regions. Moreover, for both data in the tunnel and in the open air, the trailing lorries have much smaller frontal pressures than the leading one, and their rear pressures are almost the same. As indicated in Section 6.2, the piston effect in the tunnel leads to a lower approach velocity and a weaker flow separation near the box front edge, as compared to the case in the open air. This is evident by the pressure values of the negative peaks: the lowest C_p at the box front edge of Lorry 1 is -2.14 in the tunnel, compared to the value of -3.0 in the open air. C_p at the cab front edge of Lorry 1 is also lower in the open air than that in the tunnel. This difference in the negative pressure peak becomes smaller for the trailing lorries, as a result of shielding. Another appreciative difference that can be found is the surface pressure coefficients of Lorry 8. Their values are systematically lower in the tunnel than in the open air, supported by both the experiments and simulations. However, the difference between the two cases is generally more pronounced at the rear region of the lorry than it is at the front. This suggests that the mean drag coefficient for Lorry 8 will be significantly higher inside the tunnel, as the next section will demonstrate.

6.4 Drag analysis

The aerodynamic drag coefficient is discussed now. Figure 6.12 illustrates the time history of drag coefficients of each lorry running through the tunnel and in the open air. It is clearly seen in Figure 6.12 (a) that the drag coefficients of all the lorries first rise sharply when entering the tunnel, and then decrease slowly inside the tunnel before a sudden drop at the exit. The variation in the drag coefficients can be up to 70% for the leading lorry in the tunnel, which is absent for the case in the open air (Figure 6.12 (b)). As a benefit from the shielding effect, the trailing lorries in the tunnel experience smaller variation in the drag coefficients, but they still experience larger fluctuations than those in the open air.

A similar result was obtained previously by Li et al. (2010a), who simulated a two-vehicle platoon running into a tunnel. Their work showed that the drag coefficient of the trailing vehicle did not change significantly while the drag coefficient of the leading vehicle increased during the process of entering the tunnel. It is further seen in Figure 6.12 (a) that the drag coefficient continuously decreases from Lorry 1 to Lorry 5, with the largest drop occurring at the second lorry. Note that the drag coefficient of Lorry 8 in the tunnel is much higher than the other lorries, in contrast to the case in the open air. This is largely due to the strongly negative rear pressure when the lorry travels through the tunnel, as shown in Figure 6.9 (c) and Figure 6.11 (d).

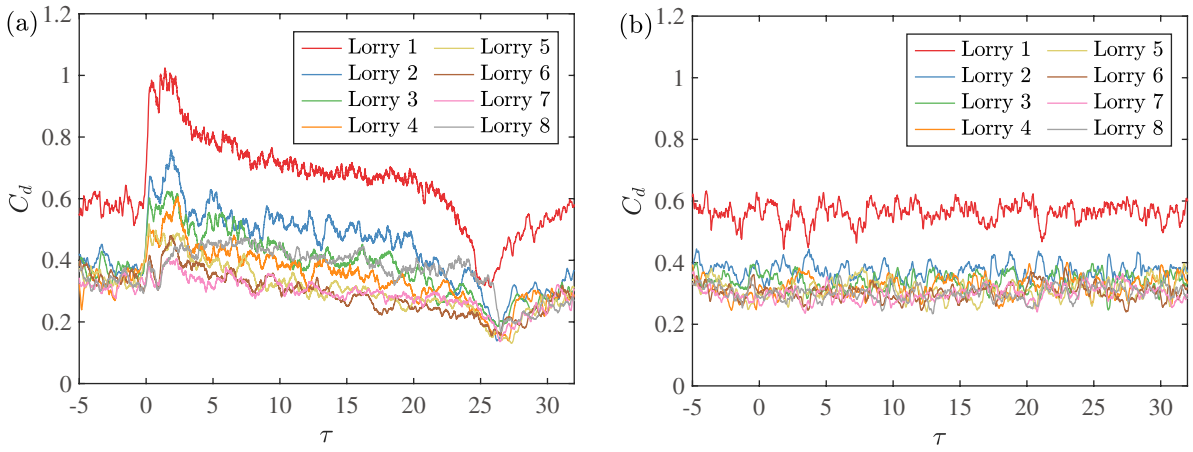

Figure 6.12: The time history of drag coefficients of different lorries in the platoon: (a) in the tunnel and (b) in the open air.

In order to compare the drag coefficients in the tunnel and in the open air directly, Figure 6.13 (a) shows the corresponding mean values. Note that the drag coefficients in the tunnel are averaged for the intermediate duration when the whole platoon is travelling inside the tunnel. It is seen that while the mean drag coefficient in the open air only changes significantly for the first three lorries and approaches a plateau after that, C_d in the tunnel continues to decrease appreciably until the fifth lorry. For the first four lorries, the presence of the tunnel tends to increase the drag coefficient due to the much higher frontal pressure, thus the C_d values in the tunnel are larger than those in the open air. The drag coefficients from the fifth to the seventh lorries are almost identical for different situations. However, for the last lorry in the tunnel, there is a large increase in the drag coefficient due to the

strongly negative rear pressures. The cumulative drag coefficients of the whole platoon is 3.314 ± 0.025 and 2.782 ± 0.025 in the tunnel and in the open air respectively. It is worth noting that whilst the drag coefficient is typically higher for a platoon travelling inside a tunnel than it is in the open air, the same is also true for single vehicles. The drag coefficient of an isolated lorry $C_{d-single}$ is 0.98 inside the tunnel and 0.64 in the open air, as discussed in Chapter 5. Therefore, to compare the benefits of platooning inside the tunnel and in the open air, it is instructive to normalise the drag coefficient by that of an isolated vehicle in their respective cases, as shown in Figure 6.13 (b). It is seen that platooning provides a drag-reduction benefit for all the lorries in both the tunnel and the open air. Interestingly, there is a much larger drag reduction due to platooning for the lorries inside the tunnel than those in the open air. This difference is as large as 20% for the lorries towards the middle of the platoon. Furthermore, the absolute difference between drag coefficients for a lorry in the platoon and a single lorry is always higher in the tunnel than it is in the open air. This suggests that platooning has a greater potential for reducing fuel consumption in the tunnel than in the open air.

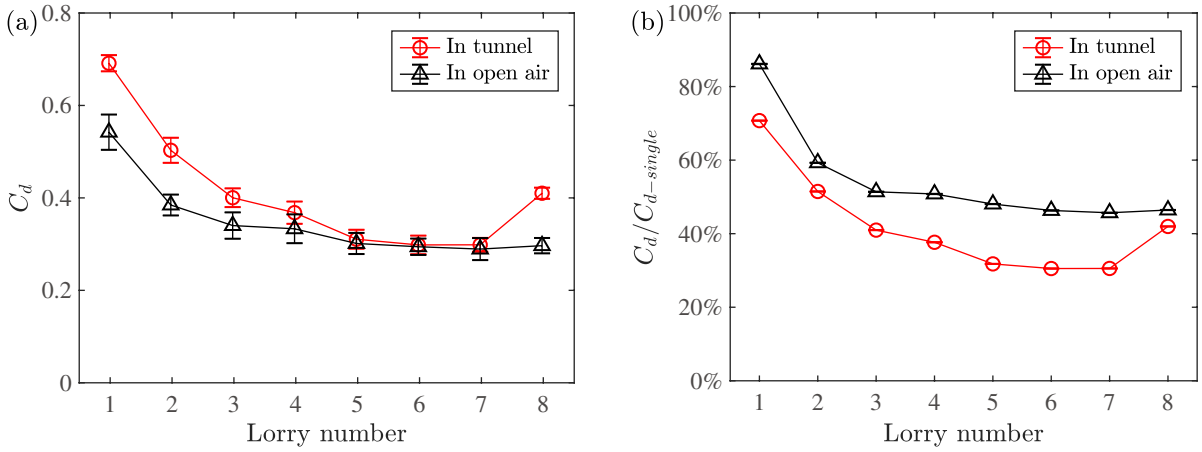

Figure 6.13: A comparison of (a) the mean drag coefficients and (b) the drag reduction ratio $C_d/C_{d-single}$ between the lorries in platoon in the tunnel and in the open air.

6.5 Conclusion

This chapter presents a detailed experimental and numerical study of the aerodynamic phenomena of a long lorry platoon running through a tunnel. The slipstream properties, surface pressure and drag force are discussed and compared to the data obtained in the open air. The main findings of this study are as follow.

- Due to the piston effect, stronger flows are induced in the frontal and rear regions of the platoon in the tunnel than in the open air. The influenced regions expand faster when the platoon is travelling inside the tunnel. Both experimental and numerical results reveal greater static pressure variations near the frontal regions of the leading lorries and the rear region of the last lorry in the tunnel.

- The flow structures around the lorry platoon are altered due to the tunnel walls: Fewer vortices are generated from the front edge of the lorry, and larger upper vortices are observed in the rear region. A weaker flow separation leads to a smaller drop in the surface pressure near the box front edge, as compared to the case in the open air.

- The variations of the drag coefficients show similar behaviours with the surface pressure, exhibiting great variations while entering and leaving the tunnel. In contrast to the case in the open air, the mean drag coefficient in the tunnel is no longer monotonically decreasing from the first to the last lorry in the platoon. Rather, it significantly decreases to a plateau at the fifth lorry and then increases again greatly at the last lorry due to strongly negative rear pressures.

- All vehicles, in both the tunnel and the open air, experience a reduction in drag due to platooning. The drag is consistently higher in the tunnel than in the open air for both isolated vehicles and platoons. However, the drag reduction due to platooning is consistently greater in the tunnel than in the open air. This implies a greater potential to reduce fuel consumption in the tunnel than in the open air.

Chapter Seven

Discussion of the effect of blockage ratio and traffic lane symmetry [1]

In this chapter, the effects of the blockage ratio and the traffic lane are investigated by analysing the slipstream, flow structure and the aerodynamic forces of the $1.5L$ platoon in four different cases. The last chapter has analysed the effect of the tunnel on this platoon by comparing the results in the small tunnel and open air. Therefore, the spacing of $1.5L$ is chosen here.

7.1 Slipstream properties

Figure 7.1 shows the aerodynamic flow around the lorry platoon, in terms of the normalised horizontal velocity and pressure coefficient in the slipstream. Note that the measuring point is located $y/H = 0.14$ away from the lorry left side and $z/H = 0.45$ from the ground level. The data in four cases are plotted together for comparison. In Figure 7.1 (a), the highest speed appears in the wake regions and a small frontal region of each lorry in all cases. In comparison to the platoon in the open air, the small tunnel induces stronger flows in the

[1] The results in this Chapter have been submitted to Journal of Wind Engineering and Aerodynamics (Zhang et al., 2022).

platoon's side and gap regions (Zhang et al. 2021). In comparison to the small tunnel, the piston effect is lessened in the large tunnel regardless of which lane the platoon is travelling. Additionally, this demonstrates that the piston effect is related to the blockage ratio rather than the traffic lane. When the platoon travels in the right lane of the large tunnel, the flow field is confined by the sidewall, breaking the flow field's symmetry, particularly for the platoon's fifth to eighth lorries. The top view of the horizontal velocity at the height $z/H = 0.57$ above the ground plane in Figure 7.2 aids in the intuitive understanding of the preceding observation. The transient velocity fields at $\tau = 22.53$ was selected to ensure the whole platoon runs in the middle of the tunnel.

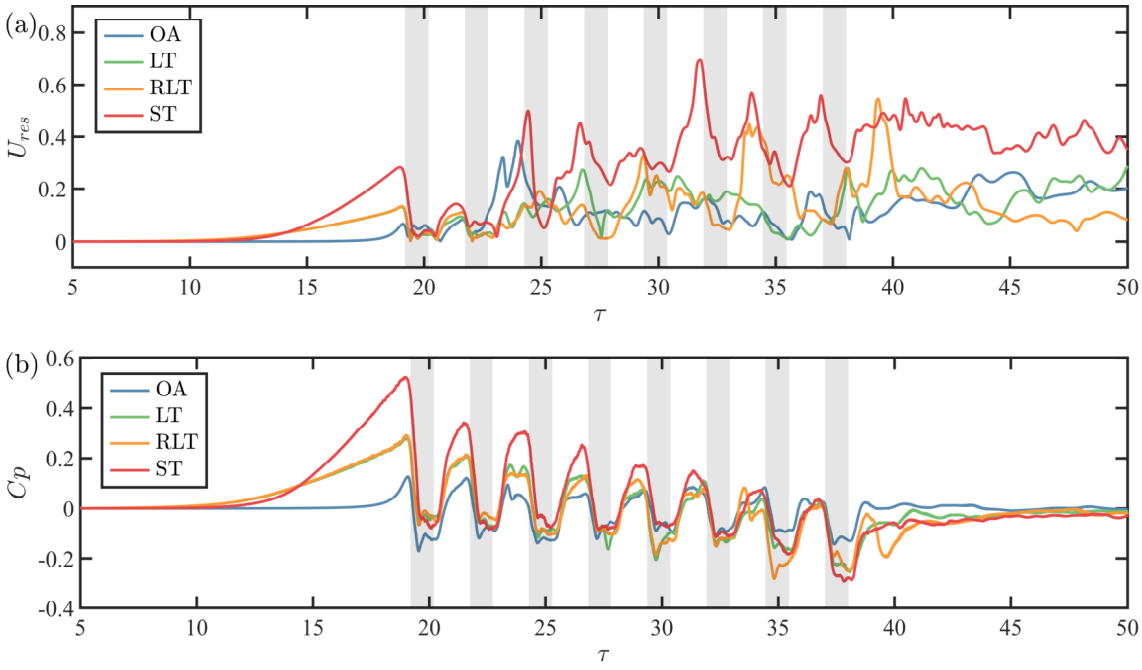

Figure 7.1: The temporal variations of the (a) normalised horizontal velocity and (b) the pressure coefficient in the open air (OA), large tunnel (LT), right lane in the large tunnel (RLT) and small tunnel (ST).

Figure 7.3 shows the corresponding TKE of the velocity field in Figure 7.2. The high turbulent kinetic energy is observed in the rear region of each lorry. The TKE is stronger for the leading and last lorry in the small tunnel. However, the TKE appears to be irrelevant to the position of the lorry in the platoon in the other three cases. The effect of the blockage ratio and traffic lane cannot be seen from the contours. The turbulent energy is basically

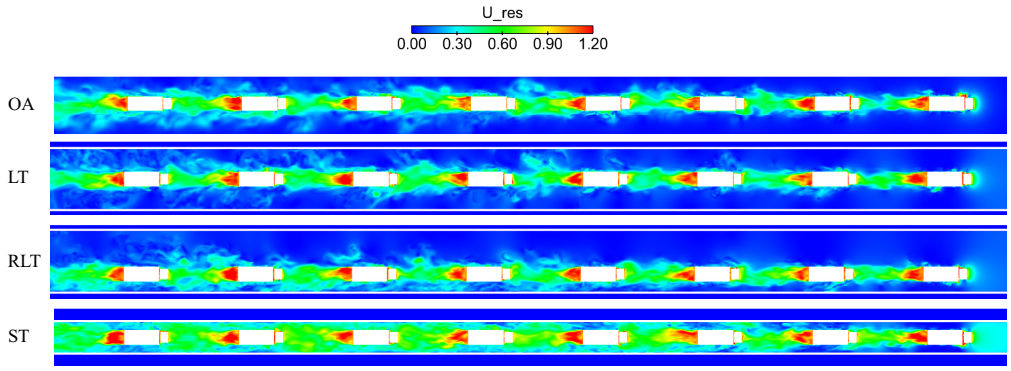

Figure 7.2: The velocity fields at a horizontal plane of $z/H = 0.57$ for the platoons running in the open air (OA), large tunnel (LT), right lane in the large tunnel (RLT) and small tunnel (ST).

concentrated in the wake region of each lorry.

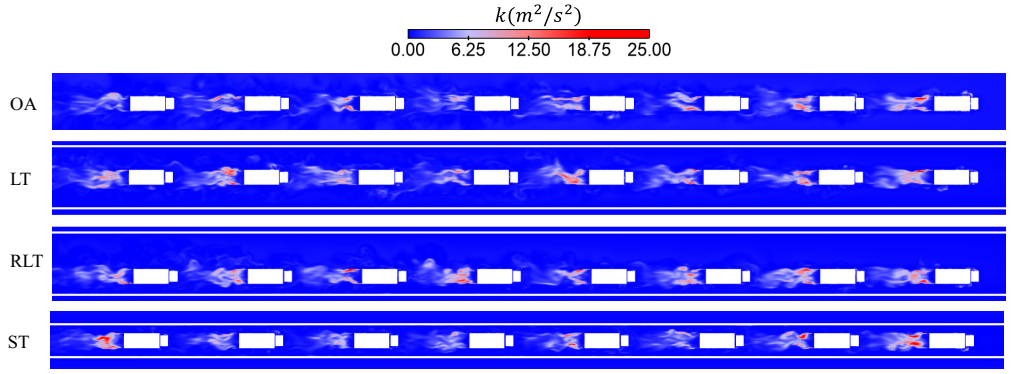

Figure 7.3: The instantaneous turbulent energy at a horizontal plane of $z/H = 0.57$ for the platoons running in the open air (OA), large tunnel (LT), right lane in the large tunnel (RLT) and small tunnel (ST).

Figure 7.4 shows the top view of the pressure distribution of the $z/H = 0.57$ plane for four cases. In the tunnels, the frontal positive pressure continuously drops from the leading lorry to the last one. The piston-induced high-pressure frontal region and low-pressure rear region of the platoon are quite apparent in the small tunnel but less so in the two large tunnels. As the pressure differential between the front and rear decreases, it is reasonable to predict that the drag in the large tunnel will decrease. However, because the frontal

pressure diminishes more quickly in the small tunnel than in the large tunnel, it can be observed that the frontal pressure is greater in the large tunnel for the fifth and sixth lorries. It is reasonable expect that the fifth and sixth lorries have a higher drag coefficient in the large tunnel than in the small tunnel. The enhanced negative pressure at the rear region of the last lorry is more noticeable in the small tunnel than in the large tunnel. When a platoon moves in an asymmetric lane, the frontal high-pressure region of the leading vehicle loses its symmetry. The potential effect of this asymmetry of pressure field on the side force is unclear.

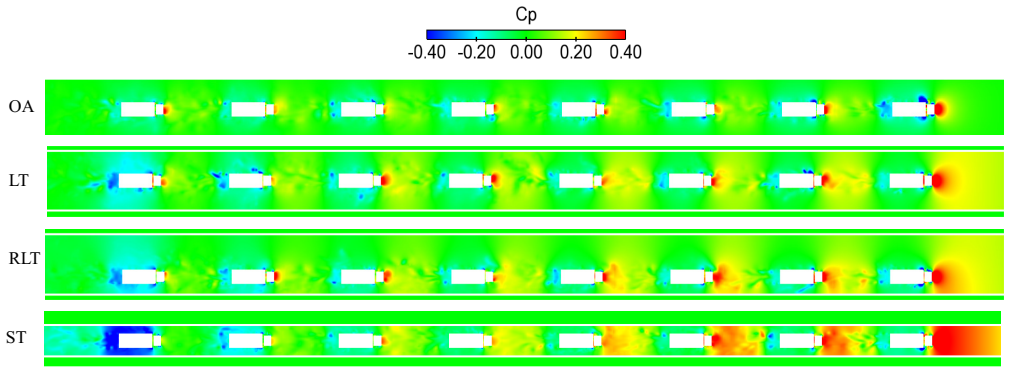

Figure 7.4: The pressure distribution at a horizontal plane of $z/H = 0.57$ for the platoons running in the open air (OA), large tunnel (LT), right lane in the large tunnel (RLT) and small tunnel (ST).

7.2 Flow structures

Figure 7.5 compares the instantaneous flow structures around the first, fifth and last lorry in four cases. As mentioned in Section 6.2, the overall flow field for all the intermediate lorries is similar, especially when compared to the lorries at each end, despite the slight difference caused by the development of the slipstream. The Lorry 5 is used as a representative of the intermediate lorries.

In both of these cases, the distributions of vortices around the lorries are similar. Due to the bluff structure of the box lorries, the flow around the platoon is highly turbulent, and

a large number of vortices are formed around the cab, box side, and rear areas. As discussed in Chapter 6, fewer vortices are observed at the lorry sides in the tunnel since the piston effect induces a smaller approach velocity. When the cross-sectional area of the tunnel is increased, the piston effect diminished, causing the vortices to increase to the level seen in the open air, which is evident in comparison between Lorry 1 in open air and in two large tunnels as shown in Figure 7.5.

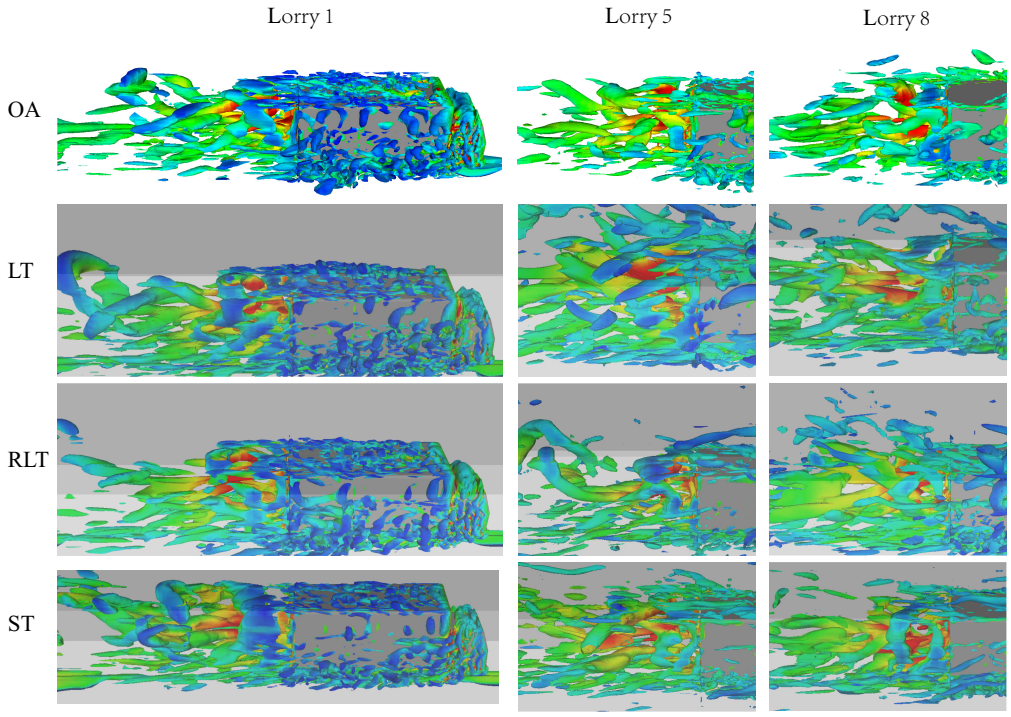

Figure 7.5: The instantaneous iso-surfaces of the second invariant Q. Left panel: Lorry 1; middle panel: Lorry 5; Right panel: Lorry 8. Here, Q is set to be $50000s^{-2}$ and coloured by the normalised velocity.

The time-averaged streamlines (over the time period of $\tau = 7.5$ 17.5) at the centreline plane in the wake region of three typical lorries (Lorry 1, Lorry 5 and Lorry 8) in the platoon are shown in Figure 7.6. In comparison to the open-air case, the existence of the upper wall enlarges the upper vortices for all lorries in the small tunnel. While in the large tunnel, the vortices behind Lorry 1 and Lorry 5 are similar to those in the open air, but the vortices behind Lorry 8 are similar to those in the small tunnel. When the platoon is running along the right lane of the large tunnel, the prominent vortex structures are similar as those in the

LT case.

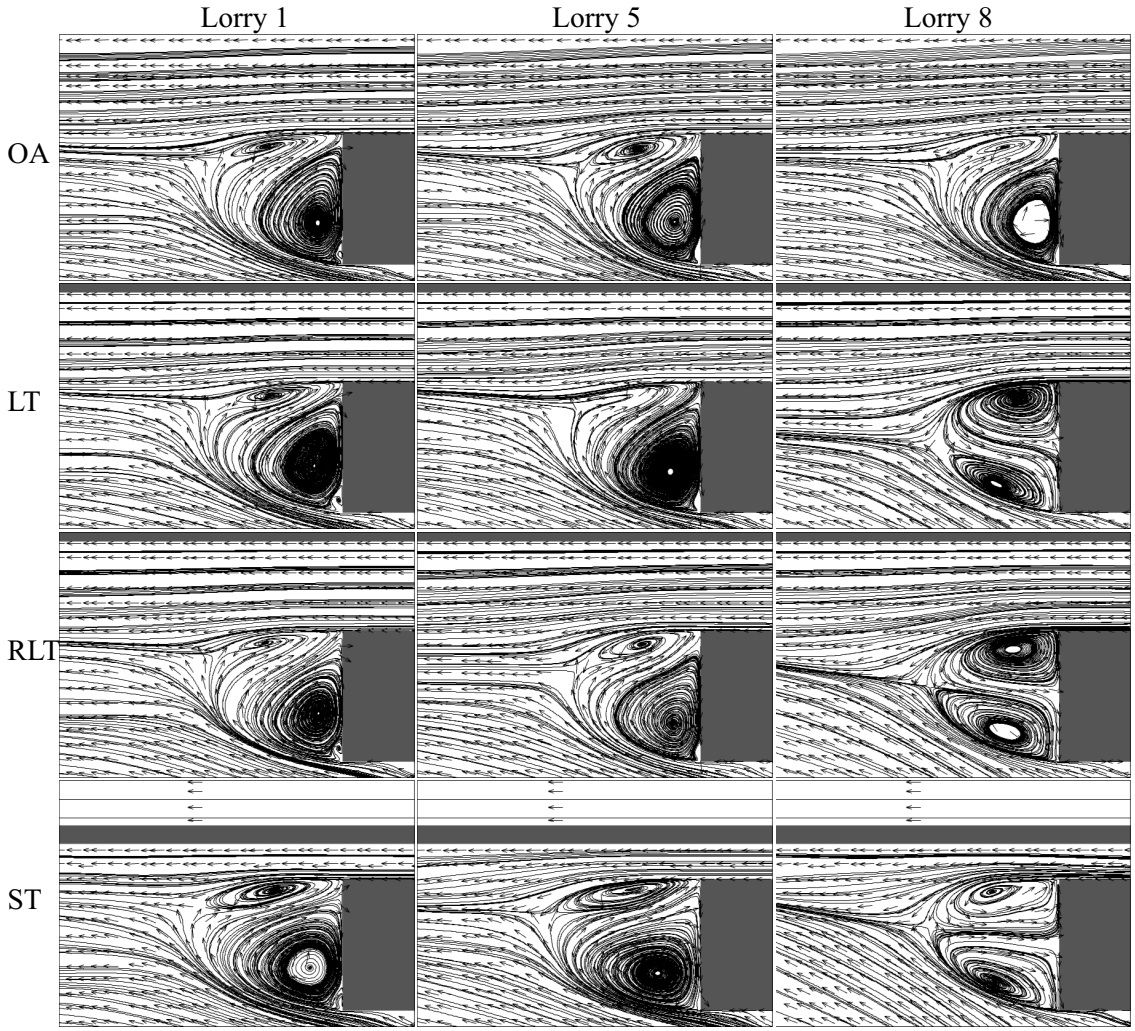

Figure 7.6: Illustrations of the rear flow structures of three representative lorries in the platoon at $y/H = 0$.

The side view of the streamlines cannot address the effect of the traffic lane on the flow structures. Figure 7.7 shows the streamline on the horizontal plane at $z/H = 0.57$. While looking at the flow field around the leading lorry in two cases, the wake structures deviates from the symmetry when the platoon is running on the right lane in the large tunnel. Figure 7.8 shows the contour of the y-axis velocity component. The results show that the maximum lateral velocity near the cab region is lower at the near-wall side for the leading lorry. Similar result is observed at the nose region when a train passing through a asymmetrical double walls (Gilbert 2014). For the wake region of each lorries, the lateral ve-

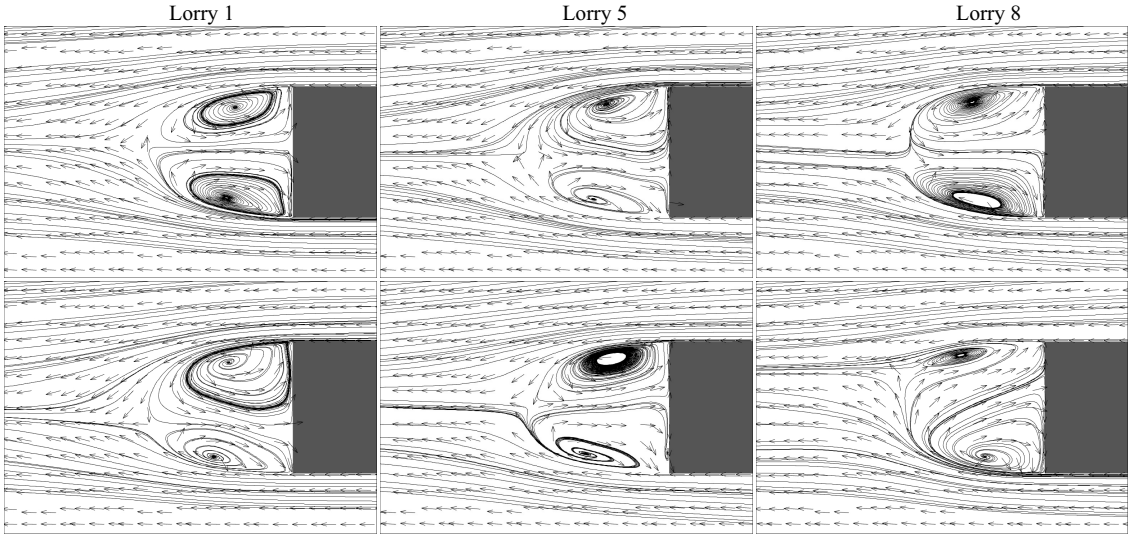

Figure 7.7: Illustrations of rear flow structures of three representative lorries in the platoon at $z/H = 0.57$. Top panel: Lorry 1, Lorry 5 and Lorry 8 in the large tunnel. Bottom panel: Lorry 1, Lorry 5 and Lorry 8 in the right lane of the large tunnel.

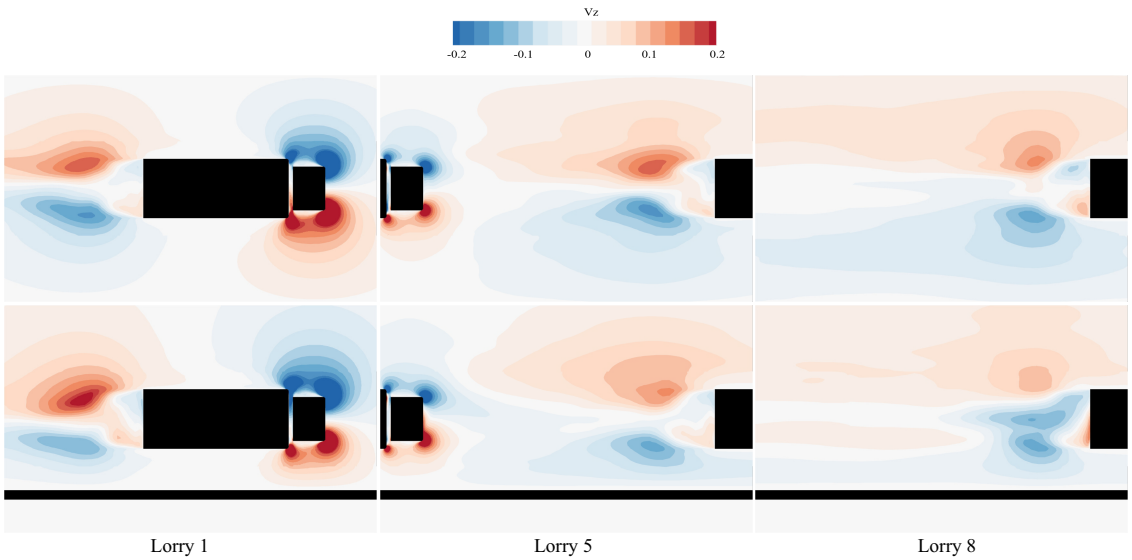

Figure 7.8: The normalised y-axis component velocity V at $z/H = 0.57$. Top panel: Lorry 1, Lorry 5 and Lorry 8 in the large tunnel. Bottom panel: Lorry 1, Lorry 5 and Lorry 8 in the right lane of the large tunnel.

locity flow to the wake center is smaller at the near wall side, resulting into the asymmetrical arrangement of the structures as shown in Figure 7.7.

7.3 Surface pressure analysis

As discussed in Chapter 6, surface pressure analysis may help us better understand the flow field and flow structure, as well as predict and comprehend the aerodynamic forces. The mean values are calculated using the same average procedure as in the previous section.

Figure 7.9 presents the time history of the surface pressure coefficient C_P at two typical surface positions (Tap 1 and Tap 8 shown in Figure 3.7) of the leading, the fifth and the last lorry in four cases. The data is synchronized with respect to the time at which each lorry arrives at the tunnel's entrance. When entering the tunnels, the frontal surface of the leading lorry rises sharply, then gradually decreases across the tunnel until it drops suddenly at the exit. When travelling through the large tunnels, the variation in amplitude is less noticeable. Because of the effective shielding effect of the platoons, the frontal surface pressure of the intermediate lorry and the last lorry is less affected by the tunnels. The fluctuations are primarily caused by driving in the highly turbulent wake of the front lorry. When it comes to the box rear regions of each lorry in four different cases, the strong negative pressure shock is only observed in the small tunnel of the leading and the fifth lorry during the entry process. As for the last lorry, when it enters the tunnels, the negative box rear pressure is significantly amplified in the small tunnel and less so in the large tunnels because of the piston effect.

Figure 7.10 shows the time-averaged surface pressure coefficients of four representative lorries along the central line in the platoon. The surface distribution of the leading lorry deviates in four cases at the frontal surface area, particularly at the front edge of the box, where flow separation occurs. As mentioned in the last chapter, the piston effect in the tunnel results in a lower approaching velocity and a weaker flow separation at the front edge of the lorry box. The piston effect becomes weaker in large tunnels, resulting in higher negative pressure peaks. The surface pressure at the box rear region of all lorries in the platoon, on

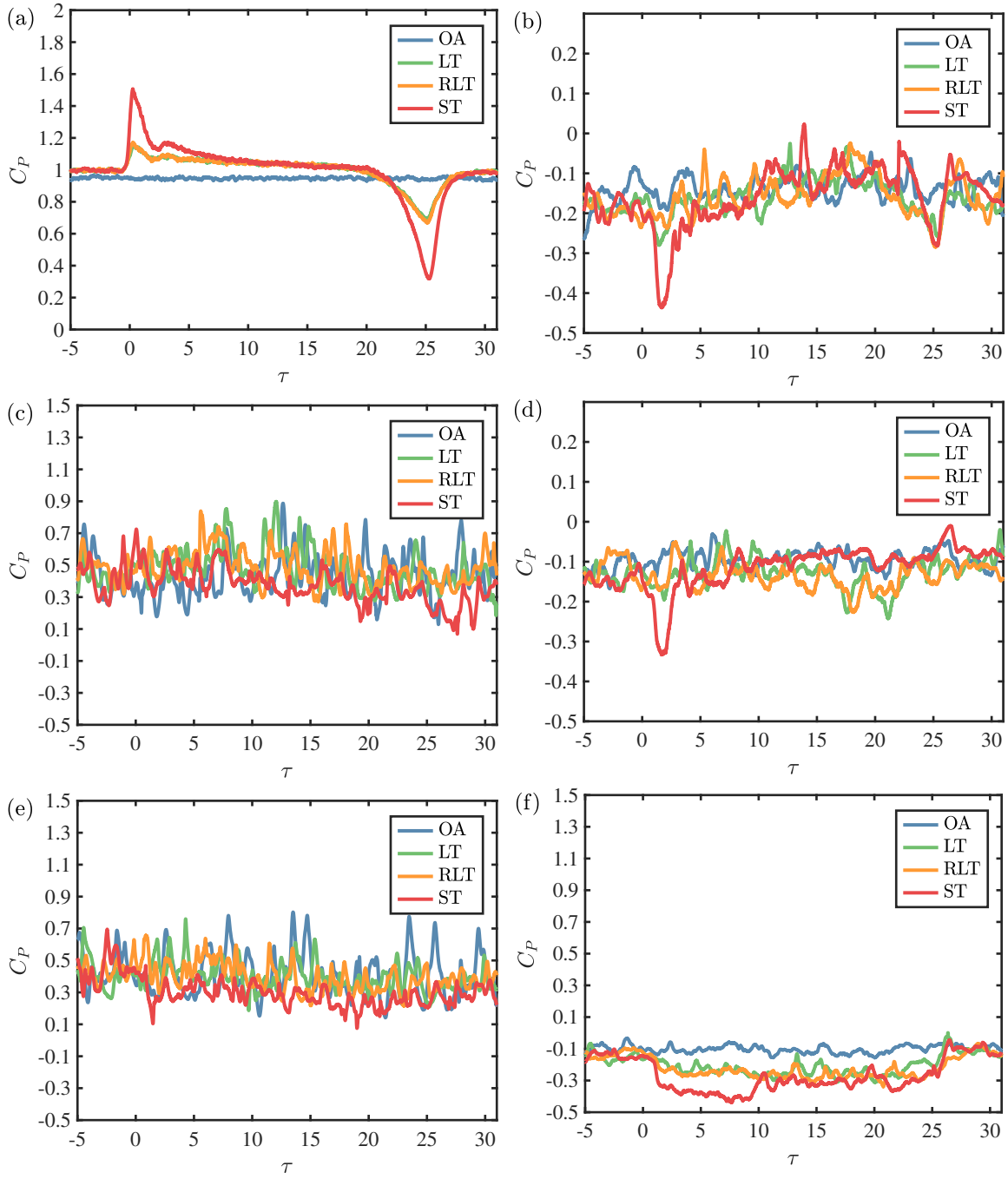

Figure 7.9: The simulated surface pressure coefficients of three representative lorries as a function of the normalised time: (a),(c),(e) cab front of the Lorry 1, 5 and 8 respectively; (b),(d),(f) box rear of the Lorry 1, 5 and 8 respectively.

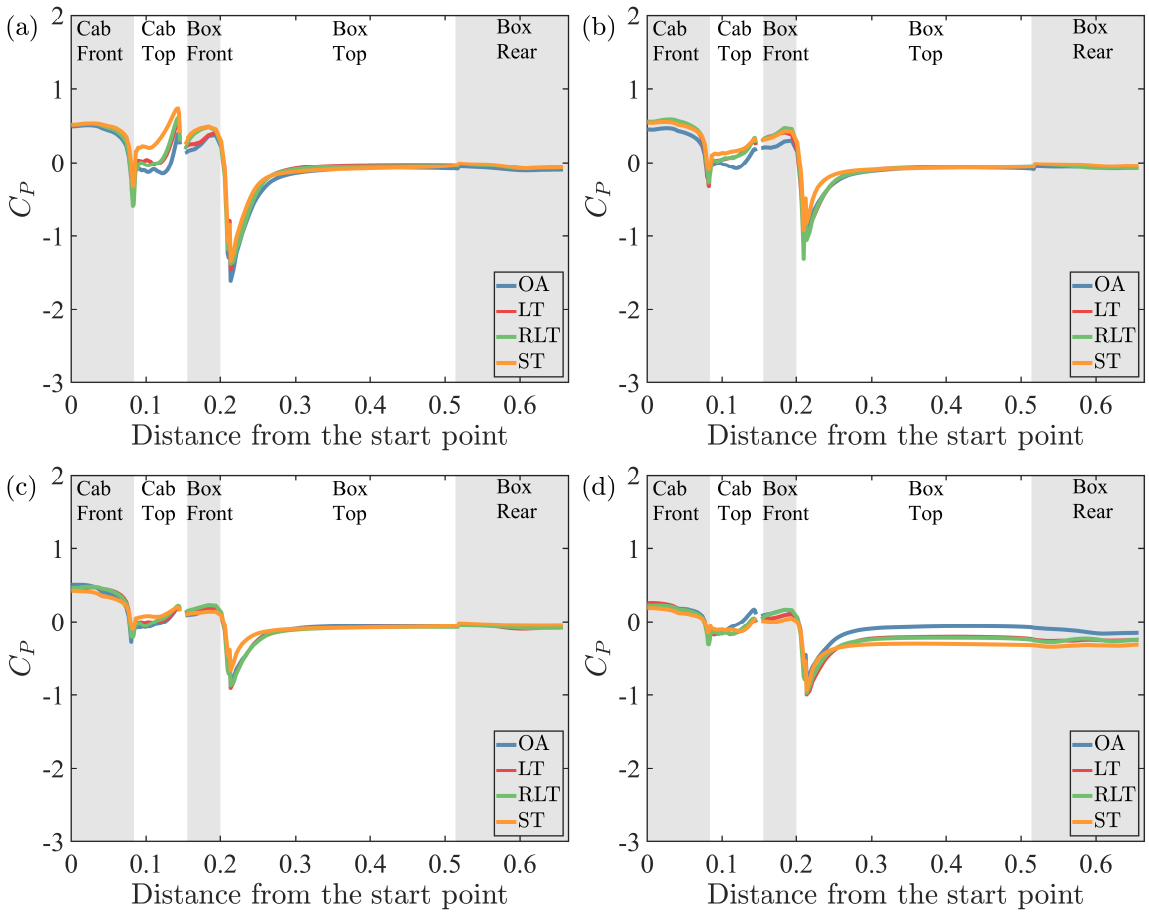

Figure 7.10: The simulated mean surface pressure coefficients of different lorries along the central line of the platoon: (a) Lorry 1; (b) Lorry 3; (c) Lorry 5; (c) Lorry 8. The shaded area is used to help to distinguish different regions along the lorry's surface.

the other hand, is only slightly affected by the blockage ratio. Specifically for the last lorry, the surface pressure at box top and rear region is consistently higher in the open air than it is in the three different types of tunnels. The location of the traffic lane has little effect on the surface pressure distribution along the central line of every lorry in the platoons.

7.4 Aerodynamics force analysis

Figure 7.11 illustrates the time history of drag coefficients of each lorry running through the open air, large tunnel, the right lane of the large tunnel and small tunnel. In the small tunnel, the drag coefficients of all vehicles increase dramatically when entering the tunnel, then gradually fall along the tunnel before abruptly decreasing at the exit. In both large tunnels, such variation is less pronounced. The trailing lorries benefit from the shielding effect in all three cases, with the most significant reduction occurring between the leading and second lorries. What makes the small tunnel different is that the drag decreases progressively from the second to the last vehicle, whereas in both large tunnels, all trailing lorries have roughly similar drag coefficients. From a time history perspective, the effect of the traffic lane on drag is negligible, as illustrated in Figure 7.11 (b) and (c).

In order to compare the drag coefficients in four cases directly, Figure 7.12 (a) shows the corresponding mean values. The contrast between the drag coefficient in the open air and the drag coefficient in a small tunnel has been extensively investigated in Chapter 6. The drag coefficient of each lorry is approximately 0.07 greater in the both large tunnels than in the open air. The drag coefficients in both large tunnels are lower for the first two lorries, but it is higher for the fourth to seventh vehicles than the drag coefficients in the small tunnel, which is in agreement with the analysis of the pressure field in Section 7.1. For a single vehicle, the drag coefficient increases from 0.71 to 0.98 when the blockage ratio increases from 15.3% to 35.8%. However, for a long platoon, increasing the blockage ratio does not lead to an increase the drag of every lorry in the platoon. For the fourth to seventh lorries, the drag coefficients is even greater in large tunnels than in small tunnel. (Note that the overall drag of the whole platoon in different size tunnels might be the same, which will be mentioned in next chapter.) In other words, the effect of blockage ratio on aerodynamic

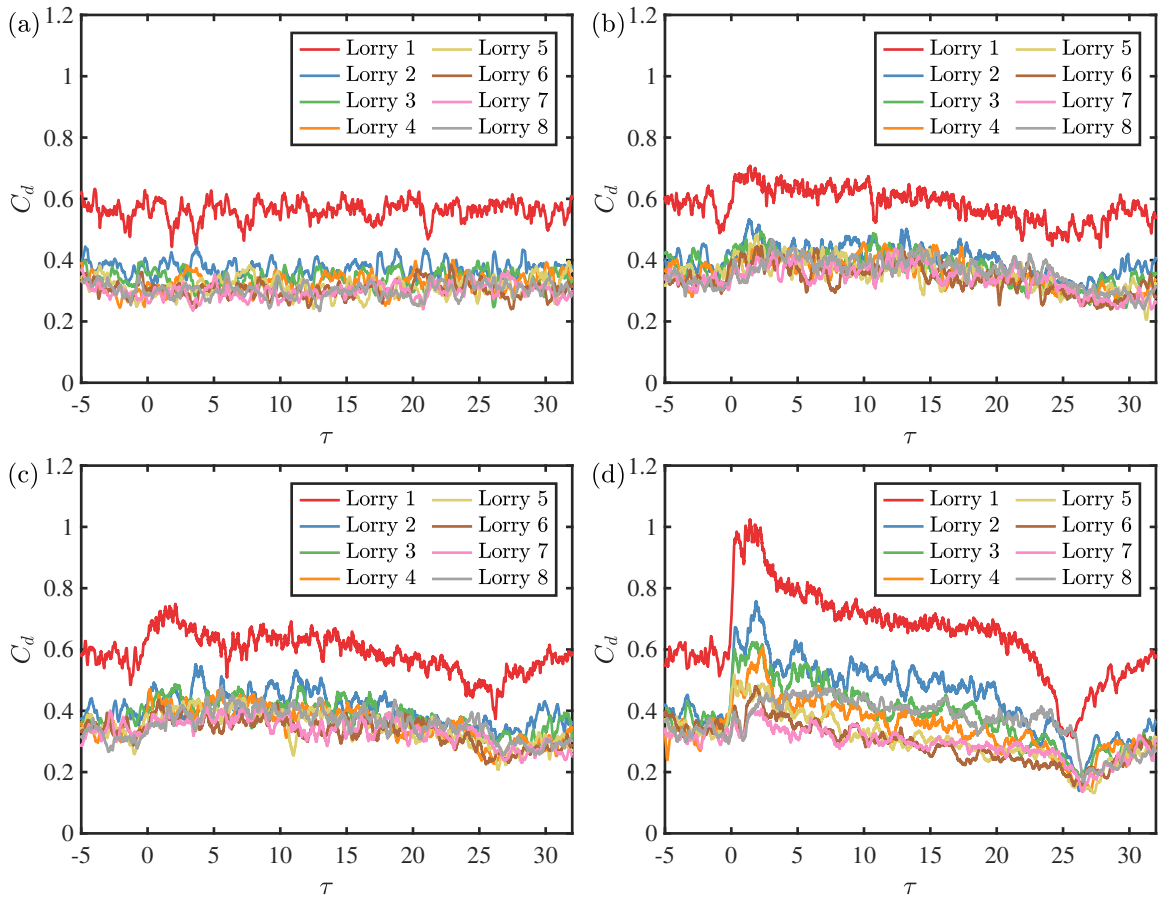

Figure 7.11: The time history of drag coefficients of all lorries in the $1.5L$ platoon: (a) in the open air, (b) in the large tunnel, (c) right lane of the large tunnel and (d) in the small tunnel.

drag is different for each lorry in the platoon. As for the effect of traffic lane, the drag coefficient of each lorry is within the range of uncertainty between the LT and RLT cases, demonstrating that the traffic lane has little influence on the drag coefficient values.

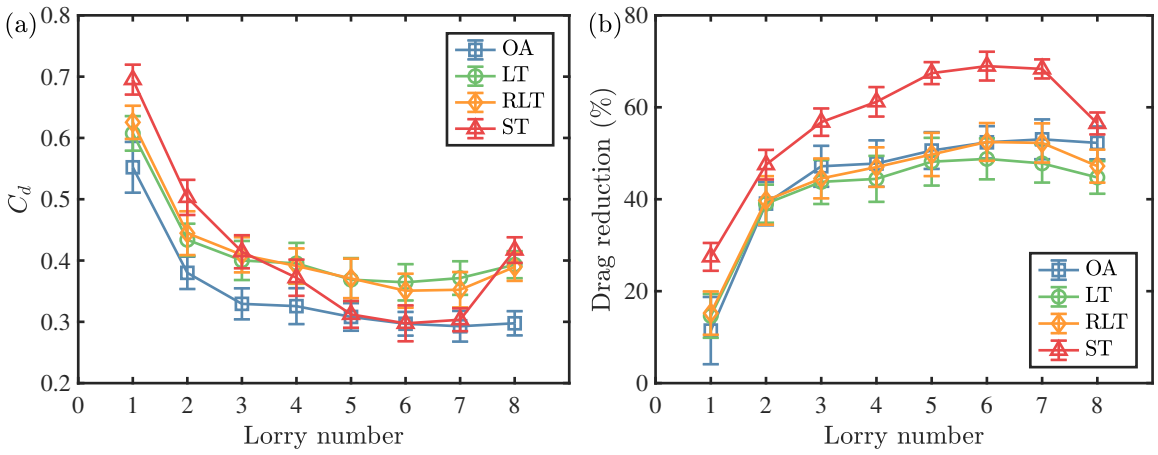

Figure 7.12: A comparison of (a) the mean drags coefficients and (b) the drag reduction ratio $(1 - C_d/C_{d-single}) \times 100\%$ among four cases.

Figure 7.12 (b) compares the drag reduction of each lorry in the platoon, relative to an isolated lorry in their respective cases. This quantity can be used to describe the advantages of platooning. The smaller the value, the higher the drag reduction ratio of platoon. It is clear that platooning has a greater potential for lowering fuel consumption in the small tunnel than it does in the open air. The drag reduction ratio is roughly the same in both the large tunnels and in the open air. To put it another way, when the blockage ratio rises, the lorries become more motivated to form a platoon in order to reduce drag.

Figure 7.13 shows the side force coefficients of each lorry in four cases. The averaged standard deviation of all lorries is shown by black error bar in the left lower corner for simplicity. It shows that Lorry 2 and Lorry 3 has large negative side force (toward the midplane of the tunnel). Gilbert, Baker, and Quinn (2013a) observed that the shedding frequency of the wake structure of the train was largely disrupted by the asymmetrical double all configuration. The consequence on side force was not mentioned. However, in present work the standard deviation of the mean side force coefficients is of the order of ± 0.05. At this specific inter-vehicle spacing ($1.5L$), it is difficult to determine the effect of the traffic lane on the side force. It is necessary to consider the spacing impact, which will

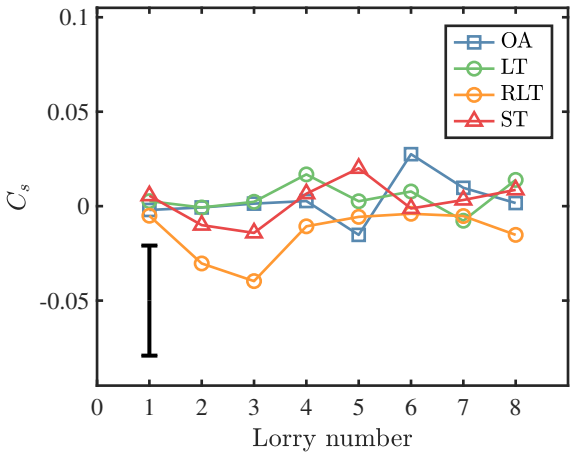

Figure 7.13: The side force coefficients of each lorry in the $1.5L$ platoon in four cases. The averaged standard deviation of all taps is shown by black error bar in the lower left corner for simplicity.

be explained in the following chapter.

7.5 Conclusion

The chapter detailed in the effect of the blockage ratio and the location of the traffic lane on the aerodynamics of the long platoon travelling inside the tunnel. The inter-vehicle spacing of $1.5L$ is selected. According to the simulation results, the following are some important findings:

- When the blockage ratio decreases, the piston effect becomes less effective, resulting in a flow field similar to that seen in the open air. Also a decrease in the peak value of the high frontal and low rear pressures has been noticed. In addition, the size of vortices surrounding the box has increased, the size of the upper vortices is reduced and the size of the lower vortices increased to a level comparable to those of the vortices in the open air. When entering the large tunnel, the magnitude of the drag variation decreases.
- Unlike a single lorry, increasing the blockage ratio does not lead to an increase of the

drag of every lorry in the platoon. In a small tunnel, the fourth to seventh lorries have smaller drag coefficients, while others have larger drag coefficients compared to the lorries in large tunnels. The variation in drag and drag reduction ratios along the platoon approaches the pattern observed in the open air.

- Driving in the right lane of the large tunnel causes the pressure field to become asymmetrical, which is noticeable in the front region of the leading lorry but has minimal impact on the strength of the piston effect. In addition, travelling on the right side of the tunnel causes the pressure and velocity flow field to deviate from its symmetrical position in the front region of the platoon and the wake region of each lorry.

- The effect of the position of traffic lane on the drag coefficient is negligible. The variation in drag and drag reduction ratios along the platoon is nearly identical between two lanes in the large tunnel.

Chapter Eight

Results and Discussion of the effect of inter-vehicle spacing [1]

In this section, the effect of inter-vehicle spacing will be discussed. The spacing of $0.5L$, $1.0L$ and $1.5L$ are determined in accordance with experimental studies (Robertson et al. 2019; Zhang et al. 2021). The spacing of $0.1L$ and $0.25L$ are set to examine the drag variation at small spacing (Ebrahim and Dominy 2020). The spacing of $0.75L$ is set to maintain an even distribution of inter-vehicle spacing. For the sake of simplicity, the flow field figures with only four spacings ($0.1L$,$0.25L$, $0.5L$ and $1.0L$) will be exhibited. The discussion of the surface pressure distribution and the aerodynamic forces will include all results from six spacings.

8.1 Flow field analysis

Figure 8.1 shows the top view of the horizontal velocity at the height $z/H = 0.57$ above the ground plane. To ensure the whole platoon runs in the middle of the tunnel, the transient velocity field at $\tau = 17.09, 17.72, 18.35$ and 20.25 were selected for $0.1L, 0.25L, 0.5L$ and

[1] The results in this Chapter have been submitted to Journal of Wind Engineering and Aerodynamics (Zhang et al., 2022).

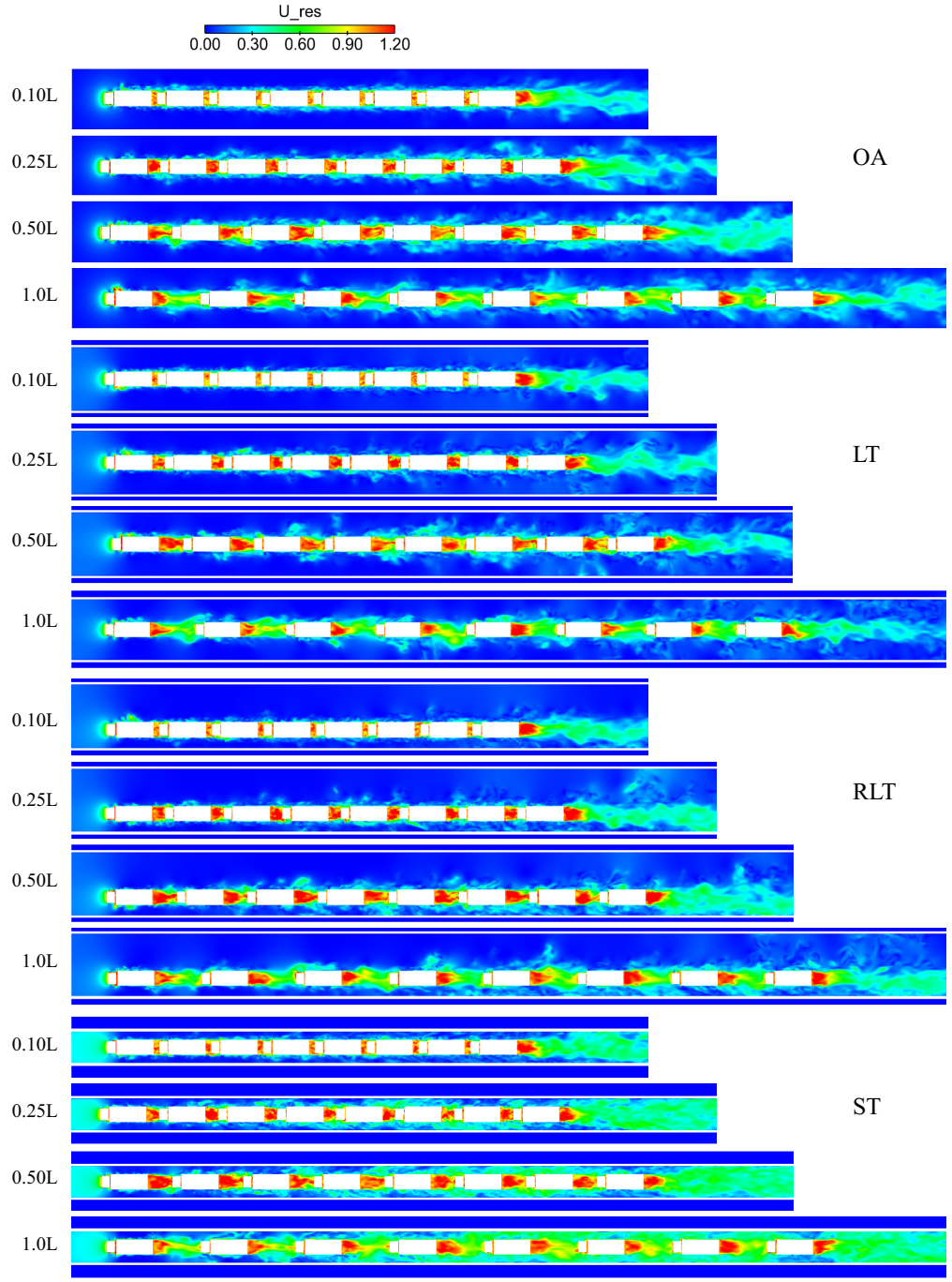

Figure 8.1: The horizontal velocity flow field during the lorry platoons of four spacings on the horizontal plane of $z/H = 0.57$ in the open air (OA), large tunnel (LT), right lane in the large tunnel (RLT) and small tunnel (ST).

$1.0L$, respectively. The highest speed appears in the wake regions and a small frontal region of all the lorries, regardless of in the tunnels or in the open air. However, when the platoon is running inside the tunnels, stronger flows are induced in the frontal and rear regions of the platoon, especially in the small tunnel. For the lateral sides of the platoons, the influence regions expand much quicker in the small tunnel than in the open air and two large tunnels. However, the lateral influence regions are not sensitive to the inter-vehicle spacing as shown in these four cases. When the spacing is reduced to $0.25L$, the high velocity wake zone begins to be squeezed, affecting the flow structures.

Figure 8.2 shows the aerodynamic flow around the lorry platoon, in terms of the normalised horizontal velocity. The monitor point is located $y/H = 0.14$ away from the lorry left side and $z/H = 0.45$ from the ground level. At the closest spacing ($0.1L$), the whole platoon resembles a single freight train. The flow around the $0.1L$ platoon can be divided into nose region, boundary layer region and near wake region, according to the (Baker et al. 2001). The normalized velocity for passenger trains is between 0.05 and 0.1 in the open air at about 3 meters from the track center (full scale), but it is higher for freight trains because of their blunt nose shapes (Baker 2014). For the lorry platoon with blunt frontal face, the normalised horizontal velocity of 0.06 around the nose region is observed (blue line), regardless of the inter-vehicle. While in the tunnel, the velocity increased due to the piston effect. In small tunnel (blockage ratio 35.8%, opening ratio 1%), the horizontal velocity when the first lorry passes the measurement point reaches 0.6, which is similar to that when a train travels through a partially-enclosed tunnel with blockage ratio of 30% and opening ratio 1% (Gilbert 2014). For the wake region, the velocities is significantly higher in small tunnel than other three cases.

Figure 8.3 shows the pressure distribution of the platoons in the middle of the tunnels on the horizontal plane. The magnitudes of the gusts generated by platoon movements, which are independent of inter-vehicle spacing, are significant in the small tunnel but less so in the large tunnels. It should be noted that the magnitudes of negative pressure at the box side and rear region of the last lorry owing to the absence of the trailing lorry are also independent of the inter-vehicle spacing. Qualitatively, when the inter-vehicle spacing reduces, the pressure differential between intermediate lorries decreases, indicating that the drag coefficients decrease.

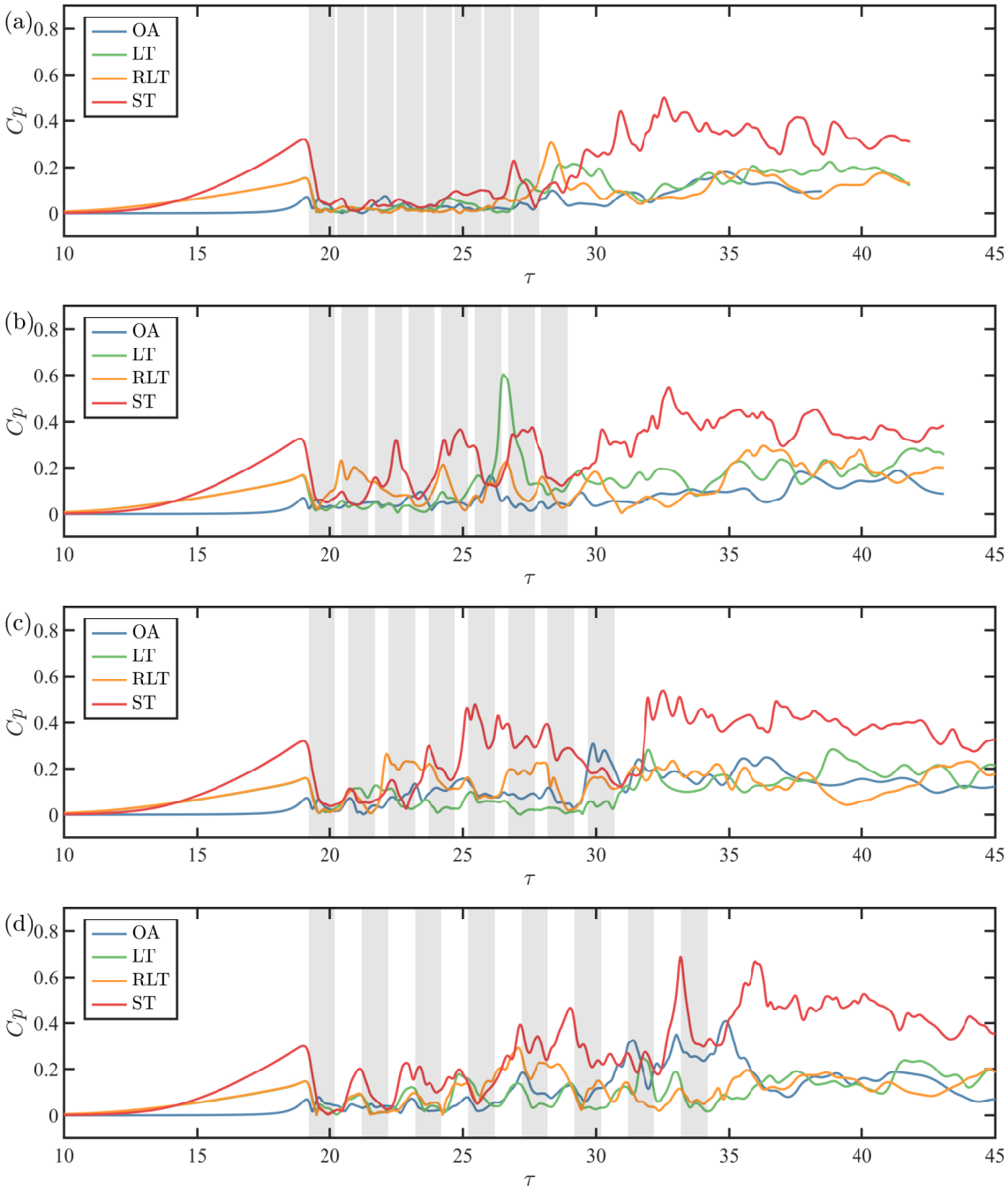

Figure 8.2: The temporal variations of the normalised horizontal velocity in the open air (OA), large tunnel (LT), right lane in the large tunnel (RLT) and small tunnel (ST). The inter-vehicle spacing is: (a) $0.1L$, (b) $0.25L$, (c) $0.5L$ and (d) $1.0L$.

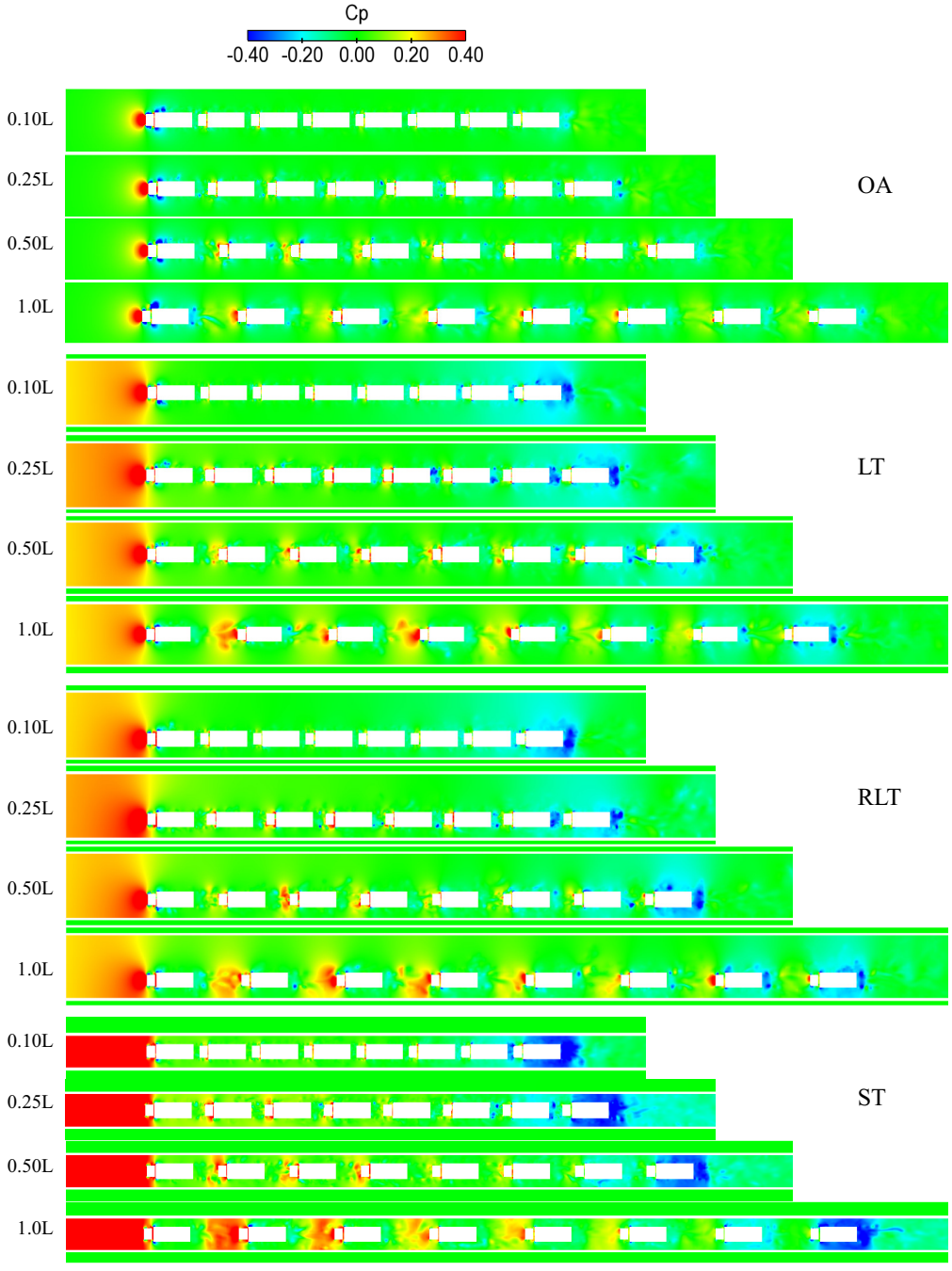

Figure 8.3: The pressure distribution during the lorry platoons of four spacings on the horizontal plane of $z/H = 0.57$ in the open air (OA), large tunnel (LT), right lane in the large tunnel (RLT) and small tunnel (ST).

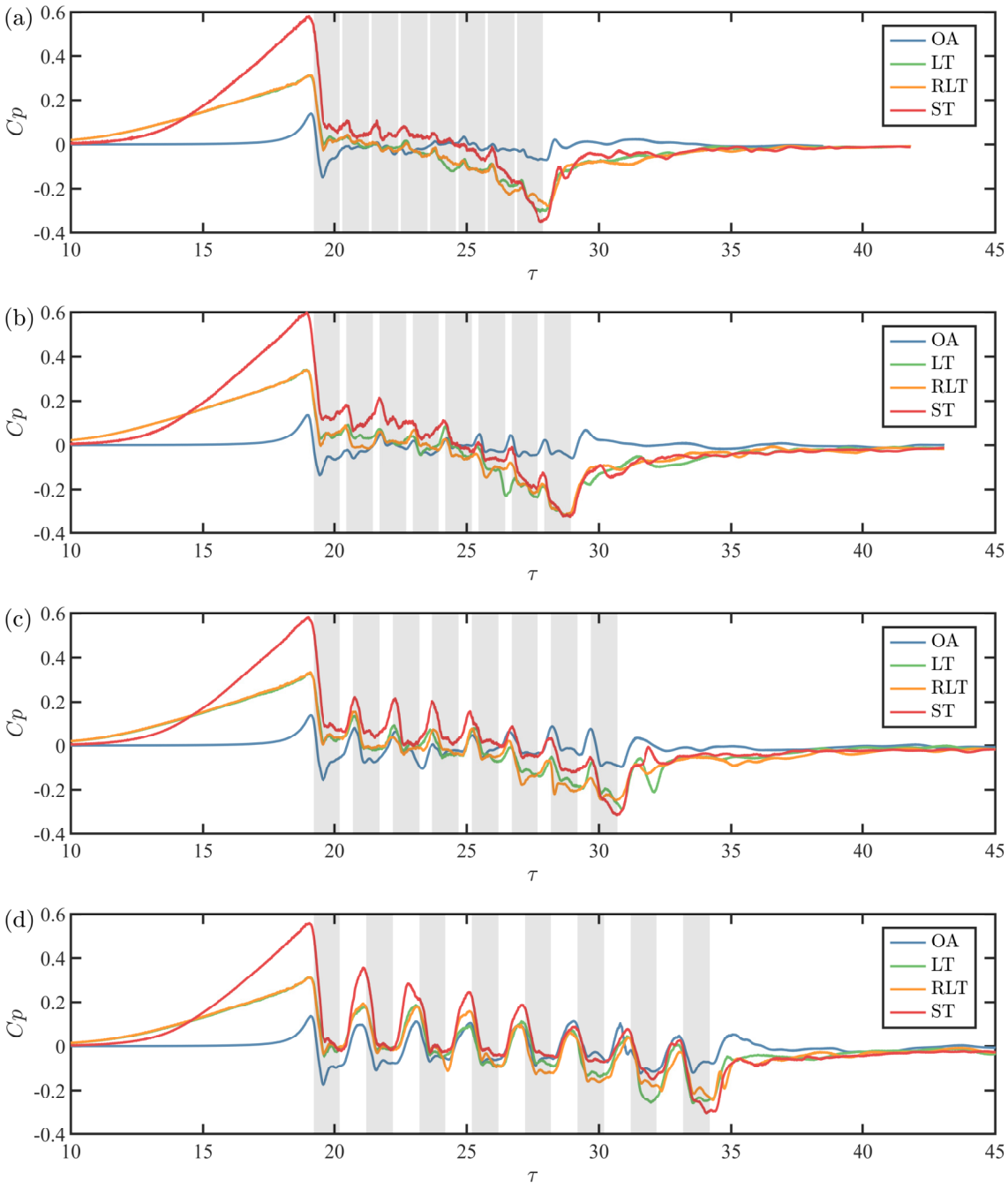

Figure 8.4: The temporal variations of the pressure coefficient in the open air (OA), large tunnel (LT), right lane in the large tunnel (RLT) and small tunnel (ST). The inter-vehicle spacing is: (a) $0.1L$, (b) $0.25L$, (c) $0.5L$ and (d) $1.0L$.

Figure 8.4 shows the aerodynamic flow around the lorry platoon, in terms of the pressure coefficients. The positive pressure peak when the leading lorry passes by and the negative pressure peak when the last lorry passes by is the same, regardless of the inter-vehicle spacing. For the shortest spacing, the pressure variation is close to the theoretical prediction as discussed in Appendix A. For large tunnels (blockage ratio 15%, opening ratio 0.6%), the positive peak reaches 0.3, which is similar to that when a train travels through a partially-enclosed tunnel with blockage ratio of 23% and opening ratio 1% (Gilbert 2014).

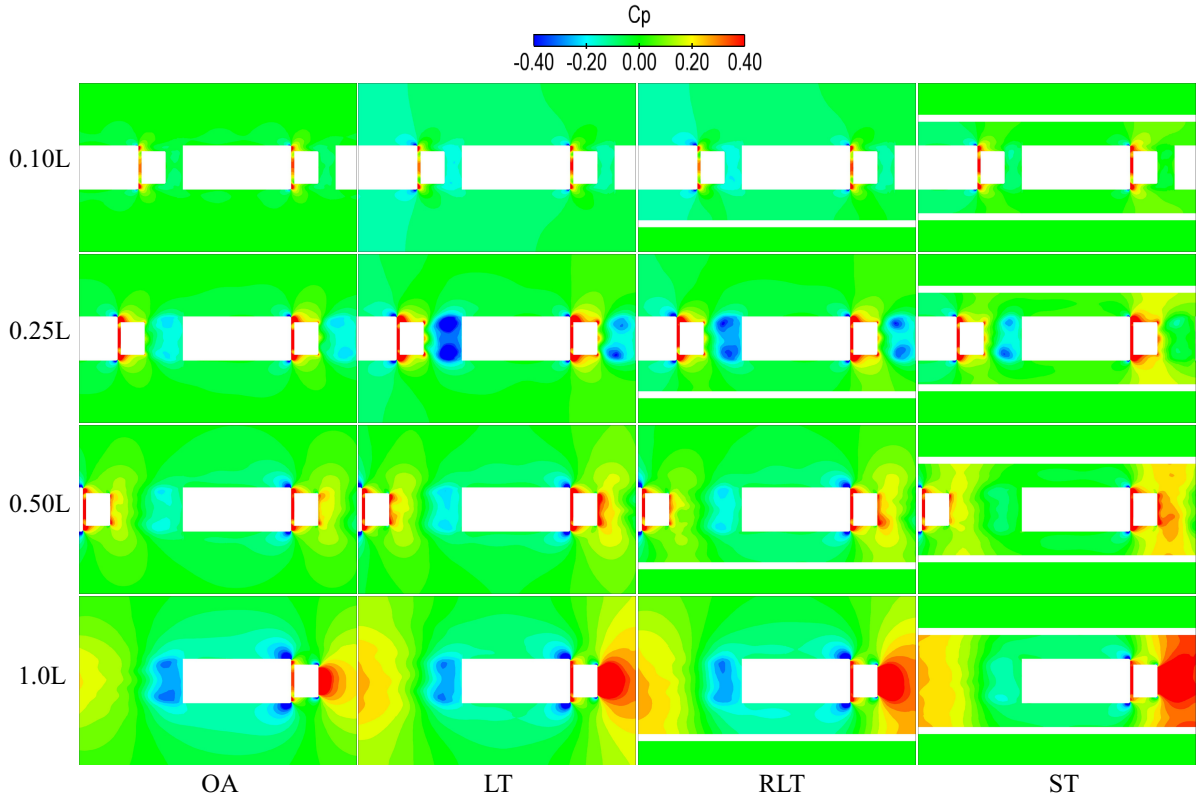

Figure 8.5: Time averaged pressure field around the fifth lorry of four spacings on the horizontal plane of $z/H = 0.57$ in the open air (OA), large tunnel (LT), right lane in the large tunnel (RLT) and small tunnel (ST).

Figure 8.5 provides the time averaged pressure field around the fifth lorry. It is clear that the frontal pressure decreases as the inter-vehicle spacing decreases. However, the rear pressure does not decrease monotonically with the spacing, being substantially larger at $0.25L$ then other spacings. This suggests that the drag variation with $0.25L$ spacing may behave differently.

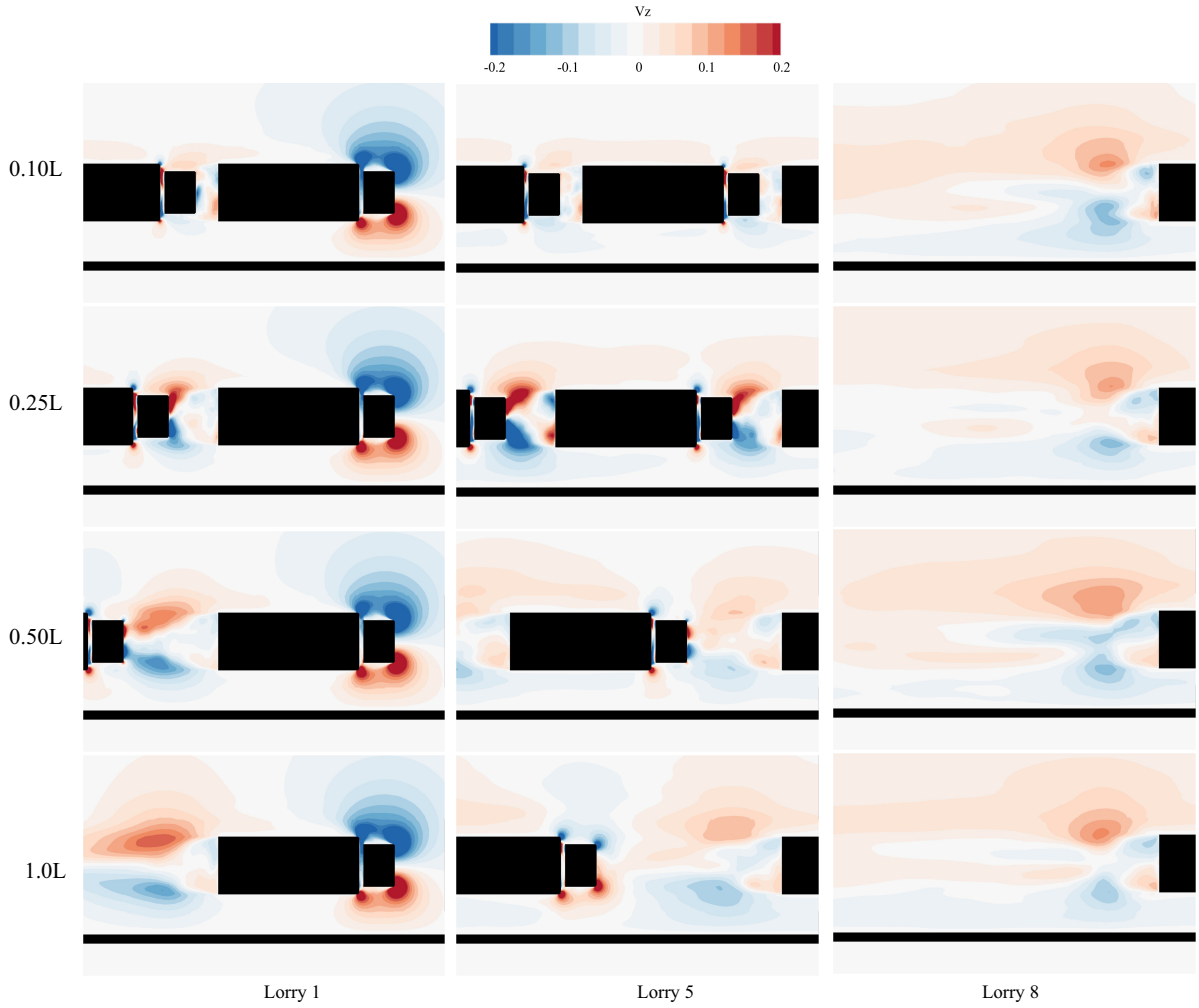

Figure 8.6: The normalised y-axis component velocity V at $z/H = 0.57$ in the right lane of the large tunnel (RLT).

To investigate the effect of spacing and traffic lane, Figure 8.6 shows the time-averaged lateral velocity on the top view. In the cab region of the leading lorry, the smaller lateral velocity to the closer wall is observed for all spacings. The lateral velocity in the wake region of the whole platoon, the lateral velocity flow to the wake center is smaller at the near wall side. At the spacing of $0.25L$, the lateral velocity in the gap region is significantly higher than that in $0.1L$ and $0.5L$ spaced platoon, indicating less air can flow to the gap region. This is consistent with the pressure field variation in Figure 8.5.

8.2 Flow structures

Figure 8.7 compares the detailed flow structures in the gap region between the fifth and the sixth lorry at the centreline plane. When the inter-vehicle spacing is larger than $0.5L$, there are two counter-rotating recirculation vortices in the near wake region. When the spacing is reduced to $0.25L$, the flow structures have been changed significantly. The bottom vortex is compressed at this spacing. As the spacing reduces to $0.1L$, the lower vortex almost disappears because there is not enough space to develop. In the open air, as the approaching of the trailing lorry, the upper vortex shrinks. At the smallest spacing ($0.1L$), the upper vortex becomes less distinguishable. However, when platoons with $0.25L$ spacing are travelling in the tunnels, the upper vortex is restricted to the top area of the cab due to the restriction of the upper wall of the tunnel. The air supposed to flow to the gap region is trapped around the lorry body, which may increase the surface pressure around the lorry box and decrease the base pressure of the intermediate lorries. When the inter-vehicle spacing is reduced from $0.25L$ to $0.1L$, the lower vortex practically vanishes, and the air flows directly upward rather than impinging on the front of the cab, which results in a significant reduction in frontal surface pressure at this spacing. It is reasonable to predict that the drag variation with spacing show different trend at $0.25L$ spacing between then open air and in the tunnels. Also, the drag of platoon will largely decrease when the spacing decreases from $0.25L$ to $0.1L$.

Figure 8.8 shows the streamline on the horizontal plane at $z/H = 0.57$. The two counter-rotating recirculation zones can be clearly identified at the $0.5L$ and $1.0L$. There is

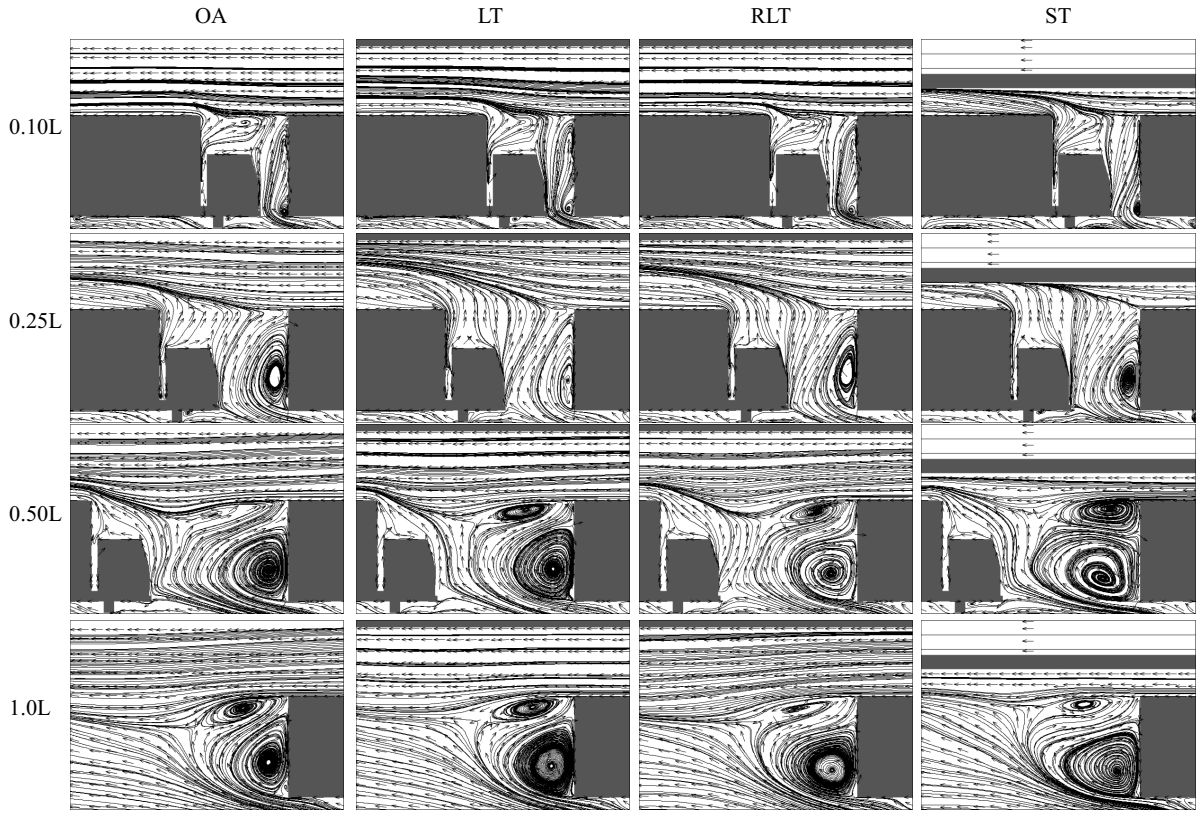

Figure 8.7: Illustrations of the wake flow structures of the fifth lorries in different platoons at $y/H = 0$.

an almost identical pattern of wake recirculation with a medium longitudinal dimension in the intermediate lorries. While at the spacing of $0.25L$, the two vortices have been squeezed. At the smallest spacing, there is no enough area for two vortices to develop in gap region. In the RLT case, the symmetry of the wake structure is marginally diminished.

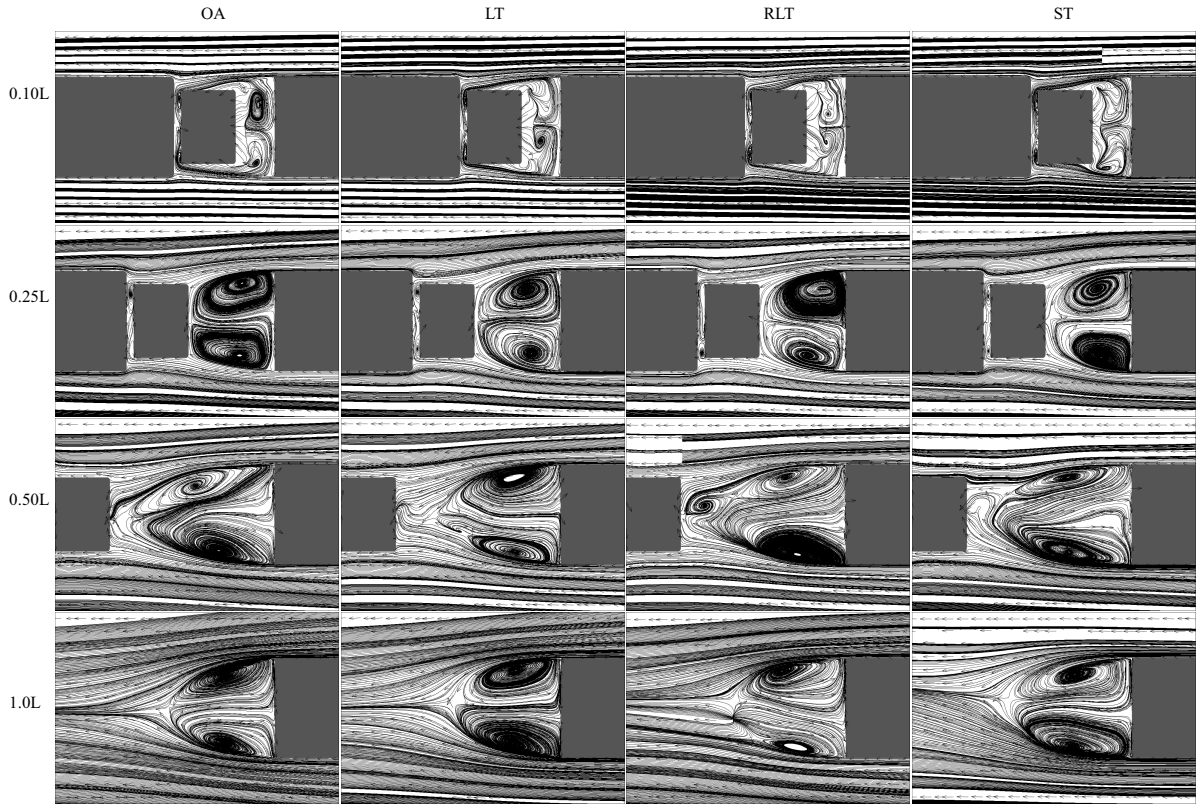

Figure 8.8: Illustrations of the wake flow structures of the fifth lorries in different platoons at $z/H = 0.57$.

8.3 Surface pressure analysis

As discussed in Section 8.2, the flow structure in the gap region is changed differently with the inter-vehicle spacing due to the existence of the tunnel walls. It is natural to expect that the pressure distributions around the middle lorries' surfaces are also different between the cases in the tunnels and the open air. Figure 8.9 illustrates a slice of the symmetry plane emanating from the O_1, which was used to evaluate the difference in frontal and rear

pressures and the flow separation along the box front edge. Additionally, the front loop of the box section, which originates from the O_2 (Tap 4 shown in Figure 3.7), is applied to examine the pressure distribution surrounding the box and to analyse the effect of the traffic lane.

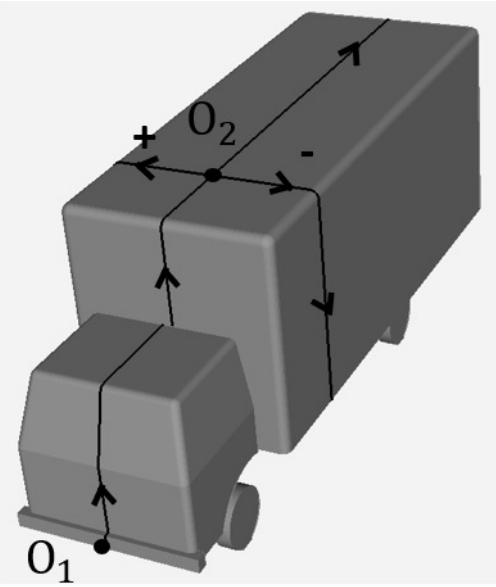

Figure 8.9: Two lines along the surface of the lorry to investigate the distribution of surface pressure coefficients.

Figure 8.10 presents the fifth lorries' time-averaged surface coefficients along the different platoons' central lines. The shaded areas are employed to distinguish different regions. The pressure on the cab front surface in the tunnels and the open-air decreases dramatically with the spacing decreases because of the more effective shielding effect. The largest drop of the frontal surface pressure occurs between $0.25L$ and $0.1L$, which is consistent with the flow structures variation discussed in Section 8.2. Box top and rear pressure likewise decrease monotonically with the spacing decrease in the open air. While in the tunnels, when the spacing reduces to $0.25L$ (denoted by the blue line), the surface pressure on the box top suddenly increases compared with the same lorry in other platoons, as shown in Figure 8.10 (b)-(d). In addition, the surface pressure in the box rear region of the middle lorry in the $0.25L$ platoon in the tunnels also show lower values than those of $0.1L$ and $0.5L$ platoons. The results are consistent with the analysis of the variation of the flow structures. The surface pressure does not change monotonically with the spacing in the tunnel, indicating

that the drag coefficient also does not change monotonically with the spacing. The high box top and side pressure of the intermediate lorry in $0.25L$ platoon may increase the skin friction combined with the lower base pressure, compared to the same lorry in the larger spacing platoon, which may increase the drag. This anomaly at a spacing of $0.25L$ can also be observed in the two large tunnels. It is reasonable to believe that the drag of intermediary vehicles does not decrease monotonically as the spacing reduces. A decrease in blockage ratio weakens the piston effect and thereby decreases approaching velocity. As a consequence, in the two large tunnels, the magnitudes of the negative peak, denotes the flow separation, are greater than those of the small tunnel on the front edge of the box, as shown in Figure 8.10.

Figure 8.11 shows the time-averaged surface pressure coefficients of the fifth lorry around the loop of the lorry box, as shown in Figure 8.9. The averaged standard deviation of all taps is shown by black error bar in each sub-figure for simplicity. With large spacing in the open air, the pressure is notably low, which past the box front edge where the separation occurs. The fifth lorry is more efficiently shielded as the spacing decreases, evidenced by the steadily increasing pressure coefficients. However, in the tunnels, the surface pressure at the lateral centreline does not increase monotonically as the spacing decreases. The surface pressure of the fifth lorry in the 0.25L platoon is higher than that in the $0.1L$ platoon, which is consistent with the analysis in Section 8.1. The upper vortex is restricted to the top area of the cab. The air supposed to flow to gap region is trapped around the lorry body, which increase the surface pressure around the lorry box, compared to lorries in other spacing platoons. A higher surface pressure around the box at this spacing means the lorry will have a higher skin fiction. When the platoon is travelling at the right lane in the large tunnel, the surface pressure around the box top remains generally symmetric, as shown in Figure 8.11 (c). The traffic lane has a negligible effect on the surface pressure.

With the help of the analysis of the surface pressure, one can gain a better understanding of the effect of inter-vehicle spacing on aerodynamic forces, which will be described in the following section.

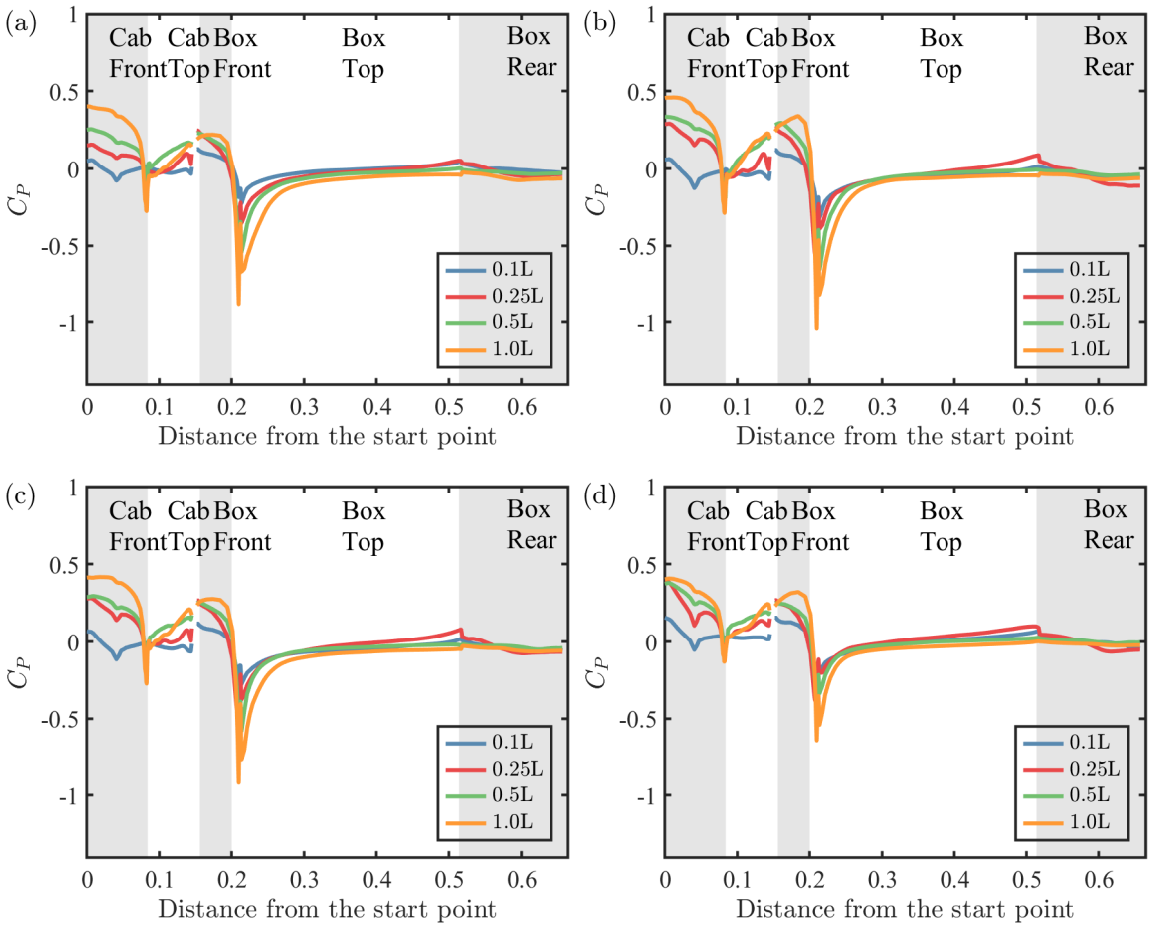

Figure 8.10: The mean surface pressure coefficients of the fifth lorries along the central line of different platoon: (a) in the open air; (b) in the large tunnel; (c) in the right lane of the large tunnel; (d) in the small tunnel. The shaded area is used to help to distinguish different regions along the lorry's surface.

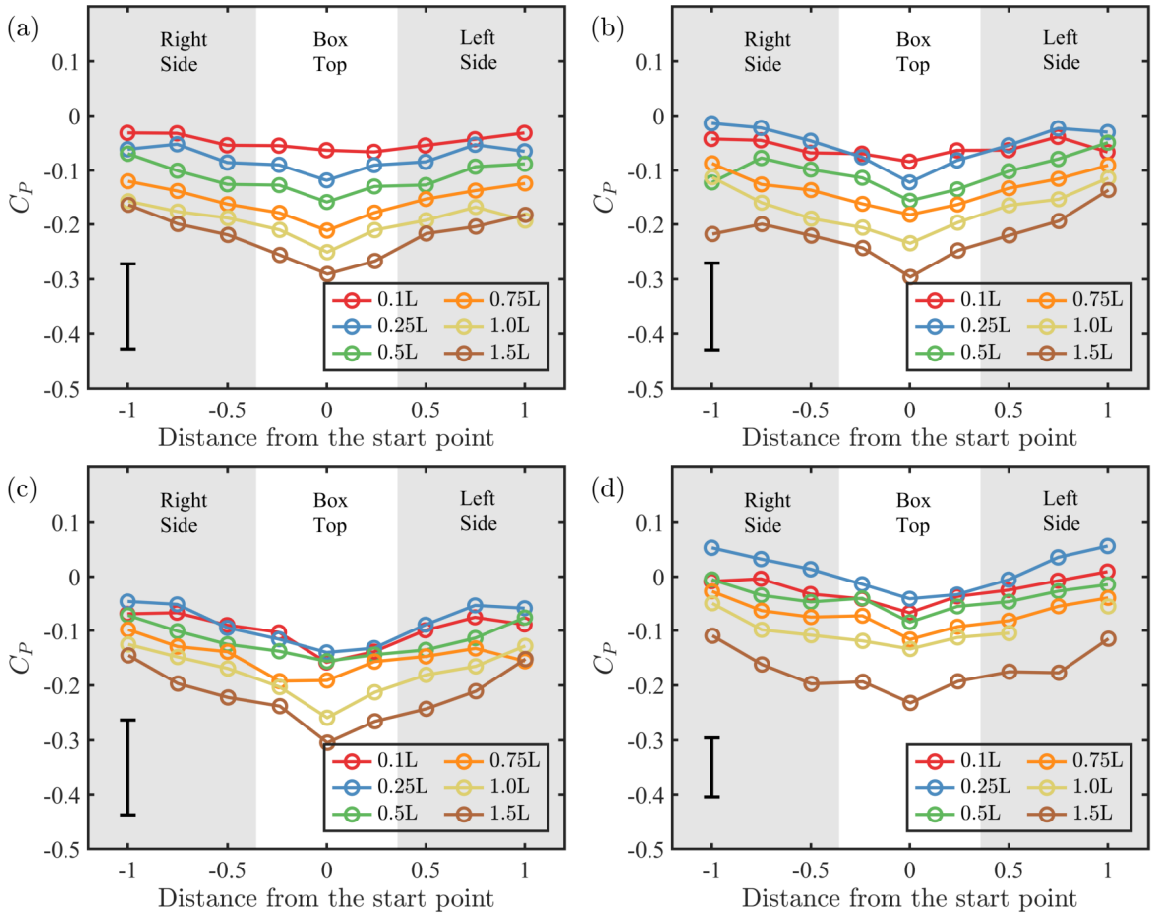

Figure 8.11: The mean surface pressure coefficients of the fifth lorries around the front loop of the lorry box: (a) in the open air; (b) in the large tunnel; (c) in the right lane of the large tunnel; (d) in the small tunnel. The shaded area is used to help to distinguish different regions along the lorry's surface. The averaged standard deviation of all taps is shown by black error bar in the lower left corner of each figure.

8.4 Force analysis

With regard to the time history of the drag, the fifth lorry is still used as the research target. Figure 8.12 shows the time history of drag coefficients of the fifth lorry in different platoons travelling in four cases. Overall, the shielding effect is more effective in narrower spacing platoons, with the fifth lorry in the $0.1L$ spacing having the lowest drag in all cases. As discussed in Section 8.2, when the spacing decreases from $0.25L$ to $0.1L$, the low vortex in the wake region almost disappears, the air flows directly upward rather than impinging on the front of the cab, leading to a considerable reduction in the frontal surface pressure. Accordingly, the greatest reduction in drag is observed between the $0.25L$ and $0.1L$ platoons, as shown in Figure 8.12. In the open air, the drag of the fifth lorry decreases in a monotonic manner with decreasing spacing. In the tunnels, however, the drag of the lorry in the $0.25L$ platoon (depicted by the blue line) is higher than in platoons with larger spacings, which is consistent with the analysis of the flow structure and the surface pressure distribution in Section 8.2 and Section 8.3.

To examine the effect of the spacing on each lorry in the platoons, the mean drag values are presented. Figure 8.13 compares the drag coefficients of each lorry in all platoons between the tunnels and the open air. The drag coefficients in the open air are monotonically decreasing with the spacing. Whilst, in the tunnel, as discussed in Section 8.2, when the spacing reduces to $0.25L$, the wake vortices are compressed, and the tunnel wall constrains the upper one. The air supposed to flow to the gap region is constrained at the side, increasing skin fiction and base drag. Therefore, the drag coefficients of the intermediate lorry in the $0.25L$ platoon in three tunnels are larger than the same lorry in the greater spacing platoon (see Figure 8.13 (b)-(d)). When the spacing keeps decreasing to $0.1L$, the drag reduce significantly in four cases, primarily due to the decrease of the frontal surface pressure. In addition, the leading lorries in all four cases benefit from the platoon, and benefit more from the smaller spacing because of the second lorry tends to progressively increase the base pressure of the first one as the spacing decreases. For the last lorry without trailing lorry tends to raise the rear pressure, there is an increase in the drag coefficient compared to its upstream lorry. This increase of the drag of the last lorry is most pronounced in the small tunnel case, where the piston effect is strongest. And the drag coefficients of the last

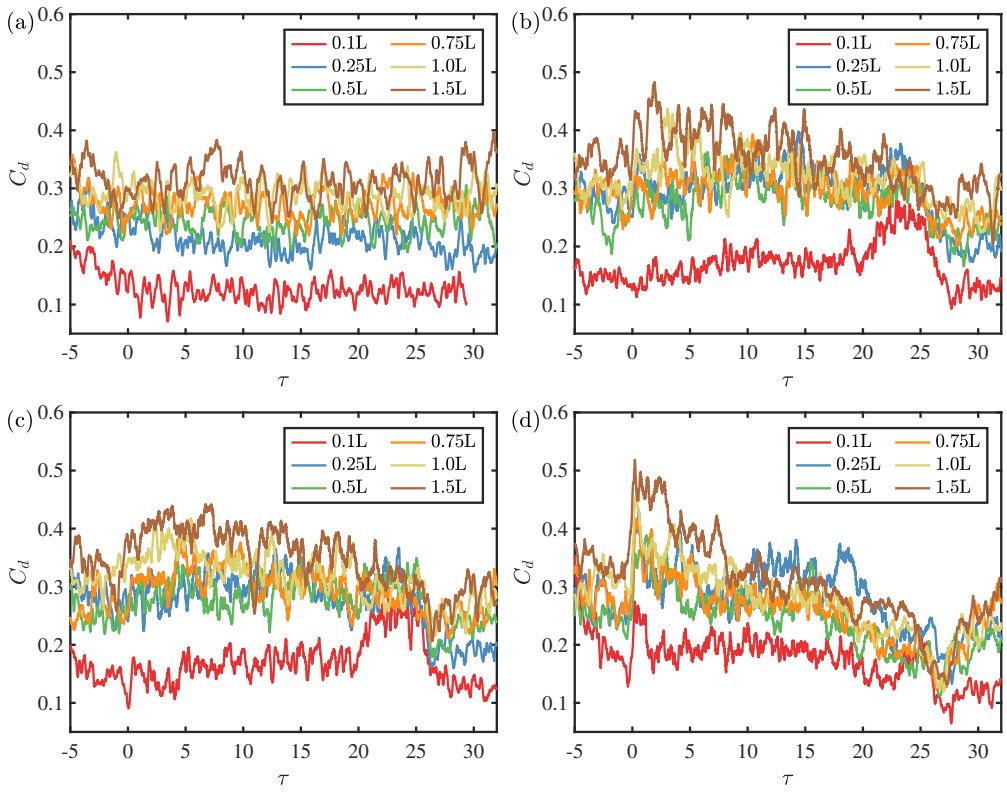

Figure 8.12: The time series of drag coefficients of different lorries in the platoon in the (a) open air, (b) large tunnel, (c) right lane in the large tunnel and (d) small tunnel.

lorry is almost irrelevant to the inter-vehicle spacings in the small tunnel.

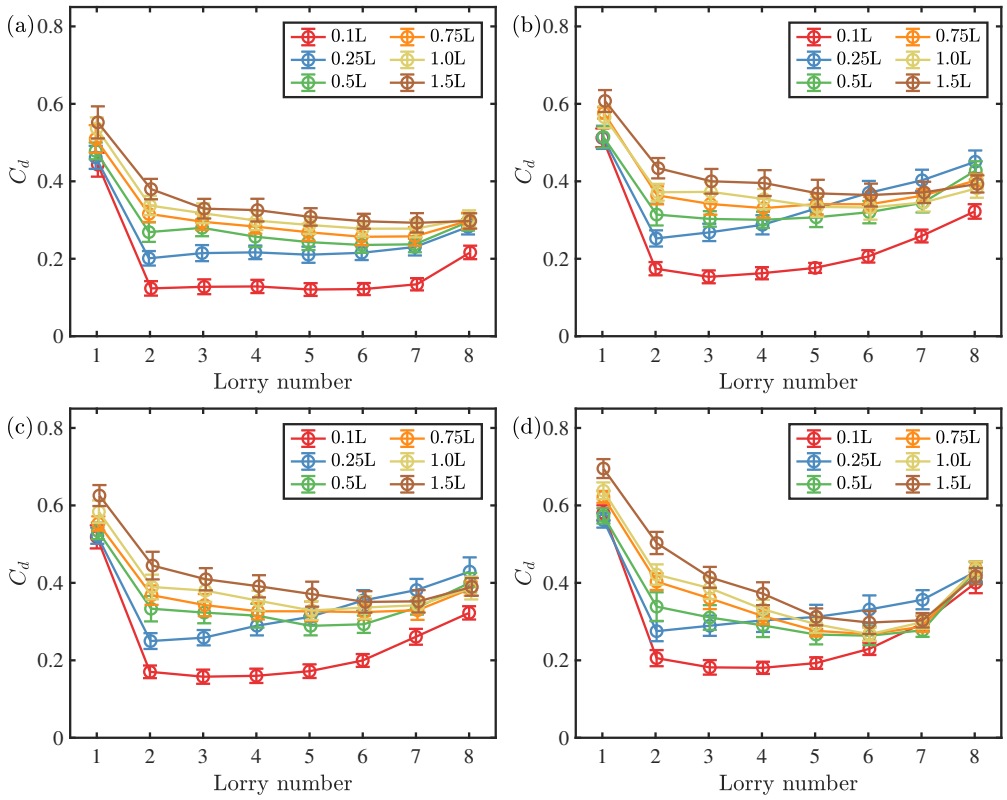

Figure 8.13: The mean drags coefficients of between lorries in platoons with different inter-vehicle spacing (a) in the open air, (b) in the large tunnel, (c) right lane of the large tunnel, (d) in the small tunnel.

To show the effect of the inter-vehicle spacing on the aerodynamic force on the entire platoon as a whole, Figure 8.14 (a) shows the overall mean drag of each the platoons verse the spacing. Generally, as the inter-vehicle distance increases, the overall drag of the whole platoon increases, but at a decreasing rate. In the open air, the overall mean drag increases monotonically with the inter-vehicle spacing. while in the tunnels, the $0.25L$ platoon has a slightly overall drag coefficient than the $0.5L$ platoon. At the same spacing, the overall drag in all tunnels is approximately 0.1 greater than that in the open air. With the exception of the $0.1L$ spacing platoon, the blockage ratio has no significant effect on the overall drag. As discussed in Section 7.4, increasing the blockage ratio does not lead to an increase the drag of every lorry in the platoon. The drag coefficient in the large tunnel is lower for the first two and the last lorries, but higher for the fourth to seventh vehicles than those in the small

tunnel, resulting in a practically equal overall drag in both tunnel sizes (see Figure 8.14 (a)). While at the closest spacing ($0.1L$), the whole platoon resembles a single freight train, with greater drag in small tunnels and lower drag in large tunnels. Therefore, the overall drag of the platoon at $0.1L$ in the small tunnel is higher than in other two large tunnels. The traffic lane also has no effect on the overall drag of the platoons.

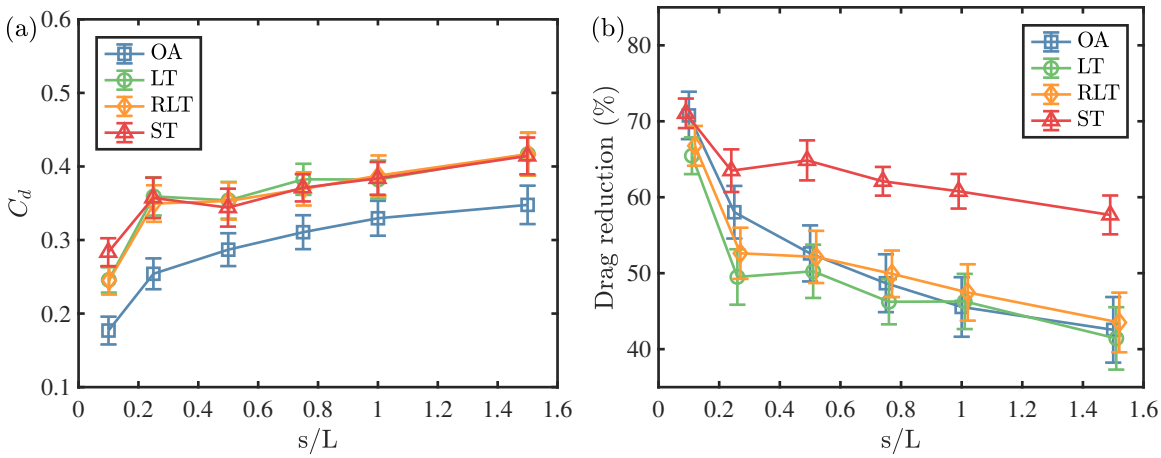

Figure 8.14: A comparison of the (a) C_d and (b) drag reduction ratio $(1-C_d/C_{d-single})\times 100\%$ across all lorries in the platoon with respect to the spacing ratio among four cases.

Figure 8.14 (b) presents the drag reduction ratio of all lorries in the platoon, relative to the eight isolated lorries in separate cases, with respect to the inter-vehicle spacing. The drag coefficients of single lorry are listed in Table 5.2. In the open air, the platoon with the smallest spacing ($0.1L$) enjoys the most significant drag reduction (72%). The drag reduction ratio decreases with the increasing spacing and declines more slowly when the spacing is relatively large, which is consistent with the experiments reported in Robertson et al. (2019). The inter-vehicle spacing has a greater impact on the total drag reduction ratio in the small tunnel than it does in the large tunnels or open air. In the tunnels, the drag reduction also decreases with the spacing increase except for the platoon with $0.25L$ spacing. The drag reduction for the $0.25L$ platoon is smaller than the $0.5L$ platoon, implying less fuel-saving benefit. It is a reasonable approach to minimize inter-vehicle spacing in open areas in order to achieve a more significant fuel-saving benefit. However, when it comes to the case in a tunnel, the inter-vehicle spacing should be carefully chosen. Considering that the $0.1L$ is too small to achieve in the actual situation, the spacing of $0.5L$ should be the best choice when the long lorry platoon is travelling inside a road tunnel.

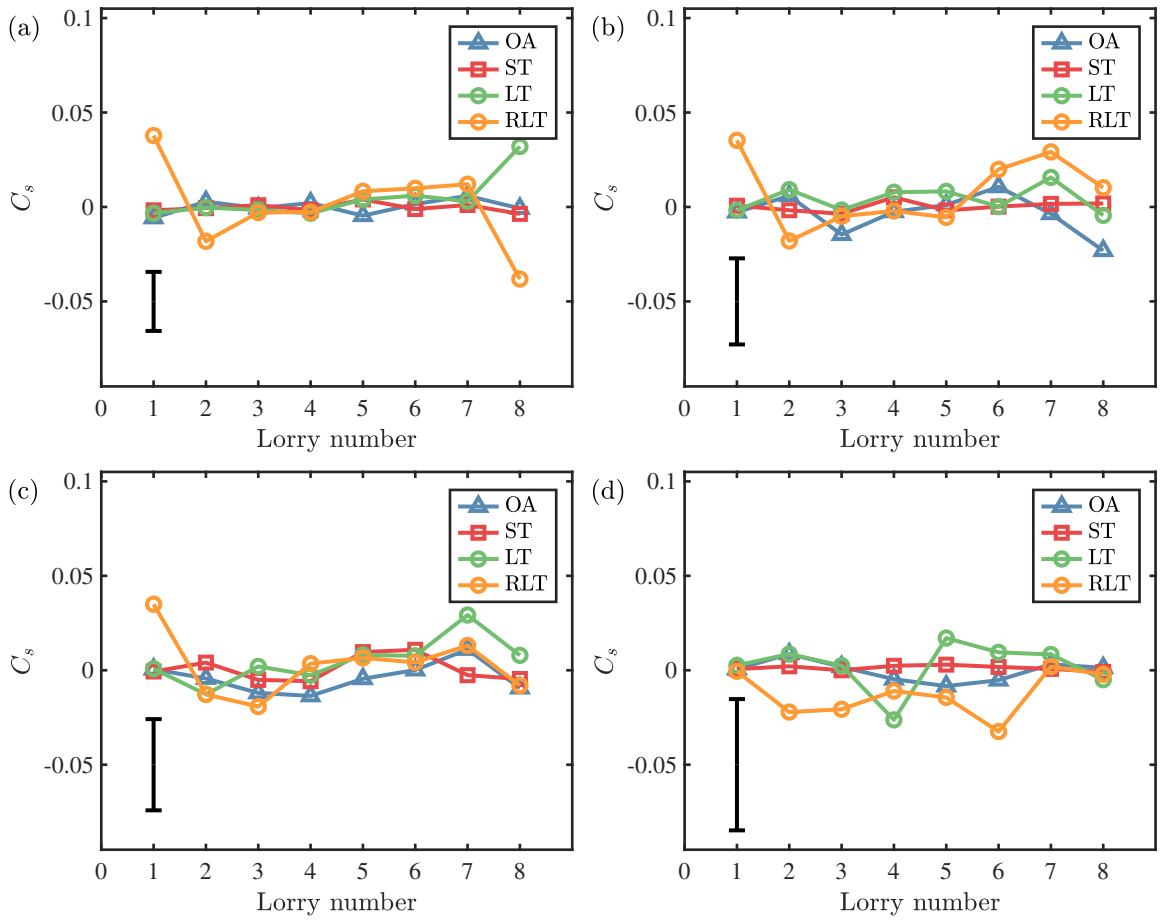

Figure 8.15: The side force coefficients of each lorry in the (a) $0.1L$, (b) $0.25L$, (c) $0.5L$ and (d) $1.0L$ platoon in four cases. The averaged standard deviation of all lorries is shown by black error bar.

Figure 8.15 compares the side force of every lorry in different spacing platoons in four cases. The averaged standard deviation of all lorries is shown by black error bar in each sub-figure for simplicity. At the closest spacing (see Figure 8.15 (a)), the leading lorry in the RLT case experiences a side force toward the near tunnel wall, but the last lorry experiences a side force in the opposite direction. This non-zero side force is created by the pressure field being asymmetric, as illustrated in Figure 7.4. In $0.25L$ and $0.5L$ spacing platoons, non-zero side forces for the leading lorry still exist, but not in larger spacing platoons ($1.0L$ in Figure 8.15 (d) and $1.5L$ in Figure 7.13). Additionally, as the spacing increases, the deviation increases, indicating a more significant side force fluctuation. With increasing inter-vehicle spacing, the influence of lanes becomes less significant. As discussed in the single lorry and $1.5L$ platoon, the r.m.s value are around one order higher than the side force coefficient itself. The analysis above can help us the to understand the effect of asymmetry of the traffic lane, but the any conclusions from current data is inconclusive. A more thorough investigation is required.

8.5 Conclusion

The chapter focuses on the inter-vehicle spacing. The effect of the inter-vehicle spacing on the slipstream properties, surface pressure and aerodynamic forces are discussed. According to the results and discussions, the following are some important findings:

- The magnitudes of the positive pressure peak before the leading lorry and the negative pressure peak after the last lorry are independent of the inter-vehicle spacing. With the decrease of the spacing, the pressure differential between intermediate lorries decreases in four cases.
- When the spacing is above $0.5L$, there are two counter-rotating recirculation vortices in the near wake region. The bottom vortex is compressed when the spacing is down to $0.25L$, and the upper vortex becomes less distinguishable in the open air. While in the tunnels, the upper vortex is confined by the tunnel wall. The air supposed to flow the gap region is trapped around the lorry body, which may increase the surface pressure

around the lorry box and decrease the base pressure of the intermediate lorries.

- In both the tunnels and the open air, the frontal surface pressure of the intermediate lorry decreases dramatically with the spacing decrease due to the more substantial shielding effect, which is the main reason for the drag reduction with the decline of spacing. However, because of the flow structure change, the intermediate lorries in the $0.25L$ platoon have higher box-side surface pressure and lower rear surface pressure than the same lorries in the $0.1L$ and $0.5L$ platoon in the tunnel.

- With the exception of the $0.1L$ spacing platoon,the blockage ratio has no significant effect on the overall drag of the platoons because the effect of blockage ratio on drag is different for each lorry in the platoon. As for the $0.1L$ platoon, the whole platoon resembles a single freight train, with greater drag in small tunnels and lower drag in larger tunnels.

- In the open air, the overall drag coefficient of the platoon is monotonically increasing with the inter-vehicle spacing increasing, but the increasing rate becomes slower for large spacings. In the small and large tunnels, the shielding effect still dominates the general trend of the drag properties. However, because of the anomalous drag behaviour at the inter-vehicle spacing of 0.25L, the overall drag coefficients of the platoons in the tunnels no longer follow a monotonic function of the inter-vehicle spacing. Although the overall drag coefficients of the platoons in the large and small tunnels are surprisingly identical, the drag reduction ratios due to platooning are more significant in the small tunnel.

Chapter Nine

Conclusions and Future work

9.1 Introduction

The main aim of the this research was to characterise the aerodynamic flow around a long lorry platoon travelling inside road tunnels and investigate the effect of the inter-vehicle spacing, blockage ratio and the traffic lane position on the aerodynamic forces. To achieve this goal, both model-scale experiments and numerical simulations were conducted. Several conclusions are summarised in this section in light of the research goal and objectives described in Chapter 1. A description of each objective is provided in the next section, followed by a review of the work done to achieve that objective and the conclusions. The next section contains a description of each objective, as well as the discussion of the work and the conclusions. Some recommendations for future work on the platoon aerodynamic in road tunnel are discussed in Section 9.3.

9.2 Conclusions

Objective 1: Compare the aerodynamics behaviors of a long platoon travelling through a road tunnel and the open air The method for performing slipstream experiments at the TRAIN rig with the model lorry platoon are presented in Chapter 3. The

numerical simulation method and validation are introduced in Chapter 4. The slipstream properties, surface pressure and drag force are discussed and compared to the data obtained in the open air. Some main findings of this study are as follow.

- The scale-down (at 1/20th) moving model vehicle experiments have been performed to the simulate the relative motion between the moving lorry platoon and the road tunnel. The slipstream pressure and velocity, as well as the surface pressure were monitored.
- Stronger flows are induced in the frontal and rear regions of the platoon in the tunnel than in the open air due to the piston effect. The influenced regions expand faster when the platoon is travelling inside the tunnel. Both experimental and numerical results reveal greater static pressure variations near the frontal regions of the leading lorries and the rear region of the last lorry in the tunnel.
- The flow structures around the lorry platoon are altered due to the tunnel walls: Fewer vortices are generated from the front edge of the lorry, and larger upper vortices are observed in the rear region. A weaker flow separation leads to a smaller drop in the surface pressure near the box front edge, as compared to the case in the open air.
- The variations of the drag coefficients show similar behaviours with the surface pressure, exhibiting great variations while entering and leaving the tunnel. In contrast to the case in the open air, the mean drag coefficient in the tunnel is no longer monotonically decreasing from the first to the last lorry in the platoon. Rather, it significantly decreases to a plateau at the fifth lorry and then increases again greatly at the last lorry due to strongly negative rear pressures.
- All vehicles, in both the tunnel and the open air, experience a reduction in drag due to platooning. The drag is consistently higher in the tunnel than in the open air for both isolated vehicles and platoons. However, the drag reduction due to platooning is consistently greater in the tunnel than in the open air. This implies a greater potential to reduce fuel consumption in the tunnel than in the open air.

Objective 2: Investigate the effects of tunnel's blockage ratio and the traffic lane position on the aerodynamic performance An in depth analysis of the effect of

the blockage ratio and the traffic lane symmetry is presented in Chapter 7. Some important findings from related discussion and analysis are as follows.

- When the blockage ratio decreases, the piston effect becomes less effective, resulting in a flow field similar to that seen in the open air. Also a decrease in the peak value of the high frontal and low rear pressures has been noticed. In addition, the size of vortices surrounding the box has increased, the size of the upper vortices is reduced and the size of the lower vortices increased to a level comparable to those of the vortices in the open air. When entering the large tunnel, the magnitude of the drag variation decreases.

- Unlike a single lorry, increasing the blockage ratio does not lead to an increase of the drag of every lorry in the platoon. In a small tunnel, the fourth to seventh lorries have smaller drag coefficients, while others have larger drag coefficients compared to the lorries in large tunnels. The variation in drag and drag reduction ratios along the platoon approaches the pattern observed in the open air.

- Driving in the right lane of the large tunnel causes the pressure field to become asymmetrical, which is noticeable in the front region of the leading lorry but has minimal impact on the strength of the piston effect. In addition, travelling on the right side of the tunnel causes the pressure and velocity flow field to deviate from its symmetrical position in the front region of the platoon and the wake region of each lorry.

- The effect of the position of traffic lane on the drag coefficient is negligible. The variation in drag and drag reduction ratios along the platoon is nearly identical between two lanes in the large tunnel.

Objective 3: Investigate the effects of inter-vehicle spacing on platoon aerodynamic performance in tunnel

An in depth analysis of the effect of inter-vehicle spacing is presented in Chapter 8. All data sets are gathered together from four cases. The following are some important findings:

- The magnitudes of the positive peak before the leading lorry and the negative peak after the last lorry are independent of the inter-vehicle spacing. With the decrease

of the spacing, the pressure differential between intermediate lorries decreases in four cases.

- When the spacing is above $0.5L$, there are two counter-rotating recirculation vortices in the near wake region. The bottom vortex is compressed when the spacing is down to $0.25L$, and the upper vortex becomes less distinguishable in the open air. While in the tunnels, the upper vortex is confined by the tunnel wall. The air supposed to flow the gap region is trapped around the lorry body, which may increase the surface pressure around the lorry box and decrease the base pressure of the intermediate lorries.

- In both the tunnels and the open air, the frontal surface pressure of the intermediate lorry decreases dramatically with the spacing decrease due to the more substantial shielding effect, which is the main reason for the drag reduction with the decline of spacing. However, because of the flow structure change, the intermediate lorries in the $0.25L$ platoon have higher box-side surface pressure and lower rear surface pressure than the same lorries in the $0.1L$ and $0.5L$ platoon in the tunnel.

- With the exception of the $0.1L$ spacing platoon,the blockage ratio has no significant effect on the overall drag of the platoons because the effect of blockage ratio on drag is different for each lorry in the platoon. As for the $0.1L$ platoon, the whole platoon resembles a single freight train, with greater drag in small tunnels and lower drag in large tunnels.

- In the open air, the drag coefficients of all lorries are monotonically decreasing with the spacing due to the stronger shielding effect. In the tunnels, the shielding effect still dominates the drag reduction. However, the overall drag reduction ratio is no longer monotonically increases with the decreasing spacing. Although the overall drag coefficients of the platoons in the large and small tunnels are surprisingly identical, the drag reduction ratios due to platooning are more significant in the small tunnel.

9.3 Directions for Future Work

The following suggestions for future research are proposed based on findings and conclusions drawn from the research conducted.

9.3.1 Geometry Variation

This research focused on the Leyland DAF 45–130, a typical commercial lorry, to investigate aerodynamics of vehicles in platoon travelling through the road tunnel. It is observed that there is a different trend in the drag with spacing in the road tunnel when compared to the open air. Other representative geometries of current production vehicles should be tested to gain a complete understanding of the effects of spacings and number of vehicles on the reduction of drag in the tunnel. For example, frontal geometry sensitivity (lorries with cabs are taller and faired), the trailer-tracker spacing and base geometry sensitivity are all required to account for the vast number of vehicles shapes currently on the road.

The second one is the tunnel geometry. Due to the experimental constraints, the present experiments were conducted in a single-lane 10-meter tunnel with rectangular cross-section. The traffic lane effect was investigated by the simulations in this work. However, the influence of the shape of cross-section and the tunnel length still remains unexplored. Tunnels with a semi-circular cross-section are more common in rural areas. Finally, extending the length of tunnel refers to the gathering of more precise mean data with less variation.

9.3.2 Unsteady Phenomena

It is critical to characterize the unsteady flow phenomena and their potential impact on the stability of the platoon in the tunnel. Some attempts to investigate the unsteady phenomena on the platoon in the open air were mentioned in the literature review. In order to achieve this, either directly measuring the force with a high response balance or, more alternatively, integrating finely populated tapping of unsteady surface pressures would be required. When the unsteady results are coupled with a vehicle dynamics response model, the stability issues

imposed by vehicle platoon can be identified and addressed. However, due to the experimental limitations of the equipment, only a few surface pressure taps were mounted on the lorry, making it difficult to analyze the platoon's unsteady characteristic inside the tunnel. Future work may improve the experimental facility to investigate the unsteady characteristics.

9.3.3 Detail study of the wake structures

In this work, the platoon is travelling in order to model the relative motion between the platoon and the tunnel. As a result, studying wake structures is a difficult task in this scenario. Existing non-intrusive technologies, such as Particle Image Velocimetry (PIV), might be utilized to validate the simulation of the wake structures and to expand on the possibilities of investigating the modes of influence in platoons using Proper Orthogonal Decomposition (POD). The critical issue is how to develop equipment that can accurately monitor the flow structures of a moving object.

List of References

Abdel Azim, Ahmed F., and Ahmed F. Abdel Gawad. 2000. "A Flow Visualization Study of the Aerodynamic Interference Between Passenger Cars". In *SAE Technical Papers*. 724. doi:10.4271/2000-01-0355. https://www.sae.org/content/2000-01-0355/.

ACIN. 2012. "Betz micromanometer-Factory Standard for pressure calibration". *Versão EN0*. Visited on 12/22/2021. https://acin.nl/.

Ahmed, S.R., G. Ramm, and G. Faltin. 1984a. "Some Salient Features Of The Time-Averaged Ground Vehicle Wake". doi:10.4271/840300. https://www.sae.org/content/840300/.

Ahmed, Syed R, G Ramm, and Gunter Faltin. 1984b. "Some salient features of the time-averaged ground vehicle wake". *SAE Transactions*: 473–503.

Alam, Assad Al, Ather Gattami, and Karl Henrik Johansson. 2010. "An experimental study on the fuel reduction potential of heavy duty vehicle platooning". In *13th International IEEE Conference on Intelligent Transportation Systems*, 306–311. IEEE. ISBN: 978-1-4244-7657-2. doi:10.1109/ITSC.2010.5625054. http://ieeexplore.ieee.org/document/5625054/.

Altaf, Alamaan, Ashraf A. Omar, and Waqar Asrar. 2014. "Passive drag reduction of square back road vehicles". *Journal of Wind Engineering and Industrial Aerodynamics* 134:30–43. ISSN: 01676105. doi:10.1016/j.jweia.2014.08.006. https://linkinghub.elsevier.com/retrieve/pii/S0167610514001640.

Altinisik, Armagan, Onur Yemenici, and Habib Umur. 2015. "Aerodynamic Analysis of a Passenger Car at Yaw Angle and Two-Vehicle Platoon". *Journal of Fluids Engineering* 137 (12): 121107. ISSN: 0098-2202. doi:10.1115/1.4030869. http://fluidsengineering.asmedigitalcollection.asme.org/article.aspx?doi=10.1115/1.4030869.

Ashrafi, Khosro, et al. 2012. "Numerical Simulation of Air Pollutant Distribution in Urban Tunnels". *Environmental Modeling and Assessment* 17 (5): 555–564. ISSN: 14202026. doi:10.1007/s10666-012-9308-4. http://link.springer.com/10.1007/s10666-012-9308-4.

Awbi, H. B. 1983. "Effect of blockage on the strouhal number of two-dimensional bluff bodies". *Journal of Wind Engineering and Industrial Aerodynamics* 12 (3): 353–362. ISSN: 01676105. doi:10.1016/0167-6105(83)90055-7.

Baker, C. J. 2014. "A review of train aerodynamics Part 2 – Applications". *The Aeronautical Journal* 118, no. 1202 (): 345–382. ISSN: 0001-9240. doi:10.1017/S0001924000009179. https://www.cambridge.org/core/product/identifier/S0001924000009179/type/journal_article.

Baker, C. J., et al. 2001. "The slipstream and wake of a high-speed train". *Proceedings of the Institution of Mechanical Engineers, Part F: Journal of Rail and Rapid Transit* 215, no. 2 (): 83–99. ISSN: 0954-4097. doi:10.1243/0954409011531422. http://journals.sagepub.com/doi/10.1243/0954409011531422.

Baker, C.J. 2001. "Flow and dispersion ground vehicle wakes". *Journal of Fluids and Structures* 15 (7): 1031–1060. ISSN: 08899746. doi:10.1006/jfls.2001.0385. https://www.sciencedirect.com/science/article/pii/S0889974601903858.

— . 1991a. "Ground vehicles in high cross winds part I: Steady aerodynamic forces". *Journal of Fluids and Structures* 5 (1): 69–90. ISSN: 08899746. doi:10.1016/0889-9746(91)80012-3. https://linkinghub.elsevier.com/retrieve/pii/0889974691800123.

— . 1991b. "Ground vehicles in high cross winds part II: Unsteady aerodynamic forces". *Journal of Fluids and Structures* 5 (1): 91–111. ISSN: 08899746. doi:10.1016/0889-9746(91)80013-4. https://linkinghub.elsevier.com/retrieve/pii/0889974691800134.

Baker, Chris. 2010. "The flow around high speed trains". *Journal of Wind Engineering and Industrial Aerodynamics* 98 (6-7): 277–298. ISSN: 01676105. doi:10.1016/j.jweia.2009.11.002. http://dx.doi.org/10.1016/j.jweia.2009.11.002.

Baker, Christopher, et al. 2016. "Transient aerodynamic pressures and forces on trackside and overhead structures due to passing trains. Part 1: Model-scale experiments; Part 2: Standards applications". *Proceedings of the Institution of Mechanical Engineers, Part F: Journal of Rail and Rapid Transit* 228 (1): 37–70. ISSN: 0954-4097 2041-3017. doi:10.1177/0954409712464859.

Barmpas, Fotios, I. Ossanlis, and N. Moussiopoulos. 2011. "Numerical study for the flow around moving cars and its effect on the dispersion of the traffic emitted pollution within a road tunnel". *International Journal of Environment and Pollution* 44 (1-4): 307. ISSN: 0957-4352. doi:10.1504/IJEP.2011.038431. http://www.inderscience.com/link.php?id=38431.

Bergenhem, Carl, et al. 2010. "Challenges of platooning on public motorways". In *17th world congress on intelligent transport systems*, 1–12.

Bergenhem, Carl, et al. 2012. "Overview of platooning systems". In *Proceedings of the 19th ITS World Congress, Oct 22-26, Vienna, Austria*.

Bhautmage, Utkarsh, and Sharad Gokhale. 2016. "Effects of moving-vehicle wakes on pollutant dispersion inside a highway road tunnel". *Environmental Pollution* 218:783–793. ISSN: 18736424. doi:10.1016/j.envpol.2016.08.002. http://dx.doi.org/10.1016/j.envpol.2016.08.002.

Biermann, D. and Jr Herrnstein, William H. 1933. "The Interference between Struts in Various Combinations". *Technical Report Archive & Image Library*.

Boussinesq, Joseph. 1877. *Essai sur la théorie des eaux courantes*. Impr. nationale.

Bradley, Ron, et al. 2000. "Technology roadmap for the 21st century truck program". *21CT-001, USA, Download from: www. doe. gov/bridge*.

Brohus, H., K. D. Balling, and D. Jeppesen. 2006. "Influence of movements on contaminant transport in an operating room". *Indoor Air* 16 (5): 356–372. ISSN: 0905-6947. doi:10.1111/j.1600-0668.2006.00454.x. https://onlinelibrary.wiley.com/doi/10.1111/j.1600-0668.2006.00454.x.

Browand, Fred. 2005. "Reducing Aerodynamic Drag and Fuel Consumption". *Workshop on Advanced Transportation*: 1–27.

Browand, Fred, John Mcarthur, and Charles Radovich. 2004. *Fuel Saving Achieved in the Field Test of Two Tandem Trucks*. Tech. rep. https://escholarship.org/uc/item/29v570mm.

Bruneau, Charles-Henri, Khodor Khadra, and Iraj Mortazavi. 2017. "Flow analysis of square-back simplified vehicles in platoon". *International Journal of Heat and Fluid Flow* 66:43–59. ISSN: 0142727X. doi:10.1016/j.ijheatfluidflow.2017.05.008. http://dx.doi.org/10.1016/j.ijheatfluidflow.2017.05.008.

Bull, M. K., et al. 1996. "Interaction between a vortex wake and an immersed rectangular plate". *Experimental Thermal and Fluid Science* 12 (2): 209–220. ISSN: 08941777. doi:10.1016/0894-1777(95)00099-2.

Burton, David, et al. 2013. "Contribution of Add-On Components to the Aerodynamic Drag of a Cab-Over Truck-Trailer Combination Vehicle". *SAE International Journal of Commercial Vehicles* 6 (2): 2013–01–2428. ISSN: 1946-3928. doi:10.4271/2013-01-2428. https://www.sae.org/content/2013-01-2428/.

Carbaugh, Jason, Datta N. Godbole, and Raja Sengupta. 1998. "Safety and capacity analysis of automated and manual highway systems". *Transportation Research Part C: Emerging Technologies* 6 (1): 69–99. ISSN: 0968090X. doi:10.1016/S0968-090X(98)00009-6. https://linkinghub.elsevier.com/retrieve/pii/S0968090X98000096.

Carlino, G, D Cardano, and A Cogotti. 2007. *A new technique to measure the aerodynamic response of passenger cars by a continuous flow yawing*. Report 0148-7191. SAE Technical Paper. doi:https://doi.org/10.4271/2007-01-0902.

Carlino, G, and A Cogotti. 2006. "Simulation of Transient Phenomena with the Turbulence Generation System in the Pininfarina Wind Tunnel". *SAE Transactions*: 1004–1018. ISSN: 0096-736X. doi:10.4271/2012-01-2045.

Chan, Eric. 2012. "Overview of the SARTRE Platooning Project: Technology Leadership Brief". *SAE Technical Paper 2012-01-9019*. doi:https://doi.org/10.4271/2012-01-9019.

Cheli, F., et al. 2006. "Numerical–experimental approach for evaluating cross-wind aerodynamic effects on heavy vehicles". *Vehicle System Dynamics* 44 (sup1): 791–804. ISSN: 0042-3114. doi:10.1080/00423110600886689. http://www.tandfonline.com/doi/abs/10.1080/00423110600886689.

Cheli, F., et al. 2011. "Wind tunnel tests on heavy road vehicles: Cross wind induced loads—Part 1". *Journal of Wind Engineering and Industrial Aerodynamics* 99 (10): 1000–1010. ISSN: 01676105. doi:10.1016/j.jweia.2011.07.009. http://dx.doi.org/10.1016/j.jweia.2011.07.009.

Chen, A. L, Omer Savas, and Karl Hedrick. 1997. *Transient Vehicle Aerodynamics In Four-car Platoons*. Tech. rep. UC Berkeley: California Partners for Advanced Transportation Technology. https://escholarship.org/uc/item/5048k2gw.

Chen, K. S., Chung Yi Chung, and S. W. Wang. 2002. "Measurement and three-dimensional modeling of airflow and pollutant dispersion in an undersea traffic tunnel". *Journal of the Air and Waste Management Association* 52 (3): 349–363. ISSN: 21622906. doi:10.1080/10473289.2002.10470783.

Chen, T.Y., Y.T. Lee, and C.C. Hsu. 1998. "Investigations of piston-effect and jet fan-effect in model vehicle tunnels". *Journal of Wind Engineering and Industrial Aerodynamics* 73 (2): 99–110. ISSN: 01676105. doi:10.1016/S0167-6105(97)00281-X. https://linkinghub.elsevier.com/retrieve/pii/S016761059700281X.

Chen, Zhengwei, et al. 2017. "Impact of ambient wind on aerodynamic performance when two trains intersect inside a tunnel". *Journal of Wind Engineering and Industrial Aerodynamics* 169 (July): 139–155. ISSN: 01676105. doi:10.1016/j.jweia.2017.07.018. http://dx.doi.org/10.1016/j.jweia.2017.07.018.

Chu, Chia-Ren, et al. 2014. "Numerical simulation of two trains intersecting in a tunnel". *Tunnelling and Underground Space Technology* 42:161–174. ISSN: 08867798. doi:10.1016/j.tust.2014.02.013. https://doi.org/10.1016/j.tust.2014.02.013.

Chung, Chung-Yi, and Pei-Ling Chung. 2007. "A Numerical and Experimental Study of Pollutant Dispersion in a Traffic Tunnel". *Environmental Monitoring and Assessment* 130 (1-3): 289–299. ISSN: 0167-6369. doi:10.1007/s10661-006-9397-0. http://link.springer.com/10.1007/s10661-006-9397-0%20https://link.springer.com/10.1007/s10661-006-9397-0.

Coleman, S.A., and C.J. Baker. 1994. "An experimental study of the aerodynamic behaviour of high sided lorries in cross winds". *Journal of Wind Engineering and Industrial Aerodynamics* 53 (3): 401–429. ISSN: 01676105. doi:10.1016/0167-6105(94)90093-0. https://linkinghub.elsevier.com/retrieve/pii/0167610594900930.

— . 1990. "High sided road vehicles in cross winds". *Journal of Wind Engineering and Industrial Aerodynamics* 36:1383–1392. ISSN: 01676105. doi:10.1016/0167-6105(90)90134-X. https://linkinghub.elsevier.com/retrieve/pii/016761059090134X.

Commission, European, Directorate-General for Mobility, and Transport. 2020. *EU transport in figures : statistical pocketbook 2020*. Publications Office. doi:doi/10.2832/491038.

Cooper, K.R. 1993. "Bluff-body aerodynamics as applied to vehicles". *Journal of Wind Engineering and Industrial Aerodynamics* 49 (1-3): 1–21. ISSN: 01676105. doi:10.1016/0167-6105(93)90003-7. https://linkinghub.elsevier.com/retrieve/pii/0167610593900037.

Cooper, Kevin R. 2012. "Wind Tunnel and Track Tests of Class 8 Tractors Pulling Single and Tandem Trailers Fitted with Side Skirts and Boat-tails". *SAE International Journal of Commercial Vehicles* 5 (1): 2012–01–0104. ISSN: 1946-3928. doi:10.4271/2012-01-0104. https://www.sae.org/content/2012-01-0104/.

Davila, Arturo, Enric Aramburu, and Alex Freixas. 2013. "Making the Best Out of Aerodynamics: Platoons". In *SAE Technical Papers*, vol. 2. doi:10.4271/2013-01-0767. https://www.sae.org/content/2013-01-0767/.

Davila, Arturo, and Mario Nombela. 2012. "Platooning - Safe and Eco-Friendly Mobility". In *SAE Technical Paper 2012-01-0488*. doi:10.4271/2012-01-0488. https://www.sae.org/content/2012-01-0488/.

Deeg, Peter, et al. 2008. "Cross-comparison of measurement techniques for the determination of train induced aerodynamic loads on the track bed". *Proceedings of the BBAA VI, Milano, Italy*: 20–24. http://bbaa6.mecc.polimi.it/uploads/treni/BPR04.pdf.

Department for Transport. 2017. *Green light for lorry 'platooning'*. Visited on 07/04/2022. https://www.gov.uk/government/news/green-light-for-lorry-platooning.

Dong, Jingliang, et al. 2017. "Numerical simulation of pollutant dispersion in urban roadway tunnels". *The Journal of Computational Multiphase Flows* 9 (1): 26–31. ISSN: 1757-482X. doi:10.1177/1757482X17694041. http://journals.sagepub.com/doi/10.1177/1757482X17694041.

Dorigatti, F., et al. 2015. "Crosswind effects on the stability of a model passenger train—A comparison of static and moving experiments". *Journal of Wind Engineering and Industrial Aerodynamics* 138:36–51. ISSN: 01676105. doi:10.1016/j.jweia.2014.11.009. https://linkinghub.elsevier.com/retrieve/pii/S0167610514002396.

Dorigatti, Francesco. 2013. "Rail vehicles in crosswinds: analysis of steady and unsteady aerodynamic effects through static and moving model tests". PhD thesis, University of Birmingham.

Drollinger, Richard A. 1987. "Heavy Duty Truck Aerodynamics". In *SAE Technical Paper 870001*. doi:10.4271/870001. https://www.sae.org/content/870001/.

E. C. Maskell. 1963. "A Theory of the Blockage Effects on, Bluff Bodies and Stalled Wings in a Closed Wind Tunnel". *Reports and Memoranda*, no. 3400.

Ebrahim, Hesham, and Robert Dominy. 2020. "Wake and surface pressure analysis of vehicles in platoon". *Journal of Wind Engineering and Industrial Aerodynamics* 201:104144. ISSN: 01676105. doi:10.1016/j.jweia.2020.104144. https://doi.org/10.1016/j.jweia.2020.104144%20https://linkinghub.elsevier.com/retrieve/pii/S0167610520300544.

Eftekharian, Esmaeel, Omid Abouali, and Goodarz Ahmadi. 2015. "An improved correlation for pressure drop in a tunnel under traffic jam using CFD". *Journal of Wind Engineering and Industrial Aerodynamics* 143:34–41. ISSN: 01676105. doi:10.1016/j.jweia.2015.04.013. http://dx.doi.org/10.1016/j.jweia.2015.04.013.

EN. 2013. *Railway applications–aerodynamics-Part4: requirements and test procedures for aerodynamics on open track*. Tech. rep.

EN, BS, et al. 2005. "Railway applications–aerodynamics-Part4: requirements and test procedures for aerodynamics on open track". *BS EN* 14067:21–23.

Fletcher, C.A.J., and G.D.H. Stewart. 1986. "Bus drag reduction by the trapped vortex concept for a single bus and two buses in tandem". *Journal of Wind Engineering and Industrial Aerodynamics* 24 (2): 143–168. ISSN: 01676105. doi:10.1016/0167-6105(86)90004-8. https://linkinghub.elsevier.com/retrieve/pii/0167610586900048.

Flynn, Dominic, et al. 2014. "Detached-eddy simulation of the slipstream of an operational freight train". *Journal of Wind Engineering and Industrial Aerodynamics* 132:1–12. ISSN: 01676105. doi:10.1016/j.jweia.2014.06.016. http://dx.doi.org/10.1016/j.jweia.2014.06.016.

Fritz, H., et al. 2004. "CHAUFFEUR assistant a driver assistance system for commercial vehicles based on fusion of advanced ACC and lane keeping". In *IEEE Intelligent Vehicles Symposium, 2004*, 495–500. IEEE. ISBN: 0-7803-8310-9. doi:10.1109/IVS.2004.1336433. http://ieeexplore.ieee.org/document/1336433/.

Fröhlich, Jochen, et al. 2005. "Highly resolved large-eddy simulation of separated flow in a channel with streamwise periodic constrictions". *Journal of Fluid Mechanics* 526:19–66. ISSN: 00221120. doi:10.1017/S0022112004002812.

Futurescot. 2021. *Driverless 40-tonne lorries to be tested for first time in UK on 5G network*. Visited on 07/04/2022. https://futurescot.com/driverless-40-tonne-lorries-to-be-tested-for-first-time-in-uk-on-5g-network/.

Gheyssens, Thomas, and Gandert Van Raemdonck. 2016. "Effect of the Frontal Edge Radius in a Platoon of Bluff Bodies". *SAE International Journal of Commercial Vehicles* 9 (2): 2016–01–8149. ISSN: 1946-3928. doi:10.4271/2016-01-8149. https://www.sae.org/content/2016-01-8149/.

Gil, N., et al. 2010. "Passenger Train Slipstream Characterization Using a Rotating Rail Rig". *Journal of Fluids Engineering* 132 (6): 0614011–06140111. ISSN: 0098-2202. doi:10.1115/1.4001577.

Gil, Nahia, Chris Baker, and Clive Roberts. 2008. "The Measurement of Train Slipstream Characteristics Using a Rotating Rail Rig". *BBAA VI International Colloquium on: Bluff Bodies Aerodynamics & Applications*: 15.

Gilbert, T., C.J. Baker, and A. Quinn. 2013a. "Gusts caused by high-speed trains in confined spaces and tunnels". *Journal of Wind Engineering and Industrial Aerodynamics* 121 (): 39–48. ISSN: 01676105. doi:10.1016/j.jweia.2013.07.015. http://dx.doi.org/10.1016/j.jweia.2013.07.015%20https://linkinghub.elsevier.com/retrieve/pii/S0167610513001608.

Gilbert, Timothy. 2014. "AERODYNAMIC EFFECTS OF HIGH SPEED TRAINS IN CONFINED SPACES". PhD thesis, University of Birmingham.

Gilbert, Timothy, Christopher Baker, and Andrew Quinn. 2013b. "Aerodynamic pressures around high-speed trains: the transition from unconfined to enclosed spaces". *Proceedings of the Institution of Mechanical Engineers, Part F: Journal of Rail and Rapid Transit* 227, no. 6 (): 609–622. ISSN: 0954-4097. doi:10.1177/0954409713494947. http://journals.sagepub.com/doi/10.1177/0954409713494947.

Gilliéron, Patrick, and Christophe Noger. 2004. "Contribution to the Analysis of Transient Aerodynamic Effects Acting on Vehicles". In *SAE Technical Paper Series*. doi:10.4271/2004-01-1311.

Gleason, Mark E. 2007. "Detailed Analysis of the Bluff Body Blockage Phenomenon in Closed Wall Wind Tunnels Utilizing CFD". In *SAE Technical Papers*, 2007:776–790. 724. doi:10.4271/2007-01-1046. https://www.sae.org/content/2007-01-1046/.

Golovanevskiy, Vladimir A., Vitaly V. Chmovzh, and Yuriy V. Girka. 2012. "On the optimal model configuration for aerodynamic modeling of open cargo railway train". *Journal of Wind Engineering and Industrial Aerodynamics* 107-108:131–139. ISSN: 01676105. doi:10.1016/j.jweia.2012.03.035. http://dx.doi.org/10.1016/j.jweia.2012.03.035%20https://linkinghub.elsevier.com/retrieve/pii/S0167610512000931.

Grandemange, M., M. Gohlke, and O. Cadot. 2013. "Turbulent wake past a three-dimensional blunt body. Part 1. Global modes and bi-stability". *Journal of Fluid Mechanics* 722:51–84. ISSN: 0022-1120. doi:10.1017/jfm.2013.83. https://www.cambridge.org/core/product/identifier/S0022112013000839/type/journal_article.

Gritskevich, Mikhail S., et al. 2012. "Development of DDES and IDDES Formulations for the k-ω Shear Stress Transport Model". *Flow, Turbulence and Combustion* 88 (3): 431–449. ISSN: 1386-6184. doi:10.1007/s10494-011-9378-4. http://link.springer.com/10.1007/s10494-011-9378-4.

Hammache, M., M. Michaelian, and F. Browand. 2002. "Aerodynamic Forces on Truck Models, Including Two Trucks in Tandem". In *SAE Technical Papers*. 724. doi:10.4271/2002-01-0530. https://www.sae.org/content/2002-01-0530/.

He, Mingzhe, et al. 2019. "Detached eddy simulation of a closely running lorry platoon". *Journal of Wind Engineering and Industrial Aerodynamics* 193 (July): 103956. ISSN: 01676105. doi:10.1016/j.jweia.2019.103956. https://linkinghub.elsevier.com/retrieve/pii/S0167610519305471.

Hemida, Hassan, and Siniša Krajnović. 2009. "Transient Simulation of the Aerodynamic Response of a Double-Deck Bus in Gusty Winds". *Journal of Fluids Engineering* 131 (3): 0311011–03110110. ISSN: 0098-2202. doi:10.1115/1.3054288. https://asmedigitalcollection.asme.org/fluidsengineering/article/doi/10.1115/1.3054288/467223/Transient-Simulation-of-the-Aerodynamic-Response.

Herriot, John G. 1947. "Blockage Corrections for Three-Dimensional-Flow Closed-Throat Wind Tunnels, with Consideration of the Effect of Compressibility". *NACA TR 995*.

Hong, Patrick, et al. 1998. "Drag Forces Experienced by Two, Full-Scale Vehicles at Close Spacing". In *SAE Technical Paper Series*. doi:10.4271/980396.

Howe, M. S. 1998. "The compression wave produced by a high-speed train entering a tunnel". *Proceedings of the Royal Society of London. Series A: Mathematical, Physical and Engineering Sciences* 454, no. 1974 (): 1523–1534. ISSN: 1364-5021. doi:10.1098/rspa.1998.0220. https://royalsocietypublishing.org/doi/10.1098/rspa.1998.0220.

Hsu, Fu-Hung, and Roger L. Davis. 2010. "Drag Reduction of Tractor-Trailers Using Optimized Add-On Devices". *Journal of Fluids Engineering* 132 (8). ISSN: 0098-2202. doi:10.1115/1.4001587. https://asmedigitalcollection.asme.org/fluidsengineering/article/doi/10.1115/1.4001587/451350/Drag-Reduction-of-TractorTrailers-Using-Optimized.

Humphreys, Hugh, and David Bevly. 2016. "Computational Fluid Dynamic Analysis of a Generic 2 Truck Platoon". In *SAE Technical Papers*. October. doi:10.4271/2016-01-8008. https://www.sae.org/content/2016-01-8008/.

Hyams, Daniel G., et al. 2011. "Computational simulation of model and full scale Class 8 trucks with drag reduction devices". *Computers & Fluids* 41 (1): 27–40. ISSN: 00457930. doi:10.1016/j.compfluid.2010.09.015. https://linkinghub.elsevier.com/retrieve/pii/S0045793010002434.

Iida, Masanobu, et al. 2005. "Steady pressure field around a train running in a vented tube". In *Proceedings of 83rd JSME Fluids Engineering Conference*, vol. 1207. doi:10.1007/BF00056599. http://www.jstage.jst.go.jp/article/rtriqr/49/2/49_2_89/_article%20https://link.springer.com/10.1007/BF00056599.

Iliadis, P., et al. 2019. "Experimental investigation of the aerodynamics of a freight train passing through a tunnel using a moving model". *Proceedings of the Institution of Mechanical Engineers, Part F: Journal of Rail and Rapid Transit* 233, no. 8 (): 857–868. ISSN: 0954-4097. doi:10.1177/0954409718811736. http://journals.sagepub.com/doi/10.1177/0954409718811736.

Iliadis, P., et al. 2020. "Numerical simulations of the separated flow around a freight train passing through a tunnel using the sliding mesh technique". *Proceedings of the Institution of Mechanical Engineers, Part F: Journal of Rail and Rapid Transit* 234, no. 6 (): 638–654. ISSN: 0954-4097. doi:10.1177/0954409719851421. http://journals.sagepub.com/doi/10.1177/0954409719851421.

Iliadis, Panagiotis. 2019. "Aerodynamics of a freight train passing through a tunnel". PhD thesis, University of Birmingham.

Ioannou, Petros. 2013. *Automated highway systems*. Springer Science & Business Media.

Ishigai, Seikan, et al. 1972. "Experimental Study on Structure of Gas Flow in Tube Banks with Tube Axes Normal to Flow : Part 1, Karman Vortex Flow from Two Tubes at Various Spacings". *Bulletin of JSME* 15 (86): 949–956. ISSN: 0021-3764. doi:10.1299/jsme1958.15.949. http://www.jstage.jst.go.jp/article/jsme1958/15/86/15_86_949/_article.

ITF Transport Outlook. 2019. ITF Transport Outlook. OECD. doi:10.1787/transp_outlook-en-2019-en. https://www.oecd-ilibrary.org/transport/itf-transport-outlook-2019_transp_outlook-en-2019-en.

Jang, Hong-Ming, and Falin Chen. 2000. "A novel approach to the transient ventilation of road tunnels". *Journal of Wind Engineering and Industrial Aerodynamics* 86 (1): 15–36. ISSN: 01676105. doi:10.1016/S0167-6105(99)00135-X. https://linkinghub.elsevier.com/retrieve/pii/S016761059900135X.

— . 2002. "On the determination of the aerodynamic coefficients of highway tunnels". *Journal of Wind Engineering and Industrial Aerodynamics* 90 (8): 869–896. ISSN: 01676105. doi:10.1016/S0167-6105(02)00156-3. https://linkinghub.elsevier.com/retrieve/pii/S0167610502001563.

Janssen, GR, et al. 2015. "Future of Transportation Truck Platooning". *Tno*, no. February: 1–36. https://www.tno.nl/en/about-tno/news/2015/3/truck-platooning-driving-the-future-of-transportation-tno-whitepaper/.

Jeong, Jinhee, and Fazle Hussain. 1995. "On the identification of a vortex". *Journal of Fluid Mechanics* 285:69–94. ISSN: 0022-1120 1469-7645. doi:10.1017/S0022112095000462. http://www.journals.cambridge.org/abstract_S0022112095000462.

Johnson, T, and S Dalley. 2002. "1/25 scale moving model tests for the TRANSAERO Project". In *TRANSAERO—A European Initiative on Transient Aerodynamics for Railway System Optimisation*, 123–135. Springer.

Jones, W.P, and B.E Launder. 1972. "The prediction of laminarization with a two-equation model of turbulence". *International Journal of Heat and Mass Transfer* 15 (2): 301–314. ISSN: 00179310. doi:10.1016/0017-9310(72)90076-2. https://linkinghub.elsevier.com/retrieve/pii/0017931072900762.

Kastner-Klein, P., E. Fedorovich, and M.W. Rotach. 2001. "A wind tunnel study of organised and turbulent air motions in urban street canyons". *Journal of Wind Engineering and Industrial Aerodynamics* 89 (9): 849–861. ISSN: 01676105. doi:10.1016/S0167-6105(01)00074-5. https://linkinghub.elsevier.com/retrieve/pii/S0167610501000745.

Katolický, Jaroslav, and Miroslav Jícha. 2005. "Eulerian-Lagrangian model for traffic dynamics and its impact on operational ventilation of road tunnels". *Journal of Wind Engineering and Industrial Aerodynamics* 93 (1): 61–77. ISSN: 0167-6105. doi:10.1016/j.jweia.2004.09.002.

Katz, Joseph. 2006. "Aerodynamics of Race Cars". *Annual Review of Fluid Mechanics* 38 (1): 27–63. ISSN: 0066-4189 1545-4479. doi:10.1146/annurev.fluid.38.050304.092016.

Khayrullina, Adelya, et al. 2015. "CFD simulation of train aerodynamics: Train-induced wind conditions at an underground railroad passenger platform". *Journal of Wind Engineering and Industrial Aerodynamics* 139:100–110. ISSN: 01676105. doi:10.1016/j.jweia.2015.01.019. http://dx.doi.org/10.1016/j.jweia.2015.01.019.

Koenig, Keith, and Anatol Roshko. 1985. "An experimental study of geometrical effects on the drag and flow field of two bluff bodies separated by a gap". *Journal of Fluid Mechanics* 156:167–204. ISSN: 14697645. doi:10.1017/S002211208500204X.

Krajnović, Siniša, and Lars Davidson. 2003. "Numerical Study of the Flow Around a Bus-Shaped Body". *Journal of Fluids Engineering* 125 (3): 500–509. ISSN: 0098-2202. doi:10.1115/1.1567305. https://asmedigitalcollection.asme.org/fluidsengineering/article/125/3/500/463229/Numerical-Study-of-the-Flow-Around-a-BusShaped.

Kumar, A., et al. 2011. "Aerodynamic Analysis of Intermodal Freight Trains Using Machine Vision". In *9 th World Congress on Railway Research*. Lille, France. ISBN: 1217244417.

Lahaye, Arnaud, Annie Leroy, and Azeddine Kourta. 2014. "Aerodynamic characterisation of a square back bluff body flow". *International Journal of Aerodynamics* 4 (1/2): 43. ISSN: 1743-5447. doi:10.1504/ijad.2014.057804.

Lai, Yung-Cheng, Christopher P.L. Barkan, and Hayri Önal. 2008. "Optimizing the aerodynamic efficiency of intermodal freight trains". *Transportation Research Part E: Logistics and Transportation Review* 44, no. 5 (): 820–834. ISSN: 13665545. doi:10.1016/j.tre.2007.05.011. https://linkinghub.elsevier.com/retrieve/pii/S1366554507000804.

Lammert, Michael P., et al. 2014. "Effect of Platooning on Fuel Consumption of Class 8 Vehicles Over a Range of Speeds, Following Distances, and Mass". *SAE International*

Journal of Commercial Vehicles 7 (2): 2014–01–2438. ISSN: 1946-3928. doi:10.4271/2014-01-2438. https://www.sae.org/content/2014-01-2438/.

Landman, Drew, et al. 2009. "Understanding Practical Limits to Heavy Truck Drag Reduction". *SAE International Journal of Commercial Vehicles* 2 (2): 2009–01–2890. ISSN: 1946-3928. doi:10.4271/2009-01-2890. https://www.sae.org/content/2009-01-2890/.

Le Good, Geoffrey, et al. 2021. "An investigation of aerodynamic effects of body morphing for passenger cars in close-proximity". *Fluids* 6 (2). ISSN: 23115521. doi:10.3390/fluids6020064.

Le Good, Geoff, et al. 2018. "Effects on the Aerodynamic Characteristics of Vehicles in Longitudinal Proximity Due to Changes in Style". In *SAE Technical Papers*, vol. 2018-May. May. doi:10.4271/2018-37-0018. https://www.sae.org/content/2018-37-0018/.

Lee, Seungjun, Yohan Park, and Jin Kim. 2018. "An evaluation of factors influencing drag coefficient in double-deck tunnels by CFD simulations using factorial design method". *Journal of Wind Engineering and Industrial Aerodynamics* 180 (July): 156–167. ISSN: 01676105. doi:10.1016/j.jweia.2018.07.018. https://doi.org/10.1016/j.jweia.2018.07.018.

Leonard, B.P. 1991. "The ULTIMATE conservative difference scheme applied to unsteady one-dimensional advection". *Computer Methods in Applied Mechanics and Engineering* 88 (1): 17–74. ISSN: 00457825. doi:10.1016/0045-7825(91)90232-U. https://linkinghub.elsevier.com/retrieve/pii/004578259190232U.

Leuschen, Jason, and Kevin R. Cooper. 2006. "Full-Scale Wind Tunnel Tests of Production and Prototype, Second-Generation Aerodynamic Drag-Reducing Devices for Tractor-Trailers". In *SAE Technical Paper 2006-01-3456*. doi:10.4271/2006-01-3456. https://www.sae.org/content/2006-01-3456/.

Li, Li, et al. 2009. "Numerical Simulation of the Transient Aerodynamic Phenomena Associated with a Van Running Into a Road Tunnel". In *2009 Asia-Pacific Power and Energy Engineering Conference*, 1:1–4. IEEE. ISBN: 978-1-4244-2486-3. doi:10.1109/APPEEC.2009.4918542. http://ieeexplore.ieee.org/document/4918542/.

Li, Li, et al. 2010a. "The Transient Aerodynamic Characteristics Around Vans Running Into a Road Tunnel". *Journal of Hydrodynamics* 22 (2): 283–288. ISSN: 1001-6058. doi:10.1016/S1001-6058(09)60056-1.

— . 2010b. "The Transient Aerodynamic Characteristics Around Vans Running Into a Road Tunnel". *Journal of Hydrodynamics* 22 (2): 283–288. ISSN: 1001-6058. doi:10.1016/S1001-6058(09)60056-1. http://dx.doi.org/10.1016/S1001-6058(09)60056-1.

Lilly, Douglas K. 1967. "The representation of small-scale turbulence in numerical simulation experiments". *IBM Form*: 195–210.

Liu, Minzhang, et al. 2018. "An alternative algorithm of tunnel piston effect by replacing three-dimensional model with two-dimensional model". *Building and Environment* 128 (July 2017): 55–67. ISSN: 03601323. doi:10.1016/j.buildenv.2017.11.022. https://doi.org/10.1016/j.buildenv.2017.11.022.

Liu, Tang-hong, et al. 2017. "Field study on the interior pressure variations in high-speed trains passing through tunnels of different lengths". *Journal of Wind Engineering and Industrial Aerodynamics* 169:54–66. ISSN: 01676105. doi:10.1016/j.jweia.2017.07.004. http://dx.doi.org/10.1016/j.jweia.2017.07.004.

Liu, Yebo, Hassan Hemida, and Zhiming Liu. 2014. "Large eddy simulation of the flow around a train passing a stationary freight wagon". *Proceedings of the Institution of Mechanical Engineers, Part F: Journal of Rail and Rapid Transit* 228 (5): 535–545. ISSN: 0954-4097. doi:10.1177/0954409713488096. http://journals.sagepub.com/doi/10.1177/0954409713488096.

Ljungkrona, Lars, and Bengt Sundén. 1993. "Flow visualization and surface pressure measurement on two tubes in an inline arrangement". *Experimental Thermal and Fluid Science* 6 (1): 15–27. ISSN: 08941777. doi:10.1016/0894-1777(93)90037-J. https://linkinghub.elsevier.com/retrieve/pii/089417779390037J.

Marcu, Bogdan, and Fred Browand. 1999. "Aerodynamic Forces Experienced by a 3-Vehicle Platoon in a Crosswind". In *SAE Technical Paper Series*. doi:10.4271/1999-01-1324.

Marcu, Fred, Bogdan; Browand. 1998. *The Aerodynamic Forces On Misaligned Platoons*. Report. UC Berkeley: California Partners for Advanced Transportation Technology. https://escholarship.org/uc/item/0fg1j34q.

Mariotti, Alessandro, and Guido Buresti. 2013. "Experimental investigation on the influence of boundary layer thickness on the base pressure and near-wake flow features of an axisymmetric blunt-based body". *Experiments in Fluids* 54 (11): 1612. ISSN: 0723-4864. doi:10.1007/s00348-013-1612-5. http://link.springer.com/10.1007/s00348-013-1612-5.

McArthur, Damien, et al. 2018. "An experimental characterisation of the wake of a detailed heavy vehicle in cross-wind". *Journal of Wind Engineering and Industrial Aerodynamics* 175:364–375. ISSN: 01676105. doi:10.1016/j.jweia.2018.01.033. https://doi.org/10.1016/j.jweia.2018.01.033%20https://linkinghub.elsevier.com/retrieve/pii/S0167610517304737.

McAuliffe, Brian R., and Mojtaba Ahmadi-Baloutaki. 2018. "A Wind-Tunnel Investigation of the Influence of Separation Distance, Lateral Stagger, and Trailer Configuration on the Drag-Reduction Potential of a Two-Truck Platoon". *SAE International Journal of Commercial Vehicles* 11 (2): 125–150. ISSN: 19463928. doi:10.4271/02-11-02-0011.

McAuliffe, Brian R., and David Chuang. 2016. "Track-Based Aerodynamic Testing of a Heavy-Duty Vehicle: Coast-Down Measurements". *SAE International Journal of Com-*

mercial Vehicles 9, no. 2 (): 2016–01–8152. ISSN: 1946-3928. doi:10.4271/2016-01-8152. https://www.sae.org/content/2016-01-8152/.

McCallen, Rose, et al. 1999. "Progress in Reducing Aerodynamic Drag for Higher Efficiency of Heavy Duty Trucks (Class 7-8)". In *SAE Technical Paper*, 1999–01–2238. doi:10.4271/1999-01-2238. https://www.sae.org/content/1999-01-2238/.

Meng, Shuang, Dan Zhou, and Zhe Wang. 2019. "Moving model analysis on the transient pressure and slipstream caused by a metro train passing through a tunnel". Ed. by Yanping Yuan. *PLOS ONE* 14 (9): e0222151. ISSN: 1932-6203. doi:10.1371/journal.pone.0222151. https://dx.plos.org/10.1371/journal.pone.0222151.

Meng, Shuang, et al. 2021. "Numerical simulation of slipstreams and wake flows of trains with different nose lengths passing through a tunnel". *Tunnelling and Underground Space Technology* 108 (November 2019): 103701. ISSN: 08867798. doi:10.1016/j.tust.2020.103701. https://linkinghub.elsevier.com/retrieve/pii/S0886779820306556.

Menter, F. R. 1994. "Two-equation eddy-viscosity turbulence models for engineering applications". *AIAA Journal* 32 (8): 1598–1605. ISSN: 0001-1452. doi:10.2514/3.12149. https://arc.aiaa.org/doi/10.2514/3.12149.

Menter, FR, M Kuntz, and R Langtry. 2003. "Ten years of experience with the sst turbulence model. Turbulence". *Heat and Mass Transfer* 4:625–632.

Miau, J. J., and M. T. Hsu. 1992. "Axisymmetric-type vortex shedders for vortex flowmeters". *Flow Measurement and Instrumentation* 3 (2): 73–79. ISSN: 0955-5986. doi:https://doi.org/10.1016/0955-5986(92)90003-N. https://www.sciencedirect.com/science/article/pii/095559869290003N.

Miau, J. J., and T. W. Liu. 1990. "Vortex flowmeter designed with wall pressure measurement". *Review of Scientific Instruments* 61 (10): 2676–2681. ISSN: 0034-6748. doi:10.1063/1.1141859. http://aip.scitation.org/doi/10.1063/1.1141859.

Michael, James B., et al. 1998. "Capacity Analysis of Traffic Flow Over a Single-Lane Automated Highway System". *ITS Journal - Intelligent Transportation Systems Journal* 4 (1-2): 49–80. ISSN: 1024-8072. doi:10.1080/10248079808903736.

MIIT. 2018. "Management Specification for Road Testing of Intelligent Connected Vehicles (Trial)". *Ministry of Industry and Information Technology of the People's Republic China*.

Mirzaei, Maryam, and Siniša Krajnović. 2016. *Large Eddy Simulations of Flow Around Two Generic Vehicles in a Platoon*. Vol. 185. Springer Proceedings in Physics. Cham: Springer International Publishing. ISBN: 978-3-319-30600-1. doi:10.1007/978-3-319-30602-5. http://link.springer.com/10.1007/978-3-319-30602-5.

Mirzaeinia, A., F. Heppner, and M. Hassanalian. 2020. "An analytical study on leader and follower switching in V-shaped Canada Goose flocks for energy management purposes". *Swarm Intelligence* 14 (2): 117–141. ISSN: 19353820. doi:10.1007/s11721-020-00179-x. https://doi.org/10.1007/s11721-020-00179-x.

Morel, T., and M. Bohil. 1980. "Flow over two circular disks in tandem". *Journal of Fluids Engineering, Transactions of the ASME* 102 (1): 104–111. ISSN: 1528901X. doi:10.1115/1.3240599.

Munoz-Paniagua, J., J García, and B Lehugeur. 2017. "Evaluation of RANS, SAS and IDDES models for the simulation of the flow around a high-speed train subjected to cross-wind". *Journal of Wind Engineering and Industrial Aerodynamics* 171, no. September (): 50–66. ISSN: 01676105. doi:10.1016/j.jweia.2017.09.006. https://doi.org/10.1016/j.jweia.2017.09.006%20https://linkinghub.elsevier.com/retrieve/pii/S0167610516306924.

News, BBC. 2017. *'Self-driving' lorries to be tested on UK roads*. Visited on 07/04/2022. https://www.bbc.co.uk/news/technology-41038220.

Niu, Jiqiang, et al. 2018. "Numerical analysis of aerodynamic characteristics of high-speed train with different train nose lengths". *International Journal of Heat and Mass Transfer* 127:188–199. ISSN: 00179310. doi:10.1016/j.ijheatmasstransfer.2018.08.041. https://doi.org/10.1016/j.ijheatmasstransfer.2018.08.041%20https://linkinghub.elsevier.com/retrieve/pii/S0017931018313061.

Niu, Ji-qiang, et al. 2017. "Numerical simulation of aerodynamic performance of a couple multiple units high-speed train". *Vehicle System Dynamics* 55 (5): 681–703. ISSN: 0042-3114. doi:10.1080/00423114.2016.1277769. https://doi.org/10.1080/00423114.2016.1277769%20https://www.tandfonline.com/doi/full/10.1080/00423114.2016.1277769.

Novak, Jakub. 2006. "Single train passing through a tunnel". In *European Conference on Computational Fluid Dynamics*. Egmond aan Zee, The Netherlands: Delft University of Technology; European Community on Computational Methods in Applied Sciences (ECCOMAS).

Ogawa, Takanobu, and Kozo Fujii. 1997. "Numerical investigation of three-dimensional compressible flows induced by a train moving into a tunnel". *Computers & Fluids* 26 (6): 565–585. ISSN: 00457930. doi:10.1016/S0045-7930(97)00008-X. https://linkinghub.elsevier.com/retrieve/pii/S004579309700008X.

Pagliarella, Riccardo M. 2009. "On the Aerodynamic Performance of Automotive Vehicle Platoons Featuring Pre and Post-Critical Leading Forms". PhD thesis, RMIT University.

Pagliarella, Riccardo M., Simon Watkins, and Angelo Tempia. 2007. "Aerodynamic Performance of Vehicles in Platoons: The Influence of Backlight Angles". In *SAE Technical Papers*, vol. 2007. 724. doi:10.4271/2007-01-1547. https://www.sae.org/content/2007-01-1547/.

Pannell, J. R., E. A. Griffiths, and J. D. Coales. 1915. "Experiments on the interference between pairs of aeroplane wires of circular and lenticular cross section". *Reports and Memoranda—Aeronautical Research Council (Great Britain), Report* 208.

Patel, Nainesh, et al. 2019. "Large-Eddy Simulation of the airflow around a truck". *Journal of Wind Engineering and Industrial Aerodynamics* 195:104017. ISSN: 01676105. doi:10.1016/j.jweia.2019.104017. https://doi.org/10.1016/j.jweia.2019.104017.

Piomelli, Ugo. 2008. "Wall-layer models for large-eddy simulations". *Progress in Aerospace Sciences* 44 (6): 437–446. ISSN: 03760421. doi:10.1016/j.paerosci.2008.06.001. https://linkinghub.elsevier.com/retrieve/pii/S037604210800047X.

Pope, Stephen B. 2000. *Turbulent Flows*. Cambridge University Press. ISBN: 978-0-521-59125-6. doi:10.1017/CBO9780511840531. arXiv: arXiv:1011.1669v3.

Prandtl, Ludwig. 1925. "7. Bericht über Untersuchungen zur ausgebildeten Turbulenz". *ZAMM-Journal of Applied Mathematics and Mechanics/Zeitschrift für Angewandte Mathematik und Mechanik* 5 (2): 136–139.

Quinn, A. D., et al. 2007. "An investigation of the wind-induced rolling moment on a commercial vehicle in the atmospheric boundary layer". *Proceedings of the Institution of Mechanical Engineers, Part D: Journal of Automobile Engineering* 221 (11): 1367–1379. ISSN: 0954-4070. doi:10.1243/09544070JAUTO537. http://journals.sagepub.com/doi/10.1243/09544070JAUTO537.

Rajamani, Gokul Krishnan. 2006. "CFD Analysis of Air Flow Interactions in Vehicle Platoons". *School of Aerospace, Mechanical and Manufacturing Engineering RMIT University*, no. August.

Rajamani, R., et al. 2000. "Demonstration of integrated longitudinal and lateral control for the operation of automated vehicles in platoons". *IEEE Transactions on Control*

Systems Technology 8 (4): 695–708. ISSN: 10636536. doi:10.1109/87.852914. http://ieeexplore.ieee.org/document/852914/.

Ricardo, TRL, and TTR. 2014. "Heavy vehicle platoons on UK roads: feasibility study". *Department for Transport and Centre for Connected and Autonomous Vehicles,* 2013–2014. https://www.gov.uk/government/publications/truck-platooning-uk-road-trial-feasibility-study.

Robbert Janssen, HZ. 2015. *Truck Platooning Driving the Future of Transportation.*

Roberts, Jack, Rick Mihelic, and Mike Roeth. 2016. "CONFIDENCE REPORT: Two-Truck Platooning". *2008_Paper_Sort3*: 73. http://www.truckingefficiency.org/sites/truckingefficiency.org/files/reports/TE%20Platooning%20CR%20FINAL%20_0.pdf.

Robertson, F.H., D Soper, and C Baker. 2021. "Unsteady aerodynamic forces on long lorry platoons". *Journal of Wind Engineering and Industrial Aerodynamics* 209:104481. ISSN: 01676105. doi:10.1016/j.jweia.2020.104481. https://doi.org/10.1016/j.jweia.2020.104481%20https://linkinghub.elsevier.com/retrieve/pii/S0167610520303913.

Robertson, Francis H., and Gregory F. Lane-Serff. 2018. "Drag on pairs of square section obstacles in free-surface flows". *Physical Review Fluids* 3 (12): 123802. ISSN: 2469-990X. doi:10.1103/PhysRevFluids.3.123802. https://link.aps.org/doi/10.1103/PhysRevFluids.3.123802.

Robertson, Francis H., et al. 2019. "An experimental investigation of the aerodynamic flows created by lorries travelling in a long platoon". *Journal of Wind Engineering and Industrial Aerodynamics* 193:103966. ISSN: 01676105. doi:10.1016/j.jweia.2019.103966. https://linkinghub.elsevier.com/retrieve/pii/S0167610519305641.

Robinson, Tom, Eric Chan, and Erik Coelingh. 2010. "Operating platoons on public motorways: An introduction to the sartre platooning programme". In *17th world congress on intelligent transport systems*, 12.

Romberg, G. F., F. Chianese, and R. G. Lajoie. 1971. "Aerodynamics of Race Cars in Drafting and Passing Situations". In *SAE Technical Paper*. doi:10.4271/710213. https://www.sae.org/content/710213/.

Roy, Christopher J., Jeffrey Payne, and Mary McWherter-Payne. 2006. "RANS Simulations of a Simplified Tractor/Trailer Geometry". *Journal of Fluids Engineering* 128 (5): 1083–1089. ISSN: 0098-2202. doi:10.1115/1.2236133. https://asmedigitalcollection.asme.org/fluidsengineering/article/128/5/1083/477713/RANS-Simulations-of-a-Simplified-TractorTrailer.

Salari, Kambiz, and Jason Ortega. 2018. "Experimental Investigation of the Aerodynamic Benefits of Truck Platooning". *SAE Technical Papers* 2018-April:1–11. ISSN: 01487191. doi:10.4271/2018-01-0732.

Sambolek, Miroslav. 2004. "Model testing of road tunnel ventilation in normal traffic conditions". *Engineering Structures* 26 (12): 1705–1711. ISSN: 01410296. doi:10.1016/j.engstruct.2004.06.001.

Schito, Paolo, and Francesco Braghin. 2012. "Numerical and Experimental Investigation on Vehicles in Platoon". *SAE International Journal of Commercial Vehicles* 5 (1): 2012–01–0175. ISSN: 1946-3928. doi:10.4271/2012-01-0175. https://www.sae.org/content/2012-01-0175/.

Shladover, S. E., et al. 1991. "Automated vehicle control developments in the PATH program". *IEEE Transactions on Vehicular Technology* 40 (1): 114–130. ISSN: 0018-9545 1939-9359. doi:10.1109/25.69979.

Shur, Mikhail L., et al. 2008. "A hybrid RANS-LES approach with delayed-DES and wall-modelled LES capabilities". *International Journal of Heat and Fluid Flow* 29 (6): 1638–1649. ISSN: 0142727X. doi:10.1016/j.ijheatfluidflow.2008.07.001. http://dx.doi.org/10.1016/j.ijheatfluidflow.2008.07.001%20https://linkinghub.elsevier.com/retrieve/pii/S0142727X08001203.

Sike, Jin, Gong Yanfeng, and Zhang Guangli. 2015. "Flow field development and energy evolution in road tunnels with unidirectional uniform traffic". *Journal of Wind Engineering and Industrial Aerodynamics* 147:66–76. ISSN: 01676105. doi:10.1016/j.jweia.2015.09.011. http://dx.doi.org/10.1016/j.jweia.2015.09.011.

Silva, Carlos B. da, et al. 2014. "Interfacial Layers Between Regions of Different Turbulence Intensity". *Annual Review of Fluid Mechanics* 46 (1): 567–590. ISSN: 0066-4189. doi:10.1146/annurev-fluid-010313-141357. https://doi.org/10.1146/annurev-fluid-010313-141357.

Smagorinsky, J. 1963. "General Circulation Experiments with the Primitive Equations. I. The Basic Experiment". *Monthly Weather Review* 91 (3): 99–164. ISSN: 0027-0644. doi:10.1175/1520-0493(1963)091<0099:GCEWTP>2.3.CO;2. http://journals.ametsoc.org/doi/10.1175/1520-0493(1963)091%3C0099:GCEWTP%3E2.3.CO;2.

Sohu, News. 2019. *Public validation test of autonomous vehicle platoon following standard*. Visited on 07/04/2022. https://www.sohu.com/a/312758422_372603.

Song, Xiaocheng, and Yu Zhao. 2019. "Numerical investigation of airflow patterns and pollutant dispersions induced by a fleet of vehicles inside road tunnels using dynamic mesh Part ii: Pollutant dispersion and exposure levels". *Atmospheric Environment* 210 (May): 198–210. ISSN: 13522310. doi:10.1016/j.atmosenv.2019.04.028. https://linkinghub.elsevier.com/retrieve/pii/S1352231019302432.

Soper, David. 2016. *The Aerodynamics of a Container Freight Train*. Springer Theses, April. Cham: Springer International Publishing. ISBN: 978-3-319-33277-2. doi:10.1007/978-3-319-33279-6. http://link.springer.com/10.1007/978-3-319-33279-6.

Soper, David, Chris Baker, and Mark Sterling. 2014. "Experimental investigation of the slipstream development around a container freight train using a moving model facility". *Journal of Wind Engineering and Industrial Aerodynamics* 135:105–117. ISSN:

01676105. doi:10.1016/j.jweia.2014.10.001. https://linkinghub.elsevier.com/retrieve/pii/S0167610514001949.

Soper, David, et al. 2018. "A comparative study of methods to simulate aerodynamic flow beneath a high-speed train". *Proceedings of the Institution of Mechanical Engineers, Part F: Journal of Rail and Rapid Transit* 232 (5): 1464–1482. ISSN: 0954-4097. doi:10.1177/0954409717734090. http://journals.sagepub.com/doi/10.1177/0954409717734090.

Soper, David, et al. 2017. "A model-scale study to assess the influence of ground geometries on aerodynamic flow development around a train". *Proceedings of the Institution of Mechanical Engineers, Part F: Journal of Rail and Rapid Transit* 231 (8): 916–933. ISSN: 0954-4097. doi:10.1177/0954409716648719. http://journals.sagepub.com/doi/10.1177/0954409716648719.

Spalart, P. R., et al. 2006. "A New Version of Detached-eddy Simulation, Resistant to Ambiguous Grid Densities". *Theoretical and Computational Fluid Dynamics* 20 (3): 181–195. ISSN: 0935-4964. doi:10.1007/s00162-006-0015-0. http://link.springer.com/10.1007/s00162-006-0015-0.

Spalart, P. R., et al. 1997. "Comments on the feasibility of LES for wings and on a hybrid RANS/LES approach". *Advances in DNS/LES* 1:4–8.

Spohn, A, and P Gilliéron. 2002. "Flow separations generated by a simplified geometry of an automotive vehicle". In *IUTAM Symposium: unsteady separated flows*, vol. 1. Kluwer Academic,

Sterling, M., et al. 2008. "A study of the slipstreams of high-speed passenger trains and freight trains". *Proceedings of the Institution of Mechanical Engineers, Part F: Journal of Rail and Rapid Transit* 222 (2): 177–193. ISSN: 0954-4097. doi:10.1243/09544097JRRT133. http://journals.sagepub.com/doi/10.1243/09544097JRRT133.

Sykes, D.M. 1973. "Advances in road vehicle aerodynamics". *BHRA Fluid Engineering, Cranfield, UK*: 311–321.

TAKEI, Yasushi, et al. 2008. "Evaluation Method for Air Pressure Variation and Station Facility Member Deterioration Caused by High-Speed Train Passage in Stations". *Quarterly Report of RTRI* 49 (2): 89–95. ISSN: 0033-9008. doi:10.2219/rtriqr.49.89. http://www.jstage.jst.go.jp/article/rtriqr/49/2/49_2_89/_article.

Tavoularis, Stavros. 2005. *Measurement in fluid mechanics*. Cambridge University Press.

Taylor, John. 1997. *Introduction to error analysis, the study of uncertainties in physical measurements*. University Science Books. https://ui.adsabs.harvard.edu/abs/1997ieas.book.....T.

Tong, Yan, et al. 2016. "Possibility of using roof openings for natural ventilation in a shallow urban road tunnel". *Tunnelling and Underground Space Technology* 54:92–101. ISSN: 08867798. doi:10.1016/j.tust.2016.02.004. http://dx.doi.org/10.1016/j.tust.2016.02.004%20https://linkinghub.elsevier.com/retrieve/pii/S0886779816300931.

Törnell, Johannes, Simone Sebben, and Per Elofsson. 2021. "Experimental investigation of a two-truck platoon considering inter-vehicle distance, lateral offset and yaw". *Journal of Wind Engineering and Industrial Aerodynamics* 213 (October 2020). ISSN: 01676105. doi:10.1016/j.jweia.2021.104596.

Travin, Andrey K., et al. 2006. "Improvement of delayed detached-eddy simulation for LES with wall modelling". *Proceedings of the European Conference on Computational Fluid Dynamics (ECCOMAS CFD 2006)* 47 (2): 345–360. doi:10.1.1.829.2813.

Tsuei, Lun, and Ömer Savaş. 2001. "Transient aerodynamics of vehicle platoons during in-line oscillations". *Journal of Wind Engineering and Industrial Aerodynamics* 89 (13): 1085–1111. ISSN: 01676105. doi:10.1016/S0167-6105(01)00073-3. https://linkinghub.elsevier.com/retrieve/pii/S0167610501000733.

Tsugawa, S., S. Kato, and K. Aoki. 2011. "An automated truck platoon for energy saving". In *2011 IEEE/RSJ International Conference on Intelligent Robots and Systems*, 4109–4114. IEEE. ISBN: 978-1-61284-456-5. doi:10.1109/IROS.2011.6094549. http://ieeexplore.ieee.org/document/6094549/.

Utsunomiya, H., et al. 1993. "Basic study of blockage effects on bluff bodies". *Journal of Wind Engineering and Industrial Aerodynamics* 49 (1): 247–256. ISSN: 01676105. doi:10.1016/0167-6105(93)90020-O. https://linkinghub.elsevier.com/retrieve/pii/016761059390020O.

Vardy, A E. 1996. "Aerodynamic Drag on Trains in Tunnels Part 2: Prediction and Validation". *Proceedings of the Institution of Mechanical Engineers, Part F: Journal of Rail and Rapid Transit* 210, no. 1 (): 39–49. ISSN: 0954-4097. doi:10.1243/PIME_PROC_1996_210_325_02. http://journals.sagepub.com/doi/10.1243/PIME_PROC_1996_210_325_02.

Vegendla, Prasad, et al. 2015. "Investigation of Aerodynamic Influence on Truck Platooning". *SAE Technical Paper Series* 1. doi:10.4271/2015-01-2895.

Volpe, Raffaele, Philippe Devinant, and Azeddine Kourta. 2015. "Experimental characterization of the unsteady natural wake of the full-scale square back Ahmed body: flow bi-stability and spectral analysis". *Experiments in Fluids* 56 (5): 99. ISSN: 0723-4864. doi:10.1007/s00348-015-1972-0. http://link.springer.com/10.1007/s00348-015-1972-0.

Wang, Feng, et al. 2014. "An improved model of traffic force based on CFD in a curved tunnel". *Tunnelling and Underground Space Technology* 41 (1): 120–126. ISSN: 08867798. doi:10.1016/j.tust.2013.12.006. https://linkinghub.elsevier.com/retrieve/pii/S0886779813002113.

Wang, Feng, et al. 2011. "Computational study of effects of traffic force on the ventilation in highway curved tunnels". *Tunnelling and Underground Space Technology* 26 (3): 481–489. ISSN: 08867798. doi:10.1016/j.tust.2011.01.003.

Wang, Shibo, et al. 2017. "The performance of different turbulence models (URANS, SAS and DES) for predicting high-speed train slipstream". *Journal of Wind Engineering and Industrial Aerodynamics* 165:46–57. ISSN: 01676105. doi:10.1016/j.jweia.2017.03.001. http://dx.doi.org/10.1016/j.jweia.2017.03.001%20https://linkinghub.elsevier.com/retrieve/pii/S0167610516307243.

Watkins, Simon, and Gioacchino Vino. 2008. "The effect of vehicle spacing on the aerodynamics of a representative car shape". *Journal of Wind Engineering and Industrial Aerodynamics* 96 (6-7): 1232–1239. ISSN: 01676105. doi:10.1016/j.jweia.2007.06.042.

Wilcox, David C. 1998. *Turbulence Modeling for CFD*. Vol. 2. DCW industries La Canada, CA. ISBN: 0963605151.

Wille, Matthias, Markus Röwenstrunk, and Günter Debus. 2008. "KONVOI: Electronically coupled truck convoys". *Human Factors for Assistance and Automation. de Waard et al.(Eds.)(Shaker Publishing, Maastricht, the Netherlands*: 243–256.

Wolf-Heinrich, Hucho. 1997. *Aerodynamics of road vehicles: from fluid mechanics to vehicle engineering*. Society of Automotive Engineers. ISBN: 0768000297.

Xia, Chao, et al. 2017. "Effects of ground configurations on the slipstream and near wake of a high-speed train". *Journal of Wind Engineering and Industrial Aerodynamics* 168:177–189. ISSN: 01676105. doi:10.1016/j.jweia.2017.06.005. http://dx.doi.org/10.1016/j.jweia.2017.06.005%20https://linkinghub.elsevier.com/retrieve/pii/S016761051630616X.

Yakhot, Victor, and Steven A. Orszag. 1986. "Renormalization-Group Analysis of Turbulence". *Physical Review Letters* 57 (14): 1722–1724. ISSN: 0031-9007. doi:10.1103/PhysRevLett.57.1722. https://link.aps.org/doi/10.1103/PhysRevLett.57.1722.

Yang, Chunxin, et al. 2000. "Ventilation and air quality in indoor ice skating arenas". *ASHRAE Transactions* 106:338. ISSN: 00012505.

Yeung, P. K. 1998. "Correlations and conditional statistics in differential diffusion: Scalars with uniform mean gradients". *Physics of Fluids* 10, no. 10 (): 2621–2635. ISSN: 1070-6631. doi:10.1063/1.869775. http://aip.scitation.org/doi/10.1063/1.869775.

Yu, K. F., et al. 2011. "Confinement Effects on Flows Past an In-Duct Rectangular Bluff Body with Semi-Circular Leading Edge". In *AIP Conference Proceedings*, 1376:154–156. September. ISBN: 9780735409361. doi:10.1063/1.3651861. http://aip.scitation.org/doi/abs/10.1063/1.3651861.

Zabat, Michael, Stefano Frascaroli, and F. K. Browand. 1994. "Drag Measurements on 2, 3 and 4 Car Platoons". In *SAE Technical Papers*. 41 2. doi:10.4271/940421. https://www.sae.org/content/940421/.

Zabat, Michael, et al. 1995. *The aerodynamic performance of platoons: A Final Report. California Partners for Advanced Transportation Technology, UC Berkeley*. Tech. rep. California Partners for Advanced Transportation Technology, UC Berkeley. http://escholarship.org/uc/item/8ph187fw.pdf.

Zdravkovich, M.M., and D.L. Pridden. 1977. "Interference between two circular cylinders; Series of unexpected discontinuities". *Journal of Wind Engineering and Industrial Aerodynamics* 2 (3): 255–270. ISSN: 01676105. doi:10.1016/0167-6105(77)90026-5. https://linkinghub.elsevier.com/retrieve/pii/0167610577900265.

Zhang, Xiao-tian, et al. 2021. "Investigation of the aerodynamic phenomena associated with a long lorry platoon running through a tunnel". *Journal of Wind Engineering and In-*

dustrial Aerodynamics 210:104514. ISSN: 01676105. doi:10.1016/j.jweia.2020.104514. https://doi.org/10.1016/j.jweia.2020.104514%20https://linkinghub.elsevier.com/retrieve/pii/S0167610520304244.

Zhao, Yu, et al. 2020. "Deposition and dispersion characteristics of ultrafine particles under different vehicle speeds in road tunnels employing dynamic mesh simulation". *Environmental Science and Pollution Research* 27 (25): 31311–31329. ISSN: 0944-1344. doi:10.1007/s11356-020-09380-1. http://link.springer.com/10.1007/s11356-020-09380-1%20https://link.springer.com/10.1007/s11356-020-09380-1.

Websites consulted

- NASA – https://turbmodels.larc.nasa.gov

Appendix One

Tunnel leakage Analysis

This appendix discusses the effect of the leakage of the experiments and simulations. The slipstream development and the drag variation will be compared in simulation. In conclusion, the reason why the gap is modeled is provided.

A.1 Introduction of the partially-enclosed tunnel

TAKEI et al. (2008) studied the pressure variation caused by high speed train passage in station (a partially-enclosed space) by moving model tests. The effect of the opening ratio (the ratio of the size of the tunnel's opening to its cross-section perimeter length) and opening shape were investigated. The pressure variation around the train in the partially-enclosed space was unique and not like the standard patterns in fully-enclosed tunnel. The continuous gap ran along the length of the tunnel ceiling. Gilbert, Baker, and Quinn (2013b) later investigated the aerodynamics transition from open air to double vertical wall, partially enclosed spaces and fully enclosed tunnels based on a single train. The typical time history of static pressure for a partially-enclosed tunnel (opening ratio 1%) is showed in Figure A.1. The positive pressure occurs when the train nose passes, while negative pressure is seen when the tail of the train passes. The positive pressure with an opening ratio of 3% are approximately $20 - 30\%$ lower than that with an opening ratio of 1%.

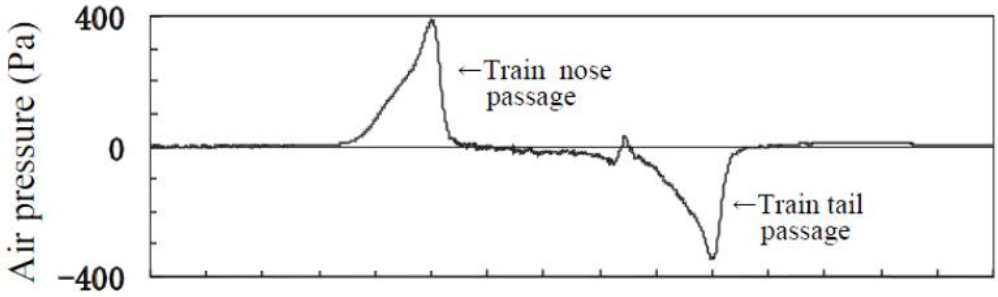

Figure A.1: Typical transient static pressure time history caused by a passing train in a partially-enclosed tunnel (TAKEI et al. 2008).

Iida et al. (2005) proposed the analytical model for the train in partially-enclosed tunnels based on the the potential flow model by (Vardy 1996; Howe 1998; Iida et al. 2005). More detailed about this analytical model are discussed in (Gilbert 2014). Figure A.2 shows the time history for partially-enclosed tunnel with different opening ratios. As the opening ratio increases, the starting point of the pressure is delayed. At the location of the train nose, the static pressure reaches its maximum value before abruptly decreasing to zero. The maximum values of the positive and negative pressure are almost the same for a same opening ratio. However, this model cannot predict accurately in certain circumstances, particularly for vehicles with bluff-noses that induce flow separation (Gilbert, Baker, and Quinn 2013b).

A.2 Simulation model

As shown in Figure 3.2, the ground plane was composed of two suspended plane halves with a minimised gap of 10 mm in width. A single long spine is running on the rig under the ground plane. This gap is inevitable because the whole platoon is installed on a single long spine. With this gap, the tunnel appears more like a partially enclosed space than a traditional tunnel. The opening ratio (the ratio of the size of the tunnel's opening to its cross-section perimeter length) is 1% for experiments and small tunnel simulation cases. For the large tunnels cases, the width of the gap is in accordance with small tunnel, resulting in a leakage ratio of 0.6%. In simulations, the effects of the leakage on a small tunnel are examined

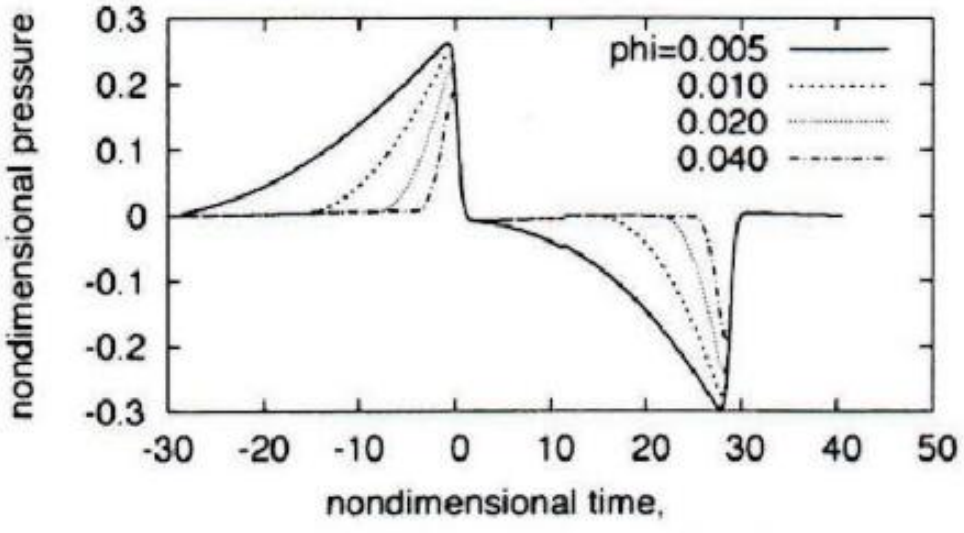

Figure A.2: The predicted pressure for different opening ratio ('phi') (Iida et al. 2005).

using a $1.5L$ platoon. Figure A.3 shows the cross-section of the tunnel with and without the tunnel. The red line in tunnel with leakage is the pressure outlet boundaries. Other simulation setup is keep in accordance with the description in Chapter 4. The numerical simulation of partial-enclosed tunnel have been validated by comparing with the results of experiments in Section 4.5.

A.3 Slipstream properties

Figure A.4 compares the simulated aerodynamic flow around the lorry platoon, in terms of the normalised horizontal velocity and pressure coefficient in the slipstream. Note that the measuring point is located $y/H = 0.14$ away from the lorry side, $y/H = 0.45$ from the ground level and 7/10 of the tunnel length from the entrance. $\tau = 0$ represents the first lorry entering the tunnel. The shaded rectangles indicate the time duration for each lorry to pass the measuring point. The slipstream development is significantly different in two tunnels. In the fully-enclosed tunnel, the horizontal velocity begins to increase from zero when the first lorry enters the tunnel, while in the partially-enclosed tunnel, the air began to be propelled forward at $\tau = 12$. However, the maximum horizontal velocity reaches the same level (at around 0.6) in two tunnels. As for the pressure variation, before the platoon arrives at the

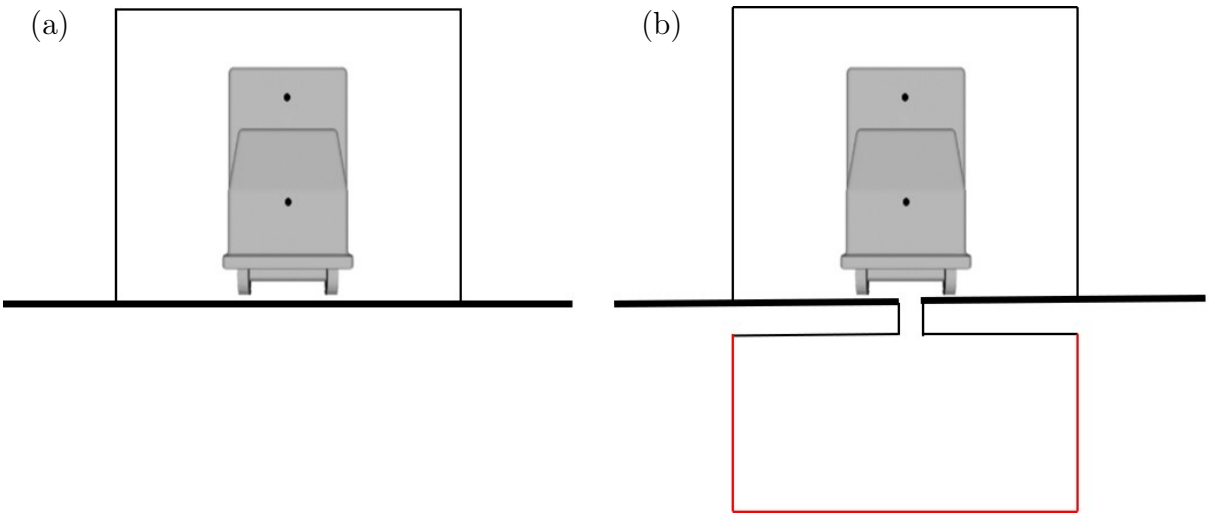

Figure A.3: The cross-section of the small (a) fully-enclosed tunnel, (b) partially-enclosed tunnel. Note that the red line represents the pressure outlet boundaries.

measuring point, the pressure coefficients fluctuates at around 0.4 in fully-enclosed tunnel. When the lorries pass by, there are eight peaks as seen with negative pressure as seen in the figure. The pressure variation trend resembles that depicted in Figure A.1, with the exception of the intermediate peaks caused by the intermediate lorries. Figure A.5 presents the side view of the velocity. During the entering process ($\tau = 11$), the air in front of the platoon escapes through the gap, while in fully-enclosed tunnel, the air keep push forward all along the whole tunnel.

Figure A.6 shows the side view of the pressure distribution at $y/H = 0$ when the platoon travels through tunnel with and without the leakage. The transient pressure fields at three distinct times are shown. At $\tau = 11.14$ when first five lorries enters the tunnel, the front positive pressure is significantly higher in the tunnel without gap (no leakage) because the air can not escape through the gap on the ground and can only move forward inside the tunnel. When the whole platoon enters the tunnel ($\tau = 22.53$), the positive frontal pressure in tunnel without gap (no leakage) becomes smaller than in the tunnel with gap, while the negative rear pressure becomes significantly lower. At $\tau = 31.39$ when then platoon leaves the tunnel, the negative rear pressure is observed significantly lower in tunnel without gap. Above all, the piston effect is stronger in tunnel without gap on the ground.

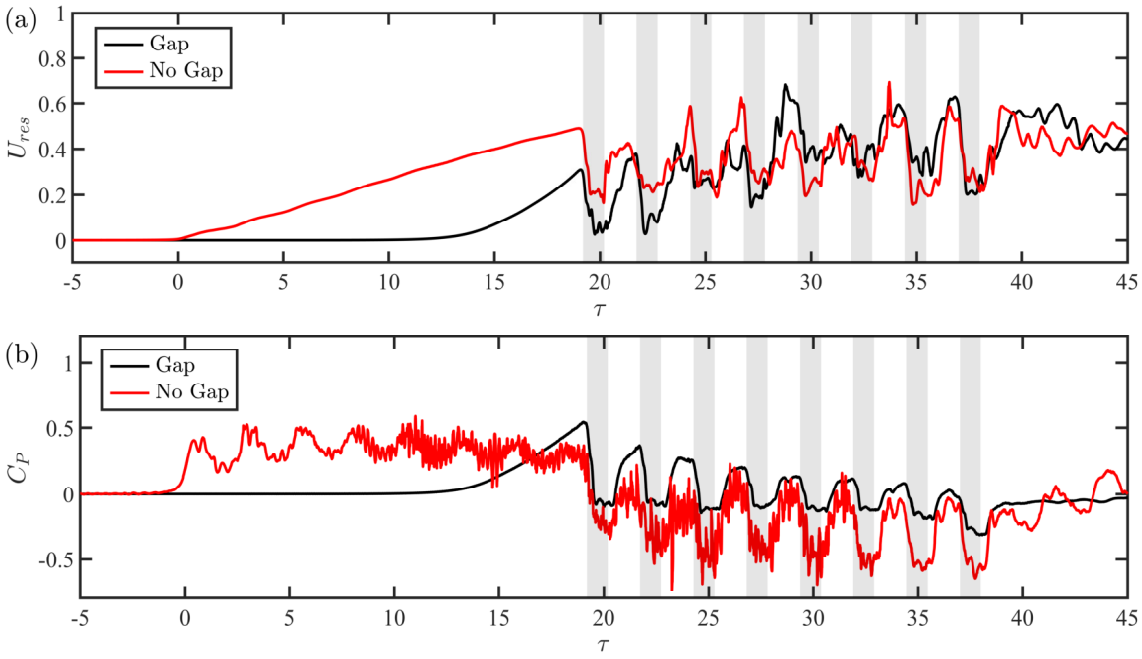

Figure A.4: The temporal variations of the (a) normalised horizontal velocity and (b) the pressure coefficient. The shaded rectangles indicate the time duration for each lorry to pass the measuring point.

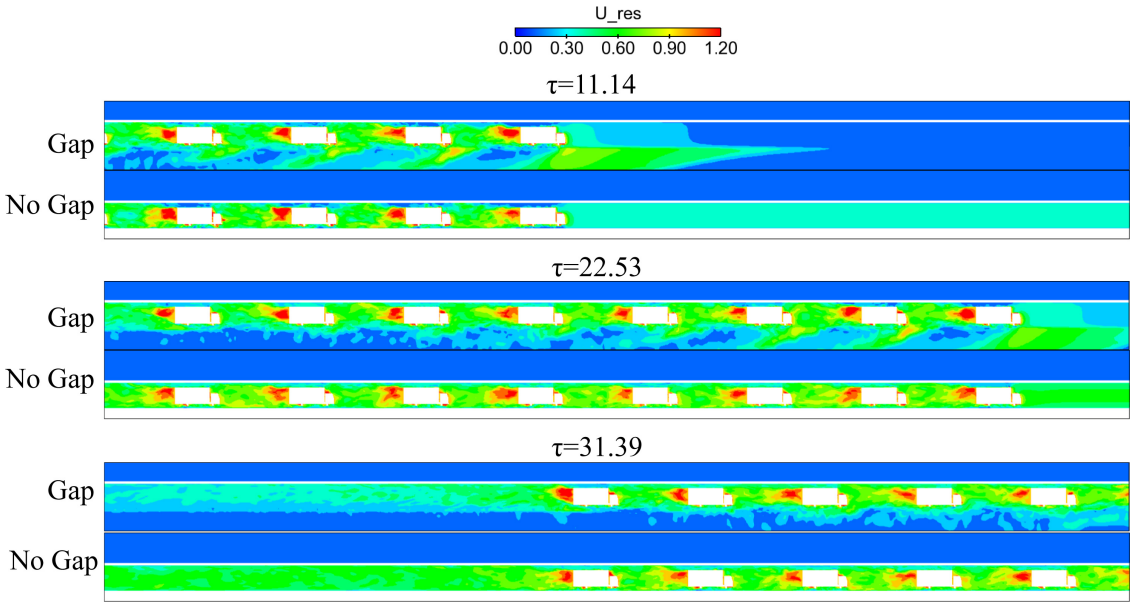

Figure A.5: The velocity field during the lorry platoon passing through two tunnels at three distinct times on the vertical plane of $y/H = 0$.

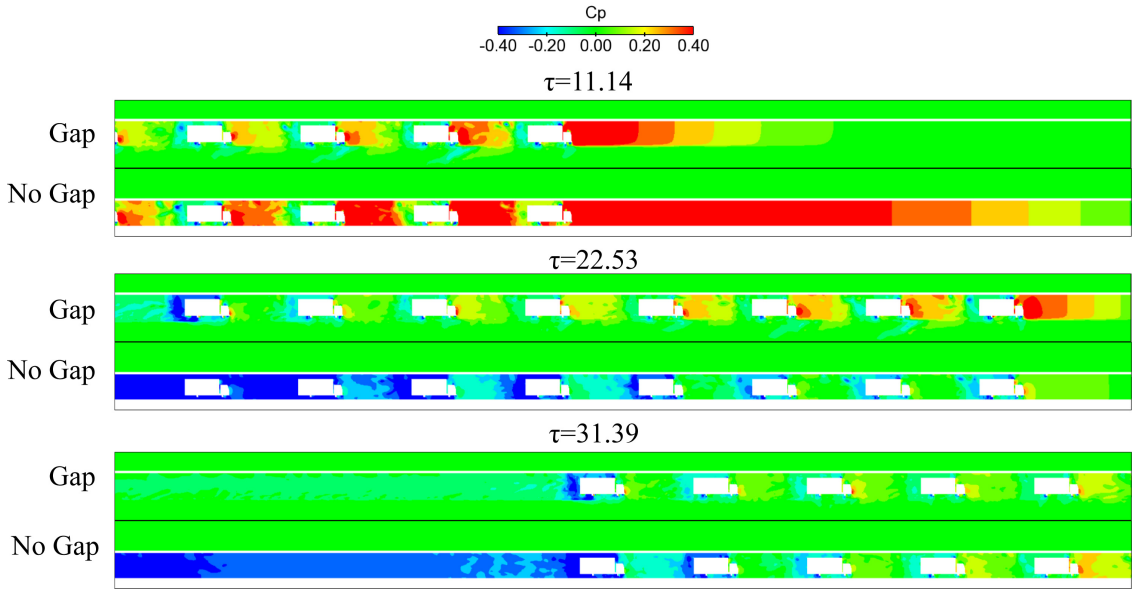

Figure A.6: The pressure distribution during the lorry platoon passing through two tunnels at three distinct times on the vertical plane of $y/H = 0$.

A.4 Aerodynamics force analysis

In previous train research (TAKEI et al. 2008; Gilbert, Baker, and Quinn 2013b), the vehicle is regarded as a single unit. For a platoon, however, it is necessary to investigate the drag coefficient of each individual vehicle. Figure A.7 illustrates the time history of drag coefficients of each lorry running through tunnel with and without leakage. In the tunnel with leakage, the drag coefficients of all vehicles increase dramatically when entering the tunnel, then gradually fall along the tunnel before abruptly decreasing at the exit. The peak drag coefficient of the leading truck reaches approximately 1, whereas the peak values for the trailing vehicles decrease gradually from 0.7 to 0.5. In the fully-enclosed tunnel (see Figure A.7 (b)). When the lorries enter the tunnel, the peak drag coefficients are significantly higher (1.6 for the leading lorry) than in a partially enclosed tunnel. Until they reach the tunnel's exit, the drag coefficients of all lorries drop dramatically to approximately 0.4. When the lorries leave the tunnel, they all experience a sudden drop of equal magnitude. The variation in drag coefficients in a fully enclosed tunnel is so extreme that it is unlikely to occur in real life. When a ground vehicle travels inside a tunnel, it experiences relative constant drag force. (Lee, Park, and Kim 2018). A fully enclosed tunnel is not a good test

case for investigating the platoon's aerodynamics.

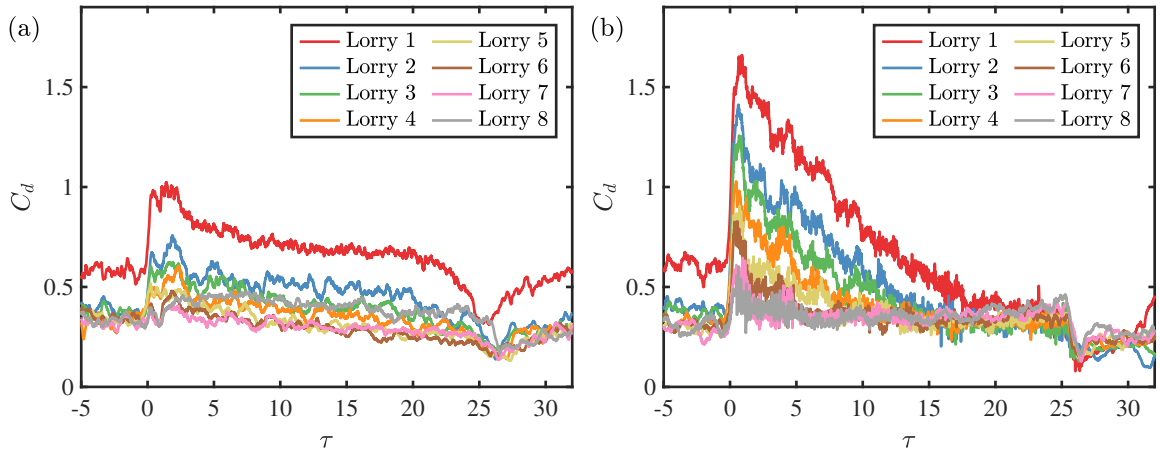

Figure A.7: The time history of drag coefficients of different lorries in the platoon: (a) in the partially-enclosed tunnel and (b) in the fully-enclosed tunnel.

A.5 Conclusion

In the appendix, the effect of the leakage of the tunnel was investigated. The slipstream development and the drag coefficient variation of the $1.5L$ spaced platoon travelling in fully-enclosed and partially-enclosed tunnel are compared and analysed. Despite the fact that the fully enclosed tunnel is unavailable in the present experiment. The main objective is to investigate the effect of the wall confinement on the aerodynamics of the platoon, a partially-enclosed tunnel is enough to provide such confinement. In addition, the significant drag variation in the fully-enclosed tunnel is not representative of the actual situation. Therefore, partially-enclosed tunnel is a better choice to represent a real road tunnel. The opening ratio is 1% for the small tunnel and 0.6% for the large tunnels. All tunnel in the main body of the thesis refer to partially-enclosed tunnel.

Appendix Two

Uncertainty Analysis

The discrepancy between the true and observed values of a certain physical quantity or derived property is called measurement error (Taylor 1997; Tavoularis 2005). Dorigatti (2013) and Soper (2016) used the uncertainty analysis method to mean pressure. Based on the data reduction methods and experimental techniques, there are two major causes of the uncertainty of experiments: bias limit and random uncertainty.

The bias limit specifies the uncertainty associated with the instrumentation's characteristics and performance. For instance, the C_ξ represents any non-dimensional coefficient calculated. the bias limit is defined as:

$$E_{\text{BIAS}} = \sqrt{\sum_k \left(\frac{\partial C_\xi}{\partial b_k} \delta b_k \right)^2} \tag{B.1}$$

where b_k indicates any generic individual quantity that was directly measured to calculate C_ξ, and δb_k presents the representative instrumentation uncertainty.

The random uncertainty is the inherent variability of the stochastic nature and unsteadiness of the physical experiments (Dorigatti 2013). Assuming a normal distribution and a 95% confidence level, the random uncertainty can be estimated as:

$$E_{\text{RND}} = \pm 2 \frac{\sigma_{C_\xi}}{\sqrt{N}} \tag{B.2}$$

where N is the number of runs and σ_{C_ξ} is the standard deviation. The bias and random

uncertainties are combined to form the total uncertainty:

$$E_{\mathrm{TOT}} = E_{\mathrm{BIAS}} + E_{\mathrm{RND}} \tag{B.3}$$

The total uncertainties are indicated as a percentage form in the paper.

B.1 Slipstream uncertainty analysis

In accordance with the prior slipstream investigations (Gil et al. 2010; Baker et al. 2016), the uncertainties of the slipstream are calculated using maximum values of static pressure and velocities.

B.1.1 Slipstream velocities

For each run, the maximum horizontal slipstream velocity is calculated at each measuring point.

Bias limit The resultant velocity is normalised with respect to lorries speed for each individual run, V_{lorry},

$$U_{res}(t)\,|_r = \frac{u_{res}(t)\,|_r}{V_{plat}} = \frac{\sqrt{u^2(t) + v^2(t)}\,|_r}{V_{plat}} \tag{B.4}$$

	Accuracy	Instrumentation	Source information
δu	0.3 m/s	Cobra probe	Manufacturer specification
δv	0.3 m/s	Cobra probe	Manufacturer specification
δu_{res}	0.3 m/s	Cobra probe	Derived from u and v
δV_{plat}	0.1 m/s	Track-side speed measuring devices	Manufacturer specification

Table B.1: The accuracies of measuring instrumentation to monitor the slipstream quantities.

The uncertainty for the measuring instrument is listed in Table B.1. The bias limits for each Cobra probe are presented in Figure B.1 (a) . The mean and maximum bias limit value for experiments in open air and the tunnel are listed in Table B.2.

	Bias limit		Random uncertainty		Total uncertainty	
	Mean	Maximum	Mean	Maximum	Mean	Maximum
In tunnel	0.012	0.012	0.035	0.042	0.047	0.054
In open air	0.012	0.012	0.054	0.058	0.066	0.070

Table B.2: The bias limit, random and total uncertainties of slipstream velocities for two series of experiments. The mean and maximum values are presented.

Random uncertainty The standard deviation of slipstream velocity is calculated using individual resultant velocity measurements for each run. Figure B.1 (b) presented the random uncertainties for two series of experiments. The mean and maximum values listed in Table B.2.

Total uncertainty The total uncertainties for two series of experiments are presented in Figure B.1 (c) and the mean and maximum values listed in Table B.2. In calculating the averages, the individual uncertainties of each of the cobra probes were used, whereas the maxima were provided by the most significant. In comparison to random uncertainty, the bias limit values are small. Previous slipstream studies Dorigatti (2013) and Soper, Baker, and Sterling (2014) show similar results to the and random uncertainties and bias limit. The magnitudes for random uncertainty in the open air experiments are relatively larger in comparison to the in the tunnel cases.

B.1.2 Slipstream static pressure

The minimum and maximum static pressure in the horizontal plane is calculated for each individual run, at each measuring position.

Bias limit The static pressure is normalised with lorries speed for each individual run, V_{plat}, and density ρ,

$$C_p = \frac{\triangle P}{1/2\rho V_{plat}^2} \tag{B.5}$$

The uncertainty for every measuring instrument is listed in Table B.3. The bias limits for

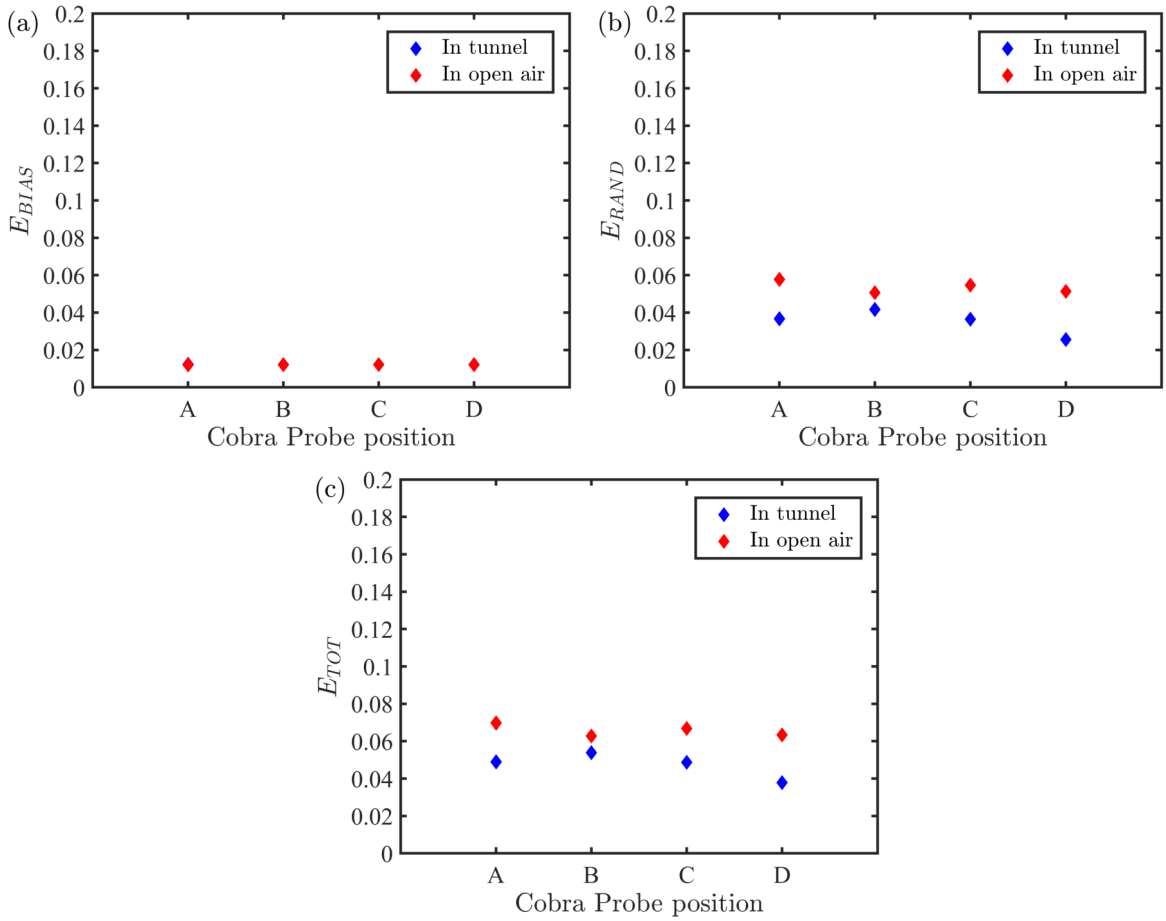

Figure B.1: The (a) bias limit, (b) random uncertainties and (c) total uncertainties for measurements of resultant velocity in the open air and in the tunnel.

each Cobra probe are presented in Figure B.2 (a) . The mean and maximum bias limit value for two series of experiments are shown in Table B.4.

Random uncertainty The standard deviation of slipstream static pressure is calculated with respect to individual static pressure measurements for each run in relation to the ensemble. The random uncertainties for two series of experiments are presented in Figure B.2(b) and the mean and maximum random uncertainty value shown in Table B.4.

Total uncertainty The total uncertainties for two series of experiments are shown in Figure B.2(c). Table B.4 summarised the mean and maximum random uncertainties for slipstream pressure. The lager bias limit are observed in tunnel experiment. Since the bias

	Accuracy	Instrumentation	Source information
$\delta \triangle P$	± 5 Pa	Cobra probe	Manufacturer specification
δV_{lorry}	0.1 m/s	Track-side speed measuring devices	Manufacturer specification
$\delta\rho$	0.005 kg/m^3	Derived from ambient conditions	Manufacturer specification

Table B.3: Accuracy of the static pressure of each measurement instruments.

limit is based on the maximum pressure coefficients (around 0.56 in the tunnel, 0.045 in the open air), the larger value for in tunnel experiment is expected according to the bias limit definition in Equation B.1.

	Bias limit		Random uncertainty		Total uncertainty	
	Mean	Maximum	Mean	Maximum	Mean	maximum
In tunnel	0.028	0.028	0.008	0.009	0.036	0.038
In open air	0.014	0.014	0.020	0.028	0.033	0.042

Table B.4: The bias limit, random and total uncertainties for slipstream static pressure for two series of experiments. The mean and maximum values are presented.

B.2 Surface pressure uncertainty analysis

The mean surface pressure coefficient is calculated for each pressure tap on all lorries in the platoon travelling through the tunnel. The mean pressure coefficient for the moving lorries is defined as:

$$\overline{C_{P_k}} = \overline{C_{P_k}(t)}\,|_{t_0<t<t_1} \tag{B.6}$$

where t_0 and t_1 represent the time when each lorry arrive and leaves the sampling section in the tunnel. The mean surface pressure coefficients in tunnel are calculated for 1 meter length near the cobra probe (7 meters from tunnel inlet to 8 meters from the tunnel inlet), in accordance with the experiments in the open air (Robertson et al. 2019).

Bias uncertainty Table B.5 summarised the uncertainty for each measuring instrument.

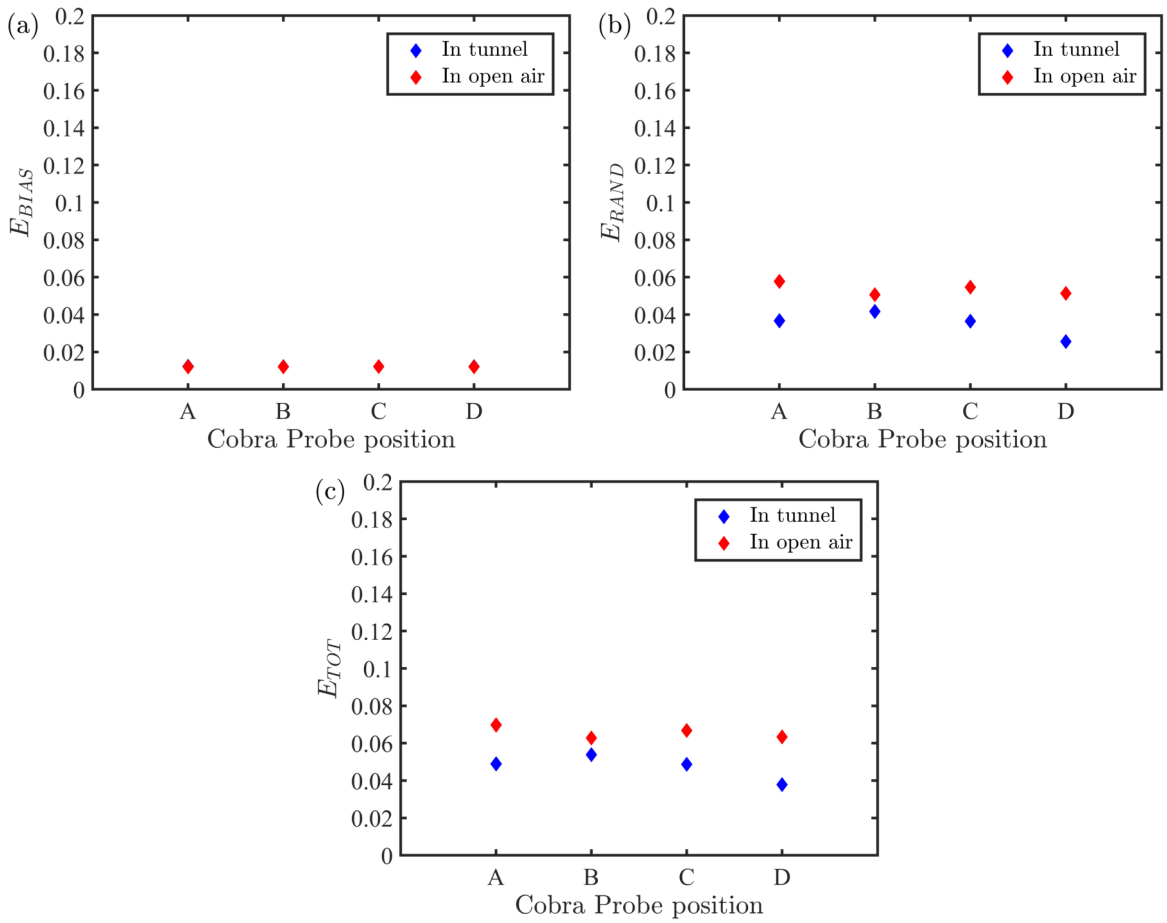

Figure B.2: The (a) bias limit, (b) random uncertainties and (c) total uncertainties for static pressure measurements in open air and in tunnel.

The ideal gas law equation was used to compute the density of air using the propagation of error theory.

	Accuracy	Instrumentation	Source information
$\delta \triangle P$	± 9 Pa	On-board pressure transducers	Static calibration
δV_{plat}	0.1 m/s	Track-side speed measuring devices	Manufacturer specification
$\delta \rho$	0.005 kg/m^3	Derived from ambient conditions	Manufacturer specification

Table B.5: The accuracies of measuring instrumentation for the static pressure.

Calibration is performed to account for the non-linearity of the pressure transducers. Instrumentation Betz micro-manometers were used to calibrate three different types of pressure transducers (ACIN 2012). The Betz manual pump is adopted to generate a nominal differential pressure ($\triangle P_N$). Time history of voltage output were recorded for 60 seconds and then time averaged to obtain $\text{Vol}_{RT}(\triangle P_N)$. The procedure is repeated 51 times over the entire pressure transducer range, including 0 Pa. Data recorded of zero differential pressure ($\triangle P_N = 0$) provided 'zero pressure offset' voltages. The data is processed considering zero pressure offset $\text{Vol}_{0,k}$ (Soper 2016),

$$\text{Vol}_k(\triangle P_N) = \text{Vol}_{RT}(\triangle P_N) - \text{Vol}_{0,k}, \tag{B.7}$$

where k denotes the serial number of pressure transducer. To reduce the error from calibration, actual cubic calibration method (Soper 2016) was used. The actual cubic calibration curve is expressed as,

$$\triangle P_{ACC,K} = C_{3,k} \triangle \text{Vol}_k^3 + C_{2,k} \triangle \text{Vol}_k^2 + C_{1,k} \triangle \text{Vol}_k, \tag{B.8}$$

where $C_{3,k}$, $C_{2,k}$ and $C_{1,k}$ are three cubic calibration coefficients. The $\triangle P_{ACC,K}$ represents the differential pressure measurement.

The calibration coefficients for pressure transducers of Lorry 8 (two types of transducers are used) are listed in Table B.6

The corresponding calibration error can be expressed as,

$$E_{ACC,k}(\triangle P_N) = \triangle P_{ACC,K} - \triangle P_N \tag{B.9}$$

	C_3	C_2	C_1
	Pa/Vol^3	Pa/Vol^2	Pa/Vol
Tap1	1.0559	-1.0059	1249.92
Tap2	1.1997	-3.1122	1245.02
Tap3	0.7660	-1.0231	1246.05
Tap4	0.9898	-4.5512	1245.32
Tap5	1.7539	-3.0643	1244.96
Tap6	0.9290	-1.4744	1247.76
Tap7	1.0602	-3.3673	1246.56
Tap8	0.6444	-0.9785	624.54
Tap9	1.5137	-2.4048	619.55
Tap10	0.9661	-1.1467	623.09
Tap11	0.5275	-1.3711	623.34
Tap12	-	-	-
Tap13	0.9581	-1.5035	626.31
Tap14	0.6032	-0.0062	623.24

Table B.6: The calibration factors of actual cubic method. Note that the transducer Tap 12 is malfunctioned.

The Actual cubic calibration errors calculated for 14 pressure transducers on Lorry 1 are shown in Figure B.3 (Note that Tap 1 to 8 is presented in Figure 3.7, while the other taps are not discussed in this writing and hence identified in 9 to 14). The error of all other pressure transducers tested have the same magnitudes of the order of ±9Pa.

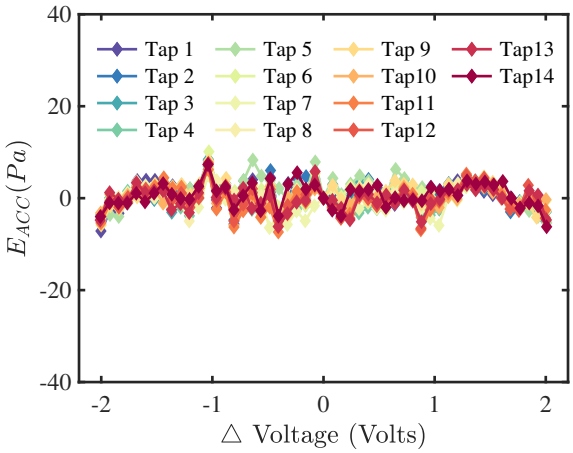

Figure B.3: The actual cubic calibration error of each pressure transducer on Lorry 1.

Random uncertainty The random uncertainties for in tunnel experiments are shown in figure Figure B.4 (b). Larger values are observed in comparison to previous study(Dorigatti 2013; Soper 2016). In Soper and Dorigatti's studies, the mean pressure coefficients are calculated for the whole open air test section length, while in this research, the pressure coefficients are calculated for only 1 meter as mentioned before, since the surface pressure changes when lorries running through the tunnel. The peak values occurs on Tap 5, where the flow stagnates. The random uncertainties are approximately the same for measurement taps located in other regions.

Total uncertainty Figure B.4 shows the magnitudes for the total uncertainties of every pressure tap. The total uncertainties of the mean surface pressure coefficients is in the range of $0.02 - 0.08$.

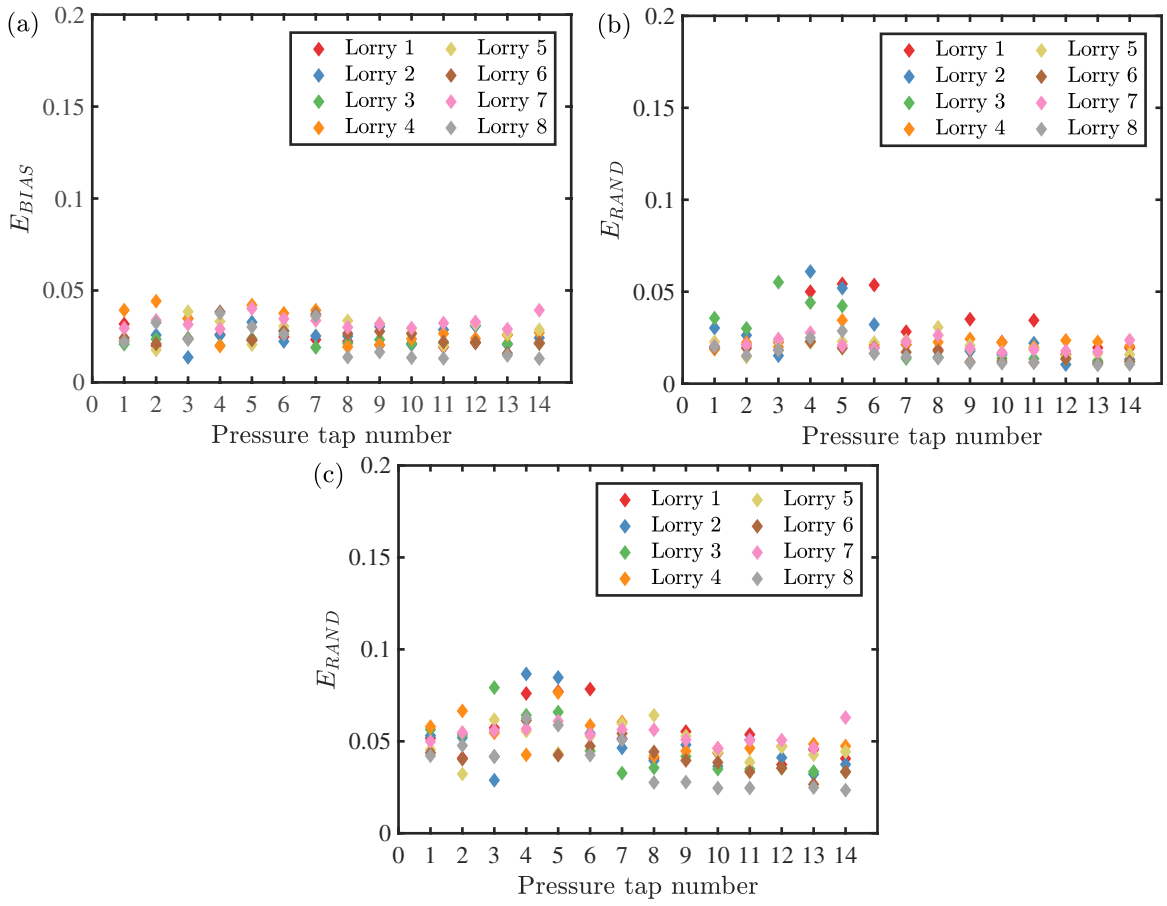

Figure B.4: The (a) bias limit, (b) random uncertainties and (c) total uncertainties for for surface pressure coefficient in the tunnel.